

**A self-emulsifying delivery system loaded with efavirenz:
The case for flax-seed oil**

A thesis submitted to Rhodes University
in Fulfilment of the Requirements of the Degree of

**MASTER OF SCIENCE (PHARMACY)
in Pharmaceutics**

by

PRIVELEDGE MAZONDE

March 2021

Faculty of Pharmacy
Rhodes University
Makhanda
South Africa

ABSTRACT

The feasibility of incorporating efavirenz (EFV), an antiretroviral agent against HIV into a lipid-based self-emulsifying drug delivery system (SEDDS) containing vegetable oils was investigated. EFV has poor aqueous solubility and is classified under the Biopharmaceutical Classification System (BCS) as a class II compound with highly permeability, its aqueous solubility is less than 10 mg/ml and is defined as a practically insoluble compound with a consequent poor bioavailability of approximately 40%, and erratic dissolution behaviour. SEDDS formulations have been shown to improve the aqueous solubility and consequently the bioavailability of BCS II compounds such as EFV. EFV is a first line antiviral agent used in combination with other agents in antiretroviral therapy (ART). Among the number of NNRTIs approved for use in HIV treatment, EFV is one of the most commonly prescribed drug.

Statistical methods and Design of Experiments (DoE) using Response Surface Methodology (RSM), specifically a Central Composite Design (CCD), were used to facilitate the development of a reversed-phase high performance liquid chromatographic (HPLC) method for the quantitation of EFV during formulation product and process development studies. A rapid, accurate, precise and sensitive HPLC method with ultraviolet (UV) detection was developed, optimised and validated for the in-vitro analysis of EFV in a total run time under 10 minutes for the elution of both EFV and loratidine which was used as the internal standard (IS). The method was then successfully applied to the determination of EFV in commercially available tablets.

Excipient screening was undertaken using solubility studies and revealed that EFV had highest solubility in flaxseed oil in comparison to soybean, macadamia, grapeseed, sunflower and olive oils. The non-ionic Tween[®] 80 and Span[®] 20 were selected as surfactant and co-surfactant, respectively with ethanol co-solvent as they exhibited improved miscibility with co-solvent. Pre-formulation studies were undertaken to investigate the compatibility of the API with excipients and to identify a nano-emulsion region and other emulsion types using pseudo-ternary phase diagrams. The phase behaviour of crude cold pressed flaxseed oil with the selected non-ionic surfactants revealed an area within pseudo-ternary phase diagrams for different surfactant-mixtures formed gels/semisolid structures which can be exploited for other drug delivery strategies that require such properties.

Fourier transform infrared spectroscopy (FT-IR), powder x-ray diffraction (XRD) and Raman spectroscopy were used to identify and assess the compatibility of EFV with chosen excipients.

A reduction in the peak intensity was observed for EFV when combined with each hydrophobic/lipid excipient evaluated revealing that there was a marked reduction in the crystallinity of the EFV. A decrease in crystallinity in comparison with the bulk API may indicate that EFV were amorphous or sequestered in a molecular dispersion and exhibited an increased solubility for the molecule.

Flaxseed oil was used as the oil phase in studies for the optimization of surfactant mixtures undertaken using DoE, specifically a D-optimal mixtures design with the flaxseed oil content set at 10% m/m was performed. Solutions from the desired optimization function were produced based on desirability and five nanoemulsion formulations were produced and characterized in terms of in vitro release of efavirenz, drug loading capacity, Zeta Potential, droplet sizes and polydispersity index (PDI). Kinetically stable nanoemulsions containing 10% m/m flaxseed oil were successfully manufactured and assessed. Droplet sizes ranged between 156 and 225 nm, Zeta Potential between -24 and -41 mV and all formulations were found to be monodisperse with polydispersity indices ≤ 0.487 .

SEDDS formulations of EFV in nano-sized carriers were developed and optimised, in vitro drug release varied with varying amounts of ethanol in the formulation producing formulations that exhibited differently modulated drug in-vitro release profiles that may be further manipulated for better performance and therapeutic outcomes in terms of solubility and possibly bioavailability of EFV when delivered using SEDDS rather than using tablets which in turn may lead to better therapeutic outcomes for patients with HIV.

ACKNOWLEDGEMENTS

Throughout the writing of this thesis, I have received a great deal of support and assistance. I would first like to thank God Almighty for the gift of life, the opportunity, and the strength to conduct this research. I present this research as my best effort unto him.

I would like to thank my supervisor Professor R.B. Walker, whose expertise were invaluable from the contextualizing and the development of this research project, questions, and methodology. Your insightful feedback pushed me to sharpen my thinking and brought my work to a higher level. I would also like to express my gratitude to the Dean and Head of the Faculty of Pharmacy, Professor S.M.M. Khamanga for playing a distinguished roll as an academic mentor throughout the process of this research project and during my undergraduate studies as well.

I would like to acknowledge my colleagues in the Biopharmaceutics Research Group at Rhodes University for their insightful collaboration and support. I would like to thank Dr B.A. Witika and Dr P.V. Ntemi particularly for their support in the early stages of my research journey even as I was completing my undergraduate studies. I would like to thank Dr P.A. Makoni, Dr M. Chikukwa, Mr. T. Mano, Mr. T. Mandava and Ms. C. Dickson for their friendship and always being enthusiastic and helpful in the laboratory and in stimulating research discussions. My sincere gratitude also goes to the technical support staff in the Faculty of Pharmacy, Mr. N. Borland, Mr. S. Ngxingo, Mr. T. Flerck, Mrs. T. Kent and Ms. L. Emslie for their consistent assistance with resources, tools and administration which made my time in the Faculty a smooth experience.

In addition, I would like to thank my parents Mr. Shepherd Mazonde and Mrs Konja Mazonde for their sacrifice throughout my life, their support throughout my educational journey, their love, wise counsel and sympathetic ear and yet the biggest investors in my dreams. Finally, I could not have completed this dissertation without the support of my special and dear friends Ms. S. Centane and Mr R. Blandin de Chalain for the unwavering support, adventures and memories outside of my research.

STUDY OBJECTIVES

The human immunodeficiency virus (HIV) remains a global health burden, but the highest mortality rate is observed in children particularly in Sub-Saharan Africa. Currently EFV among other antiretrovirals in combination are used as first line treatment for HIV infections and the use of combination therapy has improved the mortality rate. However, both EFV among other similar compounds of BCS II exhibit low oral bioavailability due to poor aqueous solubility. The absorption of EFV can be enhanced by administration with a high fat meal. BCS Class II compounds maybe typically lipophilic (oil/lipid soluble) and thus are good candidates for delivery using self-emulsifying drug delivery systems (SEDDS). The development of a dosage form of EFV that has improved aqueous solubility and likely bioavailability and may reduce the need for administration with a high fat meal and allow for improved modulation of drug release and better therapeutic possibilities. The objective of this study was to develop a lipid based SEDDS formulation to enhance the solubility of EFV through,

The specific objectives of this study were:

1. To review and interpret information relating to the pharmacological, biopharmaceutical and physicochemical properties of EFV to facilitate the development of SEDDS.
2. To develop and validate a reversed-phase high performance liquid chromatographic method for the quantitation of EFV with the aid of DoE and response surface methodology.
3. To assess the solubility of EFV in various chosen vegetable oils, characterise and investigate the compatibility of EFV and excipients and to investigate emulsion types and the formation of nano-emulsion using pseudo-ternary phase diagrams.
4. To conduct pre-formulation studies to assess the compatibility of Efavirenz and selected excipients.
5. To design, develop and optimise EFV loaded SEDDS using a D-optimal mixtures design of vegetable oil and surfactant mixtures.
6. To characterize the manufactured SEDDS with respect to in vitro release of EFV, droplet sizes, polydispersity index and Zeta Potential.

TABLE OF CONTENTS

ABSTRACT	1
ACKNOWLEDGEMENTS	3
STUDY OBJECTIVES	4
CHAPTER 1	14
EFAVIRENZ AND ANTIRETROVIRAL THERAPY	14
1.1 Introduction	14
1.1.1 Antiretroviral therapy	15
1.1.2 Biopharmaceutical Classification System (BCS)	16
1.2 Physicochemical properties of EFV	17
1.2.1 Nomenclature and structure	17
1.2.2 Solubility	17
1.2.3 Dissociation constant (pKa)	18
1.2.4 Partition coefficient (LogP)	18
1.2.5 UV absorption spectra	19
1.2.6 Melting range	19
1.2.7 Polymorphism	19
1.3 Structure activity relationships	20
1.4 Synthetic pathway	20
1.5 Clinical pharmacology	21
1.5.1 Mechanism of action (MOA)	21
1.5.2 Dosage and administration	22
1.5.3 Overdose	22
1.5.4 Contraindications and drug interactions	22
1.5.5 Pregnancy and breastfeeding	23
1.5.6 Renal impairment	24
1.5.7 Hepatic impairment	24
1.5.8 Adverse effects	25
1.5.9 Resistance	25
1.6 Clinical pharmacokinetics	26
1.6.1 Absorption	26
1.6.2 Distribution	26
1.6.3 Metabolism (metabolic pathway)	26
1.6.4 Elimination	27
1.7 Conclusions	27

CHAPTER 2	29
MICRO-, NANOEMULSIONS AND SELF EMULSIFYING DRUG DELIVERY SYSTEMS (SEDDS)	29
2.1 Introduction	29
2.1.2 Micro- and nano-emulsions	30
2.2 Formulation components of micro- and nano-emulsions	33
2.2.1 Aqueous phase	33
2.2.2 Oil phase	33
2.2.3 Surfactants and co-surfactants	34
2.2.3.1 Surfactant type	36
2.2.3.2 Co-solvents	37
2.3 Development of SEDDS	37
2.3.1 Hydrophilic-Lipophilic Balance (HLB) system	37
2.3.2 Bancroft’s Rule	38
2.3.3 Phase behaviour and diagrams	39
2.4 Methods of manufacture of micro- and nano-emulsions	40
2.4.1 Low energy methods	40
2.4.1.1 Spontaneous Emulsification	40
2.4.1.2 Phase Inversion	41
2.4.2 High energy methods	41
2.4.2.1 High pressure homogenization	42
2.4.2.2 Membrane emulsification	42
2.4.2.3 Micro-fluidization	42
2.4.2.4 Ultrasonication	42
2.5 Quality assessment and characterization of SEDDS	43
2.5.1 Droplet size	43
2.5.2 Polydispersity index (PDI)	43
2.5.3 Zeta Potential	44
2.5.4 Drug loading capacity and encapsulation efficiency	45
2.5.5 In vitro release	46
2.5.6 Stability	47
2.5.7 Crystallization, polymorphism, and compatibility	49
2.5.8 Electrical conductivity and emulsion classification	49
2.6 Conclusions	50
CHAPTER 3	52

DEVELOPMENT AND VALIDATION OF A HIGH-PRESSURE LIQUID CHROMATOGRAPHIC (HPLC) METHOD FOR THE QUANTITATION OF EFAVIRENZ	52
3.1 Introduction	52
3.2 Principles of HPLC	52
3.2.1 Distribution constant	54
3.2.2 Column efficiency	55
3.2.3 Resolution factor	56
3.2.4 Asymmetry factor	57
3.2.5 Method of detection	58
3.2.6 UV-Visible detectors	58
3.2.7 Mobile phase and buffer considerations	59
3.2.6 Internal standard	61
3.3 Method development	62
3.3.1 Statistical design of experiments	63
3.3.2 Response surface methodology	65
3.3.3 RSM notation for 2-level designs	66
3.4 Experimental	67
3.4.1 Materials and methods	67
3.4.2 System and Instrumentation	68
3.4.3 Preparation of stock solutions	68
3.4.4 Preparation of buffer and mobile phase	68
3.5 Statistical modelling and optimization	69
3.5.1 Analysis of statistical data	70
3.5.1.1 Retention time	71
3.5.1.2 Peak tailing	78
3.5.1.3 Peak resolution	79
3.5.2 Optimization and point prediction	83
3.6 Method validation	86
3.6.1 Linearity and Range	86
3.6.2 Precision	87
3.6.3 Intra-day precision	88
3.6.4 Inter-day precision	88
3.6.5 Accuracy	89
3.6.6 Limits of quantitation and detection	89
3.7 Forced degradation studies	91

3.7.1 Dry heat degradation	91
3.7.2 Neutral Hydrolysis	91
3.7.3 Acid degradation	92
3.7.4 Alkali degradation	92
3.7.5 Temperature stress studies	92
3.7.6 Oxidative degradation studies	92
3.8 Application of method	93
3.8.1 Assay of efavirenz containing tablet dosage form	93
3.9 Conclusions	93
CHAPTER 4	95
PREFORMULATION STUDIES FOR THE DEVELOPMENT OF EFAVIRENZ LOADED SEDDS	95
4.1 Introduction	95
4.2 Screening and selection of excipients	96
4.2.1 Vegetable oil triglycerides	97
4.2.2 Surfactant mixture system	101
4.3 Experimental	102
4.4 Materials	102
4.4.1 Solubility studies	102
4.4.2 Phase behaviour and pseudo-ternary phase diagram construction	102
4.4.3 Fourier Transform Infrared S Spectroscopy (FTIR)	105
4.4.4 X-ray diffraction (XRD)	106
4.4.5 Raman spectroscopy	107
4.4.6 Differential scanning calorimetry (DSC)	107
4.5 Results and discussion	108
4.5.1 Solubility studies	108
4.5.2 Pseudo-ternary phase diagram construction	109
4.5.3 Fourier Transform Infrared Spectroscopy (FTIR)	112
4.5.4 Raman Spectroscopy	118
4.5.5 X-ray diffraction (XRD)	121
4.5.6 Differential scanning calorimetry (DSC)	124
4.6 Conclusions	125
CHAPTER 5	127
FORMULATION DESIGN, OPTIMISATION AND CHARACTERISATION OF EFAVIRENZ LOADED FLAXSEED OIL SEDDS	127
5.1 Introduction	127

5.1.2 Surfactant mixture optimization	129
5.1.3 Phase behaviour and exploitation of design spaces.....	130
5.2 Experimental (manufacture and characterisation of SEDDS)	132
5.2.1 Materials	132
5.2.2 Preparation of nano-emulsions	132
5.2.3 Droplet size and polydispersity index.....	133
5.2.4 Zeta Potential	133
5.2.5 Transmission electron microscopy	133
5.2.6 Fourier Transform Infrared Spectroscopy (FTIR)	134
5.2.7 Raman spectroscopy	134
5.2.8 X-ray diffraction	134
5.2.9 EFV loading capacity.....	135
5.2.10 In-vitro EFV release	135
5.2.11 Comparison of release profiles.....	136
5.2.12 Stability	137
5.2.12.1 Phase separation.....	137
5.2.12.2 Heat cool cycles.....	137
5.3 Results and discussion	137
5.3.1 Statistical design and analysis.....	137
5.3.1.1 Droplet size	146
5.3.1.2 Polydispersity Index.....	147
5.3.1.3 Zeta Potential	149
5.3.1.4 Statistical optimization	151
5.4.2 Characterization and in vitro assessment of optimized nano-emulsions	153
5.4.2.1 EFV loading.....	153
5.4.2.2 Droplet size and PDI.....	154
5.4.2.3 Zeta Potential (ZP).....	155
5.4.2.4 Transmission electron microscopy	155
5.4.2.5 Raman spectroscopy	157
5.4.2.6 X-ray diffraction	158
5.4.2.7 In vitro EFV release.....	159
5.4.2.8 Stability studies	160
5.5 Conclusions	162
CHAPTER SIX	164
CONCLUSIONS	164
References.....	167

LIST OF TABLES

Chapter 1

<i>Table 1.1 Antiretroviral drugs on the 22nd WHO essential medicines list and their BCS classification</i>	17
<i>Table 1.2 Drugs that are contraindicated with EFV.</i>	23

Chapter 2

<i>Table 2.1 Commercially available approved LBDDS products</i>	30
<i>Table 2.2 Differences between micro and nanoemulsions</i>	32
<i>Table 2.3 Some commonly used compounds and associated HLB values</i>	38

Chapter 3

<i>Table 3.1 Modes of HPLC, their common stationary phase material and applications in analysis characterization of stationary phases</i>	53
<i>Table 3.2 Commonly used HPLC solvents with relevant properties</i>	60
<i>Table 3.3 Results of internal standard suitability selection studies</i>	61
<i>Table 3.4 Published methods of HPLC quantitation of efavirenz</i>	62
<i>Table 3.5 Central Composite Design for two factors, two-level full factorial design matrix (2²) with two input factors (X1, X2)</i>	67
<i>Table 3.6 Central Composite Design for three factors, two-level full factorial design matrix (2³) with three input factors (X1, X2 and X3)</i>	67
<i>Table 3.7 Design constraints for three percent organic phase, pH and temperature and associated levels with actual responses for minimum and maximum values obtained</i>	69
<i>Table 3.8 Experimental conditions for the CCD with actual design values used and observed responses</i>	70
<i>Table 3.9 Fit Summary for retention time, transformed inverse Sqrt Constant: -0.5</i>	72
<i>Table 3.10 ANOVA data for retention time quadratic model, transformed sqrt, constant = -0.5</i>	75
<i>Table 3.11 Fitting statistics for peak tailing</i>	79
<i>Table 3.12 ANOVA data for peak tailing factor for a mean model</i>	79
<i>Table 3.13 Fitting statistics for the quadratic model for peak resolution</i>	80
<i>Table 3.14 ANOVA quadratic model for peak resolution power transformed with lambda 2.03</i>	82
<i>Table 3.15. Constraints for the optimization of the separation</i>	84
<i>Table 3.16. Intra-day precision data for analysis of EFV.</i>	88
<i>Table 3.17. Inter-day precision data for EFV</i>	89
<i>Table 3.18. Accuracy results for RP-HPLC analysis of EFV (n=3)</i>	89
<i>Table 3.19 LOQ data for HPLC analysis of EFV</i>	90
<i>Table 3.20. Assay data of efavirenz containing tablets</i>	93

Chapter 4

<i>Table 4.1 Typical composition of some common vegetable oils, * = < 2 % Adapted from</i>	98
<i>Table 4.2 Titration chart for each dilution line to generate data to plot phase diagrams with proportions of each component in the nano-emulsion along dilution line 9.</i>	105
<i>Table 4.3 Saturation solubility of EFV in vegetable oils.</i>	108

Table 4.4 Observed and reported FTIR signals for EFV	113
Table 4.5 Theoretical (reported) and experimental vibrational wavenumbers for Raman spectrum of EFV	118

Chapter 5

Table 5.1 Published methods for in-vitro EFV release testing	135
Table 5.2 Input variable constraints for D-optimal design.....	138
Table 5.3 Surfactant mixture composition for the D-optimal design and actual experimental responses for 10 % m/m flaxseed oil nano-emulsions.	138
Table 5.4 PRESS statistic values for each applied and Sum of squares for all models applied to the data.	139
Table 5.5 Constraints used for identifying the optimized composition.	151
Table 5.6 Solutions for specified optimization criteria.....	151
Table 5.7 Compositions of surfactant mixtures used for the manufacture and characterization of 10 % w/w EFV loaded flaxseed nano-emulsions.....	153
Table 5.8 CQA results of formulations assessed after various stability conditions.....	161

Appendix 1

Table 7.1 Solutions produced by CCD optimization criteria in section 3.5.2 to produce the selected conditions solution 3.	209
Table 7.2 Table of results obtained for producing the calibration curve using the optimized HPLC conditions.....	209

LIST OF FIGURES

Chapter 1

Figure 1.1 Chemical structure of EFV.....	17
Figure 1.2 Synthesis of EFV through the asymmetric addition of zinc-cyclopropylacetylde to amino ketone.	21

Chapter 2

Figure 2.4. Winsor type of emulsion.	32
Figure 2.5. Schematic representation of the preferential orientation of surfactants between bipolar phases (A) (water and surfactant system) and (B) (oil and water system, self-association of surfactants to form micelles (C) (o/w) system and (D) (w/o) system.	34
Figure 2.6. Schematic representation of a micelle formed using a surfactant and co-surfactant in an o/w system.	35
Figure 2.7. Schematic of a typical phase diagram depicting the regions in which different types of emulsions from.	39
Figure 2.8. Visual representation of emulsion coalescence and flocculation redrawn from.	47
Figure 2.9. Visual representation of sedimentation, creaming and phase separation of emulsions. ...	48

Chapter 3

Figure 3.1. Schematic representation of (A) Gaussian or symmetrical peak shape and (B) Asymmetrical chromatographic peak.	57
Figure 3.2. Typical chromatogram for the separation of EFV 250 µg/mL and LRT 100 µg/mL using the optimized conditions	62

Figure 3.3 A 'Black Box' Process Model Schematic, with k = number of factors, r = number of output responses.....	64
Figure 3.4. Box-Cox plot for the non-transformed quadratic model for retention time.	73
Figure 3.5. Box-Cox plot for the inverse square root transformed quadratic model for retention time.	74
Figure 3.6. Plot of residual versus predicted and externally studentized residuals for the transformed quadratic model for retention time.	75
Figure 3.7. Effect of % ACN on retention time at pH 4.5 and 37.5° C.....	77
Figure 3.8. 3D surface response plot for peak retention time.....	78
Figure 3.9. Box-Cox diagnostic plot for peak resolution quadratic model (non-transformed).....	80
Figure 3.10. Box-Cox diagnostic plot for peak resolution quadratic model (power transformed).	81
Figure 3.11. Diagnostics normal plot of residuals for peak resolution quadratic model (transformed).	81
Figure 3.12. 3D Response surface plot showing the effect of % ACN and column temperature with a buffer of pH 4.5 on peak resolution.....	83
Figure 3.13. Chromatogram for the separation of EFV 250 µg/mL and LRT 150 µg/mL.....	85
Figure 3.14. Overlay plot of the desirable area (yellow) derived using the specified optimization criteria listed in Table 3.14.....	86
Figure 3.15. Typical calibration curve obtained by the chosen optimized HPLC conditions.	87

Chapter 4

Figure 4.1. Schematic representation of the structure of stearic acid triglyceride, saturated hydrocarbon chain with zero (0) double bonds.	99
Figure 4.2. Schematic representation of the structure of oleic acid triglyceride, mono-unsaturated hydrocarbon chain with one (1) double bond.....	100
Figure 4.3. Schematic representation of the structure of the linoleic acid triglyceride, poly-unsaturated hydrocarbon chain with two (2) double bonds.	100
Figure 4.4. Schematic representation of the structure of linolenic acid triglyceride, poly-unsaturated hydrocarbon chain with three (3) double bonds.....	101
Figure 4.5. Pseudo-ternary phase diagram and dilution line (in red points) used to plot diagrams, points in red represent P1 to P20 along dilution line 9 beginning from 10 % flaxseed oil using Table 4. 2.104	
Figure 4.6. Scanned image investigation of turbidity and transparency for phase identification studies and critical quality attributes (CQA) droplet size (DS), polydispersity index (PDI) and Zeta Potential (ZP).	110
Figure 4.7. Pseudo-ternary phase diagram of flaxseed oil with surfactant mixture S1 in which a (0.5: 1: 1 m/m ratio of ethanol: Tween [®] 80: Span [®] 20 is used.....	110
Figure 4.8. Pseudo-ternary phase diagram of flaxseed oil with surfactant mixture S2 in which a (1: 1: 1 m/m of Ethanol: Tween [®] 80: Span [®] 20).....	111
Figure 4.9. Pseudo-ternary phase diagram of flaxseed oil with surfactant mixture S3 in which a (1.5: 1: 1 m/m of Ethanol: Tween [®] 80: Span [®] 20).	112
Figure 4.10. FTIR spectrum of EFV.	112
Figure 4.11. FTIR spectrum a of 1:1 m/m mixture of EFV and flaxseed oil.....	114
Figure 4.12. FTIR spectrum of 1:1 m/m mixture of EFV and soybean oil.....	114
Figure 4.13. FTIR spectrum a of 1:1 m/m mixture of EFV and macadamia oil.	115
Figure 4.14. FTIR spectrum of 1:1 m/m mixture of EFV and Span [®] 20.	116
Figure 4.15. FTIR spectrum of a 1:1 m/m mixture of EFV and Tween [®] 80.	116
Figure 4.16. FTIR spectrum of a 1:1 m/m mixture of EFV and a ternary emulsion mixture (1:1:1 m/m of Tween [®] 80, Span [®] 20 and ethanol).	117
Figure 4.17. Raman spectrum for pure EFV.....	118
Figure 4.18. Raman spectrum of a 1:1 m/m mixture EFV and flaxseed oil.....	119
Figure 4.19. Raman spectrum of a 1:1 m/m mixture of EFV and Span [®] 20.....	120
Figure 4.20. Raman spectrum of a 1:1 m/m mixture of EFV efavirenz and Tween [®] 80.....	120
Figure 4.21. Raman spectrum of 1:1 m/m mixture of EFV and components of a ternary emulsion mixture i.e. 1:1:1 m/m of Tween [®] 80, Span [®] 20 and ethanol.....	121

Figure 4.22. XRD pattern of pure EFV.....	121
Figure 4.23. XRD pattern of 1:1 m/m mixture of EFV and flaxseed oil.	122
Figure 4.24. XRD pattern of 1:1 m/m mixture of EFV Tween [®] 80.	122
Figure 4.25. XRD pattern of 1:1 m/m mixture of EFV Span [®] 20.....	123
Figure 4.26. XRD pattern of 1:1 m/m mixture of EFV and ternary mixture of excipients (1:1:1 m/m of Tween [®] 80, Span [®] 20 and ethanol).....	123

Chapter 5

Figure 5.1. Schematic representation of standard simple linear and simplex lattice designs.....	129
Figure 5.2. Phase diagram for screening for emulsion regions.	130
Figure 5.3. Real contour plot of the simplex lattice design applied to surfactant mixture optimization	132
Figure 5.4. Diagnostic Box-Cox plot non-transformed for the special quartic model for droplet size	141
Figure 5.5. Diagnostic Box-Cox plot for non-transformed for the special quartic model for PDI	141
Figure 5.6. Diagnostic Box-Cox plot for non-transformed for the linear model for ZP.	142
Figure 5.7. Normal plot of residuals for the special quartic model for droplet size.	143
Figure 5.8. Residuals vs predicted plot for the special quartic model for droplet size.	143
Figure 5.9. Normal plot of residuals for the special quartic model for PDI.	144
Figure 5.10. Predicted vs actual diagnostic plot for the special quartic model for PDI.....	144
Figure 5.11. Normal plot of residuals for the linear model for ZP.	145
Figure 5.12. Predicted vs actual diagnostic plot for the linear for ZP.....	145
Figure 5.13. Contour plot depicting the impact of surfactant mixture content on droplet size.....	146
Figure 5.14. Contour plot depicting the impact of surfactant mixture content on PDI.....	148
Figure 5.15. Contour plot depicting the impact of surfactant mixture composition on ZP.....	150
Figure 5.16. Overlay plot of the desirable area (yellow) derived using the specified criteria listed in	154
Figure 5.17. Droplet size distribution for batches F1 - F5.....	154
Figure 5.18 Transmission electron micrograph of nano-emulsion F5.	156
Figure 5.20. FTIR spectrum of EFV loaded nano-emulsions.	157
Figure 5.21. Raman spectrum of EFV loaded nano-emulsion F1.	158
Figure 5.22. XRD signal of pure EFV loaded nano-emulsion F1-F5.....	158
Figure 5.23. Mean \pm SD (n = 3) dissolution profiles for batches F1, F2, F3, F4 and F5 and EFV powder.	159

Appendix 3

Figure 7.1. Diagnostic Normal plot of residuals for the inverse transformed quadratic model for retention time.	207
Figure 7.2. Diagnostic Box-Cox plot for peak tailing mean model.	207
Figure 7.3. Diagnostic normal plot of residuals for peak tailing mean model.....	208
Figure 7.4. Diagnostic plot of residual versus predicted and externally studentized residuals for the transformed quadratic model for peak resolution.	208
Figure 7.5. FTIR Spectra of 1:1 m/m mixtures of EFV and grapeseed oil.	214
Figure 7.6. FTIR Spectra of 1:1 m/m mixtures of EFV and olive oil.....	214
Figure 7.7. FTIR Spectra of 1:1 m/m mixtures of EFV and sunflower oil.....	215
Figure 7.8. 3D Response surface showing the effect of the concentration of Span [®] 20, Tween [®] and Ethanol on droplet size.	216
Figure 7.9. 3D response surface plot for PDI showing the effect of surfactant concentrations.....	217
Figure 7.10 3D Response surface plot for Zeta potential.....	218
Figure 7.11. Transmission electron image of formulation emulsion F4.....	219
Figure 7.12. Transmission electron image of formulation nano-emulsion F2.	220
Figure 7.13. Transmission electron image of formulation nano-emulsion F3.	220

CHAPTER 1

EFAVIRENZ AND ANTIRETROVIRAL THERAPY

1.1 Introduction

Approximately 25.4 million people were accessing antiretroviral therapy in 2019, with at least 31.6 million people globally living with the human immunodeficiency virus (HIV) in the same year [1]. HIV continues to be a major global public health issue, having claimed almost 33 million lives so far according to the World Health Organization (WHO) with the regions most affected being Sub-Saharan Africa including South Africa [2]. South Africa has the largest population of people living with HIV in the world with an estimated 7.1 million people with HIV and the country has the world's largest Antiretroviral Therapy (ART) program [3]. As a response to this disease burden, concerted efforts by the country and the international community at large has resulted in an increase of access to health services and essential medicines used for ART. Approximately 90% of people living with HIV were aware of their status in 2018 in South Africa, in 2019, 68% of adults and 53% of children living with HIV globally were receiving ART [4]. Despite improvements on access to essential medicines, African healthcare systems continue to face severe challenges which negatively impact access to affordable quality healthcare leading to morbidity and mortality from easily treated conditions. The challenges include a high infectious disease burden, a growing burden due to chronic disease, a shortage of human resources and infrastructure to deliver healthcare services in addition to significant funding and budgetary constraints amongst others [5,6]. In efforts to improve access to HIV drugs, simplification of process chemistry, reformulation, dose reduction, inclusion of new drug classes and new therapeutic strategies have been developed and used as tools to contribute to the reduction of the HIV burden [7].

HIV belongs to a class of viruses called retroviruses and a subgroup of retroviruses known as lentiviruses with the course of infection with such viruses characterized by a long interval between initial infection and the onset of serious symptoms [8]. There are two types of HIV, HIV-1 and HIV-2, and both can cause acquired immune deficiency syndrome (AIDS) however most AIDS infections are due to HIV-1 strains, while HIV-2 represents a significant minority of all HIV infections in some countries, such as Guinea-Bissau and Portugal [9].

HIV can replicate only inside cells using the enzyme reverse transcriptase to convert their ribonucleic acid (RNA) into deoxyribonucleic acid (DNA), which can be incorporated into the human cell's genes through integration between viral DNA and human DNA and results in the replication of the virus [10]. Upon transmission to a new host, HIV targets CD4⁺ effector memory T cells, resulting in acute, massive depletion of these cells from mucosal effector sites and over time, HIV weakens an individual's immune system and the patient becomes at risk to opportunistic infections and AIDS [11,12]. CD4⁺ cells play a major role in mediating immune response through the secretion of specific cytokines and a higher count measured in cells per cubic milliliters of blood provides a picture of the immune system health, with higher CD4⁺ counts typically signifying healthier immune systems [13,14]. Since CD4⁺ lymphocytes are a primary target of HIV, CD4⁺ counts are therefore one of the factors used to measure disease progression in HIV-positive individuals [15]. CD4⁺ effector memory T cell counts vary in uninfected individuals and across populations due to a variety of demographic, environmental, immunological and genetic factors that probably persist throughout however, in HIV infected individuals initiation of ART is recommended at CD4⁺ cell counts <400 cells/ μ L [16,17].

1.1.1 Antiretroviral therapy

ART is a treatment regimen typically comprised of a combination of antiretroviral drugs for the treatment of HIV. The goals of ART are to provide maximum and long term suppression of the viral load, restore and preserve immune function, reduce HIV-related infectious and non-infectious morbidity, prevent onward transmission of HIV, prolong life expectancy and improve quality of life [18]. With prolonged viral suppression, the CD4⁺ lymphocyte count usually increases, which is accompanied by a restoration of pathogen-specific immune function. For most patients, this results in a dramatic reduction in the risk of HIV-associated morbidity and mortality. For patients who start ART with preserved CD4⁺ counts, ART can prevent the decline in CD4⁺ count which has been observed in untreated patients and prevent clinical complications of HIV infection. Long-term cohorts show that patients who adhere well to ART have a near-normal life expectancy [19,20].

There are seven classes of antiretroviral agents currently in use and the classes are, nucleoside reverse transcriptase inhibitors (NRTI), non-nucleoside reverse transcriptase inhibitors (NNRTI), protease inhibitors (PI), fusion inhibitors, integrase strand transfer inhibitors (INSTIs), post-attachment inhibitors and CCR5 inhibitors [21,22].

International HIV treatment guidelines recommend first-line use of a combination of three drugs usually two NRTIs with an NNRTI, a boosted PI or an integrase inhibitor in order to achieve sufficient HIV RNA suppression with unique patient circumstances e.g., concomitant diseases and conditions, potential for pregnancy, cost guiding the treatment choice [23]. ART co-administration of different drugs inhibits viral replication by several mechanisms so that propagation of a virus with resistance to a single agent becomes inhibited by the action of the other two agents [24]. CD4+ cell count, HIV RNA level, genotype, and other laboratory tests for general health and co-infections are recommended at specified points before and during ART [25]. In April 2013, South Africa began initiating eligible first-line patients on a once-daily, single-tablet fixed dose combination (FDC) regimen of tenofovir (TDF), emtricitabine (FTC) and efavirenz (EFV) [26]. TDF and FTC are NRTIs with especially TDF becoming an integral part of several ARV drug regimens [27]. Currently, there are a number of NNRTIs approved for use in HIV treatment, with EFV being one of the most commonly prescribed drug [28].

1.1.2 Biopharmaceutical Classification System (BCS)

With a large number of candidates of active compounds from diverse sources, the classification of active compounds and understanding their biopharmaceutical behavior in classes can be a useful approach for accelerated drug development activities. The biopharmaceutical classification system (BCS) has become an increasingly important tool for regulation of drug products world-wide since its inception in 1995 [29]. The BCS is a prognostic tool for assessing the potential effects of formulation on the human drug oral bioavailability used in conjunction with in vitro dissolution tests, the BCS can support the prediction of in vivo product performance and the development of mechanistic models that support formulation assessments. [30]. Identification and classification of API may provide insight into a formulation strategy, Table 1.1 shows the classification of antiretroviral compounds on the 22nd and latest WHO essential medicines list [31]. Atazanavir is highly permeable but poorly soluble in aqueous media and is thus BCS II [32]. Ritonavir is a BCS IV compound with low solubility and low permeability [33]. Ideal oral dosage forms should produce both a reasonably high bioavailability and low inter and intra subject variability in absorption therefore BCS II compounds may be better suited in formulations that increase solubility and BCS IV compounds may be better suited for formulation strategies that increase both solubility and provide permeability enhancement [34].

Table 1.1 Antiretroviral drugs on the 22nd WHO essential medicines list and their BCS classification [35–37].

Class I	Class II
High solubility and high permeability e.g. Emtricitabine,	Low solubility and high permeability e.g. Efavirenz, Atazanavir, Duranavir, Raltegravir, Nevirapine
Class III	Class IV
High solubility and low permeability e.g. Tenofovir,	Low solubility, low permeability e.g. Etravirine, Ritonavir, Lopinavir

1.2 Physicochemical properties of EFV

1.2.1 Nomenclature and structure

Efavirenz, chemically 2H-3, 1-benzoxazin-2-one, 6-chloro - 4- (cyclopropylethynyl) -1, 4-dihydro-4-(tri-fluoromethyl)-(4S) and is a white crystalline no hygroscopic powder [38]. The chemical structure of EFV is depicted in Figure 1.1 and the molecular formula of EFV is C₁₄H₉ClF₃NO₂ [39].

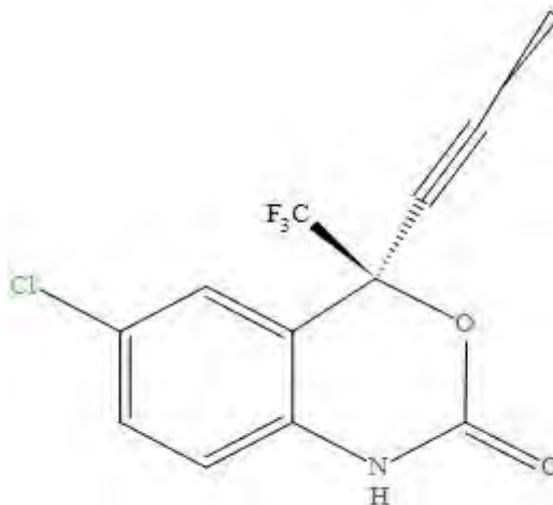


Figure 1.1 Chemical structure of EFV

1.2.2 Solubility

Efavirenz is practically insoluble in water having a solubility of approximately 0.01 mg/ml [40]. This drug is classified as a BCS II with high permeability and low solubility. The poor

aqueous solubility and wettability of EFV gives rise to difficulties in pharmaceutical formulations for oral delivery, which may lead to a low bio-availability currently reported to be 40 % [41].

1.2.3 Dissociation constant (pKa)

The acid-base dissociation constant (pKa) of a drug is a key physicochemical parameter influencing various biopharmaceutical characteristics such as the ionization state of the API which is controlled by both solution pH and therefore exists in different states in different pH environments [42]. These different ionization states cationic, anionic or neutral often have different properties with respect to water solubility, UV absorption, and reactivity. The ionized form is usually more water soluble, while the neutral form is more lipophilic and has higher membrane permeability [43]. Efavirenz pKa value is 10.2 and is a weakly acidic drug and therefore in acidic conditions it is largely unionized and in alkaline environments it is ionized and practically insoluble at physiological pH (7.4), therefore enabling formulations such as SEDDS may influence the solubility and in turn bioavailability of EFV may yield better therapeutic performance [44–46].

1.2.4 Partition coefficient (LogP)

The partition coefficient (Log P) of a compound is a value defined as ratio of unionized drug distributed between aqueous and organic phase or how a solute is distributed between two immiscible solvents [47,48]. The oil and water partition coefficient helps determine the ability of a compound to cross the lipid bilayer membrane [49]. LogP values can be obtained experimentally using Equation 1.1.

$$\text{LogP} = \left(\frac{C_{oil}}{C_{water}} \right)_{equilibrium}$$

Equation 1.1

Where,

C_{oil} = Concentration of compound in oil and

C_{water} = Concentration of compound in water.

A value of Log P of zero indicates that the drug has equal distribution in water and partition solvent while values of Log P less than one indicate higher aqueous solubility and values greater than one are indicative of higher lipid solubility [50]. Due to the hydrophobic nature of the biological membrane, the amount of drug absorbed depends heavily on its lipophilicity [51]. The unionized form of the EFV molecule has greater lipophilicity and hence it has received so much importance and has a logP value of approximately 4.6, Caco-2 and intestinal permeability studies suggest EFV is highly permeable and the clinical efficacy may be limited by low solubility [52–54].

1.2.5 UV absorption spectra

Ultraviolet (UV) visible absorption spectroscopy involves the valence electrons of a molecule and is dependent on the nature and type of chemical bonds in a molecule [55]. The UV spectrum is used to determine API concentrations, characterize chemical reactions and kinetics thereof. UV spectroscopy has been used as detection systems when monitoring chromatographic separations. Identification of the maximum and minimum absorption in a spectrum due to different chromophore functional groups is valuable when selecting a wavelength applicable for detection using HPLC as a mode of analysis [56,57]. EFV has a UV absorption maximum of 246-247 nm and has a chromophore and therefore can be detected and quantified using methods such as UV high pressure liquid chromatography UV-HPLC [58,59].

1.2.6 Melting range

The melting point of EFV is reported to be between 138-141 °C [60]. The melting point range was determined using as Stuart° SMP 30 melting point instrument from Bibby Scientific Limited, Stone, Staffordshire, ST150SA, United Kingdom. The melting point range was observed to be from 137-141 °C for the raw material which is similar to that reported [61].

1.2.7 Polymorphism

Polymorphism is the ability of solid materials to exist in two or more crystalline forms with different arrangements or conformations of the constituents in the crystal lattice [62]. These polymorphic forms of a drug differ in the physicochemical properties such as dissolution and solubility, chemical and physical stability. These forms also differ in various important drug outcomes like drug efficacy, bioavailability, and even toxicity [63]. Polymorphic studies are important as a particular polymorph can be responsible for a particular property which might

not be exhibited by any other form [64]. EFV has more than 23 polymorphs reported in literature, but very little information has been reported on them [65]. It is claimed that Form I is the thermodynamically stable form and has the highest melting point of $\pm 137^{\circ}$ C and exposure to high temperatures convert all other known forms into Form I [66]. Although Form I of EFV may have erratic dissolution behavior, compared to other known forms, it is claimed to be the preferred form in the pharmaceutical industry, due to its thermodynamic stability [67].

1.3 Structure activity relationships

EFV like most NNRTIs has been identified to have high accommodation capacity in the binding pocket of the reverse transcriptase enzyme (RT) which is hydrophobic in nature. When the interactions occur, this leads to conformational changes on the RNA sequence of the reverse transcriptase. These conformation changes, induced by the binding of the NNRTIs to the RT are thought to be at the basis of their inhibitory action against the enzyme [68]. NNRTIs display a common pharmacophoric model, which contains an aromatic ring capable of participate the π - π stacking interactions, amides or thioamides that can form hydrogen bonds and conformation that could be capable to help the drug to maintain its activity against strains of HIV-1 [69]. Most EFV interactions with HIV reverse transcriptase involve hydrophobic contacts and hydrogen bonding is formed between the NH group of the benzoxazin-2-one nucleus and the carbonyl oxygen atom of the main chain of lysine (Lys101) of the reverse transcriptase enzyme, furthermore, there is an interaction between the carbonyl oxygen atom of the main chain of Lys103 and the nitrogen atom of the benzoxazin-2-one ring of EFV [70].

1.4 Synthetic pathway

EFV was first developed in 1992 by Merck in eight linear steps of a medicinal chemistry route with an overall yield of 12% with the starting material as 4-chloro-3-cyanoaniline [71]. Various other methods with less steps and greater yield have been developed for the synthesis of EFV such as the asymmetric synthesis of EFV by an organocatalyzed enantioselective trifluoromethylation of nonfluorinated aryl alkynyl ketone 1-(5-chloro-2-nitrophenyl)-3-cyclopropylprop-2-yn-1-one with Ruppert–Prakash reagent, (trifluoromethyl- trimethylsilane (Me_3SiCF_3) has been reported to yield up to 99 % EFV, however, extra steps to protect then de-protect p-Methoxybenzyl groups which are chemically sensitive and could hinder selectivity in the synthesis process have been sighted as major drawback [72,73]. A second generation asymmetric addition of zinc-cyclopropylacetylide to amino ketone in the presence

of amino alcohol (1R, 2S)-1-Phenyl-2-(1-pyrrolidinyl) propan-1-ol is part of most currently used manufacturing routes with overall process from amino ketone in a two-step process to yield EFV up to 87% reported and quite high purity of the isolated compound, the reaction scheme is shown in Figure 1.2 [74].

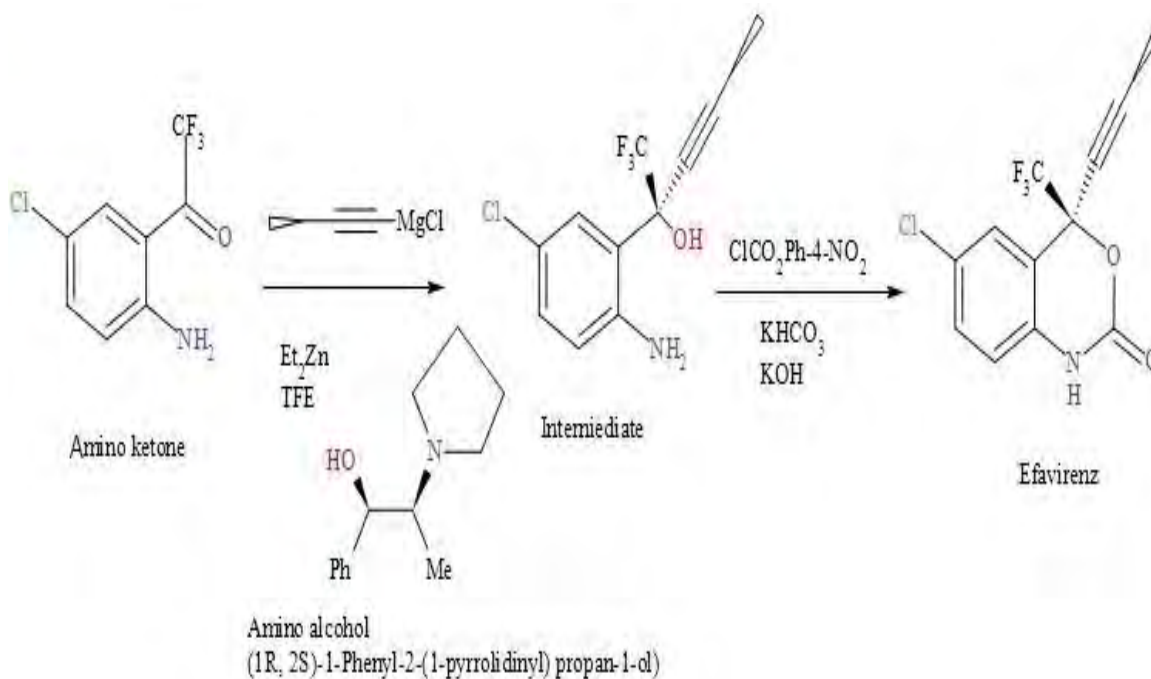


Figure 1.2. Synthesis of EFV through the asymmetric addition of zinc-cyclopropylacetylide to amino ketone [74].

1.5 Clinical pharmacology

1.5.1 Mechanism of action (MOA)

The mechanism of action of EFV is by inhibiting HIV-1 replication directly by binding noncompetitively to HIV-1 reverse transcriptase [75]. EFV has unique specificity for HIV-1 and is not active against other viruses [76]. The drug binds to a hydrophobic region of the HIV-1 reverse transcriptase through an allosteric mechanism that alters the enzyme conformation and prevents access to the substrates and prevents or slows down the process of reverse transcription which is the method the virus uses to translate its RNA onto host cell's DNA for replication [77,78].

1.5.2 Dosage and administration

Efavirenz is available as 600 mg tablets, 50, 100 or 200 mg capsules. Standard adult dosage of efavirenz is 600 mg once daily for those over 40 kg taken when fasting, preferably at bedtime. Pediatric dosing for children 3 months of age and older is weight based with target dose of 15 mg/kg/day once daily recommended by the WHO [79,80]. For geriatrics, with aging, hepatic and kidney function typically decline, suspected in part due to loss of functional tissue of these organs as a result of aging resulting in altered metabolism [81]. As a result, older patients will often have increased drug exposure and consequently increased adverse effects. The therapeutic window between an effective drug level and a toxic level for many drugs is often reduced in the older population owing to increased drug sensitivity associated with aging, which further heightens the need to monitor for toxicity and adverse effects in this patient population [82].

1.5.3 Overdose

The overdose of EFV is reported in various case reports with a reported greatest amount of 3 grams ingested at once and some prominent effects reported were aggravated depression, apathy, emotional lability, euphoria, burning sensation in the throat immediately after ingestion, visual impairment and motor deficits in lower limbs [83,84]. In general overdose effects of EFV are its severe already known side effects [85].

1.5.4 Contraindications and drug interactions

The use of efavirenz is contraindicated in patients with previously documented hypersensitivity to EFV and patients with a history of mental illness and those concurrently receiving co-administered drugs that are cytochrome P450 (CYP) 3A4 substrates due to a (CYP) 3A4 interaction which is the most abundant hepatic and intestinal phase I enzyme that metabolizes approximately 50% of marketed drugs [86–89]. EFV is therefore contraindicated with several drugs although the mechanism of the apparent increase in (CYP) 3A4 activity by efavirenz and the magnitude of change relative to other known inducers are not known [90,91]. This interaction results in the increased systemic clearance of contraindicated and co-administered drugs that are cytochrome P450 (CYP) 3A4 substrates [91,92]. EFV may also substantially slow the elimination of drugs predominately cleared by (CYP) 2B6, (CYP) 2C19 or by both enzymes and may also lower the area under the plasma concentration time curve (AUC) of

active metabolites of some pro-drugs such as clopidogrel and proguanil by up to 30% [93–95]. Commonly contraindicated drugs with EFV are listed in Table 1.2.

Table 1.2. Drugs that are contraindicated with EFV [96,97].

Drug class	Examples of drugs within class contraindicated with EFV	Clinical comment
Benzodiazepines	midazolam, triazolam	Potential for serious or life-threatening reactions such as prolonged or increased sedation or respiratory depression.
GI Motility Agents	cisapride	Potential for serious or life-threatening reactions such as cardiac arrhythmias.
Anti-Migraine	ergot derivatives (dihydroergotamine, ergonovine, ergotamine)	Potential for serious or life-threatening reactions such as acute ergot toxicity characterized by peripheral vasospasm and ischemia of the extremities and other tissues
Neuroleptic	pimozide	Potential for serious or life-threatening reactions such as cardiac arrhythmias.
Herbal Products	St. John's wort (<i>Hypericum perforatum</i>)	May lead to loss of virologic response and possible resistance to efavirenz or to the class of non-nucleoside reverse transcriptase inhibitors (NNRTIs).

1.5.5 Pregnancy and breastfeeding

The administration of antiretroviral agents during pregnancy and around delivery has been shown to be effective in reducing mother-to-child transmission of HIV, EFV is categorized as a category D drug by the Food and Drug Administration (FDA) with positive evidence of human fetal risk from case reports, nevertheless, potential benefits may outweigh the potential risks [98,99]. However, drugs are commonly assigned high-risk FDA categories based on limited information, evidence of teratogenicity linked to the use of EFV in pregnancy has been limited and current evidence suggests that the risk is lower than previously thought [100,101]. Current WHO guidelines recommend avoiding EFV in the first trimester only, but also note that overall rates of birth defects in infants exposed to EFV, NVP and TDF are similar to those in the general population [101]. The WHO guidelines on antiretroviral therapy recommend that EFV can be included as part of first-line therapy in adults regardless of sex, and that it can be used throughout pregnancy after the first trimester with surveillance warranted, however some reports suggests findings that favored dolutegravir over EFV in ART regimens for pregnant women [102,103].

While the transmission of HIV from mother to child after birth via breast milk remains a major concern in areas of the world where formula feeding is not safe, affordable, or practical, EFV

is widely used during breastfeeding and is excreted into breastmilk and small amounts are found in the serum of some infants and treatment of HIV-positive mothers with EFV does not appear to affect growth and development of their HIV-negative breastfed infants [104–106]. The extension of maternal ART through the period of breast feeding has been proposed as one strategy to reduce breast milk HIV transmission by reducing plasma and breast milk HIV concentrations and/or by providing prophylaxis to the infant through ingestion of antiretrovirals present in breast milk [107]. The extent of antiretroviral transfer from mother to infant via breast milk and the resulting infant antiretroviral drug exposure have not been well delineated however other reports suggest that most breastfed infants are exposed to <10% of the weight-adjusted therapeutic pediatric dose, the safety threshold for exposure to maternal drugs from breast milk [108,109].

1.5.6 Renal impairment

Although the use of EFV has been associated with the development of renal stones, data suggest however that EFV carries a low risk [110,111]. The available limited data on patients with renal impairment suggests that 1% of efavirenz is excreted unchanged in urine therefore, dosage adjustment does not appear necessary due to the demonstrated safety renal profile in controlled trials although instances of case reports linked efavirenz to renal toxicity on the basis of a hypersensitivity reaction involving pneumonitis, hepatitis, and interstitial nephritis to which symptoms recurred after a re-challenge [112].

1.5.7 Hepatic impairment

EFV has been associated with hepatotoxic effects and alterations in lipid and body fat composition, however data is very limited with reports that suggest that the frequency of grade 3-4 transaminase elevations associated with EFV-based ART combinations under clinical practice conditions is low and similar to that found in patients receiving protease inhibitors currently used as substitutes in ART regimens, however, mitochondrial function has been reported to be undermined in vitro by EFV to varied extents depending on concentration in particular, respiration and intracellular adenosine triphosphate (ATP) levels were reduced whereas reactive oxygen species production increased [113,114].

1.5.8 Adverse effects

Despite the widespread use of EFV, patients receiving EFV containing therapy frequently report central nervous system (CNS) disturbances [115]. Symptoms of efavirenz-associated adverse drug reactions occur at a high frequency and can include impaired concentration, anxiety, abnormal dreams, suicidal ideation, hallucinations, nausea, and vomiting [116,117]. The majority of patients report symptoms which typically arise in the first few days of treatment and decline within a few weeks of continued therapy with a minority of patients continuing to experience symptoms for the duration of efavirenz use [118]. As with other NNRTIs, efavirenz can also cause rash and hepatotoxicity [119]. In addition to the negative impact on the quality of the patient's life, EFV side effects may also lead to a decrease in patient adherence and most clinicians tend to avoid efavirenz in patients with a psychiatric history [120,121]. EFV is effective as a once-a-day dose and reaches therapeutic levels in the CNS and may potentially be used to manage HIV in the CNS, however, EFV levels in the CNS are generally high due to dose-dumping that is associated with the use of conventional dosage forms and can lead to severe psychiatric side effects [122].

1.5.9 Resistance

Despite high levels of treatment success, resistance to efavirenz can develop. EFV as most NNRTIs are prone to rapid development of resistance stemming from mutations in the drug-binding pocket of the enzyme [28]. EFV resistance mutations development have been reported in some clinical reports finding 6%-8% of patients treated with efavirenz plus two NRTIs for 2-3 years developed resistance which suggest a high risk of resistance of EFV [123]. Emulsion based combinatorial nano-formulations explored to overcome the drawbacks of EFV have also been reported to overcome the problem of drug resistance owing to their ability to provide controlled release profile and targeted drug delivery which augments bioavailability, therapeutic efficacy and reduce the side effects of the EFV through convenience of dosing and improving patient adherence to antiretroviral medication which is a major concern, in particular for drugs displaying a low genetic barrier to resistance [124].

1.6 Clinical pharmacokinetics

1.6.1 Absorption

EFV exhibits a relatively low intra-individual variability of pharmacokinetics although some reports find high inter-individual variability but a dosing regimen of 600 mg a day for adults assures plasma concentrations that are adequate for inhibition of viral replication [118,125]. EFV is readily absorbed and achieves peak serum concentration (C_{\max}) of in approximately 3 to 5 hours following a 600 mg standard adult oral dose with increases in C_{\max} and area under the plasma concentration-time curve (AUC) have been reported to be dose proportional for 200, 400, and 600 mg EFV doses except proportional for a 1,600 mg EFV dose, suggesting reduced absorption at higher doses [126]. EFV has a long serum half-life of 45 hours and reaches steady-state plasma concentrations in 6 to 10 days. The bioavailability of EFV is increased by a high-fat/high-caloric meal when compared to fasting [127].

1.6.2 Distribution

EFV is widely distributed into the liver, brain, and heart following administration. Additionally, hydroxylated EFV, which is a cytochrome P450-dependent mono-oxygenated metabolite of EFV, has been detected in the liver, brain, spleen, and heart tissue [128]. An oral volume of distribution of 252 L has been reported at an absorption rate constant of 0.3 per hour meaning the drug has a propensity to leave the plasma and enter the extravascular compartments of the body, therefore, a high dose of the drug is required to achieve a given plasma concentration [129,130]. The drug is highly protein bound up to 99%, predominantly to albumin, and has a low CNS to plasma ratio for total drug and food increases the systemic exposure to EFV, however, higher exposure results in higher rates of adverse events and efavirenz may be taken when fasting to reduce the dose dumping effect [79].

1.6.3 Metabolism (metabolic pathway)

Efavirenz (EFV) is principally metabolized by (CYP) 2B6 to 8-hydroxy-efavirenz (8OH-EFV) and to a lesser extent by (CYP) 2A6 to 7-hydroxy-efavirenz (7OH-EFV) up to 23% of overall EFV metabolism [93,131]. EFV-N-glucuronide has also been reported in other literature even though it represents a minor percentage of EFV metabolites present in vivo [132]. The (CYP) 2B6 is also the major enzyme involved in formation of the secondary metabolite 14-dihydroxy-EFV [133,134].

1.6.4 Elimination

About 16-61% of EFV is eliminated in the feces primarily as parent drug and 14-34% in the urine primarily as metabolites [79,94]. The predominant mode of EFV excretion is as glucuronides due to the (UGT) 2B7 enzyme in the urine, with 8-hydroxy-EFV-N-glucuronide as the major metabolite found [135]. The formation rate of EFV-N-glucuronide shows large variability between human microsomal samples, whereas formation of 7-hydroxy-EFV-G, 8-hydroxy-EFV-G and 8, 14-hydroxy-EFV-G does not [131].

1.7 Conclusions

The great need for improved access to medicines for effective ART especially those on the essential drug list of the WHO remains a focus for sub-Saharan Africa. Recommended ART regimens for first-line use are a combination of three drugs usually two NRTIs with an NNRTI with EFV being the most prescribed NNRTI and included in the FDC combination with tenofovir and emtricitabine. Efavirenz is available as 600 mg tablets, 50, 100 or 200 mg capsules and is part of the 22nd and latest WHO essential medicines list.

EFV is an NNRTI which is practically insoluble in water having a solubility of approximately 0.01 mg/ml other physicochemical properties of EFV such as the logP reveal that it is highly lipophilic with a log P = 4.6. It is weakly basic and readily dissolves in non-polar and/or aprotic organic solvents and has distribution across cellular membranes which is favorable however the rate limiting step is dissolution necessitating biopharmaceutical modification of the molecule within its dosage form. EFV is effective as a once-a-day dose and reaches therapeutic levels in the CNS and may potentially be used to manage HIV in the CNS, however, EFV levels in the CNS are generally high due to dose-dumping that is associated with the use of conventional dosage forms and can lead to severe psychiatric side effects, therefore more enhanced drug delivery strategies may enhance the therapeutic effect of EFV or reduce side effects.

EFV is contraindicated with several drugs particularly those that are cytochrome P450 (CYP) 3A4 substrates therefore the prescription of EFV must be done with the complete knowledge of the patient history and any co-administered drugs. EFV widely used during breastfeeding and is excreted into breastmilk, however the risk to breastfeeding infants is relatively low. Although EFV has been associated with the development of renal stones, clinical data reveals that the risk is very low as only 1% of efavirenz is excreted unchanged in urine therefore,

dosage adjustment does not appear necessary due to the demonstrated safety renal profile in controlled trials. The frequency of grade 3-4 transaminase elevations associated with EFV-based ART combinations under clinical practice conditions is also reported to be very low despite case reports with positive association.

Based on the physicochemical properties, BCS class, clinical pharmacology, and clinical pharmacokinetics of EFV, a nano-lipid-based formulation approach in the form of self-emulsifying drug delivery systems (SEDDS) will be investigated to increase the surface area available for aqueous dissolution of EFV. The lipid-based formulation could facilitate API availability through self-emulsification as droplets that may be manipulated for droplet sizes with an ability to penetrate intracellular membranes from the systemic circulation or via the lymphatic system distributions that provide sufficient viral suppression in all tissues with minimum side effects. This approach may ensure a consistent temporal profile with reduced frequency of dosing and dose levels which is of particular importance for the use of combination formulations of ART to promote adherence and patient outcomes. Furthermore, reduced frequency of dosing may play role in mitigating for the shortcoming of a low genetic barrier to resistance of EFV.

CHAPTER 2

MICRO-, NANOEMULSIONS AND SELF EMULSIFYING DRUG DELIVERY SYSTEMS (SEDDS).

2.1 Introduction

Over 30% of commercially available drugs and 90% of the molecules in the discovery pipeline exhibit poor aqueous solubility presenting pharmaceutical and formulation scientists with challenges when developing effective formulations for such API [136–138]. The rate and extent of absorption of API that exhibit poor aqueous solubility is largely dependent on the rate of dissolution particularly if conventional solid oral dosage forms which must disintegrate and dissolve in the gastrointestinal tract before absorption is possible [139]. The formulation approach plays an important role in overcoming the shortcomings of API that exhibit poor aqueous solubility [140]. Lipid-based drug delivery systems (LBDDS) which are self-micro emulsifying drug delivery systems (SMEDDS) and self-nano emulsifying drug delivery systems (SNEDDS) have recently been the focus as an approach for overcoming the poor solubility and oral bioavailability of API particularly those classified as BCS II and IV compounds [141–143]. LBDDS deliver an API dissolved in a mixture of one or more excipients which may include mono, di and tri-glycerides, lipophilic and hydrophilic surfactants and or co-surfactant/s [144–146]. When an API is administered via the oral route using lipid formulations, it remains in a dissolved state throughout transit along the gastrointestinal tract (GIT) and absorption of the compound may be enhanced as dissolution step prior to absorption is avoided [147]. LBDDS in which nano-size droplets occur may lead to an increase in AUC or drug exposure by increasing the gastric residence time through mucosal adhesion or by increasing cell or tissue entry [148–150].

Among the many classes and types of LBDDS reported, micro- and nano-emulsions comprised of water, oil and surfactant are some of the simplest forms of LBDDS. Their inherent stability, ease of manufacture and suitability for different applications has attracted attention in a variety of fields and industries including the nutraceutical, colouring and flavouring, antimicrobial, cosmetic and drug delivery industries [151,152]. Micro- and nano-emulsion drug delivery systems enhance intestinal lymphatic transport of API and may circumvent the hepatic first pass effect. Mechanisms of transport include increasing membrane fluidity thereby facilitating transcellular absorption and inhibition of cytochrome P450 (CYP) 450 enzymes increasing

intracellular concentrations and residence time by surfactants [153]. Due to their unique performance and interest in drug delivery strategies, a number of LBDDS drug formulations have been approved for the commercial market. Table 2.1 contains a list of commercial products approved by regulatory authorities and their listed excipients.

Table 2.1 Commercially available approved LBDDS products [154,155].

Product / compound	Dosage form	Oils	Water insoluble surfactants	Water soluble surfactants	Hydrophilic co-solvents
Norvir®/ Ritanovir USA and Europe	Soft gelatine capsules		Oleic acid	Polyoxyl 35, castor oil	Ethanol
Prometrium® / Progesterone USA	Soft gelatine capsules	Peanut oil			
Neoral® / Cyclosporin A USA	Soft gelatine capsules	Corn oil mono-triglycerides		Polyoxyl 40, hydrogenated castor oil	Ethanol 11.9%, glycerol, propylene glycol
Gengraf® / Cyclosporin A USA	Oral solution			Polyoxyl 40, hydrogenated castor oil, Polysorbate 80	Propylene glycol
Sandimmune® / Cyclosporin A USA	Oral solution	Olive oil		Polyoxyethylated oleic glycerides	Ethanol 12.5%
Rapamune® / Sirolimus USA and Europe	Oral solution	Phosphatidylcholine, mono- and di-glycerides, soy fatty acids, ascorbyl palmitate		Polysorbate 80	1.5–2.5% ethanol, propylene glycol

2.1.2 Micro- and nano-emulsions

Micro- and nano-emulsions may exist as oil in water (o/w) or water in oil (w/o) emulsions depending on the continuous and dispersed phases in dynamic equilibrium and may differ in respect of droplet size, shape and morphology [156]. Schematic representation of an o/w emulsion in which oil droplets are dispersed in an aqueous phase or a w/o emulsion in which water droplets are dispersed in an oil phase are depicted in Figures 2.1 (A) and 2.1 (B) respectively.

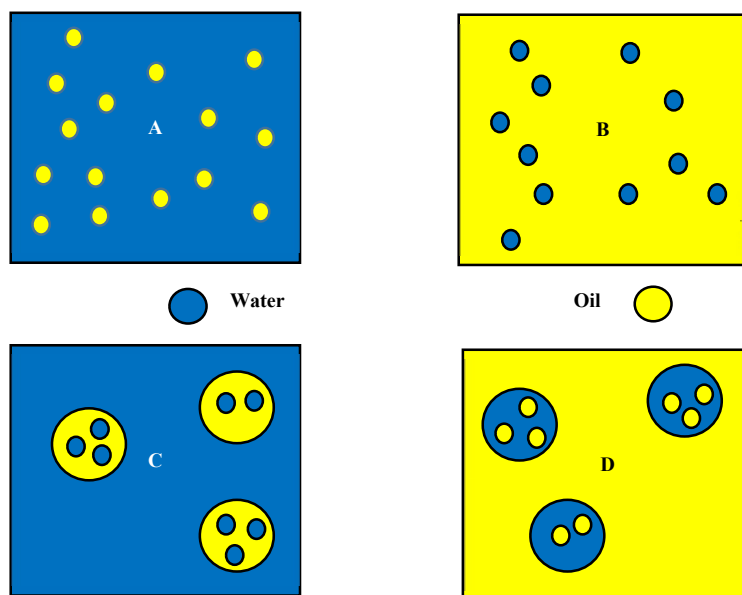


Figure 2.1. Visual representation of (A) oil in water (o/w), (B) water in oil (w/o), (C) water in oil in water (w/o/w) (D) oil in water in oil (o/w/o).

Emulsions may exist in a state in which a second degree of continuous phase and dispersed phase classification is introduced and produces water in oil in water (w/o/w) emulsions as depicted in Figure 2.1 (C) or oil in water in oil (o/w/o) emulsions as depicted in Figure 2.1 (D) [157,158].

Micro-emulsions were first reported by Hoar and Schulman in 1943 [159]. Micro-emulsions are thermodynamically stable and usually transparent due to the fact that the droplet size is smaller than the wavelength of visible light at $\lambda = 150 \text{ nm}$ [160]. These emulsions are single optically isotropic liquids with droplets ranging in size from 5nm to 100 nm which form spontaneously and are therefore inherently thermodynamically stable [161,162]. Although micro- and nano-emulsions are prepared using similar components there is considerable confusion relating to the use of the term micro-emulsion and nano-emulsions in the scientific literature [163]. In fact these systems are a distinct type of colloidal dispersion with the most significant difference being stability or state of equilibrium where micro-emulsions are thermodynamically stable, whereas nano-emulsions are generally not and a summary of critical parameters and differences listed in Table 2.2. [164,165]. The disadvantages of micro-emulsion based systems however include the need to use high concentrations of surfactant and co-surfactant to stabilize nano-sized droplets and the limited solubilizing capacity for high-melting point substances [166].

Table 2.2. Differences between micro- and nano-emulsions.

Parameter	Micro-emulsion	Nano-emulsion
Droplet size	10 – 100 nm	10 – 1000 nm
Stability	Thermodynamically stable	Kinetically stable
Manufacture methods	Spontaneous	High energy methods
Advantages	Low energy for formation, high stability	Lower surfactant concentration used
Disadvantages	High surfactant concentration needed	Lower stability

Phase behaviour studies using equilibrium phase diagrams for polar/amphiphilic/non-polar systems provides essential information relating to the formation and structure of a micro-emulsion. Winsor suggested four types of equilibrium systems exist and was later proved experimentally as depicted in Figure 2.2.

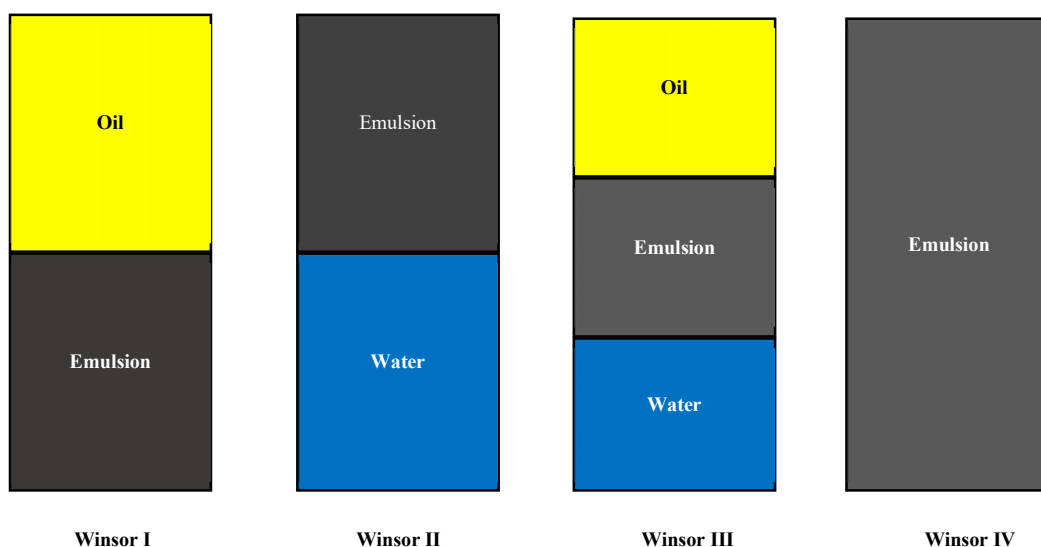


Figure 2.2. Winsor type of emulsion.

Winsor I systems are oil-in-water (o/w) emulsion system in which the surfactant-rich aqueous phase coexists with an oil phase in which the surfactant is only present as a monomer(s). Winsor II systems are water-in-oil (w/o) emulsions in which the surfactant rich oil phase coexists with a surfactant deficient aqueous phase. Winsor III or middle phase systems are three-phase system in which a bi-continuous middle-phase emulsion, rich in surfactant, coexists with excess water and oil phases. Winsor IV systems are single-phase or isotropic

micellar solutions or micro-emulsions that form spontaneously on addition of sufficient surfactant with little or no agitation [167].

2.2 Formulation components of micro- and nano-emulsions

2.2.1 Aqueous phase

The aqueous phase may be the continuous or dispersed phase of an emulsion system in which a hydrophilic API and other components such as preservatives, electrolytes such as sodium chloride (NaCl), hydrophilic polymers and/or minerals are dissolved and which may affect or alter and in some cases be used for the control of pH, ionic strength, rheological characteristics and, phase behaviour and other physicochemical properties of the system [168,169]. The aqueous phase exists in an optimum proportion within a micro- or nano-emulsion system and an excess or too little may lead to phase inversion or separation of the system thereby compromising stability of the emulsion [168,170].

2.2.2 Oil phase

The oil phase of micro and nano-emulsions may be comprised of vegetable oils, vegetable oil derivatives and/or some commonly used dietary oils such as grapeseed, sunflower, soybean and olive oil, amongst others [171]. The common chemical components of oils are triglycerides although these may differ in type, structure, chain length, saturation and/or purity. The selection of an oil is a vital aspect in the development process particularly in the context of ensuring safety and minimizing toxicity and for which the route of administration dictates which oil(s) may be preferred. For food-grade materials or orally administered API oils that are generally recognised as safe (GRAS) according to the Food and Drug Administration (FDA) can be used such as for example of corn oil in the commercially available product Neoral[®] for the administration of cyclosporine [172]. However, there is a paucity of information relating to the phase behaviour, formation and microstructure of nano-emulsions produced using food grade materials which may, in part, be due to the fact that crude edible oils are known to be difficult to solubilize in o/w nano-emulsion systems [173,174].

Vegetable oils are comprised of mono, di and triglycerides and are classified according to the chain length of the fatty acids viz., as short chain triglycerides (SCT), medium chain triglycerides (MCT) and long chain triglycerides (LCT). MCT usually have fewer double bonds

in the fatty acids compared to LCT and therefore MCT are not as susceptible to oxidation. Triglycerides containing unsaturated or short-chain fatty acids exhibit better dispersion properties in micro-emulsions than triglycerides with saturated or long-chain fatty acids [175]. However the solubilisation capacity of micro-emulsions increases as the chain length of surfactant molecules used increase [176]. In some cases, oils derived from aromatic plants that exhibit pharmacological effects have been used for their preservative and medicinal properties and have been delivered using micro or nano-emulsion systems [177–179].

2.2.3 Surfactants and co-surfactants

Surfactants are usually amphiphilic compounds which exhibit two characteristic behaviours viz., and ability to preferentially locate at an interface between a polar and a non-polar phase such as an aqueous and oil phase as depicted in Figure 2.3 (A and B) or an ability to self-associate in aqueous or non-aqueous solutions as depicted in Figure 2.3 (C and D) by forming micelles [180,181].

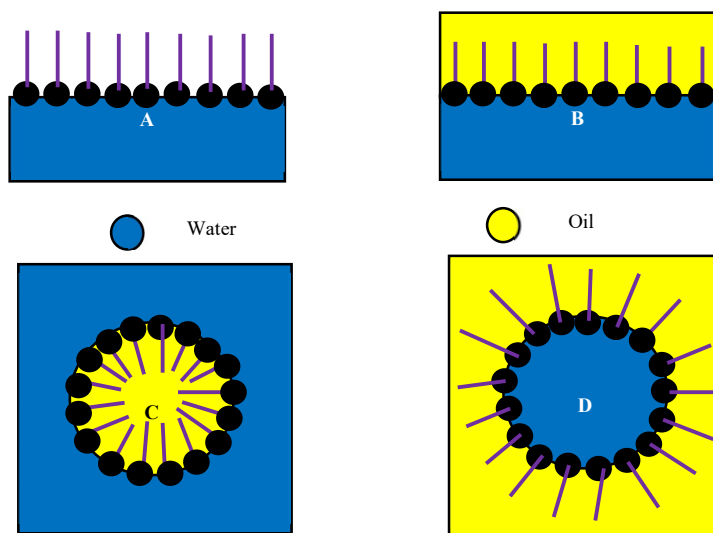


Figure 2.3 Schematic representation of the preferential orientation of surfactants between bipolar phases (A) (water and surfactant system) and (B) (oil and water system, self-association of surfactants to form micelles (C) (o/w) system and (D) (w/o) system.

Adsorption which is a phenomenon determining which molecule moves from the bulk solution to the interface in a specific orientation is a well-known characteristic of amphiphilic molecules such as surfactants [182]. Since the surfactant molecule has a lower free energy when it is adsorbed at the interface than in the bulk solvent phase, the equilibrium in the system will tend towards an adsorbed state where the molecules are arranged in a specific pattern driven by an

energy reduction process which is largely dependent on structural, geometric and prevailing thermodynamic conditions [183,184]. When the surfactant concentration in the aqueous phase increase surfactant molecules initially saturate the interface after which they accumulate in the bulk solution to a point where self-associating surfactant molecules form micelles in which the hydrophobic tail of the molecule is oriented away and the hydrophilic heads oriented towards the aqueous phase in that system (Figure 2.3 (C and D) [185,186].

The concentration of surfactant at which the micelles first form is the Critical Micelle Concentration (CMC) which is specific for a specified temperature and pressure [187]. At this concentration the factors which favour micelle formation dominate the effects which oppose micelle formation. The CMC can be experimentally determined by plotting the surface tension of a solution versus log of the bulk phase concentration for an aqueous solution of a surfactant [188]. In solutions in which the concentration of surfactant is high but lower than the CMC the lower the surface tension of the system however, at concentrations $> \text{CMC}$ the surface tension of the solution is essentially constant [189]. In most cases, single-chain surfactants used alone are unable to reduce the interfacial tension between the aqueous and oil phase sufficiently, to enable a micro-emulsion to form spontaneously [190]. Medium chain length alcohols which are commonly added as co-surfactants have the effect of further reducing the interfacial tension between the phases and increase the mobility of the hydrocarbon tail whilst increasing the fluidity of the interface thereby increasing the entropy of the system and an example of a surfactant and co-surfactant stabilized micelle is depicted in Figure 2.4 [191].

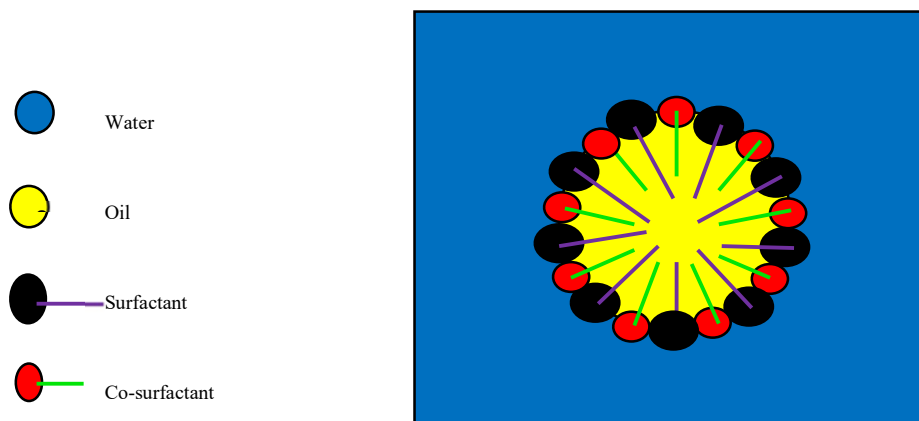


Figure 2.4 Schematic representation of a micelle formed using a surfactant and co-surfactant in an o/w system.

2.2.3.1 Surfactant type

Surfactants are classified according to the nature of the polar head group resulting in anionic, cationic, amphoteric or Zwitterionic and non-ionic surfactants [192]. Ionic surfactants dissociate in aqueous environments to form surface-active anions or cations [193]. Some examples of anionic surfactants include sodium dodecyl sulphate (SDS) and sodium bis-2-ethylhexylsulphosuccinate (AOT) and examples of cationic surfactants include quaternary ammonium alkyl salts such as cetyltrimethylammonium bromide (CTAB) and the twin-tailed surfactant didodecyl ammonium bromide (DDAB) [194]. Generally, ionic surfactants exhibit greater surface activity at lower concentrations than non-ionic surfactants and are generally more effective [195]. A combination of ionic and non-ionic surfactant can be effective at increasing the extent of the micro-emulsion region of a phase system particularly when ionic surfactants such as sodium dodecyl sulphate which have HLB values > 20 are used as these require the presence of a co-surfactant to reduce the effective HLB to a level suitable for micro-emulsion formation [196].

Non-ionic surfactants may be homologous structures comprised of different lengths of alkyl chains with at least one hydrophobic or water insoluble and one oxygen containing functional group which generally do not ionize but dissolve in water [197]. Examples of non-ionic surfactants include polyoxyethylene surfactants such as Brij 35 (C12E35) or sugar based esters such as sorbitan monooleate or Span[®] 80, sorbitan monolaurate or Span[®] 20 and polyoxyethylene sorbitan mono-oleate or Tween[®] 80 [198]. Since non-ionic surfactants do not contain ionisable functional groups, they are less sensitive to changes in the pH of the dispersion medium or the presence of electrolytes and therefore tend to exhibit fewer interactions with cell membranes when compared to anionic and cationic surfactants resulting in formulation scientist preferably using non-ionic surfactants for oral and parenteral formulations because due to low tissue irritation and toxicity effects [199].

The structure of Zwitterionic surfactants include a dipolar head group in the molecule, one of which is positively and the other negatively charged [200]. Phospholipids are an example of Zwitterionic surfactants which exhibit excellent biocompatibility and other examples include 3-(1-alkyl-3-imidazolio)propane-sulfonate (ImS3-n), betaine and sulfo-betaine [201]. Zwitterionic surfactants can be separated into pH-sensitive and insensitive materials [202]. These surfactants usually exhibit low irritant potential and minimize the irritation potential of anionic surfactants although large quantities of the surfactant may cause gastrointestinal and

skin irritation when administered orally or topically requiring careful consideration when selecting surfactants for use in dosage forms [203,204].

2.2.3.2 Co-solvents

Co-solvents may be added to lipid-based systems improve formulation quality and performance characteristics. Some commonly used co-solvents include ethanol, propylene glycol, and polyethylene glycol of different molecular weight [205]. The inclusion of a co-surfactant and co-solvent to solubilise a multi-component oil phase or crude cold pressed oil may be necessary to form a system that resembles a Winsor IV system [206,207]. Specific attention must be paid to safety consideration when using organic solvents in dosage forms intended for paediatric patient use [208]. Ethanol is the only permissible second most commonly used solvent in oral dosage forms and can also be used as a microbial preservative in oral liquid medicines. The American Academy of Paediatrics Committee on Drugs has recommended that the amount of ethanol used in any preparation must not result in a blood alcohol concentration >25 mg/ dL after a single dose, whereas the European Medicines Agency (EMA) has recently proposed that blood ethanol levels should not exceed 1 mg/dL after a single dose or a dose of 6 mg/kg) in children < 6 years of age [209].

2.3 Development of SEDDS

The development of micro- and nano-emulsions commences with an understanding of the type of emulsion to be produced viz., o/w or w/o as this facilitates selection of appropriate surfactants, co-surfactants and/or co-solvents for the emulsion to be produced. Several approaches can be used to rationalize the selection of each excipient and includes use of the HLB system, Bancroft's rule in addition to phase behaviour studies.

2.3.1 Hydrophilic-Lipophilic Balance (HLB) system

The hydrophilic-lipophilic balance (HLB) system was created in the late 1940s to describe and rationalize surfactant behaviour and assist in making decisions about the amount and type of surfactants to be used to form stable emulsions [210]. Surfactants are characterized according to the balance between the hydrophilic and lipophilic constituents of the molecules. The HLB number reflects the polarity of the molecules over a range of 1-40, with the most common emulsifiers falling in the range of 1-20, some examples of which are listed in Table 2.3.

Table 2.3. Some commonly used compounds and associated HLB values [211–213].

Surfactant HLB Value	Uses	Examples	Type	HLB value
1-3	Anti-foaming agents/ surface films	Vegetable oils, hydrocarbon waxes	Non-ionic	< 3
3-6	Water in oil emulsifier	Span® 60 (sorbitan monostearate)	Non-ionic	4.7
7-9	Wetting agents	Span® 20 (sorbitan monolaurate)	Non-ionic	8.6
8-15	Oil in water emulsifiers	Tween® 80 (polyoxyethylene sorbitan mono-oleate)	Non-ionic	15
13-15	Detergents	PEG 400 monolaurate	Non-ionic	9.7
15-18	Solubilizers	Tween® 20 (polyoxyethylene sorbitan mono-laurate)	Non-ionic	16.7

HLB values >10 reflect emulsifiers that are comprised of a large number of hydrophilic groups and are therefore more hydrophilic and water miscible whereas HLB values <10 reflect the molecules are lipophilic or oil miscible (Table 2.3) [214]. Specific oils will require incorporation of emulsifiers with a specific HLB to be effectively emulsified and produce an emulsion that exhibits maximum stability, usually surfactants with similar HLB values to that of the respective oils will ensure better stabilization than when those of divergent HLB are used [215]. It is generally accepted that HLB values between 3 and 6 favour the formation of w/o micro-emulsions whereas surfactants with HLB values between 8 and 18 are preferred when producing o/w micro-emulsion systems and for a specific oil, the required HLB value of surfactant to produce an o/w emulsion is usually higher than that required HLB to produce a w/o emulsion [216].

2.3.2 Bancroft's Rule

Bancroft developed a set of empirical rules to describe the nature of an emulsion that can be stabilized using a specific emulsifier and the rule specifies for both micro- and macro-emulsions, the phase in which the surfactant is most soluble is the continuous phase [217]. The rule implies that o/w emulsions are likely formed by addition of a water-soluble emulsifier whereas w/o emulsions are formed when an oil-soluble emulsifier is used, however, there are limitations and some cases the type of emulsion formed is dependent on a number of factors other than solubility and include the ratio of oil to water used and thermodynamic conditions in which the system is formed [218].

2.3.3 Phase behaviour and diagrams

Phase behaviour studies using equilibrium phase diagrams for three component systems containing water, oil and surfactant or mixture of surfactants can provide information essential to understanding the formation and structure of micro-emulsions. Phase diagrams or pseudo ternary phase are called Gibbs triangle plots and have been used to describe and optimize three component surfactant, oil and aqueous solution systems that form micro- and nano-emulsions and a typical representation of such a diagram is depicted in Figure 2.5.

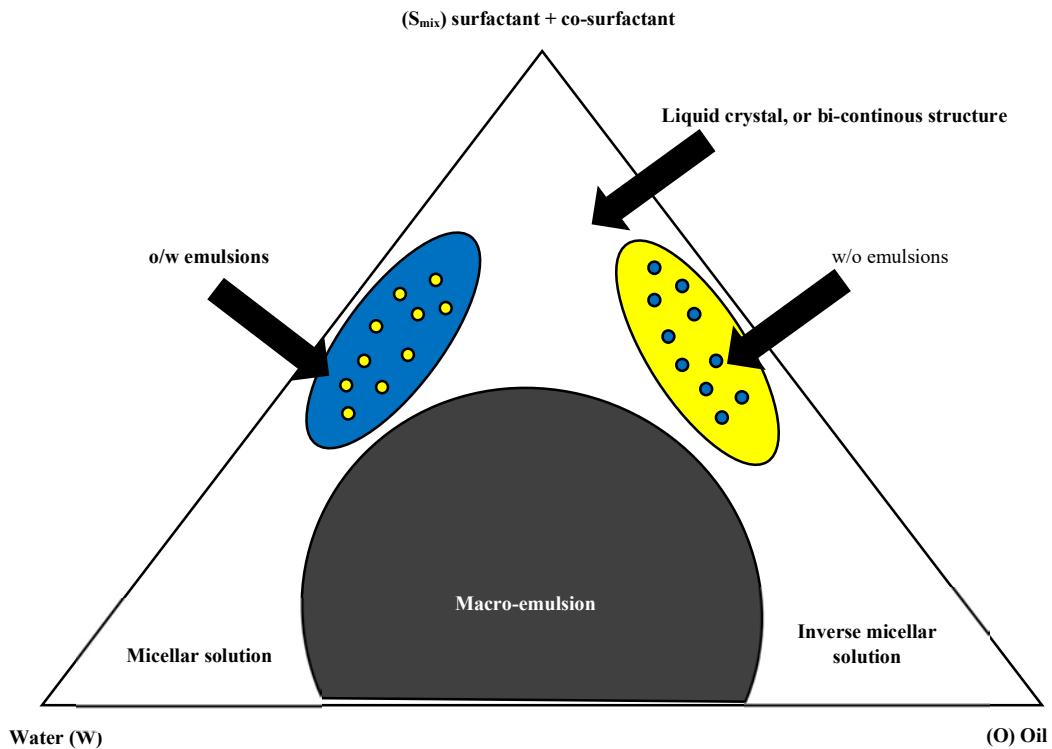


Figure 2.5. Schematic of a typical phase diagram depicting the regions in which different types of emulsions from [219].

Pseudo-ternary phase diagrams take the form of an equilateral triangle sub-divided into a set of smaller equilateral triangles which may be further be sub-divided. Each of the sides of the largest equilateral triangle represent the proportion as a percentage of each of the three components used in the micro-emulsion, viz., oil, water and surfactant or surfactant mixture with each vertex representing 100 % of each of the individual components whereas the smaller divisions reflect are a more accurate and precise composition of the ternary mixture [220,221].

Pseudo-ternary plots are used to identify the boundaries and distinct areas in which the ternary mixture exists in biphasic, mono-phasic, non-isotropic, or liquid crystalline and co-existing regions in a state of dynamic equilibrium [222,223]. When the proportion of oil and surfactant in combination is greater than the aqueous phase reverse micelles which are capable of solubilising low volumes of water in the hydrophilic core, are formed due to the orientation of surfactant molecules in the system. On addition of more water in hydrophilic core w/o micro-emulsions, in which water occurs as droplets of the dispersed phase stabilized by an interfacial layer of the surfactant /co-surfactant mixture, are formed [224]. At very low concentrations of surfactant along the water and oil baseline as depicted in the phase diagram (Figure 2.5), macro-emulsions form due to the surface tension and bipolar nature of the system. Emulsions with smaller droplets form at high surfactant concentrations but usually occur on opposite sides of the phase diagram in terms of the classification as o/w and w/o micro- or nano-emulsions. In general along the water and surfactant mixture baseline where minimal oil is included, o/w emulsions form whereas and on the opposite side of the diagram along the oil and surfactant mixture baseline where minimal water is present w/o emulsions generally form [225,226].

2.4 Methods of manufacture of micro- and nano-emulsions

Different techniques can be used to manufacture micro- and nano-emulsions which may involve a single or series of consecutive steps, depending on the type of emulsion to be produced, the starting materials and methods used. The methods of manufacture of emulsions can be grouped as low- or high-energy methods and are mechanical or chemical in nature. Low energy methods do not require input of mechanical energy input, result in spontaneous formation of small oil droplets as a result of intrinsic chemical energy whereas high energy methods require energy in mechanical, chemical and/or thermodynamic form to be applied to produce an emulsion.

2.4.1 Low energy methods

2.4.1.1 Spontaneous Emulsification

Spontaneous emulsions formed when an aqueous phase and oil phase are mixed in the presence of an emulsifier with gentle stirring at a pre-defined temperature. Mixing of the phases with gentle agitation by magnetic stirring results in distribution of the emulsifier in the aqueous

phase leading to an increase in interfacial oil-water area resulting in oil droplet, formation. A major disadvantage of this approach is that highly synthetic surfactants are required on a large scale which may not be economically feasible economically or may have regulatory constraints in the food industry as a consequence of the usually high surfactant concentrations used [227,228].

2.4.1.2 Phase Inversion

Phase inversion makes use of phase inversion properties molecules, which, in this is the change in hydrophilicity or lipophilicity of emulsifiers as a function of temperature when prepared in specific ratios [229]. At low temperatures oil-in-water emulsions are formed and at high temperatures water-in-oil emulsions are formed as the aqueous solubility of emulsifier(s) decreases as the temperature of the systems increase. Phase inversion is a consequence of solubility behaviour with changes in temperature and as temperature increases, o/w emulsions may change to w/o emulsions. Phase inversion can be exploited to produce emulsions characterized by fine droplet size and long-term emulsion stability [230]. The phase inversion temperature (PIT) is the temperature at which an oil-in-water emulsion becomes a water-in-oil emulsion and is a critical process parameter to monitor. The higher the PIT and the more stable the resultant oil-in-water emulsion is at ambient temperatures. The PIT depends on the relative concentrations of the emulsifier mixture used, the nature of the emulsified oils in addition to the individual HLB values of the excipients used [231,232].

2.4.2 High energy methods

High energy methods are used extensively to manufacture nano-emulsions as the use of high mechanical energy levels creates strong disruptive forces, which break up large droplets to form nano-sized droplets resulting in the formation of nano-emulsions with high levels of kinetic energy. The disruptive forces are imparted to the system using mechanical devices such as ultrasonic baths/probes, microfluidizers or high-pressure homogenizers [233]. The use of high energy methods permit greater control over the resultant droplet for a formulation composition in addition to control of the stability and rheology of the resultant emulsion.

2.4.2.1 High pressure homogenization

High-pressure homogenizers are used to impart high energy into a system by applying homogeneous flow to a system through a small orifice to reduce droplets to a small size. Initially a coarse emulsion is passed through a small with high pressure usually of 500 to 5,000 psi and turbulence, hydraulic shear and cavitation forces are applied simultaneously during this process, to produce a nano-emulsion of extremely small droplet sizes [234]. In some cases a combinations of high pressure homogenization (HPH) and ultrasound (US) or high shear homogenization can o be used to produce nano-emulsions [235].

2.4.2.2 Membrane emulsification

Membrane emulsification has emerged as a relatively new energy-efficient approach for the preparation of micro and nano-emulsions of tuneable droplet size. Membrane technologies function primarily on the principle of size exclusion and is a promising technological approach to nano-emulsion production as membrane pore size can be tailored within a range of 50-220 nm [236]. Direct membrane emulsification involves formation of droplets following mixing of two immiscible liquids by injecting the intended dispersed phase under pressure through a microporous membrane made usually from polymers such as porous glass (SPG) membrane which are the most commonly used membrane for the preparation of emulsions, ceramic (titanium oxide) membranes have also been used [237–239].

2.4.2.3 Micro-fluidization

Micro-fluidization is an approach that follows mixing an aqueous and oily phase together in an inline homogenizer to produce a coarse emulsion which is then is forced through an interaction chamber comprised of micro-channels using a high-pressure positive displacement pump at pressures between 200 and 500 psi [240]. The process forces the two liquid phases through the micro-channels into an impingement area forming droplets in the submicron size range [241].

2.4.2.4 Ultrasonication

In this approach emulsions are formed following ultrasonic agitation of the system using sound waves generated at > 20 kHz which disrupts the integrity of coarse droplets into nano-sized

droplets to form a nano-emulsion [242]. Sound waves are applied using a sonotrode to produce mechanical vibration and acoustic cavitation which subsequently collapse and the resultant shock waves generated disrupt the coarse droplets, at high mHz frequencies nano-emulsions can be produced without an emulsifier [243–245].

2.5 Quality assessment and characterization of SEDDS

2.5.1 Droplet size

Quantitative data and measurements of droplet size, size distribution and Polydispersity index (PDI) can be obtained using Dynamic Light Scattering (DLS) or Photon Correlation Spectroscopy (PCS) which is commonly used for the determination of particle size of micro-, nanoparticles, micro- and nano-emulsions [246]. This approach is based on the assumption that all particles/droplets in a system are very small, spherical and display Brownian motion when in a solution/suspension [247]. The scattering of laser light occurs when light rays hit particles their size can be determined based on the physical properties of scattered light such as the angular distribution. Laser light irradiated onto macromolecules in DLS scattering the incident light in all directions the intensity of which is recorded by the detector [248]. Although PCS is used as a complementary tool to determine particle size and the PDI of micro and nano-emulsions, this technique cannot provide information relating to the shape and surface morphology of nanoparticles or nano-droplets. Transmission electron microscopy (TEM) is a powerful technique used to characterize the size, shape and morphology of droplet or aggregates in micro-emulsions which is commonly used in conjunction with DLS as a confirmatory analytical technique to provide information relating to the shape and size of nano or micro-particles and droplets [249,250].

2.5.2 Polydispersity index (PDI)

The successful formulation and production of stable and efficient nano-carrier drug delivery systems requires the preparation of homogenous or monodisperse nano-carriers of specific size. The polydispersity index (PDI) is a measure of the extent of uniformity of the size distribution of particles, is dimensionless and scaled such that values < 0.05 are observed for highly monodisperse analytical standards. Values for $PDI > 0.7$ indicate that the sample has a broad particle size distribution and it is likely that the formulation cannot be analysed using

dynamic light scattering (DLS) [251]. High PDI values also mean that the size uniformity of the formulation is not guaranteed, and equal volumes of the product may not contain the same amount of API indicating that adequate control of the formulation, manufacture and administration process may not be guaranteed.

2.5.3 Zeta Potential

The Zeta potential (ZP) of a system describes electro-kinetic potential and is a measure of surface charge in colloidal systems. In other words the ZP is a measure of the potential difference between a dispersion medium and the stationary layer of that dispersion medium adjacent to dispersed particles in that medium [252]. Several factors such as pH of the medium, ionic strength, concentration of solutes and temperature affect the ZP of a system. Furthermore, the ZP may influence the stability of systems, cellular uptake and intracellular trafficking of emulsion droplets. In general, emulsions with a high negative or positive ZP are stabilized whereas emulsions with a low ZP tend to coagulate or flocculate which may lead to poor physical stability. High positive or negative values for the $ZP > \pm 30$ mV tend to reflect monodisperse systems [253], whereas $ZP < \pm 5$ mV show agglomeration and poor PDI. In some cases the ZP is not a directly relevant parameter for establishing stability particularly when the differences in ZP between emulsions is small [254]. Laser Doppler Anemometry (LDA) can be used to determine the electrophoretic mobility of particle in aqueous dispersion, which in turn can be used to establish the ZP using Smoluchowski's formula (Equation 2.1) [255].

$$\bar{y} = \frac{\epsilon_r \epsilon_0}{\eta} \zeta$$

Equation 2.1

Where,

\bar{y} = electrophoretic mobility

ζ = Zeta Potential

ϵ_r = relative permittivity

ϵ_0 = permittivity of a vacuum

η = viscosity of dispersion fluid

2.5.4 Drug loading capacity and encapsulation efficiency

Drug-loading capacity (DLC) and encapsulation efficiency (EE) are two important parameters to characterize when assessing the quality of nanomedicines. The two parameters are useful for establishing the fill volumes of capsules which is required to identify capsule size in order to assure that the required dose of API is in each capsule with a general desirability of lower EE and DLC values [256]. The DLC is affected by the structure, physical and chemical properties of the vehicle of the carrier material and is a measure of the mechanism of loading, mass of API in the feed process during manufacture, the DLC is defined as the ratio of the weight of incorporated API to the total weight of the lipid composition, and can be calculated using Equation 2.2 and reflects the mass ratio of API to nanomedicine during the manufacture of nanomedicines [257].

$$\text{Drug loading capacity} = \frac{W_a - W_s}{W_a - W_s + W_L} \times 100$$

Equation 2.2

Where,

W_a = weight of API added

W_s = weight of API in supernatant (after centrifugation)

W_L = weight of lipid added

EE which is an indicator of loading efficiency of the API in the carrier technology [258]. The EE is the ratio of weight of incorporated API to total weight of API and it is calculated using Equation 2.3.

$$\text{Encapsulation efficiency} = \frac{W_a - W_s}{W_a} \times 100$$

Equation 2.3

Where,

W_a = weight of API added

W_s = weight of API in supernatant (after centrifugation)

Compared to conventional drug-delivery systems, the size of the reservoir in which the API is loaded is extremely small nano-sized carriers [259]. Consequently, a high entrapment efficiency is preferred as this reduces the total size of the dosage form to be administered to the patient which may, in turn, increase adherence.

2.5.5 In vitro release

Although nano-particulate systems are a promising approach for the treatment of a variety of human disease issues of toxicity, loss of or altered efficacy may occur if unanticipated changes in product quality or performance occur [260]. Consequently, there is a need to develop standardized test methods for novel drug delivery systems to ensure product performance and quality which should as far as possible be simple, reliable and reproducible and in vitro release testing is necessary for all novel dosage forms, irrespective of intended route of administration [261]. Product quality and performance may be characterized using in vivo and/or in vitro experiments however due to cost, time, labour and need for human and/or animal subjects for in vivo drug release kinetic studies the use of in vitro release is used as a surrogate assessment of in vivo product performance [262].

API release from nanoparticle matrices in vivo, occurs by diffusion of API and/or the digestion of lipids by lipase, colipase or other enzymes [263]. The initial rapid release of API from nanoparticles may be due to an improvement in solubility of the API, or due to high API concentrations near the particle surface in the case of drug-enriched shell technologies. Factors that affect or control API release from nanoparticles include the physicochemical properties of the API and lipid, API to lipid ratio, method of incorporation of API, type and concentration of surfactant, type and concentration of co-surfactant used. Consequently, drug release from nano-sized dosage forms may be assessed using sample and separate (SS), continuous flow (CF) or dialysis membrane (DM) methods [264].

When using the SS approach the nano-particulate dosage form is introduced into the in vitro release test medium maintained at a constant temperature, after which API release is monitored by sampling the medium or the nanoparticles [265]. USP Apparatus I (basket) or II (paddle) are commonly used and the pH of the dissolution medium used in in vitro release studies should as far as possible mimic in vivo conditions [266,267]. Floating, swelling, beads, coated and uncoated tablets, suppositories, immediate and modified release formulations can be evaluated using USP Apparatus I and solid dosage forms such as tablets and capsules or particulate

dosage forms such as suspensions and powders can be evaluated using USP Apparatus II provided the dosage forms do not float [261,268]. The USP III and IV have also been used and reported to demonstrate superior discriminatory power for a testing formulations containing drug nanoparticles [269].

2.5.6 Stability

During the emulsification process, emulsifying agents adsorb onto freshly formed interfacial films, which weaken interfacial forces and permit partial mixing of the immiscible phases of the system. Following formation of the first drop the initial emulsion changes due to different time-dependent processes such as Ostwald ripening, coalescence, flocculation, sedimentation, and creaming or phase separation which important and of interest to the pharmaceutical and food industry [270]. Depending on prevailing thermodynamic conditions these processes may occur at different rates and some may reversible and others irreversible. The formation of flocs or floccules by the phenomenon flocculation is depicted in Figure 2.6 which is usually induced by the presence of excess surfactant and may be reversible [271].

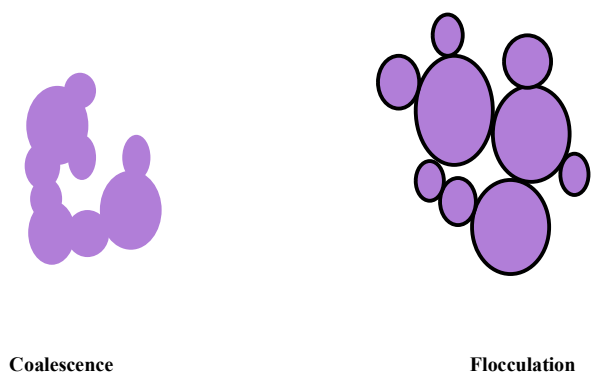


Figure 2.6. Visual representation of emulsion coalescence and flocculation redrawn from [272].

Coalescence in emulsions is an irreversible process in which two or more droplets merge on contact to form a single daughter droplet as depicted in Figure 2.6. The driving force for coalescence is thinning and disruption of the liquid film between droplets which occurs if emulsion droplets are in close proximity in the cream layer, in floccules or as a consequence of Brownian motion and diffusion. As the droplets converge the liquid film between them undergoes thermal fluctuation and when the film thickness approaches a critical value the film collapses resulting in rupture and coalesce [273]. Flocculation occurs when attractive

interaction forces arise following depletion of surfactant micelles which leads to a fluid-solid phase transition. The formation of droplet flocs in the emulsion has an impact on the creaming rate and increased flocculation promotes creaming [274]. In dilute emulsions, flocs which do not or exhibit limited interaction with each other, tend to increase the creaming velocity, since bigger particles are subject to gravitational effects and the presence of flocs tends to increase the viscosity of emulsions [275]. Emulsions maybe susceptible to kinetic instability which manifest as sedimentation and creaming resulting suspended or emulsified particles or droplets settling or rising in the continuous phase as depicted in Figure 2.7 [276].

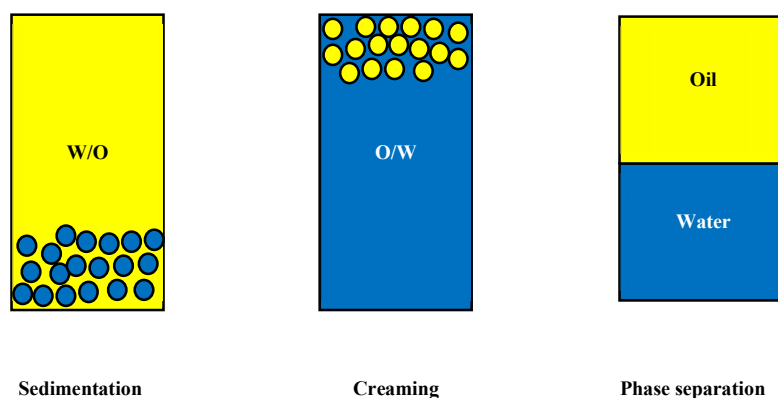


Figure 2.7. Visual representation of sedimentation, creaming and phase separation of emulsions.

Creaming, as depicted in Figure 2.7 is essentially mass migration of emulsion droplets to the surface of the emulsion and is driven by the buoyancy of the emulsion droplets in the continuous phase and the velocity of creaming velocity increases as flocculation increases or decreases with increasing droplet concentrations [270,277]. Sedimentation or creaming occur due to gravitational effects and depends on the relative densities of the dispersed and continuous phase. If the density of dispersed phase is lower than that of the continuous phase the droplets will tend to move upwards and separate from continuous phase resulting in the formation of a separate layer at the top of the continuous phase whereas the converse occurs during sedimentation (Figure 2.7). The dispersion droplets of the creamed layer do not normally coalesce and are generally re-dispersed with gentle shaking [278]. Phase separation may or may not be evident visually however creaming, coalescence and flocculation occur prior to phase separation making identification and quantitation of this phenomenon difficult to evaluate. By centrifugation of samples or establishing a creaming index permits characterization and quantitative evaluation of this phenomenon [279].

2.5.7 Crystallization, polymorphism, and compatibility

Crystalline polymorphs of compounds may have the same chemical composition, but different internal crystal structures, and therefore possess different physicochemical properties such as energy, melting point, density, stability, and in particular solubility, may offer an improvement on the original form due to different lattice structures and/or different molecular conformations [280]. The phenomenon of polymorphism is quite common among organic molecules, and many drugs can crystallize into different polymorphic forms as they interact with their excipients [281,282]. Polymorphic forms of drugs can prove interesting for drug development, generally, the solubility of metastable polymorphs is kinetically higher than that of a thermodynamically more stable polymorph, offering, at least in theory, a solution to bioavailability problems [283,284].

Conducting API compatibility evaluation with potential excipients are important pre-formulation and early product development studies for any dosage form. Potential physical and chemical interactions between an API and excipients may have an impact on the chemical nature, stability, and bioavailability of the API. Consequently, the therapeutic efficacy and safety of an API must be evaluated prior to commercialisation of a product. Fourier Transform Infrared spectroscopy (FTIR), Raman spectroscopy and X-ray Powder Diffractometry (XRD) are rapid analytical approaches commonly used to evaluate potential API-excipient interactions and to detect different polymorphs [285,286].

2.5.8 Electrical conductivity and emulsion classification

Ion movement or transport in micro- or nano-emulsions can provide information relating the internal dynamics of the system. For o/w emulsion the continuous phase is aqueous in nature and conduction of electrical inputs occurs with limited influence of the dispersed oil concentration. Conversely for w/o systems, where conduction is dependent on dispersed aqueous phase. Ion transport in w/o micro-emulsion systems may occur by a hopping mechanism in which droplets associate and surfactant ions hop from droplet to droplet resulting in an increase in conductance or droplet fusion and subsequent fission occurs with transfer of ions resulting in electrical conduction [287]. The ion conductance of Winsor I o/w systems is reasonably high and resembles that of aqueous solutions since water is the dispersion medium whereas conductance in Winsor II w/o systems is very low since the dispersion medium is oil. In Winsor III systems where o/w and w/o dispersions are simultaneously present in a bi-

continuous system electrical conduction is reasonably large. Conductance increased sharply after a threshold concentration of the aqueous phase at a constant temperature. This phenomenon is known as percolation and the concentration or temperature at which the change occurs is the percolation threshold [288]. For w/o micro- and nano-emulsion systems two percolation thresholds may be observed due to composition and/or temperature [289].

2.6 Conclusions

SEDDS such as micro- and nano-emulsions have been developed to minimize the challenges associated with the administration and delivery of compounds of poorly aqueous solubility such as EFV. The advantages of nano sized SEDDS is that they provide a large surface area which facilitates absorption which may improve bioavailability of these API. The design of SEDDS focusses on ensuring API release is independent of gastrointestinal tract physiology and the fed/fasted state of the patient possibly resulting in more consistent formulation performance for all patients. SEDDS are generally isotropic mixtures of API, oil, surfactant and/or co-surfactant with or without addition to a co-solvent with a droplet size ranging from 10 nm up-to 100 nm for micro-emulsions and up to 1000 nm or several μm in diameter for the broad category of nano-emulsions, SNEDDS or SEDDS. The API is dispersed or dissolved in oil droplets which are protected from gastrointestinal conditions with an ability to penetrate intracellular membranes from the systemic circulation or via the lymphatic system distributions. Non-surfactants usually exhibit low irritant potential and are preferred in pharmaceutical formulation development studies. Co-solvents such as propylene glycol and ethanol are permissible for oral applications with however maximum recommended amounts per single dose varying in different countries.

Investigation of phase behavior of LBDDS components using pseudo-ternary phase diagrams and Winsor phase behavior is useful for optimization of formulations and pre-formulation studies assist in defining appropriate proportions of each component to use and the facilitation of decisions in relation to manufacturing processes such as whether high pressure or high shear homogenization can be used. Such decisions are required to ensure that an optimum product with predefined quality attributes is produced together with exploitation of the potential advantage of manufacturing SEDDS using facile manufacturing procedures which are simple and readily scalable.

During SEDDS formulation development studies, critical quality attributes (CQA) of nano-emulsions include droplet size (DS), polydispersity index (PDI), zeta potential (ZP) and drug loading capacity (DLC) are monitored for optimization. Droplet size may influence physiological processes such as hepatic uptake and accumulation, tissue diffusion, tissue extravasation and renal excretion. Nano carriers of diameter between 100 and 150 nm circulating in blood vessels do not easily leave the capillaries that perfuse tissues such as the kidney, lung, heart and brain. In contrast smaller droplets between 20 and 100 nm may distribute into the bone marrow, spleen and liver sinusoids and may leave the vasculature via fenestrated capillaries in the perfused organs. Tailored droplet sizes may provide preferential distribution into specific organs such as the CNS but provide sufficient viral suppression with minimum side effects.

Successful formulation of safe, stable, and efficient nano-carriers requires the preparation of homogenous (monodisperse) populations of nano-carriers of a certain size. Therefore, it is important to consider the composition of the nano-carriers and the nature of the solvents and co-solvents used during their preparation to control the droplet size distribution for more tailored design approach of SEDDS and desirably those with a low PDI < 0.7. The ZP of a system describes electro-kinetic potential and is a measure of surface charge in colloidal systems, it may influence the stability of systems, cellular uptake, and intracellular trafficking of emulsion droplets. In general, emulsions with a high negative or positive ZP are stabilized whereas emulsions with a low ZP tend to coagulate or flocculate which may lead to poor physical stability. High positive or negative values for the ZP > ± 30 mV tend to reflect monodisperse systems, the migration or change in CQA over periods of time is also used for assessing the stability of SEDDS and their ability to resist changes in the physicochemical properties over time.

CHAPTER 3

DEVELOPMENT AND VALIDATION OF A HIGH-PRESSURE LIQUID CHROMATOGRAPHIC (HPLC) METHOD FOR THE QUANTITATION OF EFAVIRENZ

3.1 Introduction

High-Performance Liquid Chromatography (HPLC) is one of the most versatile, dependable and rapid chromatographic techniques used for qualitative and quantitative analysis of pharmaceutical and biological samples [290]. HPLC is commonly used for quality control of pharmaceutical formulations, for therapeutic drug monitoring and life sciences research including food and flavour analysis and forensic evaluation of non-volatile compounds [291]. Rapid progress in the use of HPLC has been facilitated by the development of reliable, reasonably priced equipment and efficient stationary phases [292]. HPLC can be used to analyse samples of a wide range of polarity, ionic and thermally unstable compounds. The technique is also adaptable and compatible with the analysis of a wide range of molecular weight of compounds, ranging from < 2000 Daltons to large proteins presenting with molecular weight > 2000 Daltons when used in size exclusion mode [293].

3.2 Principles of HPLC

In HPLC, a liquid phase (mobile phase) is used to transport soluble analytes along a stationary phase usually in the form of a column of known dimension and material including silica, cyano and C₁₈ based amongst others [294,295]. The stationary phase may be a solid, gel, or liquid and if liquid, it may be sequestered on a solid material that may or may not contribute to the separation [296]. The liquid may be covalently bonded to the solid or support particles of the column to produce a bonded phase which may improve column selectivity for specific analytical methods. The mobile phase may be a binary, ternary or quaternary mixture of solvents, aqueous and some organic compound such as include methanol, ethanol and/or acetonitrile which are moved along the column. The separation of compounds can be successfully achieved through differences in mass transfer of an analyte between the stationary and mobile phase. The difference in mass transfer leading to separation is a result of specific and nonspecific interactions amongst which partitioning, adsorption, ion exchange, and size exclusion are common mechanisms [297–299]. The mobile and stationary phases are usually

materials of different hydrophobicity chemically bonded to the solid support. The chemical nature of the stationary phase governs the strength of analyte retention, therefore HPLC separations are driven by the selectivity achieved using the two interacting phases as summarized in Table 3.1.

Table 3.1 Modes of HPLC, their common stationary phase material and applications in analysis characterization of stationary phases [300,301].

Mode	Stationary phase	Typical compounds	Mobile phase
Normal phase	Cyano, Silica, Amino, Diol	Compounds insoluble in water	Organic
Reversed phase	C ₄ , C ₈ , C ₁₈ , Cyano, Amino	Neutrals, weak acids, weak bases	Aqueous buffers with organic modifiers
Size exclusion	Polystyrene Silica	High molecular weight compounds, polymers, proteins	Aqueous gel filtration Organic gel permeation
Ion exchange	Anion or Cation exchange resin	Ionic/Inorganic ions	Aqueous buffers Counter Ion

HPLC can be operated in several modes which is primarily determined by the type of stationary phase used. A polar stationary and non-polar mobile phase are used in normal phase HPLC in which the most common substituents attached to the silicone backbone of a stationary phase diol, amino, cyano, inorganic oxides, and dimethyl amino substituents [302,303]. Non-polar compounds elute early in normal phase HPLC whereas in reversed phase HPLC where the mobile phase is polar, and the stationary phase is non-polar polar compounds in the sample elute early. Reversed phase HPLC is the most common liquid chromatographic mode used and common stationary phases include C₈, C₁₈, or other hydrocarbons. Reversed-phase chromatography can also use water as the mobile phase, which is advantageous since water is more economical, nontoxic, and invisible in the UV region of the electromagnetic spectrum when using UV detection [304].

Column selection is a critical step in HPLC method development and is a process driven mainly by considering factors such as the type of HPLC system, compound to be analysed and performance requirements of the analysis used. Columns are usually packed with pellicular or porous particles. Pellicular particles are usually polymers or glass beads ranging between 30 μm and 40 μm in diameter [305]. A thin uniform layer of silica, polystyrene synthetic resin, alumina or other types of ion-exchange resin are included to surround the pellicular particles [306]. Porous particles are more commonly used and exhibit diameters between 3 μm to 10 μm with stationary phases that exhibit different physical and chemical properties such as porosity, specific area, particle size and shape and length [307]. The choice of an analytical column is

dependent on physicochemical properties such as solubility, molecular weight and ionic nature of the analyte to be monitored. The retention of an Active Pharmaceutical Ingredient (API) by a stationary phase is also a function of the packing material and column dimensions used. The efficiency of columns increases as the particle size of the stationary-phase decreases and therefore, the smaller the particles used, the better the resolution and sensitivity that can be achieved with that column. However smaller particle sizes often result in higher back pressures on the system resulting in greater risk of blockage by buffers when recrystallization in the mobile phase occurs [308]. The resolution of a column is proportional to column length i.e. the longer the column, the more efficient it is however increasing column length also increases analysis time and therefore for each HPLC method column suitability must be performed to assess the number of theoretical plates and column efficiency. The mobile phase composition and column temperature are also constitute important experimental conditions that can be altered when a mixture of several compounds is separated [309]. An increase in temperature is usually predicted to increase the rate of the interphase mass transfer and thus one can operate at much higher linear velocities with improved column efficiency and faster analysis times [310].

3.2.1 Distribution constant

The separation of analytes in HPLC is a function of the difference in equilibrium between the stationary and mobile phase and distribution constant (K) which is calculated using Equation 3.1.

$$K = \frac{C_s}{C_m}$$

Equation 3.4

Where,

K = distribution constant

C_s = concentration of analyte in the stationary phase

C_m = concentration of analyte in the mobile phase

The distribution constant is the ratio of analyte concentration in either the stationary and mobile phases at equilibrium within the HPLC column. Compounds that are well retained by the stationary phase or that exhibit long retention times have high distribution constants [311]. The

extent of retention of compounds along a stationary phase is an important factor to consider during HPLC method development, long retention times maybe unnecessarily costly on the amount of mobile solvents used and the run time of the system. A good balance of adequate retention to separate a compound and its internal standard with adequate resolution is desirable in a short run time preferably below 10 minutes under various specified conditions such as temperature, flow rate, column length and solvent used.

3.2.2 Column efficiency

Column efficiency is a measure of how a column performs through calculating the number of theoretical plates (N) or more often, the height equivalent of theoretical plates (HETP or H) [312]. The parameter N is a widely used approach for assessing the efficiency of separation of a chromatographic system. The greater the number of theoretical plates the better the efficiency of the column under investigation. The number of theoretical plates can be calculated using Equations 3.2 and 3.3. The longer columns exhibit greater numbers of theoretical plates whereas short columns produce separations with shorter retention or separation times. Although the value of N depends on elution time, the Food and Drug Administration (FDA) recommends generally an N value > 2000 [313,314].

$$N = 16 \left(\frac{tr}{wb} \right)^2$$

Equation 3.5

$$N = 5.54 \left(\frac{tr}{w_{1/2}} \right)^2$$

Equation 3.6

Where,

N = the number of theoretical plates

t_r = retention time of the analyte

w_b = peak width at baseline

w_{1/2} = peak width at one half the maximum height of the peak

The height equivalent of a theoretical plate (HETP) expresses the height (H) of a single theoretical plate and is a ratio of efficiency per unit length (L) of a column that is calculated using Equation 3.4. [315]. The greater the efficiency of a column the smaller the value of the

theoretical height will be. Measuring H is necessary when comparing the efficiency of columns of different length or stationary phase [316].

$$H = \frac{L}{N}$$

Equation 3.7

Where,

H = height of one theoretical plate

L = length of column

N = the number of theoretical plates

The number of theoretical plates was used to determine the suitability of columns for a separation by evaluation of a sample mixture containing uracil, acetophenone, benzene and naphthalene dissolved in acetonitrile (ACN). The chromatographic separation conditions used a mobile phase of ACN and H₂O in a 65: 35 v/v ratio at 22 °C. The injection volume was 20 μL and the flow rate was 1 mL/min with the detection wavelength set at 247 nm. The average theoretical plate number of the column tested was 9784 ± 0.085. The column was therefore considered suitable for use in the development of an analytical method for the quantitation of EFV.

3.2.3 Resolution factor

The resolution factor (*Rs*) provides an indication of the degree of separation between adjacent peaks in a chromatogram and is a function of the column, operating conditions and instrument variables of a system [317]. The *Rs* is calculated using Equation 3.5.

$$Rs = \frac{t_2 - t_1}{0.5(w_1 + w_2)}$$

Equation 3.8

Where,

Rs = peak resolution

*t*₂ = retention time of second eluting peak

*t*₁ = retention time of first eluting peak

*w*₁ = width of first eluting peak at base

*w*₂ = width of second eluting peak at base

A resolution factor > 1.5 is considered desirable as the resultant separation is suitable for accurate integration and quantitation of individual peaks. A $R_s < 1.5$ indicates poor resolution and is unacceptable since inaccurate results may be produced [317]. A Phenomenex Luna[®] C₁₈ 150mm x 4.6mm i.d. stationary phase of 5 μ m particle size (Separations[®], Randburg, South Africa) was used and exhibited an R_s of 6.1 when evaluated using the conditions described in § 3.2.2, indicating that the peaks of interest were well resolved and the column was therefore suitable for these studies.

3.2.4 Asymmetry factor

When calculating the efficiency of a column it is assumed that the peak(s) of interest will be symmetrical, or Gaussian as depicted in Figure 3.1A. Where the peak is not symmetrical and tailing occurs, the peak will be asymmetrical as depicted in Figure 3.1B.

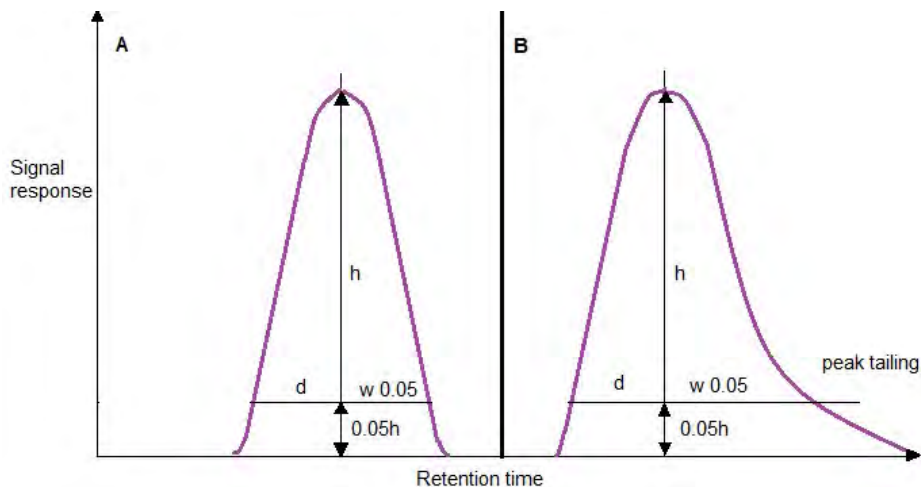


Figure 3.1. Schematic representation of (A) Gaussian or symmetrical peak shape and (B) Asymmetrical chromatographic peak.

Symmetrical peaks are ideal for chromatographic separations and quantitation, for which a constant, α , is assigned and equal to 5.45 when peak width is measured at half peak height. This is the easiest and often used peak width to measure. The symmetry factor (A_s) is a measure of peak shape and can be calculated using Equation 3.6 [318].

$$A_s = \frac{W_{0.05}}{2d}$$

Equation 3.9

Where,

A_s = peak symmetry factor

$W_{0.05}$ = is width at one-twentieth peak height

d = the distance between a perpendicular line drawn from the peak maximum and the front of a peak corresponding to one-twentieth of the peak height.

A value for A_s value of 1 signifies peak symmetry, whereas when peak tailing occurs (Figure 3.1B) the value for A_s becomes > 1 and if peak fronting occurs the asymmetry factor is < 1 . Asymmetry factor of between 0.8 and 1.2 is recommended as appropriate for HPLC analyses [319,320].

3.2.5 Method of detection

In any HPLC system the component responsible for turning a specific physico-chemical property of the analyte into a measurable signal corresponding to concentration or identity is the detector [321]. The most common detectors used in liquid chromatography are ultraviolet (UV) detectors, electrochemical detectors (ECD) are also to a lesser extent but more often than nuclear magnetic resonance detectors (NMR) [322].

3.2.6 UV-Visible detectors

Standard UV detectors for HPLC separations measure absorbance of monochromatic light produced by a tungsten lamp of fixed wavelength in the visible wavelength range of the electromagnetic spectrum between 190 nm and 400 nm against that of a reference beam [323,324]. The magnitude of the absorbance observed is correlated to the concentration of analyte in the eluent passing through the flow cell of the instrument, prior to using a UV-Vis detector the maximum UV absorbance of the compound of interest should be identified to select an appropriate wavelength of detection for that compound. Sample concentration reflected as absorbance is determined by the fraction of light transmitted through the detector cell in accordance to the Beer Lambert law and only compounds with chromophores are detected [325]. Typically such molecules contain unsaturated bonds, aromatic or functional groups containing heteroatoms with π^* and σ^* nonbonding orbitals into which electrons are promoted and absorb incident energy. If the molar absorptivity coefficient for the analyte is unknown, the use of standard solutions of known concentration can be used to calibrate the instrument for a concentration versus absorbance response through a calibration curve or response factor. The analyte concentration can be determined with the aid of the Beer-Lambert

law reported in Equation 3.7 [326]. According to the Beer-Lambert law, the light intensity transmitted from the detector is directly proportional to analyte concentration in dilute solutions.

$$A = \varepsilon \times c \times l$$

Equation 3.10

Where,

ε = molar absorptivity coefficient in $\text{dm}^3 \text{mol}^{-1} \text{cm}^{-1}$,

c = concentration in mol dm^{-3} ,

A = the absorbance, and

l = path length of the light through the flow cell in cm.

Diode array detectors are a sub-set of UV detectors in which the tungsten lamp is combined with a deuterium lamp which emits radiation in the 190 nm - 850 nm range of the electromagnetic spectrum. These detectors are used to detect absorption at multiple or a single wavelength and acquire spectra for peak purity analysis dynamically. Photodiode array detectors (PDA) are used to monitor a sample at more than one wavelength which is especially useful when the wavelength maximum absorption of the components of a mixture are different. The wavelengths to monitor can be selected to analyse each compound at a setting reflecting the highest sensitivity of that system [327]. In this research a diode array detector was used for the initial identification of the UV maximum absorbance of efavirenz (EFV) between a ranges of 210 – 600 nm. A simple UV was used for method development and validation studies.

3.2.7 Mobile phase and buffer considerations

The components of the mobile phase are selected in a manner to ensure sample solubility, extent of ionization of analyte and the stability of the analyte and stationary phase are maintained [328]. It is recommended that HPLC-grade solvents are used in order to optimise the reproducibility of a separation and to minimise contamination. The solvents used to prepare the mobile phase must be miscible with one another in binary or ternary mixtures and produce a solution without high column backpressures, furthermore the solvents must have a low UV cut off to minimise noise when low wavelength UV detection is required [329]. The most commonly used HPLC solvents and relevant chromatographic properties are summarised in Table 3.2. For the purposes of this research, analytical grade acetonitrile was selected for use as it has a low viscosity and only absorbs UV light at a wavelength of 190 nm. Methanol is

slightly more viscous than acetonitrile and forms more viscous solutions with water than acetonitrile (ACN) and absorbs UV light at 205 nm [330,331].

Table 3.2 Commonly used HPLC solvents with relevant properties [332,333].

Solvent	Viscosity cP	UV-cut off nm	Refractive Index	Boiling Point ° C	Miscibility with water
Acetonitrile	0.358	195	1.341	82	Miscible
Methanol	0.584	205	1.326	65	Miscible
Ethanol	1.19	205	1.359	78	Miscible
Isopropanol	2.39	205	1.375	82	Miscible
Tetrahydrofuran	2.20	215	1.404	66	Miscible
Water	1.00	185	1.333	100	--

For the purposes of formulation development activities and assay of dosage forms it is recommended to that a mobile phase in which the excipients used in the products are soluble be used in the solvent system in order to avoid increasing column backpressure during analyses. This approach permits the peaks of active pharmaceutical ingredients (API) and those of the excipients to be separated if they are detected at the wavelength used. Both acetonitrile and methanol were investigated for use in the mobile phase for the assaying of EFV. Crude cold pressed vegetable oils are insoluble in acetonitrile and methanol but are soluble in ethanol, therefore ethanol was used for the dissolution of samples during sample preparation for injection into HPLC.

To minimise retention time variability and peak distortion of weak acids and bases mobile phase pH must be strictly controlled and buffers are commonly used for this purpose in reversed-phase liquid chromatography to control the ionization state of analytes [334]. Changes in pH may affect the elution of acid/base compounds which has a strong dependence of their degree of ionization at any time [335]. The non-ionized form of a compound is less polar than the ionized form and is thus more strongly retained by the reversed-phase system delaying elution to beyond the solvent front. Consequently at low pH, acids are better retained than bases and the converse occurs at more alkali pH [336].

As the polarity of a molecule increases the retention time decreases as when an acid or base ionizes the molecule becomes polar or hydrophilic and retention time is reduced [334]. The pH of the buffer selected is primarily based on the pKa of the analyte(s) of interest. Rapid analysis can be achieved if analytes are predominantly in their ionised form in which they interact with

the mobile phase and will thus travel at a similar velocity to the mobile phase during the separation. EFV is a weak acid with a pKa of 10.1 ± 0.1 and at a pH of 4 the compound is largely unionised and therefore will be retained by the stationary phase. In this way chromatographic retention times can be controlled [53,337]. Since EFV is largely unionized close to a neutral pH such as that of water and an organic solvent alone without the presence of a buffer. The analysis of EFV using a non-buffered mobile phase has also been achieved [338].

3.2.6 Internal standard

In order to improve the accuracy and precision of this method, an internal standard (IS) was used to compensate for variable injection volumes and day-to-day instrumental variability [33]. The major criteria used when selecting an internal standard are that the physicochemical and analytical properties of the compound are similar to those of the analyte of interest. In other words the standard must be sufficiently soluble in the mobile phase and exhibit a similar mechanism of retention to the analyte by the stationary phase [340]. In order to identify and select an IS for the analysis of efavirenz, four compounds viz., carbamazepine, indomethacin, loratidine and emtricitabine were evaluated using preliminary conditions with a mobile phase of ACN and HPLC grade water in a 60:40 % v/v ratio at a flow rate of $1 \text{ mL}\cdot\text{min}^{-1}$ and temperature of $25 \text{ }^\circ\text{C}$. The results observed are summarized in Table 3.3. Loratidine was selected as the IS as the peak resolution, symmetry and retention time was ideal. A typical chromatogram is depicted in Figure 3.2.

Table 3.3 Results of internal standard suitability selection studies

Compound	Retention time minutes	Comments
Carbamazepine	2.05	Too close to solvent front
Emtricitabine	1.52	Too close to solvent front
Loratidine	8.50	Ideal for IS, narrow symmetrical peak
Indomethacin	2.47	Broad peak with peak tailing, Too close to solvent front

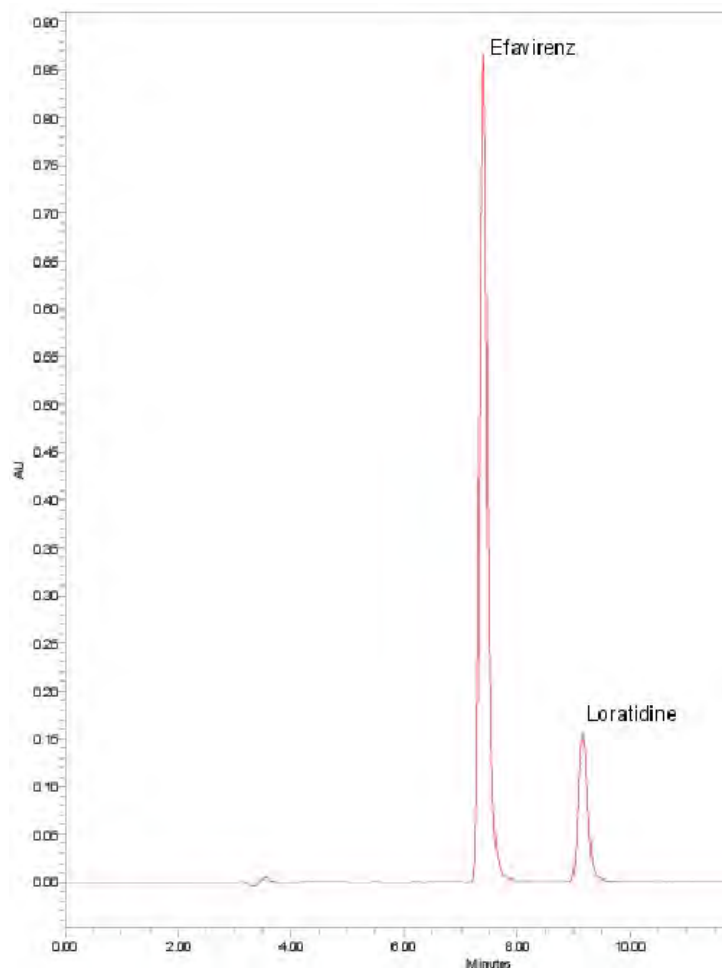


Figure 3.2. Typical chromatogram for the separation of EFV 250 $\mu\text{g/mL}$ and LRT 100 $\mu\text{g/mL}$ using the optimized conditions

3.3 Method development

The development of an HPLC method commences by considering factors such as the nature of the analyte and sample matrix to be analysed and subsequently identifying the best initial conditions to be applied [341]. Prior to the development of the HPLC method for the analysis of EFV, a literature review was undertaken and published conditions used for the analysis of EFV are summarised in Table 3.4 from which the initial conditions used for the development of a method for this research were elucidated.

Table 3.4 Published methods of HPLC quantitation of efavirenz.

Column	Sample material	Mobile phase % v/v	Detection	Reference
C ₁₈ (100Å 4.6 mm i.d.) KinetexW, PhenomenexW, Torrance CA, USA	Blood plasma	75 % ACN and 25% water with pH adjusted to 3.2 using 0.1% formic acid.	UV at 247 nm	[342]

Shim-packVP-ODS. 150 x 4.6mm i.d	Efavirenz raw material	50% ACN and 50 % ammonium acetate buffer, pH 7.4.	UV at 246 nm	[343]
C ₁₈ Waters X-Terra Shield, RP18 50 x 4.6 mm, 3.5 µm		ACN and phosphate aqueous buffer pH 3.5	UV at 260 nm	[344]
Nova-Pak® cartridge	Tablets	55% ACN and 45% phosphate buffer at pH 4.5	ECD detector at +1400 mV and 1.0 µA 252 nm	[345]
C ₁₈ , 250 mm x 3.9 mm i.d, 10 µm	Tablets	70% ACN and pH adjusted aqueous phase orthophosphoric acid (0.1%).		[346].
Zorbax SB CN, 250 × 4.6 mm i.d, 5 µm		Methanol (A) and buffer at pH 4.5(B) using the gradient: 0–10 min (90% B), 10–22 min (35% B), and 22–25 min (90% B).	UV at 260 nm	[58]
C ₁₈ Waters Spherisorb® 5 µm ODS	Polymer-lipid nanoparticles	70% ACN and 30% 10 mM phosphate buffer at pH 6.8.	UV at 246 nm	[347]

The methods of analysis of EFV have been reported in raw material, tablets, plasma, and polymer-based lipid nanoparticles among many other types of materials not listed in the table. Of the methods described in literature, a significant number used a hydrophobic C₁₈ column with a mobile phase of an acidic buffer with ≥ 50 % organic solvent of either acetonitrile or methanol. Most methods were isocratic with UV detection at 246, 247 or 260 nm. Preliminary experiments were performed to select an internal standard, mobile phase composition, determine system and column suitability. Method optimization was then undertaken using response surface and statistical analysis to locate an optimal point for the analysis. During optimization, retention time, peak resolution and peak tailing responses were monitored to ensure that the analysis time was short, peak resolution was greatest and that the peaks had lowest peak tailing. A CCD was developed using Design-Expert version 12.0 software (Stat-Ease Inc., Minneapolis, MN, United States of America). The method was validated according to the ICH guidelines for accuracy, precision, linearity and range, limits of detection (LOD) and quantitation (LOQ) [348,349].

3.3.1 Statistical design of experiments

The use of statistical design of experiments (DoE) is an efficient approach for planning and conducting experiments in order to make valid, objective conclusions to be derived from the data generated thereby preventing false assumptions [350]. Well-chosen experimental designs maximizes the information that can be generated for defined experimental effort. DoE commences with determination of the objectives of an experiment and selecting input factors to be evaluated in that study. Experimental design involves assessment and multivariate optimization of the experimental conditions for, in this case a reversed phase HPLC analytical method for EFV. The factors derived using DoE can easily be optimized using a Quality by

Design (QbD) approach. QbD is a systematic approach that includes evaluation of multi-dimensional combinations of input variables using DoE to define the optimum conditions to meet predetermined goals whilst assuring quality by selecting and identifying critical quality attributes that can be optimized [351].

In the context of HPLC method development, factors that can be monitored then manipulated to produce the desired efficient HPLC method result in the input factors. These factors can be either be categorical or numerical, an example of factors for example is the type of organic solvent used in the mobile phase while numerical examples include temperature, pH of mobile phase and composition of organic solvent in the mobile phase.

The statistical theory underlying DoE generally begins with the concept of process models as to describe the dynamics of an experiment, a collection of all factors that may affect the output can be described by a Black Box Process model depicted in Figure 3.3 defined with k input factors and r outputs or responses which may be considered as critical quality attributes [352]. The process is a matrix of statistical and mathematical approaches that permits elucidation of the factors that have an impact on the response monitored (Y) and the influence on changes in the levels of input factors in an experimental domain or the process and design matrix. This approach facilitates an understanding of the relationship(s) between one or more measured responses viz., Y_1 (retention time), Y_2 (peak tailing) and Y_3 (peak resolution) and input factors, X_1 (% ACN), X_2 (column temperature) and X_3 pH of mobile phase. The primary purpose of using a sequential strategy is that first or second order polynomial mathematical relationships that describe the system can be elucidated.

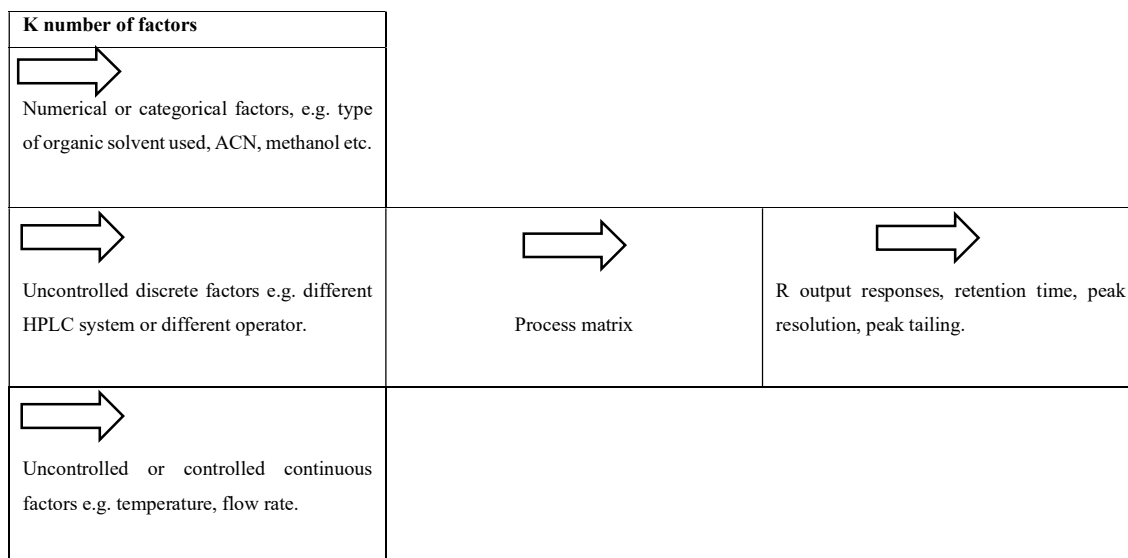


Figure 3.3. A 'Black Box' Process Model Schematic, with k = number of factors, r = number of output responses.

When the experimental data are analysed, all unknown parameters are identified and estimated, and the coefficients of the terms are tested to see determine those that are significantly different from zero. The most common empirical models to which experimental data are fitted take either a linear form or quadratic form and an example of a linear model with two factors viz., X1 and X2 is shown as Equation 3.8 [353].

$$Y = \beta_0 + \beta_1X1 + \beta_2X2 + \beta_{12}X1X2 + \varepsilon$$

Equation 3.11

Where,

ε = experimental error

β = coefficient of term(s)

X1 = % ACN

X2 = column temperature

A more complicated example of a linear model with three factors viz., X1, X2, X3 and one response, Y, is presented as Equation 3.9 [353]. if all possible terms were to be included in the model. Y is the defined response for given levels of the effects of the inputs X1 and X2 and the term X1X2 is included to account for possible interaction effect between X1 and X2 just as for X1X2X3 combined. The constant β_0 is the response of Y when both inputs are zero.

$$Y = \beta_0 + \beta_1X1 + \beta_2X2 + \beta_3X3 + \beta_{12}X1X2 + \beta_{13}X1X3 + \beta_{23}X2X3 + \beta_{123}X1X2X3 + \varepsilon$$

Equation 3.12

Where,

ε = experimental error

β = coefficient of term(s)

X1 = % ACN

X2 = column temperature

X3 = pH of buffer

3.3.2 Response surface methodology

The most relevant multivariate approaches used for in analytical method optimization is response surface methodology (RSM), RSM is a collection of mathematical and statistical

techniques based on the fitting of experimental data to linear or polynomial models to determine which best describes the data set with the objective of making statistical predictions [354]. RSM can be applied when a response or a set of responses of interest are influenced by multiple variables, the objective of RSM is to simultaneously optimize the input levels of variables to define optimum system performance, this can be exploited in the development of HPLC methods [355]. An optimized HPLC method is defined by independent and dependent categorical or numerical factors which will contribute to repeatable and reliable HPLC analyses. Categorical factors include the type of organic solvent in the mobile phase, column type and buffer type used. Numerical factors include amount of organic solvent and aqueous phase, pH and molarity of the buffer and temperature. The optimum separation is achieved when the levels of input variables used are located within maximum and minimum levels and can be modified to enhance the separation of analytes of interest. This approach is more efficient at achieving an optimized separation with fewer experiments than the use of the traditional approach of changing one variable at a time during method development [356].

RSM is generally performed to achieve a specific target, to maximize or minimize a response, reduce variability by locating the region where a process is easier to manage or ensure a process robust. Popular experimental designs are two-level designs since they are ideal for use for screening, are simple and result in economic approaches to data generation, the most popular approach used is based on a full factorial central composite design (CCD), which enables one to estimate the coefficients for second-order models [357]. The CCD contains an embedded factorial or fractional factorial design with centre points that is augmented with a group of axial points that allow estimation of curvature of the system [352].

3.3.3 RSM notation for 2-level designs

The standard layout for a 2-level design uses a +1 and -1 notation to denote the high and low level for each factor. The centre points determine the experimental error and how well the data can be reproduced. The axial points are taken in a way to ensure repeatability, and the model prediction variance is constant at every point equidistant from the centre of design [358]. By way of example an experiment in which 4 trials (or runs) are conducted with each factor set to high or low levels during a run according to whether the matrix has a +1 or -1 set for the factor during that trial is depicted in Table 3.5. A 2^3 design matrix with three factors and consequently eight trial runs is shown in Table 3.6 [359]. If an experiment had more than three input factors, there would be an additional column in the matrix for each additional factor therefore

increasing the number of design points to 2^4 (16) experimental runs, consequently, the number of runs rises exponentially as the number of factors evaluated in the design increases. This gives rise to the need for screening of the most relevant factors through literature and robust preliminary experiments to augment statistical DoE techniques.

Table 3.5 Central Composite Design for two factors, two-level full factorial design matrix (2^2) with two input factors (X1, X2)

Run	X1	X2
1	-1	-1
2	+1	-1
3	-1	+1
4	+1	+1

Table 3.6 Central Composite Design for three factors, two-level full factorial design matrix (2^3) with three input factors (X1, X2 and X3)

Run	X1	X2	X3
1	-1	-1	-1
2	-1	-1	+1
3	-1	+1	-1
4	-1	+1	+1
5	+1	-1	-1
6	+1	-1	+1
7	+1	+1	-1
8	+1	+1	+1

3.4 Experimental

3.4.1 Materials and methods

All chemicals were at least of analytical reagent grade and were used without further purification. Efavirenz was donated by Adcock Ingram[®] Limited (Wadeville, Gauteng, South Africa) and loratadine (LRT) which was used as the internal standard (IS) was donated by Aspen Pharmacare (Port Elizabeth, Eastern Cape, South Africa). Romil HPLC-grade acetonitrile UV cut-off of 195 nm acetonitrile was purchased from Microsep (2 Saturn Cres, Linbro Business Park, Gauteng, South Africa). Potassium triacetate, citric acid, potassium dihydrogen phosphate was purchased from Associated Chemical Enterprises (Southdale, Gauteng, South Africa) and sodium hydroxide pellets from Merck[®] Chemicals (Midrand, Gauteng, South Africa). HPLC-grade water was produce using a Direct-Pure[®] Ultrapure and

RO Water system, (RephiLe Bioscience, Ltd, Boston, United States of America) and consisted of a three-stage pre-filtration kit, RO membrane, tank vent filter with CO₂ remover, two RephiDuo pack cartridges and a 0.2 µm capsule filter. EFV tablets were purchased from a local pharmacy and the manufactures included, Adco-Efavirenz (Adcock Ingram Limited, Midrand, South Africa), (Cipla Medpro, Cape Town South Africa), Efavirenz (Aspen Pharmacare Limited, Woodmead, South Africa) and Erige by (Aurobindo Pharma Limited, Alberton, South Africa).

3.4.2 System and Instrumentation

The HPLC separation was achieved using a Waters® Alliance e2695 separation module equipped with an autosampler, an online degasser and a model 2489 UV-Vis Detector (Waters®, Milford, MA, USA). Data was acquired, processed and reported using Waters® Empower™ 3 software version 3.6.0. The separation of efavirenz and the internal standard loratidine was achieved under isocratic conditions using a Phenomenex® Luna 5 µm C₁₈ (2) 250 × 4.6 mm i.d column.

3.4.3 Preparation of stock solutions

The standard stock solutions of efavirenz and the internal standard were prepared by accurately weighing approximately 25 mg efavirenz and 10 mg loratidine using a Mettler® Model AE 163 analytical balance (Mettler® Inc., Zurich, Switzerland) into separate 100 mL A-grade volumetric flasks and the adding mobile of ethanol and water phase 70: 30 v/v solvent. The stock solutions were sonicated using a Model B12 Branson® ultrasonic bath (Branson Inc., Shelton, Conn, USA) for 5 minutes after which the solutions were made up to volume to produce a 250 µg/mL efavirenz and 100 µg/mL loratidine solution. The mobile phase was ACN and HPLC water in a 65:35 v/v ratio. The standard stock solutions were serially diluted to produce concentrations of 250, 150, 100, 75, 35, 17.5, 2.5 and 1.5 µg/mL. The internal standard was added to all calibration standards prior to analysis in concentration of 10 µg/mL. All solutions were protected from light using aluminium foil and stored at 4 °C in a refrigerator prior to use. The standard solutions were used within two days of preparation.

3.4.4 Preparation of buffer and mobile phase

0.15 M acetate buffer solutions were prepared by accurately weighing 1.002 g potassium triacetate and 0.784 g citric acid into a 500 mL A-grade volumetric flask and making up to

volume with HPLC grade water. The pH of the buffers was monitored using a model GLP 21 pH-meter (Crison Instruments, Barcelona, Spain at 25 °C and was adjusted to 4.5 using a 0.05 M potassium hydroxide solution or 0.05 M hydrochloric acid. Mixing and degassing of the buffer solution under vacuum was undertaken using a Model A-2S Eyela Aspirator degasser (Rikakikai Co., Ltd, Tokyo, Japan) and filtering through a 0.45 µm HVLP Durapore® membrane filter (Millipore® Corporation, Bedford, MA, USA) prior to use. Buffers were freshly prepared and used when HPLC analysis was performed.

3.5 Statistical modelling and optimization.

Three independent factors viz., percent acetonitrile in the mobile phase, pH of buffer and column temperature were the input factors used to build mathematical models for the responses monitored. A central composite (CCD) experimental design was used to study the response surface for the effects of these independent factors on the responses monitored. A desirability function was applied for simultaneous optimization of retention time, peak tailing, and peak resolution of EFV. Fisher's test for Analysis of Variance (ANOVA) was applied to assess the significance of differences, if any, of factors under investigation. The design space for three factors was set to a minimum and maximum for the numerical factors listed in Table 3.7. The variables and ranges initially selected were identified from literature and preliminary experiments. The ACN concentration (A) was kept at a minimum 65 % v/v and maximum 90 % v/v with respect to buffer content. The minimum value for column temperature (B) was set at 25° C and the maximum at 50° C. The minimum and maximum values for buffer pH (C) were 3 and 6 respectively. The influence of these factors on retention time, peak tailing and resolution were monitored and described using different plots.

Table 3.7 Design constraints for three percent organic phase, pH and temperature and associated levels with actual responses for minimum and maximum values obtained.

Variable/Response	Units	Factor/Response	Std. Dev.	Low	High
ACN	% v/v	Factor	0	65	90
Column temperature	°C	Factor	0	25	50
Buffer pH		Factor	0	3	6
Retention time	minutes	Response	0.812102	3.285	14.009
Resolution		Response	0.476482	1.59	8.688
Tailing factor		Response	0.0337216	1.002	1.155

A CCD design consisting of 20 experimental runs, with 14 axial points and 6 centre points was generated for these studies and the order and combination of variables is summarised in Table 3.8.

Table 3.83 Experimental conditions for the CCD with actual design values used and observed responses.

Run	Input factors			Response factors		
	ACN % v/v	Column temperature °C	Buffer pH	Retention time minutes	Resolution	Peak tailing
1	77.5	37.5	4.5	5.086	6.44	1.002
2	77.5	37.5	4.5	5.074	6.46	1.096
3	77.5	37.5	4.5	5.082	6.46	1.09
4	77.5	58.5224	4.5	4.46	6.76	1.091
5	77.5	37.5	1.9	5.167	1.59	1.1002
6	77.5	37.5	4.5	5.081	6.46	1.089
7	77.5	37.5	4.5	5.095	6.48	1.086
8	65	25	3	8.118	1.76	1.024
9	65	50	3	6.205	6.273	1.13
10	65	50	6	7.766	8.688	1.099
11	77.5	37.5	7.0	5.185	6.559	1.104
12	77.5	16.4776	4.5	5.094	6.471	1.093
13	77.5	37.5	4.5	5.088	6.423	1.105
14	90	25	6	3.994	6.191	1.107
15	65	25	6	7.981	5.345	1.113
16	56.4776	37.5	4.5	14.009	6.511	1.106
17	90	50	3	3.285	2.178	1.054
18	98.5224	37.5	4.5	3.82	4.844	1.155
19	90	25	3	3.994	5.559	1.1
20	90	50	6	4.02	4.926	1.117

3.5.1 Analysis of statistical data

The responses recorded for the CCD experiments were analysed. The retention time and peak resolution followed quadratic polynomial models, whereas peak tailing followed a mean model later discussed the specific response analysis section. Higher polynomial models were investigated only after simple linear polynomial models produced inadequate description and analysis of the experimental data. The predicted residual sum of squares (PRESS statistic value) is used to establish the suitability of each model in terms of data fitting and the model with the lowest PRESS is considered suitable for that response. The PRESS value analyses the prediction ability of models and the model with a minimum PRESS is usually considered the best predictive model for a specific set of data and is automatically suggested by the software [360].

Prior to analysis of the suggested model, residual analysis was undertaken to confirm that the assumptions for ANOVA analysis were met. For this purpose, diagnostic plots viz., Box-Cox and normal plots of residuals are generated to assess whether data transformation is necessary. Data transformation may be necessary to improve the applicability and usefulness of a applied statistical test [361]. ANOVA was used to evaluate model adequacy and fitness of the model.

The probability (p) value is used to establish if the responses monitored are statistically significant. The p-value is used to determine whether to accept or reject the null hypothesis, where a p-value < 0.05 implies that the model used is significant, and that the model term/s or in this case the input or combination of input factors) has a coefficient significantly different from zero and can be estimated [362]. The model F-value is used to determine the utility of a model and establish if that model best fits the data set in question. The F-value is a ratio of explained to unexplained variability where the explained variability is based on the value for R^2 and that for unexplained variability is based on $1 - R^2$ and each is divided by the corresponding degrees of freedom. The larger the F-value, the more useful the model [363]. The R^2 value for responses indicates the quality of the model and R^2 values approaching 1 reflect a good correlation between the observed experimental data and the model predicted response. Adjusted (Adj) R^2 values in close agreement with predicted R^2 values indicate reliability of a model [364,365]. Adequate (Adeq) precision is a comparison of the range of predicted values at the design points and the average prediction error. Adequate precision is also defined as the signal-to-noise ratio, where a ratio > 4 is desirable, and indicates that there is adequate model discrimination with that model [366].

3.5.1.1 Retention time

One of the objectives of any HPLC method is short analysis times, the retention time is one of the most important factors as it determines the run time of a method where shorter run times are preferred as solvent use is limited as is wear and tear of the HPLC system [367]. Following modelling and understanding of all input factors can assist in selecting a short analysis time. The retention time of EFV followed a transformed quadratic model which exhibited the lowest PRESS in comparison to those for the linear, cubic, and quartic models. The experimental data were automatically fitted to models by the software to linear, quadratic, cubic, special cubic, quartic and special quartic models. The best fit mathematical model was identified based on the comparison of statistical parameters of R^2 , adjusted R^2 and PRESS. The predicted residual sum of squares (PRESS) was used to establish the suitability of each model in respect of data fitting and the model with the lowest PRESS was identified as suitable for that response. The PRESS value analyses the prediction ability of models and the model with the minimum PRESS is usually considered the best predictive model for a set of data [368,369]. Based on this data therefore, retention time followed a quadratic model.

The R^2 value is a measure of the variance of the response variables and the closer the R^2 value is to one or > 0.9 , the smaller the standard deviation therefore the more accurate the response predicted by the model. The predicted R^2 is in reasonable agreement with the adjusted R^2 i.e., $< 2\%$ difference and therefore the model is adequate to navigate the design space. The Fit statistics summary is given in Table 3.9 for the suggested transformed quadratic model for retention time. The statistics summarized in Table 3.9 reveal a predicted R^2 value of 0.9080 which is in reasonable agreement with the Adjusted R^2 of 0.9770 with a difference < 0.2 .

Table 3.9 Fit Summary for retention time, transformed inverse Sqrt Constant: -0.5.

Source	Sequential p-value	Lack of Fit p-value	Adjusted R^2	Predicted R^2	
Linear	< 0.0001	< 0.0001	0.9014	0.8493	
2FI (2 factor interactions)	0.4020	< 0.0001	0.9023	0.8573	
Quadratic	0.0005	< 0.0001	0.9770	0.9080	Suggested
Cubic	0.2184	< 0.0001	0.9834	-0.1519	Aliased

Prior to ANOVA analysis of the model terms, diagnostic plots to determine if power transformations were required were reviewed and the Box-Cox plot at $\lambda = 1$ is depicted in Figure 3.4. This procedure finds the appropriate Box-Cox power transformation for a data set containing a response value divided among two or more groups. The data were eventually analyzed by a one-way ANOVA F-test (two or more groups). This procedure is often used to modify the distributional shape of the data so that the residuals are more normally distributed and/or the within-group variances are closer to equality. This is done so that tests and confidence limits that require normality can more appropriately be used. It cannot correct every data ill. For example, data that contain outliers may not be properly adjusted by this technique [370]. Without transformation at $\lambda = 1$ the blue line fell outside the 95 % confidence interval (red lines) which is the optimum range of the parabola where the estimated $\lambda = -0.37$.

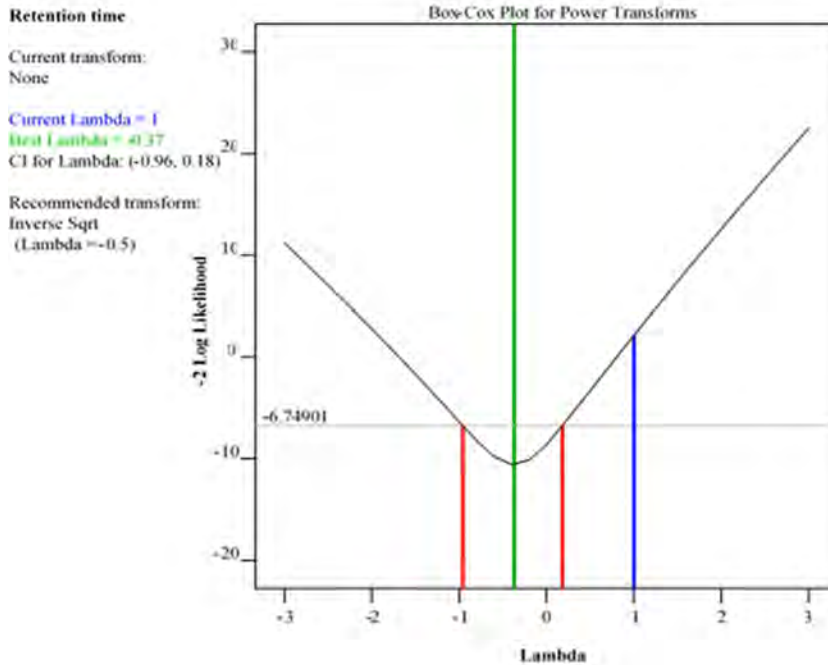


Figure 3.4. Box-Cox plot for the non-transformed quadratic model for retention time.

Analysis of the Box-Cox revealed that an inverse square root (sqrt) transformation with $\lambda = 0.5$ was necessary to fitting to the 95 % confidence interval between 0.8 and 0.26 for the statistical analysis [371]. An inverse sqrt transformation ($\lambda = -0.5$) was performed and the resulting Box-Cox depicted in Figure 3.5 was produced allowing for the $\lambda = -0.5$ to fall within the 95 % confidence interval of -0.8 and 0.26 . For a model to be adequate for navigating the design space, the λ must fall in the 95 % confidence interval, if not a transformation is recommended so as to ensure that the model provides an adequate approximation to the optimization process. After transformation the ANOVA analysis produced a Lack of Fit F-value of 90.7 implying that the Lack of Fit was not significant which is desirable for design space navigation.

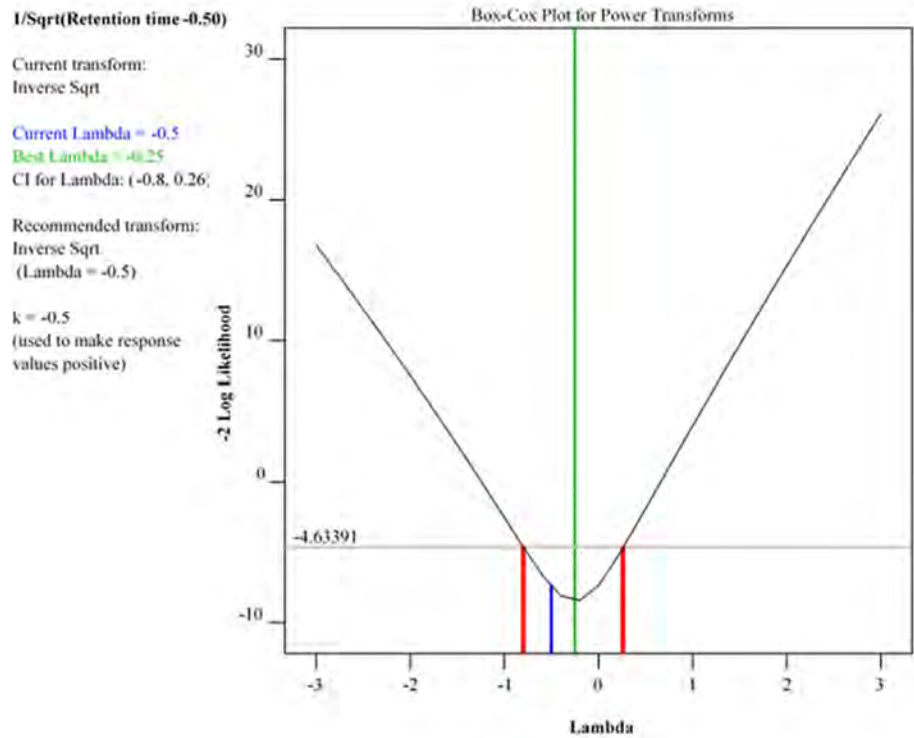


Figure 3.5. Box-Cox plot for the inverse square root transformed quadratic model for retention time.

The residual versus predicted response plots also did not show an obvious pattern as depicted in Figures 3.6. The plots reveal an almost equal scatter above and below the x-axis, implying that the proposed models were adequate i.e. the normality of distribution for ANOVA was met and there is no reason to suspect any violation of the independence or constant variance assumption.

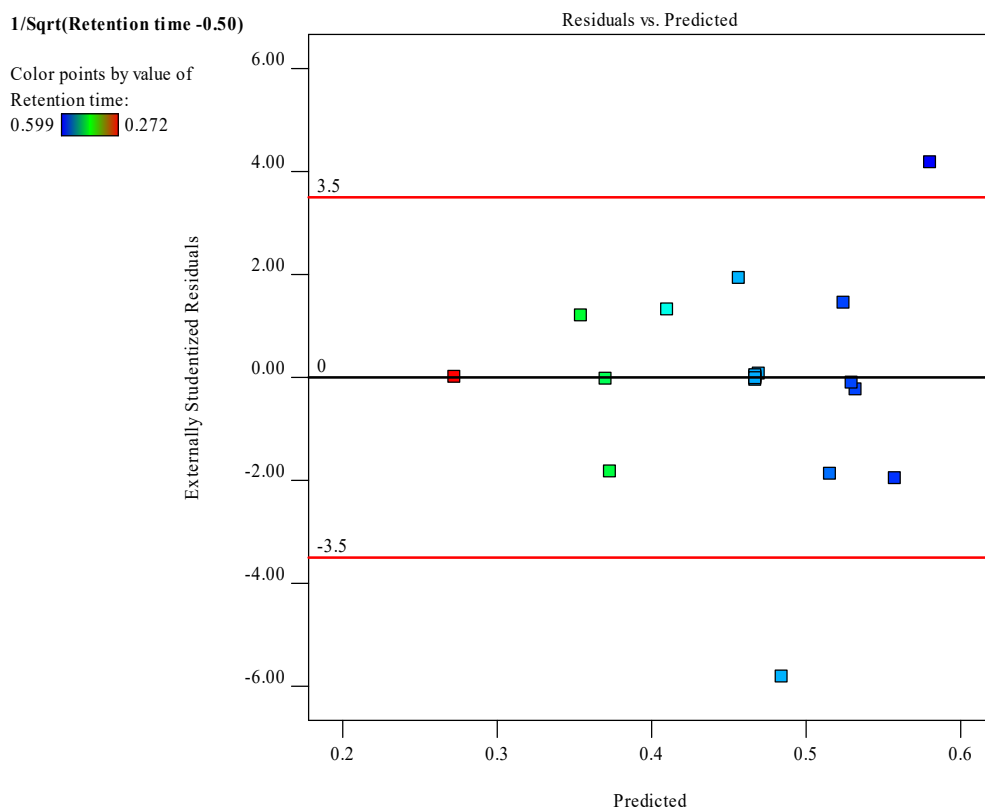


Figure 3.6. Plot of residual versus predicted and externally studentized residuals for the transformed quadratic model for retention time.

The normal plot of residuals for retention time is depicted is given Appendix 1 in Figure 7.1 was also used to confirm diagnostic testing. It was observed that data points generally fall on roughly on a straight line, indicating that the errors are normally distributed after transformation, thus supporting the fact that the model fits the data adequately.

The ANOVA data for the quadratic model for retention time are summarized in Table 3.10. The model F-value of 90.71 implies the model is significant and there is only a 0.01% chance that an F-value this large could occur due to noise. For each model term, p-values < 0.05 indicate that specific model term(s) are significant. In this case the terms A, B, C, BC, A² and B² are significant in other words % v/v ACN (A), buffer pH (B), column temperature (C), the combination of pH and column temperature (BC), A² and B² produced coefficients significantly different from zero and therefore had a significant effect on retention time.

Table 3.4. ANOVA data for retention time quadratic model, transformed sqrt, constant = -0.5

Source	Sum of Squares	df	Mean Square	F-value	p-value	
Model	0.1080	9	0.0120	90.71	< 0.0001	significant
A-% organic phase	0.0968	1	0.0968	731.97	< 0.0001	
B-Column temp	0.0025	1	0.0025	18.83	0.0015	
C-Buffer pH	0.0009	1	0.0009	6.95	0.0249	
AB	3.512E-08	1	3.512E-08	0.0003	0.9873	
AC	0.0001	1	0.0001	0.4504	0.5174	

BC	0.0017	1	0.0017	12.98	0.0048	
A ²	0.0043	1	0.0043	32.18	0.0002	
B ²	0.0012	1	0.0012	8.83	0.0140	
C ²	0.0000	1	0.0000	0.1558	0.7013	
Residual	0.0013	10	0.0001			
Lack of Fit	0.0013	5	0.0003	2012.00	< 0.0001	significant
Pure Error	6.573E-07	5	1.315E-07			
Cor Total	0.1093	19				

Due to the number of insignificant model terms the model was reduced by excluding model terms with p-values > 0.05 were excluded from ANOVA (Table 3.10) to produce a reduced surface response model. The Lack of Fit F-value of 2012.00 implies the Lack of Fit is significant and there is only a 0.01% chance that a Lack of Fit F-value this large could occur due to noise. The significant lack of fit could result in model prediction inaccuracies; however, this model was considered adequate to navigate the design space as it had an adequate precision > 4 which is desirable. The relationship between input factors and retention time is described mathematically using Equation 3.10.

$$\frac{1}{\text{Sqrt}(\text{Retention time} - 0.50)}$$

$$= -0.821694 + 0.024427A + 0.000241B + 0.030326C + 4.24E - 07AB$$

$$- 0.000146AC - 0.000781BC - 0.000110A^2 + 0.00058B^2 + 0.000532C^2$$

Equation 3.13

The results suggest that all input factors influenced retention time and therefore multiple interactions were observed. The effect of % ACN on retention time at pH 4.5 and column temperature of 37.5 °C is depicted in Figure 3.7. The % v/v ACN exhibited the greatest effect on retention time i.e. with the steepest slope of correlation. As the % v/v ACN was increased from 65 % v/v to 90 % v/v the retention time decreased from approximately 8 minutes to 4 minutes at 37.5 column temperature and a buffer pH of 4.5.

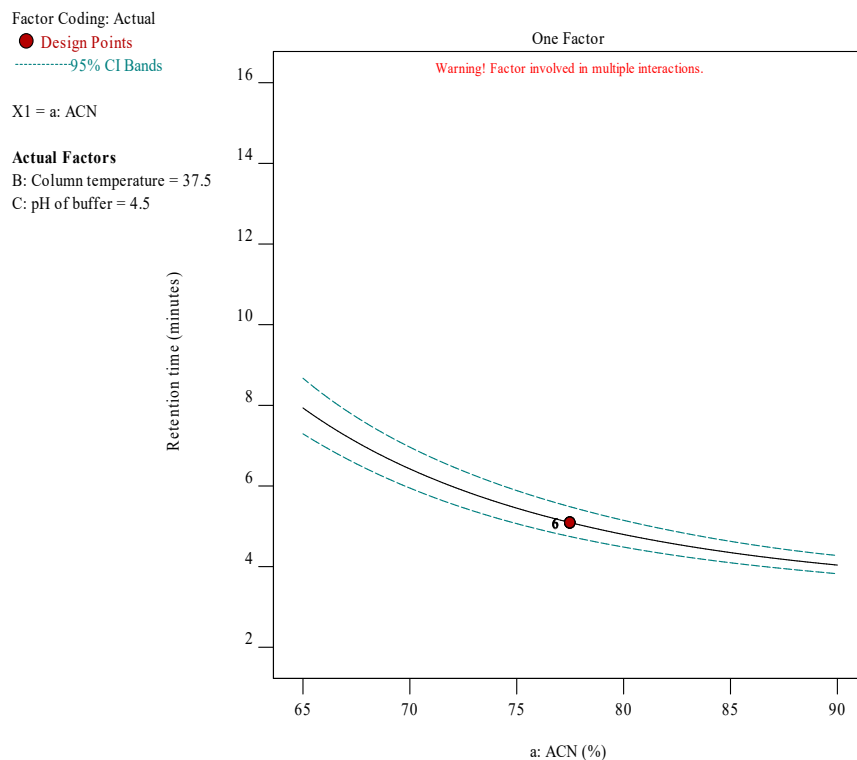


Figure 3.7. Effect of % ACN on retention time at pH 4.5 and 37.5° C

As the column temperature was increased, the retention time decreased slightly and as the buffer pH was increased from 3 to 6 the retention time increased slightly. Figure 3.8 shows a 3D response surface plot of the three factors and their effect on retention time. The longest retention time is observed 25° C and a composition of ACN of 65 % in the mobile phase, while higher temperatures and high composition of organic phase reduced the retention time significantly. Due to the hydrophobic nature of EFV, reduced % organic phase resulted in more aqueous phase in the mobile phase resulting in high retention times as the drug prefers hydrophobic environments.

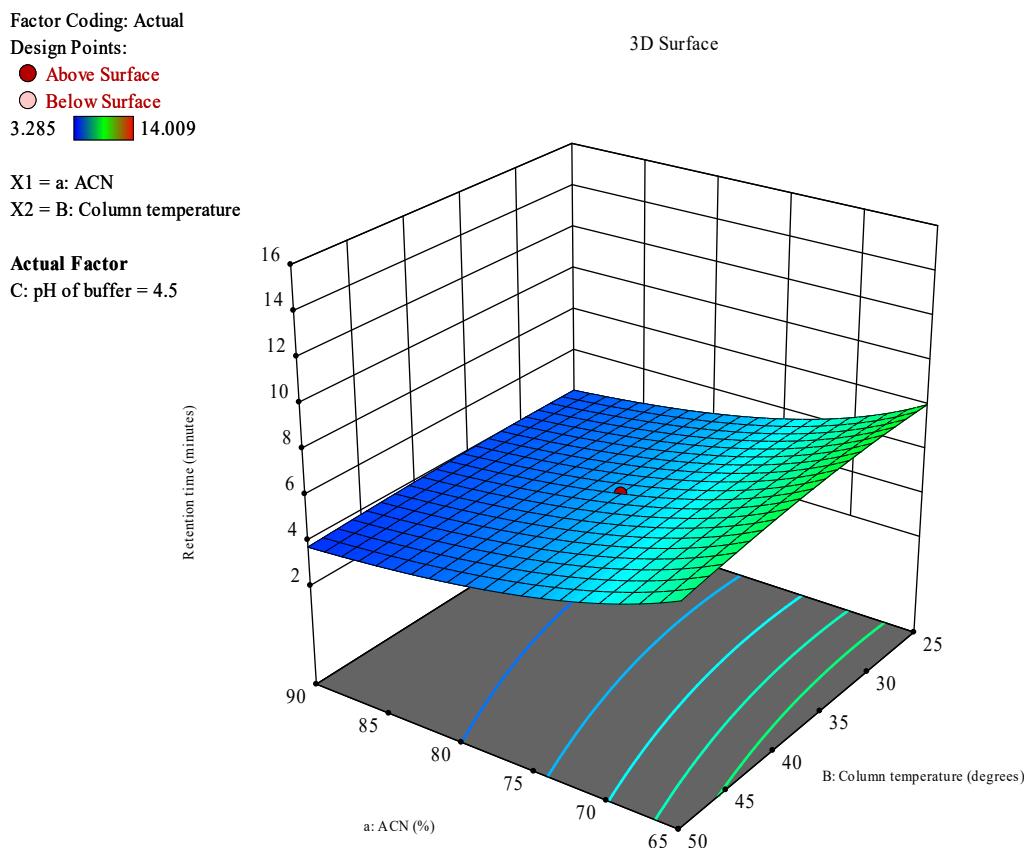


Figure 3.83. 3D surface response plot for peak retention time

3.5.1.2 Peak tailing

Peak tailing was analysed using ANOVA which revealed that peak tailing data did not fit a model and the mean estimate was adequate to represent peak-tailing with a factor of 1.093 which was, in this design space, a constant = 1.093 as reported in Equation 3.11.

$$\text{Peak tailing} = 1.09$$

Equation 3.14

The statistical data for this analysis are summarized in Table 3.11 and ANOVA data in Table 3.12. A negative value for Predicted R² implies that the overall mean might be a better predictor of the peak tailing factor than the current model. In some cases, a higher order model may be required for better prediction.

Table 3.11. Fitting statistics for peak tailing.

Std. Dev.	0.0337	Adjusted R²	0.0000
Mean	1.09	Predicted R²	-0.1080
C.V. %	3.09	Adeq Precision	NA
R²	0.0000		

Table 3.12. ANOVA data for peak tailing factor for a mean model.

Source	Sum of Squares	df	Mean Square	F-value	p-value	
Model	0.0000	0				
Residual	0.0216	19	0.0011			
Lack of Fit	0.0144	14	0.0010	0.7209	0.7123	not significant
Pure Error	0.0072	5	0.0014			
Cor Total	0.0216	19				

A p-value < 0.05 indicates model terms that are significant and in this case, there are no significant model terms and values > 0.05 indicate the model terms are not significant. The Lack of Fit F-value of 0.72 implies the Lack of Fit is not significant relative to the pure error. There is a 71.23% chance that a Lack of Fit F-value this large could occur due to noise. A non-significant lack of fit is good as we want the model to fit. The mean peak tailing factor of 1.09 was sufficient for this chromatographic separation and well below the 1.2 recommended by the ICH [372].

3.5.1.3 Peak resolution

Peak resolution data were best fitted by a quadratic model and the fit summary is given in Table 3.13. The fit statistics summarized in Table 3.13 reveals a predicted R² of 0.8941 which is in reasonable agreement with the adjusted R² of 0.9734 in other words the difference is < 0.2. Adequate precision measures the signal to noise ratio and a ratio > 4 is desirable and the observed ratio of 37.009 indicates an adequate signal indicating the model could be used to navigate the design space.

Table 3.13. Fitting statistics for the quadratic model for peak resolution.

Std. Dev.	2.66	Adjusted R²	0.9734
Mean	33.42	Predicted R²	0.8941
C.V. %	7.95	Adeq Precision	37.0093
R²	0.9860		

Diagnostic testing for model suitability was undertaken using Box-Cox plots for power transformation. The Box-Cox plot prior to model transformation is depicted in Figure 3.9 where $\lambda = 1$ (blue line) falls outside the 95 % confidence interval of 1.5 and 2.7 (red lines) in the optimum range of the parabola. A power transformation of $\lambda = 2.03$ was recommended and

when performed resulted the Box-Cox plot depicted in Figure 3.10 with the desired λ within a 95 % confidence interval.

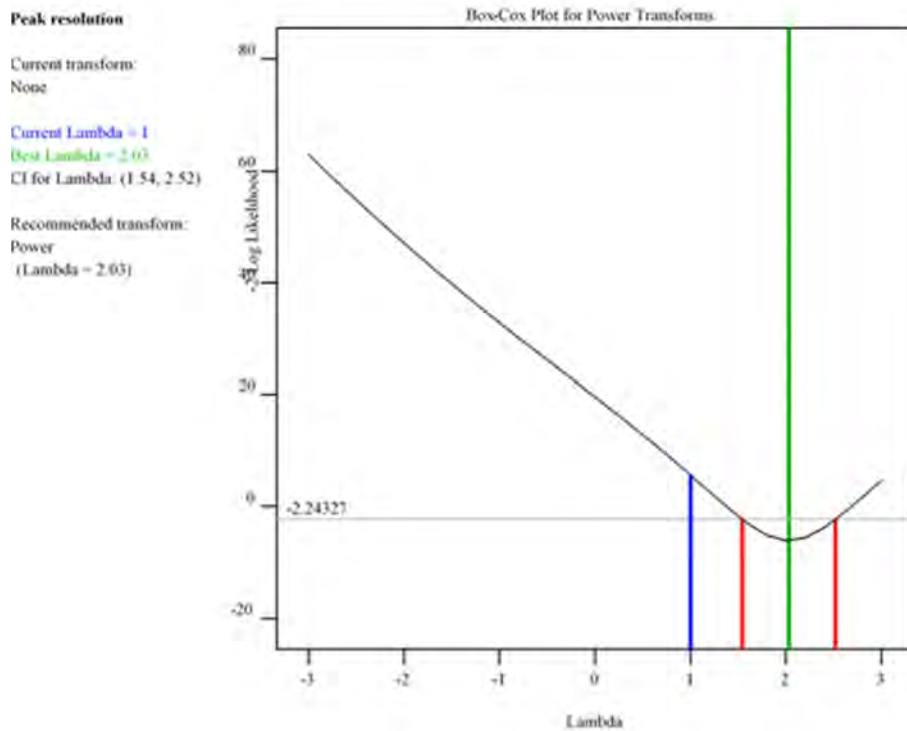


Figure 3.94. Box-Cox diagnostic plot for peak resolution quadratic model (non-transformed).

A power transformation ($\lambda = 2.03$) was performed, and the resulting Box-Cox depicted in Figure 3.10 was produced allowing for the $\lambda = 2.03$ to fall within the 95 % confidence interval of 1.54 and 2.52. The normal plot of residuals for retention time is depicted is given in Figure 3.11 also used to confirm diagnostic testing with that data points generally falling on roughly a straight line, indicating that the errors are normally distributed after transformation, thus supporting the fact that the model fits the data adequately. The residual versus predicted response plots also did not show an obvious pattern and the Figure is shown in Figure 7.4 of Appendix 1.

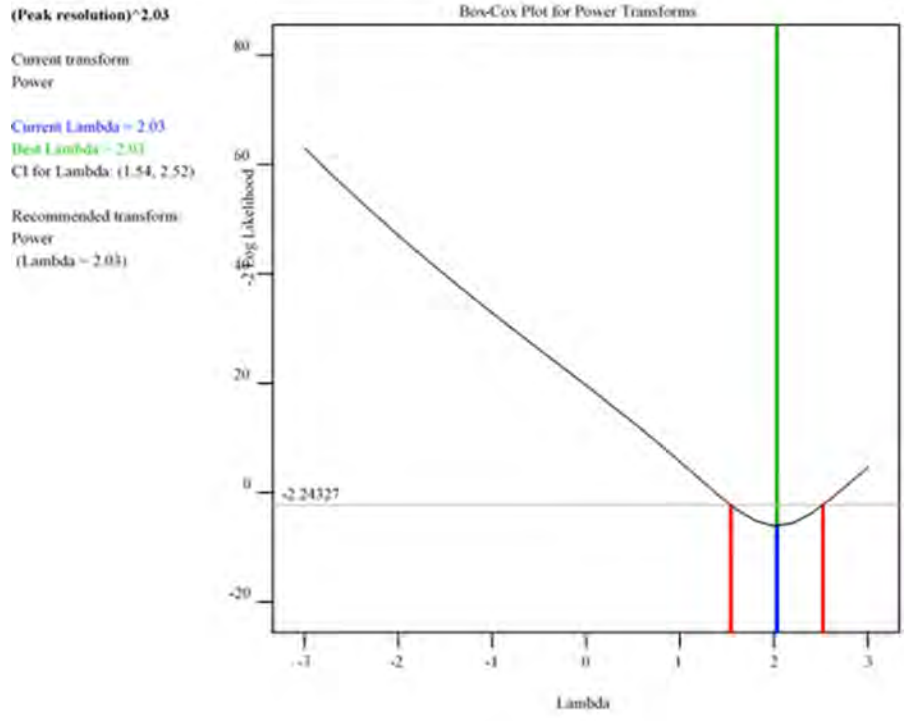


Figure 3.105. Box-Cox diagnostic plot for peak resolution quadratic model (power transformed).

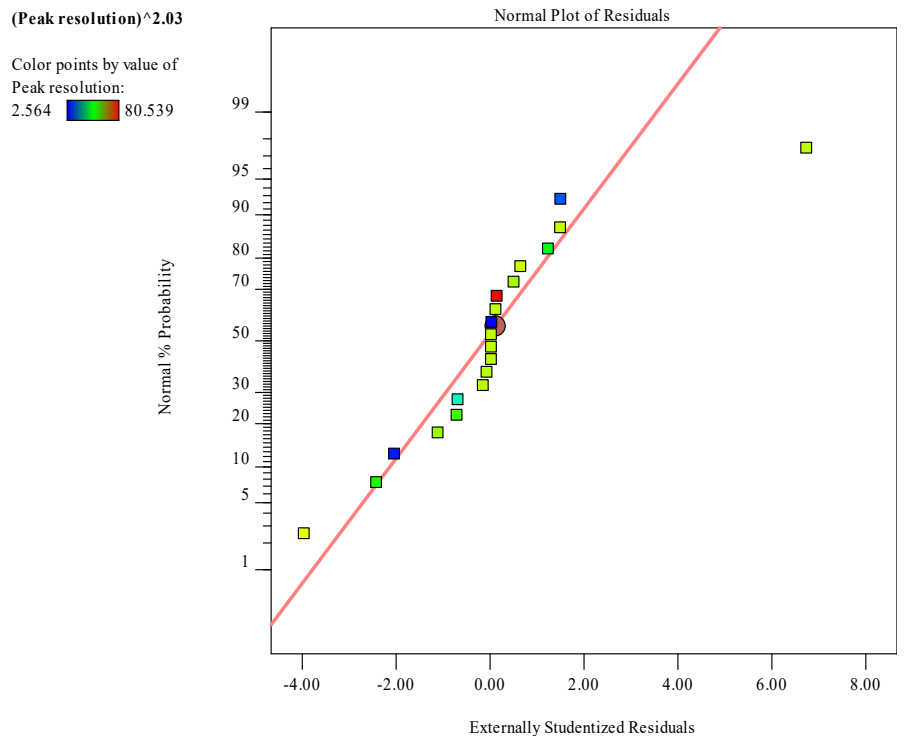


Figure 3.116. Diagnostics normal plot of residuals for peak resolution quadratic model (transformed).

ANOVA analysis of quadratic model data was undertaken and revealed a Model F-value of 78.35 which implies the model was significant and there was only a 0.01% chance that an F-value this large could occur due to noise. A p-value < 0.05 indicates significant model terms showing that all these factors influenced peak resolution. In this case the terms % ACN (A), column temperature (B) and pH of buffer (C), had significant model terms as summarized in Table 3.14. A value for $p > 0.1000$ indicates the model terms are not significant. Due to the number of model terms that were not significant, the model was reduced and model terms with p-values > 0.05 were excluded to produce a reduced response surface model for which the relationship between input factors and retention time is described mathematically using an actual equation.

Table 3.14. ANOVA quadratic model for peak resolution power transformed with lambda 2.03.

Source	Sum of Squares	df	Mean Square	F-value	p-value	
Model	4984.48	9	553.83	78.35	< 0.0001	significant
A-% ACN	426.87	1	426.87	60.39	< 0.0001	
B-Column temp	161.89	1	161.89	22.90	0.0007	
C-Buffer pH	1654.58	1	1654.58	234.08	< 0.0001	
AB	1745.65	1	1745.65	246.97	< 0.0001	
AC	136.08	1	136.08	19.25	0.0014	
BC	57.92	1	57.92	8.19	0.0169	
A ²	163.62	1	163.62	23.15	0.0007	
B ²	1.29	1	1.29	0.1825	0.6783	
C ²	674.26	1	674.26	95.39	< 0.0001	
Residual	70.68	10	7.07			
Lack of Fit	70.40	5	14.08	244.40	< 0.0001	significant
Pure Error	0.2880	5	0.0576			
Cor Total	5055.16	19				

A multiple interaction relationship was observed, % v/v ACN, buffer pH and column temperature each resulted in a significant effect on resolution. The minimum value for the resolution factor was 1.59 and the maximum 8.68 in the design space. The effect of % ACN and column temperature interaction relationship at pH of 4.5 is observed with the 3D response surface plot depicted in Figure 3.12. Specifically, resolution was observed to decrease with increasing % v/v ACN and decreased from approximately 7 to as the % v/v ACN increased from 65 % v/v to 90% v/v. Resolution increased from approximately 6 to 7 as the temperature of column increased from 25°C to 50°C. Of all parameters buffer pH of the buffer had greatest effect on resolution with an increase in pH from 3 to 6 resulting in the value for resolution increasing from approximately 5 to 7. The overall equation for resolution in mathematical terms is given in Equation 3.12.

$$\begin{aligned}
 \text{Resolution} = & -50.56 + 0.750A + 0.770B + 5.585C - 0.010002AB - 0.01747AC \\
 & + 0.0063BC - 0.002135A^2 - 0.000013B^2 - 0.400176C^2
 \end{aligned}$$

Equation 3.15

Factor Coding: Actual
 Design Points:
 ● Above Surface
 ○ Below Surface
 1.59  8.688

X1 = a: ACN
 X2 = B: Column temperature

Actual Factor
 C: pH of buffer = 4.5

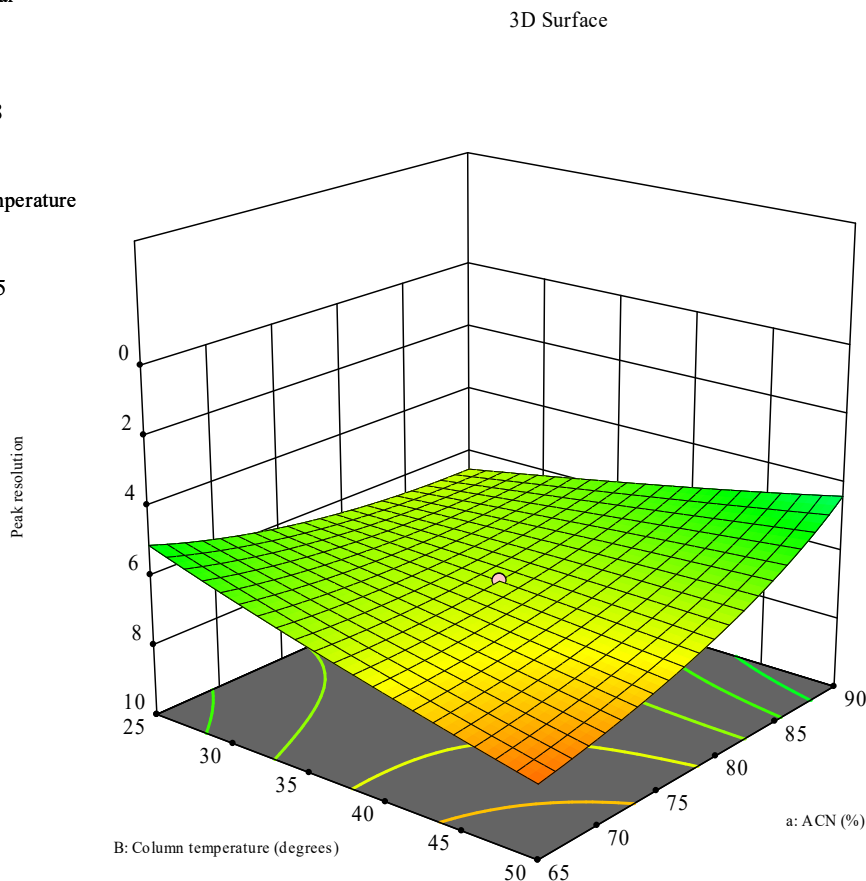


Figure 3.127. 3D Response surface plot showing the effect of % ACN and column temperature with a buffer of pH 4.5 on peak resolution

3.5.2 Optimization and point prediction

The models generated provide an approximation of the true relationship between the input variables and responses in the region of parameter levels known to affect the separation under development. The models were used to optimize the chromatographic separation by specifying the numerical values for each input factor investigated and these are listed in Table 3.15. The goal was a retention time for EFV of between 3 and 8 minutes. Peak resolution was set to maximise in the range 1.5 and 10. Similarly, peak tailing was set to minimise in the range between 1 and 1.2.

Table 3.15. Constraints for the optimization of the separation

Parameter	Goal	Lower Limit	Upper Limit	Lower Weight	Upper Weight	Importance
A: % v/v acetonitrile	in range	65 %	90 %	1	1	3
B: Column temp °C	in range	25	50	1	1	3
C: Buffer pH	in range	3	6	1	1	3
Retention time min	in range	3	8	1	1	3
Resolution	maximize	1.5	10	1	1	3
Tailing factor	minimize	0	1.2	1	1	3

Twenty-one potential solutions were generated based on the numerical optimization constraints set and a desirability value was associated with each and are listed in Appendix 1 in Table 7.1. Of all solutions, solution 3 exhibited the largest value for peak resolution at a relatively short retention time. Solution 3 conditions were therefore selected for validation and method application studies. The conditions for the chosen optimised method were, 80 % ACN, a buffer pH of 4.5 and column temperature of 40 °C at a flow rate of 1 mL/min. A retention time of 7.35 minutes was observed. Sharp symmetrical peaks were observed when using the optimized conditions and typical chromatogram of the separation is depicted in Figure 3.13. The prediction error of the model was calculated using Equation 3.13. The % RSD for retention time of EFV in relation to the predicted retention time was -12.04%, peak resolution -3.69 % and peak tailing value of 1.091. The low value for calculated prediction error indicates the applicability and robustness of the mathematical model used to determine the optimized conditions [373].

$$\text{Prediction error} = \frac{(\text{experimental value} - \text{predicted value})}{\text{experimental value}} \times 100$$

Equation 3.16

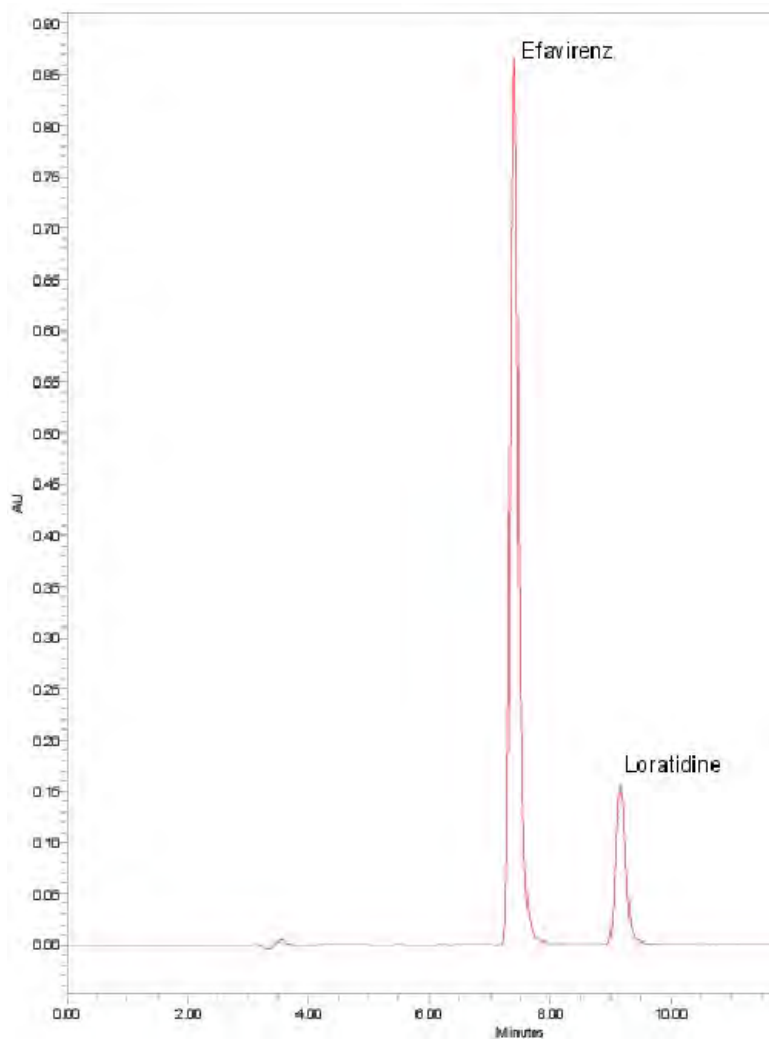


Figure 3.138. Chromatogram for the separation of EFV 250 $\mu\text{g}/\text{mL}$ and LRT 150 $\mu\text{g}/\text{mL}$

There were many solutions produced from the optimization criteria and also the overlay plot of the desired area where the optimization criteria were met is depicted in Figure 3.14 and the area shown in yellow, this show that only a small region of the design space in grey where the % ACN was < 67.5 % at pH 5.3 did not meet the criteria.

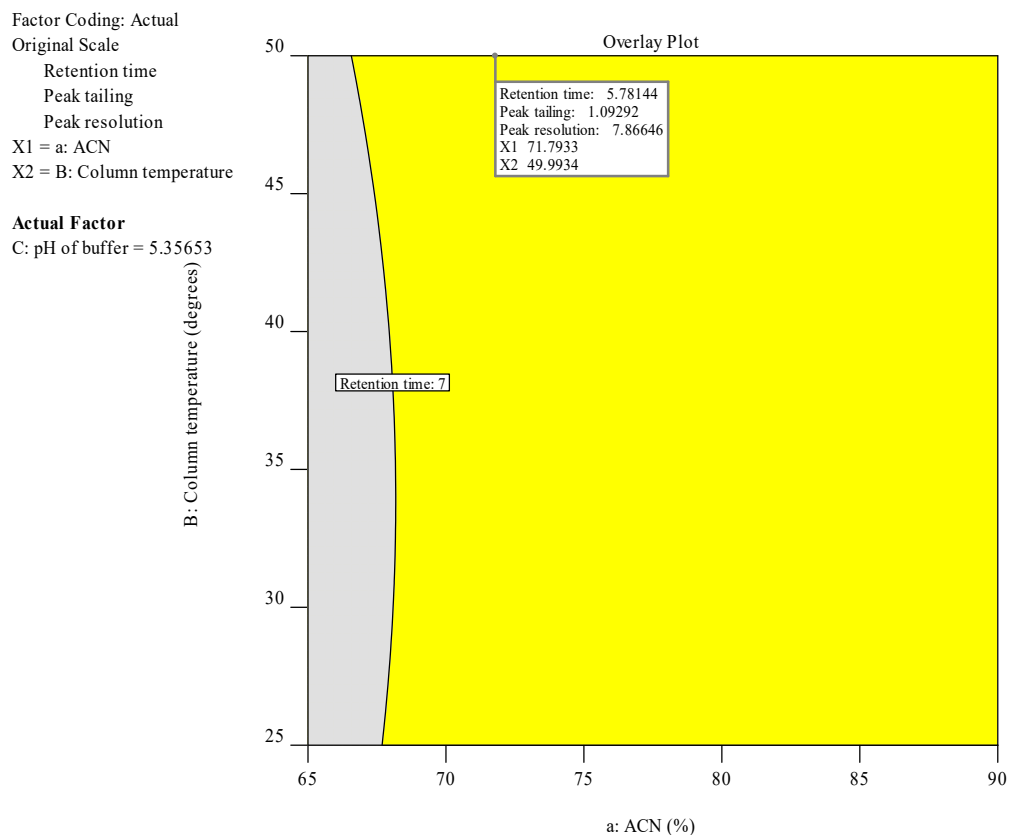


Figure 3.14. Overlay plot of the desirable area (yellow) derived using the specified optimization criteria listed in Table 3.14

3.6 Method validation

Validation of an analytical method is a process used to ensure the performance of the method meet the requirements of the method for its intended purpose [374]. Method validation includes an assessment of the adequacy of the analytical procedure using statistics, linear regression analysis and determination of the relative standard deviation. The method should be reliable, precise, accurate and robust when used by all analysts when using similar or equivalent instruments or conducting analysis on different days throughout the lifecycle of a product. Therefore validation parameters include accuracy, precision, linearity, range, limits of detection (LOD) and quantitation (LOQ), selectivity and be stability indication with system suitability assessed on daily basis, therefore the optimized method was validated according to ICH guidelines [375].

3.6.1 Linearity and Range

Linearity is defined as the ability of a method to produce test results that are directly proportional to analyte concentration over a specific range [376]. The mean peak area ratio of

EFV/LRT generated using the HPLC method was plotted against corresponding serially diluted concentrations to produce a calibration curve. The linearity of the calibration curve is depicted in Figure 3.15. To generate the calibration curve eight efavirenz standards over the concentration range from 17.5, 35, 70, 105, 140, 175, 227.5 and 280 µg/mL were analysed in triplicate, the table of results is reported in Appendix 1 in Table 7.2. Linear regression analysis resulted in an equation for the line $y = 0.0144x - 0.0579$, and the goodness-of-fit (R^2) was 0.9988 indicating a linear relationship exists between the concentration of analyte and ratio of area under the peaks.

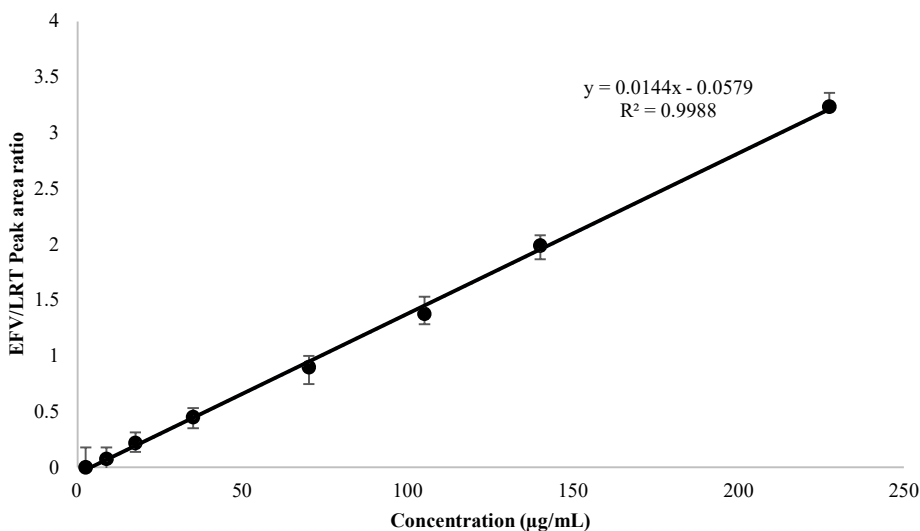


Figure 3.15. Typical calibration curve obtained by the chosen optimized HPLC conditions.

To establish the linearity of a method, a correlation coefficient ≥ 0.99 is considered sufficient over the tested range. The y-intercept should be $< 2\%$ of the concentration closest to zero. For this calibration curve the y-intercept was $y = 0.018\%$ of the response and therefore these data satisfied the criteria for linearity [377].

3.6.2 Precision

The degree of scatter of a set of data around a point is known as precision and is assessed using multiple injections of solutions of known concentration and evaluating the percent RSD around each point [378]. There are three levels of precision viz., repeatability or intra-day precision, intermediate or inter-day precision and reproducibility or robustness which evaluates the analysis between laboratories or analyses conducted by different analysts. The percent RSD tolerance level at all three levels of precision is set at $< 5\%$ for in vitro analysis [379,380].

3.6.3 Intra-day precision

Intra-day precision or repeatability studies are conducted to establish if an analytical method yields accurate and precise results when used under the same operating conditions or when experiments are conducted on the same day [381]. According to the ICH guidelines at least nine analyses are necessary for precision studies to be valid. For this study, repeatability was determined by analysing three different concentrations viz., 5, 25 and 100 µg/mL each sample prepared and analysed in triplicate, representing a low, medium and a high concentration respectively and calculating the % RSD at each concentration. The % RSD at all levels was ≤ 5 % and the results shown in Table 3.16 indicating that the method was repeatable, and the intra-day precision of the method is adequate.

Table 3.16. Intra-day precision data for analysis of EFV.

Efavirenz	Concentration µg/mL	Calculated concentration Mean ± SD µg/mL	% RSD
Low	5	4.87 ± 0.031	0.98
Medium	25	24.96 ± 0.19	1.14
High	100	100.94 ± 0.077	1.10

3.6.4 Inter-day precision

Intermediate precision is the variability in data that may occur when a method is used in the same laboratory at a different time or condition(s) [382]. The results of inter-day precision studies are summarized in Table 3.17. Inter-day precision experiments were undertaken on three consecutive days at three concentration levels, viz., low (5 µg/mL), medium (25 µg/mL) and high (100 µg/mL) as the average of 3 replicates. At all levels, the SD was < ± 1.05, the % RSD was < 5% indicating that the analytical method exhibited adequate intermediate precision.

Table 3.17. Inter-day precision data for EFV.

Day	Theoretical concentration µg/mL	Actual Concentration Mean ± SD µg/mL	RSD %
Day 1	5	5.27 ± 0.007	0.72
	25	26.03 ± 0.013	0.41
	100	98.8 ± 0.090	0.53
Day 2	5	5.14 ± 0.071	0.28
	25	23.7 ± 0.101	1.09
	100	101.8 ± 0.029	0.87
Day 3	5	4.79 ± 0.075	0.36
	25	24.8 ± 0.053	0.29
	100	102.4 ± 0.048	0.38

3.6.5 Accuracy

The accuracy of an analytical method is a measure of closeness of experimental data to an accepted reference [383]. The ICH recommends acceptance criteria for accuracy at % RSD < 5% determined at three different concentration levels. Three levels of EFV concentration samples of 5, 50 and 100 µg/mL were prepared in triplicate and analysed by HPLC against their theoretical concentrations. The resulting mean at each level and % RSD are given in Table 3.18.

Table 3.18. Accuracy results for RP-HPLC analysis of EFV (n=3)

Theoretical concentration µg/mL	Actual concentration mean ± SD	% RSD	% Bias
5.0	4.94 ± 0.18	1.07	- 1.21
50	50.31 ± 0.09	0.52	0.616
100	101.47 ± 0.12	0.98	1.47

Bias is a calculated measure of the extent of deviation of an experimental data set from the true value and is determined using Equation 3.14 [384]. The ICH acceptance criterion for % bias is < 2 %. The data summarized in Table 3.18 indicate that the method meets the criteria set for accuracy and bias. The resultant % RSD values were all < 5%, indicating that the analytical method is accurate and suitable for use, in addition, the largest value for % bias was 1.47 %, which indicates that no value deviated by > 5% of the stated value or theoretical value.

$$\% \text{ Bias} = \frac{\text{Actual value} - \text{Theoretical value}}{\text{Actual value}} \times 100$$

Equation 3.17

3.6.6 Limits of quantitation and detection

The limit of quantitation (LOQ) of an individual analytical procedure is defined as the lowest concentration of analyte that can be reliably measured using the analytical procedure [385]. The limit of detection (LOD) is the lowest concentration of an analyte in a sample that can be detected but not necessarily quantified using the experimental conditions of the analysis [386]. Signal to noise (s/n) ratios can be used to establish the LOQ and LOD, and ratios of 3:1 or 2:1 and 10:1 are used for these parameters, respectively [387]. The s/n ratio is calculated by dividing the peak height of a signal by the range of the baseline noise observed for the analytical method [375]. The LOQ is generally a compromise between the lowest concentration detected

or the sensitivity and acceptable precision and accuracy for the method. UV detectors generally exhibit diminished precision when monitoring low concentration samples due, in part, to a gradual loss of sensitivity of detector lamps as they age or due to different for different makes and models [388]. The LOQ can be determined based on the standard deviation of the response and the slope. The limit of quantitation may be estimated using Equation 3.16. The LOD was determined based on the standard deviation of the response and the slope of the calibration curve using Equation 3.15.

$$LOQ = \frac{10\sigma}{S}$$

Equation 3.18

$$LOD = \frac{3.3\sigma}{S}$$

Equation 3.19

Where,

σ = standard deviation of the response

S = slope of the calibration curve

The slope (S) is estimated from the calibration curve for the analyte and an estimate of σ may be determined by using a specific calibration curve with sample concentrations of the analyte in the range of the LOQ and LOD. The y-intercept of the least squares linear regression line may be used as the standard deviation [389]. The LOQ can be determined following sequential injection of samples prepared from a standard stock solution with decreasing concentration of the analyte of interest and the lowest standard concentration with a % RSD $\leq 5\%$ is the LOQ.

The LOQ and LOD were determined using the % RSD approach by analysing different concentrations of EFV (n=6) and the LOQ data were generated are listed in Table 3.19. A % RSD of $< 5\%$ was observed at 0.5 $\mu\text{g/mL}$, therefore this concentration was considered to be the LOQ. The LOD calculated as a third of the LOQ which was therefore 1.5 $\mu\text{g/mL}$.

Table 3.19 LOQ data for HPLC analysis of EFV.

EFV Concentration $\mu\text{g/mL}$	SD	% RSD
1	0.0418	0.85
0.75	0.0252	1.31
0.5	0.0143	2.86
0.25	0.0068	5.24
0.1	0.0170	6.07

3.7 Forced degradation studies

Forced degradation or stress studies are a crucial step for validation of methods. A stability indicating HPLC method must monitor changes in the chemical, physical, and microbiological properties of a compound over time [390]. The HPLC method must also be able to accurately quantitate the analyte without interference from degradation products and/or impurities [341]. Recommendations by regulatory authorities of analytical methods used in industry also invariably call for forced degradation studies such as for example that listed in the ICH drug stability test guidance Q1A (R2) where stress studies on a drug to establish its inherent stability characteristics to support the suitability of the proposed analytical procedure(s) are recommended [391]. In addition to establishing specificity, forced degradation studies also provide information relating to degradation pathways of a compound, structural elucidation of degradation products, determination of the intrinsic stability of a compound in a solution and solid state. Stress studies are used to determine the thermolytic, hydrolytic, oxidative, and photolytic degradation mechanisms of an active compound [392]. Forced degradation studies were conducted by exposing EFV to acidic, alkaline, neutral hydrolytic, dry heat and photolytic, conditions prior to analysis using the developed RP-HPLC method [393]. The degradation of API up to 10 % of the original label claim is set as the limit of stability and tolerance levels between 10 and 15 % degradation were set for this study [394]. HPLC analysis of EFV was performed with pure EFV sample and the chromatogram is depicted in Figure 7.5 in appendix 1.

3.7.1 Dry heat degradation

To perform dry heat stress studies, 250 mg efavirenz powder was weighed then placed on a glass petri dish, covered with aluminium foil then placed in an oven (Gallenkamp®, Loughborough UK) set at 90 °C for 8 hrs after which a 100 µg/mL stock solution was prepared by dissolving 10 mg of the EFV powder in 100 mL in an A-grade volumetric flask with 70: 30 ACN/H₂O v/v and analysed using the HPLC conditions in section 3.5.2. Approximately 99.65 ± 0.102 % of EFV was recovered i.e., not degraded.

3.7.2 Neutral Hydrolysis

Neutral hydrolysis studies were performed by refluxing an aqueous solution of API for 12 hours. 50 mL of 100 µg/mL solution of efavirenz was mixed with 50 mL of HPLC grade water,

the resultant mixture was refluxed at 70° C for 8 hours. The sample was allowed to cool down to room temperature before HPLC analysis. The extent of degradation under these conditions was determined and $98.89 \pm 0.273\%$ of EFV was recovered suggesting that EFV is quite stable under neutral degradation due to its nonpolar nature [395].

3.7.3 Acid degradation

As per ICH Q1A (R2) recommendation [372,396]. A 50 mL solution of 100 µg/mL efavirenz was refluxed with 50 mL 0.1 M HCL at 90 °C for 8 hours. The solution was allowed to cool to room temperature prior to HPLC analysis. The extent of degradation was somewhat slower in acidic conditions with $97.9 \pm 0.73 \%$ of EFV which was recovered.

3.7.4 Alkali degradation

A solution of 50 mL of 100 µg/mL efavirenz was refluxed with 50mL of 0.1 M sodium hydroxide (NaOH) at 90 °C for 8 hours. The solution was allowed to cool to room temperature (22 °C) prior to HPLC analysis. Degradation peaks observed on the chromatogram indicate that EFV is susceptible to alkaline hydrolysis with a $3.69 \pm 0.107 \%$ quantity of EFV recovered. Hydrolysis was rapid and the extent of degradation was more pronounced. At t = 0 hours only 8.3 % EFV was recovered with the resulting chromatogram, given in Figure 7.6 in appendix 1, and at t = 1.5 hrs only 4.5 % of EFV was recovered.

3.7.5 Temperature stress studies

Temperature stress studies were performed by exposing 100 µg/mL solution of EFV in 70:30 v/v ACN and water to heat at 80 °C for 8 hours using a Colora Model NB-34980 Ultra-Thermostat water bath (Colora, Lorch, Germany) and allowed to cool to room temperature (22 °C) prior to HPLC analysis. Degradation was observed with $46 \pm 0.89 \%$ of EFV recovered, the resulting HPLC chromatogram is given in Figure 7.7 in appendix 1.

3.7.6 Oxidative degradation studies

Oxidation stress studies were performed using hydrogen peroxide as the oxidising agent. A 50 ml solution of efavirenz 100 µg/ml was refluxed with 50 mL 3 % v/v hydrogen peroxide at 70 °C for 8 hours. The mixture was cooled to room temperature (22°C) prior to HPLC analysis.

38.4 ± 1.34 % of EFV was recovered i.e., not degraded, the resulting HPLC chromatogram is depicted in Figure 7.8 in appendix 1.

3.8 Application of method

3.8.1 Assay of efavirenz containing tablet dosage form

Branded efavirenz tablets 600 mg were used for the assay. Twenty tablets were weighed using a Mettler Toledo balance (Mettler® Instruments Inc, Zurich, Switzerland) and crushed using a mortar and pestle. An amount equivalent to 10 mg of efavirenz was weighed and dissolved in 100 mL of an ACN: Water mixture (35: 65) v/v in an A-grade 100 mL volumetric flask. The resulting solution was filtered twice using Millipore® automation compatible 0.45-µm PVDF membrane syringe filters from (Merck Group, Darmstadt, Germany) then analysed using RP-HPLC. A summary of the results is presented in Table 3.20.

Table 3.20. Assay data of efavirenz containing tablets.

Product	Theoretical efavirenz	Actual efavirenz	RSD % (n=3)
Aspen	10	9.92	1.021
Erige	10	9.98	0.965
Adcock	10	10.02	0.084
Cipla	10	9.94	0.994

3.9 Conclusions

A reversed phase HPLC method for the in vitro quantitation of EFV was successfully developed, validated and subsequently applied to the assessment of commercially available dosage forms. The linearity of the EFV/LRT peak area ratio versus EFV concentration was demonstrated and statistical analysis proved that the method is repeatable for the analysis of EFV as raw material drug and in pharmaceutical formulations producing a separation that was free from interference by the excipients. The method was also linear and precise, and the total chromatographic run time was under 8 minutes which permits the analysis of a large number of samples in a short period of time. LRT was selected for use as the IS due to its retention time relative to that of EFV. The chromatographic conditions yielded sharp, symmetrical peaks with a high degree of resolution between EFV, and LRT were well separated and resolved, and the retention times were approximately 4.4 and 6.3 minutes, respectively.

RSM is a collection of mathematical and statistical techniques that are used to model and to analyse problems in which input variables affect outputs or responses. Of the types of RSM available, a CCD approach was adopted and used to evaluate several input variables that affected analytical method performance. During method development, ACN content (X1), buffer pH (X2) and column temperature (X3) were investigated as input variables in twenty experiments. Their impact on three critical quality attributes of the separation viz. retention time of EFV (Y1), resolution of EFV (Y2) and tailing of EFV (Y3) were investigated.

The results of statistical analysis revealed that the models used to fit the data are suitable to navigate the design space. 3D response surface plots facilitated the explanation of the interactive effects of input variables on the responses monitored and predicted values were in good agreement with experimental values. The ACN content had a significant effect on the retention time for EFV and the peak resolution between EFV and LRT. As ACN % increased, the retention time decreased. The pH of the buffer had a significant impact on the retention time for EFV. As the pH of the buffer increased, the retention time also increased. An increase in column temperature resulted in a slight decrease in the retention time.

The solution chosen from optimization criteria had chromatographic conditions that required a mobile phase of a mixture of ACN and 5mM tri-acetate buffer (pH 4.5) in an 80:20 % v/v ratio respectively delivered at a flow rate of 1 mL/min. The optimised method was validated according to ICH, USP and FDA guidelines and forced degradation studies were performed. EFV was observed to be relatively stable under dry heat stress, acid degradation and neutral hydrolysis but significant amounts of EFV were degraded under alkali conditions, high temperature in solution and oxidative stress studies. Commercially available EFV tablets were successfully analysed. The main advantage of this method over existing methods is its simplicity, low cost and speed which renders it applicable for use in low-income areas. This method was applied to the evaluation of the API content and release of EFV SEDDS during formulation development and assessment studies.

CHAPTER 4

PREFORMULATION STUDIES FOR THE DEVELOPMENT OF EFAVIRENZ LOADED SEDDS

4.1 Introduction

Pre-formulation studies are performed to identify incompatibilities between an Active Pharmaceutical Ingredient (API) and potential excipients since incompatibilities such may have significant implications for long term stability, dissolution and bioavailability of the API [397,398]. Pre-formulation studies are an important component of risk management required by regulatory agencies where understanding and identifying critical raw material attributes necessary for the successful development of an optimised dosage form [399,400]. Pre-formulation studies may minimize the risk of unexpected stability or incompatibility occurring during product development thereby avoiding an increase in the time and cost of product development activities [401].

Pre-formulation aim to detect and identify different types of interaction between an API and potential excipients including but not limited to physical interactions which are usually difficult to detect when formation or destruction of chemical bonds in a compound are not evident [402]. Physical interactions may affect the manufacturing process or manifest as a change in taste, colour, and smell of an API and may be due to crystallization and/or segregation of a product following manufacture. Chemical interactions between an API and potential excipients may affect the stability of a product and consequently result in degradation, polymorphic transitions, oxidation, hydrolysis, dehydration, isomerization, photolysis or esterification which are some of the common chemical interactions that have been observed between an API and potential excipients [403,404]. During pre-formulation activities the solubility, melting point and other physicochemical properties of excipients and API should be identified as these may be used to elucidate potential incompatibilities or manufacturing challenges as different molecular conformations of an API may exhibit different interactions with excipients inducing different therapeutic activity or instability with reduced performance of the formulation or product a direct consequence thereof [405].

Despite the importance of pre-formulation studies, no universally accepted protocol is available. Several spectroscopic techniques have been used for such activities including Fourier Transform Infrared Spectroscopy (FTIR), Raman spectroscopy and X-ray diffraction (XRD)

for identification of amorphous, crystalline and polymorphic forms of an API [406–408]. Different crystalline, amorphous, and hydrate forms of a compound may display different physical, thermal, dissolution and bioavailability characteristics to each other [283,409]. FTIR spectroscopy detects vibrational changes, if any, and a reduction in peak intensity, appearance of new absorption bands, or the disappearance of signal peaks may indicate the existence of potential interactions between an excipient and API or be evidence of potential intermolecular interactions between the components of a dosage form [410]. Raman spectroscopy and XRD are valuable for distinguishing the presence of different phases or polymorphs as a consequence of by their unique diffraction pattern. Since the choice of polymorph is important in relation to properties such as solubility, bioavailability and stability it is vital these be identified during pre-formulation activities [140,411].

4.2 Screening and selection of excipients

Excipients typically form the majority of a dosage form, consequently knowledge and characterization of excipients is necessary to predict dosage form performance attributes [412]. The performance criteria to be met by excipients for different routes of administration are outlined in the United States Pharmacopoeia (USP), European Pharmacopoeia (pH.Eur.) and Japanese Pharmacopoeia (JP) including quality attributes and test procedures required to assure the quality of pharmaceutical products in which they are used [413–415]. The guidelines recommend that all materials must be non-toxic, safe and physiologically inert and must be generally regarded as safe (GRAS) materials [416].

Knowledge of excipient performance can be used to justify selection of quality attributes of an excipient, product and product specifications [417]. The solubility of an API in excipients is an important factor that can be determined experimentally using thermodynamic and kinetic solubility approaches. Since most API are developed for oral administration, adequate aqueous solubility vital to ensure bioavailability and small unit doses are preferred from a patient convenience and adherence perspective [418]. The selection of excipients for SEDDS formulations is dependent on the ability of excipients to solubilise API in addition to their capability to self-emulsify in with the surfactant used [419,420]. The intended target, dosage form, route of administration and release profile must be considered when identifying and selecting excipients [415,421]. The optimum combination and quantity of excipients are of critical importance for the assurance of performance of a formulation or product. Furthermore

the API and the excipients should exhibit no physical or chemical interactions with packaging materials or the equipment to use during manufacture and quality control analyses [422].

4.2.1 Vegetable oil triglycerides

Crude edible vegetable oils are relatively cheap, readily available products of green chemistry with functional food properties that exhibit numerous health benefits for patients and have been used in LBDDS [423]. Grapeseed, flaxseed and soybean oil are rich in poly-unsaturated fatty acids including α -linoleic acid which is positively associated with cardiovascular health due to down-regulation of low-density lipoprotein cholesterol production [424]. Flaxseed oil is a source of, viscous fibre and phytochemicals such as lignans and protein that have demonstrated clinical activity and is one of the six plant materials currently under investigation of as a cancer-preventive food [425]. Diets rich in α -linoleic acid inhibit lymphocyte proliferation and the immune response in healthy humans and thus may be beneficial to individuals that present with autoimmune disorders [426]. Epidemiologic studies reveal little evidence to suggest that vegetable oils contribute to cardiovascular disease, cancer, or inflammation, nevertheless, consumption of these in quantities higher than recommended must be carefully considered since insufficient data to adequately evaluate adverse effects at higher levels of intake exists [427].

Vegetable oils are primarily comprised of triglycerides which are classified according to the fatty acid chain or hydrocarbon chain length which may range between 4 and 28 carbons. Fatty acids of < 6 carbons are short chain, between 6 and 12 carbons are medium chain and from 13 to 21 carbons) are long chain compounds [428]. The typical compositions of some selected vegetable oils are summarized in Table 4.1 as average amounts taken from various literature where, saturated fatty acid (SFA), mono-unsaturated fatty acid (MUFA) and poly-unsaturated fatty acid (PUFA) content are listed.

Table 4.5 Typical composition of some common vegetable oils, * = < 2 % Adapted from [429–431].

Fatty acid composition (% w/w)	SFA			MUFA		PUFA	
	Palmitic	Stearic	Palmitoleic	Oleic	Eicosenic	Linoleic	Linolenic
	C _{16:0}	C _{18:0}	C _{16:1}	C _{18:1}	C _{20:1}	C _{18:2}	C _{18:3}
Flaxseed oil	6	*	*	19	*	14	50
Soybean	10	4	*	18	0	55	13
Macadamia oil	13	*	36	51	2	*	*
Grapeseed oil	6	3	*	14	*	74	*
Olive oil	16	2	*	62	*	16	*
Sunflower oil	6	3	0	17	0	74	*
Canola oil	5	2	*	55	*	24	8

The distribution and fatty acid content of oils differs depend on the source plant and process technology used for the production therefore chemo-metric and principal component analysis was undertaken to evaluate oils [432]. Soybean oil is composed of five fatty acids viz., palmitic (16:0), stearic (18:0), oleic (18:1), linoleic (18:2) and linolenic acids (18:3). The percent composition of these fatty acids was 10%, 4%, 18%, 55%, and 13%, respectively on average of which the principal component linoleic acid constitutes the largest proportion [433]. Olive oil is constituted of oleic C_{18:1} in compositions of between 55 % and 83 % [434]. Linoleic acid is the predominant fatty acid in sunflower seed oil and grapeseed oil constituting > 60% of the total composition with approximately 8-15% saturated fatty acids which is mainly palmitic and stearic acid [435,436].

Vegetable oil triglycerides structures have three hydrocarbon chains linked to a glycerol backbone by ester bonds and long chain saturated triglyceride stearic acid denoted C_{18:0} i.e. 18 carbons and zero double bonds is depicted in Figure 4.1.

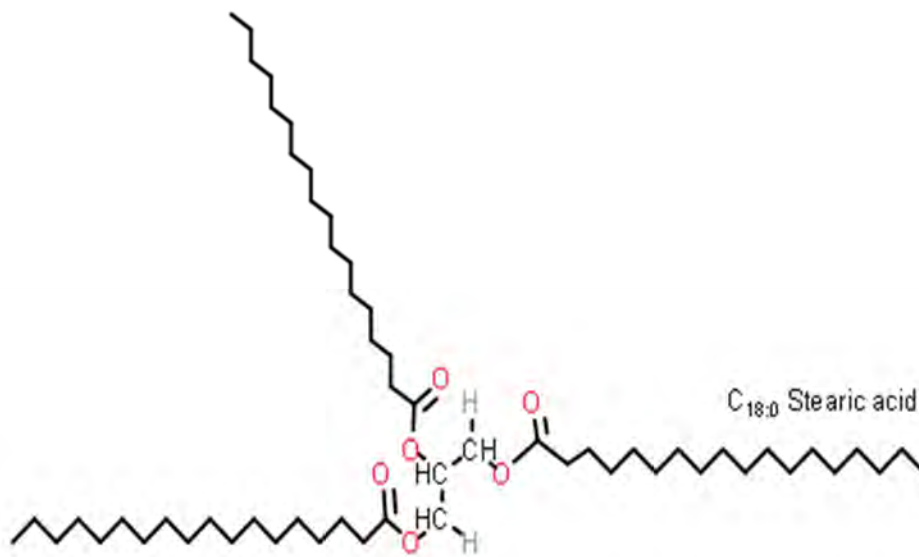


Figure 4.19. Schematic representation of the structure of stearic acid triglyceride, saturated hydrocarbon chain with zero (0) double bonds.

The chain length and saturation extent may play a crucial role in the characteristics of the emulsion system, the effect of these differences in chain length and saturation in vegetable oil may be confirmed as the reason why the oils may have varied dissolution capacity of each oil to EFV, and the fluidity of the emulsion formed. It is important therefore to assess such interaction of vegetable oil triglycerides with specific compounds for future reference in drug formulation development studies. MCT and LCT may also present with different transport routes where MCT are directly transported by the portal blood to the systemic circulation, whereas the LCT are transported via the intestinal lymphatics. The LCT are likely to augment the lymphatic transport of a lipophilic drug substance leading to enhance oral bioavailability [437]. The structure of mono-unsaturated triglyceride oleic acid C_{18:1} is depicted in Figure 4.2.

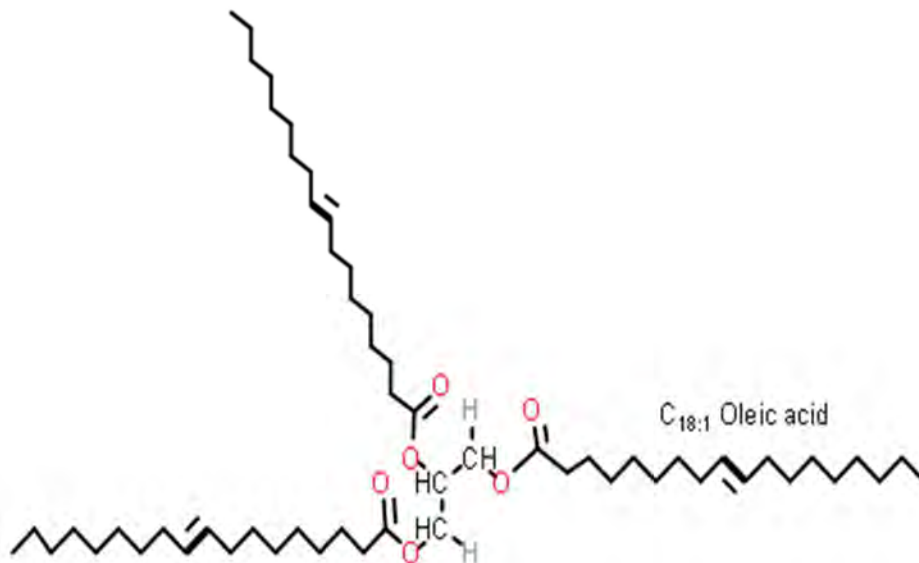


Figure 4.210. Schematic representation of the structure of oleic acid triglyceride, mono-unsaturated hydrocarbon chain with one (1) double bond.

The structures of poly-unsaturated linoleic triglycerides (C_{18:2}) and linolenic (C_{18:3}) acid are depicted in Figures 4.3 and 4.4 respectively.

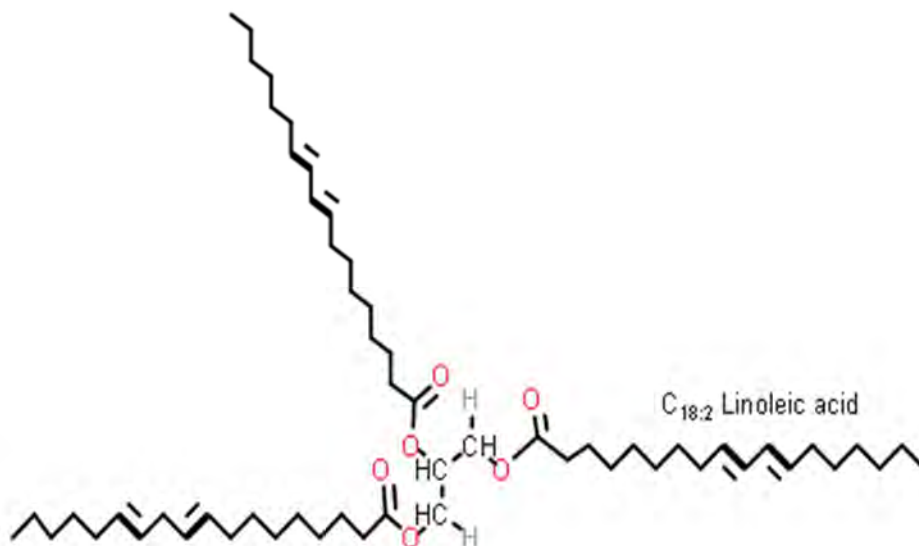


Figure 4.3. Schematic representation of the structure of the linoleic acid triglyceride, poly-unsaturated hydrocarbon chain with two (2) double bonds.

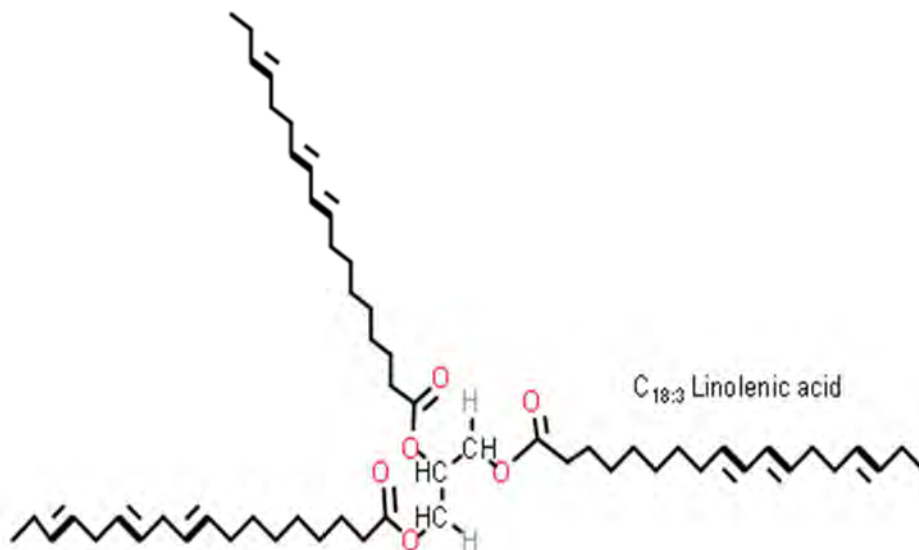


Figure 4.4. Schematic representation of the structure of linolenic acid triglyceride, poly-unsaturated hydrocarbon chain with three (3) double bonds.

Vegetable oils may also contain a wide range of minor components such as sterols, tocopherols, carotenoids, phenolic, chlorophyll, free fatty acids and other minor derivatives in addition to trace metal ions [438]. The intensity colour of the bulk oil depends on the presence of colouring pigments such as carotenoids and chlorophyll [439].

4.2.2 Surfactant mixture system

The surfactant system used is generally comprised of a surfactant and co-surfactant which ensures maximum solubility and miscibility of the components of the formulation system and are critical parameters to establish during pre-formulation activities as this translates to isotropy and dispersity indexes as described § 2.6.2. Non-ionic surfactants specifically Tween[®] 80 and Span[®] 20 are non-toxic profile and do not contain an ionisable group which makes these less sensitive to pH changes and the presence of electrolytes whilst minimizing interactions with cell membranes when compared to anionic and cationic surfactants [440,441]. Consequently non-ionic surfactants are preferred for oral and parenteral formulations because of their low tissue irritation and toxicity potential [204]. Polysorbates are emulsifiers used in pharmaceutical, cosmetic and food preparations to solubilize essential components or oils into water-based products. Polysorbates are oily liquids derived from ethoxylated sorbitan (a derivative of sorbitol) esterified with fatty acids, Tween[®] 80 has an HLB value of 15 and is water soluble whereas Span[®] 20 with a HLB value of 8.6 is oil soluble [442]. Organic solvents

such ethanol and propylene glycol are often used to improve the solubility of compounds, are readily available and easy to process however specific attention to safety issues, particularly in paediatric patients is required and adherence to regulatory guidelines as described in Chapter 2 a necessity [208,443]. Some properties of co-solvents such as ethanol which make it an antimicrobial preservative impart additional stability to emulsion systems [444].

4.3 Experimental

4.4 Materials

Cold pressed flaxseed, soybean, sunflower, olive, grapeseed and macadamia oils were purchased from Escentia products (Johannesburg, Gauteng, South Africa). Span[®] 20 and Tween[®] 80 were purchased from Merck (Johannesburg, Gauteng, South Africa). Ethanol was purchased from Anatech (Olivedale, Gauteng, South Africa). EFV was donated by Adcock Ingram[®] Limited (Wadeville, Gauteng, South Africa).

4.4.1 Solubility studies

The solubility of EFV in the different vegetable oils was determined by adding an excess of efavirenz to 5 mL of flaxseed, sunflower, soybean, macadamia, grapeseed and olive oil in Kimax[®] test-tubes sealed with a Teflon[®]-lined screw cap (DWK Life Sciences, Hattenbergstr, Mainz, Germany). The tubes were agitated with the aid of cylindrical BRAND[®] (Wertheim, Germany) PTFE 5 mm x 2 mm magnetic stirrer bars at 100 rpm for 48 hours at room temperature ($22 \pm 2^{\circ}\text{C}$) using an FMH STR-MH hot plate magnetic stirrer (Lasec[®] Group, Cape Town, South Africa). Samples were removed and centrifuged using a Damon IEC HN-SII centrifuge (Thermo Scientific, Waltham, MA, United States of America) at 3000 rpm for 15 minutes after which a 500 μL aliquot of the supernatant was collected and added to 50 mL ethanol and water in a 3:2 v/v ratio prior to filtration through a Millipore[®] automation compatible 0.45- μm PVDF membrane syringe filter from (Merck Group, Darmstadt, Germany). The concentration of EFV in the oils was determined using the validated HPLC method described in Chapter 3.

4.4.2 Phase behaviour and pseudo-ternary phase diagram construction

The water titration method was used to construct phase diagrams and identify the type of emulsions that result following emulsification in addition to characterizing the behaviour of mixtures along dilution paths [445]. Preliminary studies with mixtures of flaxseed oil and a Tween[®] 80 and Span[®] 20 surfactant 1:1 m/m mixture in 9:1, 4:1, 7:3, 3:2, 1:1, 2:3, 3:7, 1:4 m/m ratios and Winsor type I products with no isotropic regions were produced at $22 \pm 2^\circ \text{C}$ following 48 hours of incubation. Therefore, a surfactant, co-surfactant and co-solvent mixture was investigated for further phase behaviour evaluation. Surfactant solutions of Tween[®] 80, Span[®] 20 and ethanol were mixed using a Genie two vortex mixer (Scientific Industries Inc. [™], Bohemia, New York, United States of America) at 800rpm for 30 ± 2 seconds. Three surfactant mixtures viz., S1, S2 and S3 comprised of combinations of ethanol: Tween[®] 80: Span[®] 20 in 0.5:1:1, 1:1:1 and 1.5:1:1 m/m ratios were prepared and added to flaxseed oil to produce pseudo-binary solutions in 9:1, 4:1, 7:3, 3:2, 1:1, 2:3, 3:7, 1:4, 1:9 m/m ratios to produce surfactant and oil mixtures in Kimax[®] test-tubes (DWK Life Sciences, Hattenbergstr, Mainz, Germany). The pseudo-binary pre-concentrates mixtures contained no additional water. To minimize the effect of water, 500 mL > 98 % ethanol was placed in a Schott Duran bottle (DWK Life Sciences, Hattenbergstr, Mainz, Germany) containing 300g of 3A and 4A in a 1:1 m/m ratio as molecular sieve pellets from (B & M Scientific, Cape Town, South Africa). The bottle was sealed and kept at room temperature for 7 days [446,447]. The ethanol was then degassed under vacuum with the aid of a Model A-2S Eyela Aspirator degasser (Rikakikai Co., Ltd, Tokyo, Japan) and filtered through a 0.45 μm HVLP Durapore[®] membrane filter (Millipore[®] Corporation, Bedford, MA, United States of America) prior to use. Each of the ratios tested represent a dilution line from one to nine on the Gibbs phase triangle depicted in Figure 4.5 on which dilution line is depicted as red crosses. Water was added in $5 \pm 1\%$ increments to each pseudo-binary mixture following the titration chart summarized in Table 2 and after 48-hour incubation at room temperature, $22 \pm 2^\circ \text{C}$ the regions of the phase diagram were identified and characterized visually for Winsor behaviour prior to further characterization of pre-defined formulation attributes.

The titration chart and Gibb's triangle plots were developed using Triplot version 4.1.2 software (Todd A. Thompson, LA, USA). Points located within the phase diagram were observed and evaluated against Winsor phase behaviour descriptions viz., Winsor I, II, III and IV as described in Chapter 2. The data were plotted as a phase diagram and graphical overlay plot using a Triplot software spreadsheet. The resultant pseudo-ternary phase diagrams for

surfactant mixtures S1, S2 and S3 are a representative sample of the types of structures that form when different amounts of ethanol are used.

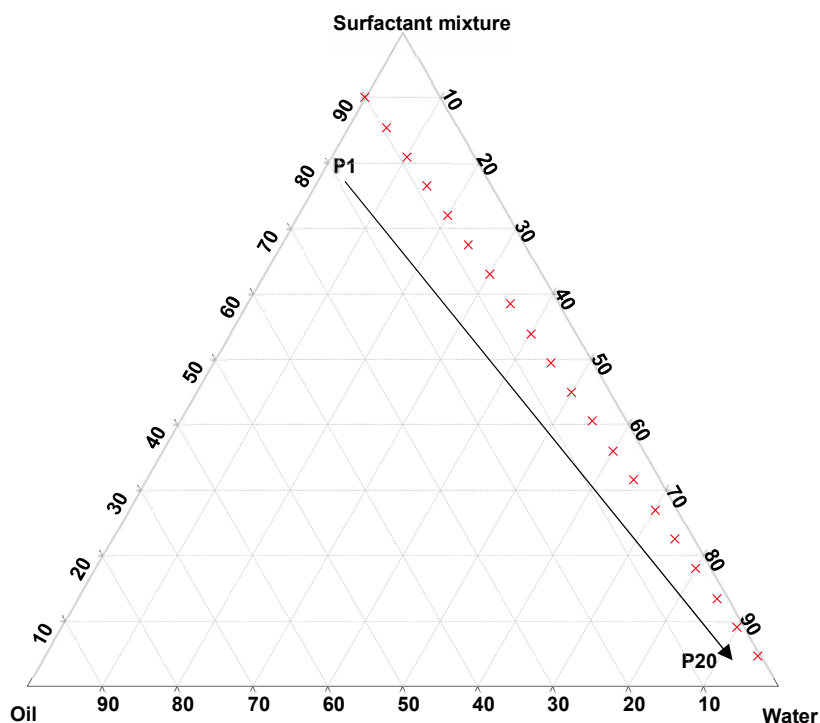


Figure 4.511. Pseud-ternary phase diagram and dilution line (in red points) used to plot diagrams, points in red represent P1 to P20 along dilution line 9 beginning from 10 % flaxseed oil using Table 4. 2.

The nine pseudo-binary solutions mixtures produced along the oil and surfactant mixture baseline in Figure 4.5 from 10 % w/w flaxseed oil at P1 to 90 % w/w flaxseed oil were vortexed using a Genie two vortex mixer (Scientific Industries Inc. TM, Bohemia, New York, United States) and placed into a clear Falcon[®] 24-well cell culture microplate with a lid (Corning[®] Inc, New York, United States). The bottom surface of the plate was placed onto a Xerox WorkCentre 3655 scanner (XeroxTM, Norwalk, CT, United States of America) with the top surface lid and sides covered with clean white background paper. The transparency and turbidity of the phase diagram dilution line ratio mixtures were visualized using the scanner in addition to determining the droplet size, PDI and Zeta Potential. The images for each of the pseudo-binary solutions and corresponding droplet size, PDI and ZP elucidated immediately within 6 minutes of vortexing are reported given in the results in section 4.4.2.

The mixtures used to generate points P1 to P20 summarized in Table 4.2 and Figure 4.5 represent 5 % w/w increment points from 0 % water to 95 % water approaching the water

vertex along dilution line 9 for surfactant mixture 1 (S1). The electrical conductivity was measured using a FiveEasy™ F30 Conductivity meter (Mettler Toledo, Greifensee, Switzerland) for these solutions and was used to classify emulsion microstructure and establish if w/o or o/w emulsions had been formed as o/w systems exhibit higher electrical conductivity than w/o emulsions [448]. Electrical conductivity measurements along dilution line nine from the pseudo-binary solutions of the surfactant/oil phase to the water vertex suggest that phase-inversion of system from a w/o to an o/w nano or micro-emulsion occurs at a specific point or range of values between P7 and P12 highlighted and summarized in the titration chart in Table 4.2.

Table 4.2 Titration chart for each dilution line to generate data to plot phase diagrams with proportions of each component in the nano-emulsion along dilution line 9.

Water addition points on dilution line	Oil mg	S1 mg	Water μ L	Total mg	S 1 %	Oil %	Water %	Conductivity μ S cm^{-1}
P1	250	2250	0	2500	90.00	10.00	0.00	0.18
P2	250	2250	133	2633	85.45	9.49	5.05	0.2
P3	250	2250	280	2780	80.93	8.99	10.07	0.28
P4	250	2250	440	2940	76.53	8.50	14.96	0.45
P5	250	2250	625	3125	72.00	8.00	20.00	0.96
P6	250	2250	835	3335	67.46	7.49	25.03	1.67
P7	250	2250	1075	3575	62.93	6.99	30.06	7.76
P8	250	2250	1350	3850	58.44	6.49	35.06	11.43
P9	250	2250	1675	4175	53.89	5.98	40.11	25.3
P10	250	2250	2050	4550	49.45	5.49	45.05	119.6
P11	250	2250	2500	5000	45.00	5.00	50.00	142.2
P12	250	2250	3050	5550	40.54	4.504	54.95	147.6
P13	250	2250	3750	6250	36.00	4.00	60.00	173.6
P14	250	2250	4625	7125	31.57	3.50	64.91	173.9
P15	250	2250	5875	8375	26.86	2.98	70.14	202
P16	250	2250	7500	10000	22.50	2.50	75.00	261
P17	250	2250	9950	12450	18.07	2.00	79.91	278
P18	250	2250	14275	16775	13.41	1.49	85.09	356
P19	250	2250	22500	25000	9.00	1.00	90.00	389
P20	250	2250	46600	49100	4.58	0.50	94.90	433

4.4.3 Fourier Transform Infrared S Spectroscopy (FTIR)

Fourier-transform infrared spectroscopy is an analytical technique used to generate infrared absorption or emission spectra of solid, liquid or gas and permits simultaneous collection of high-resolution spectral data over a frequency specified to produce a vibrational spectrum [286]. The FTIR spectrum of a molecule is used as a fingerprint for identification purposes as it is a unique property of molecules based on the unique structural features of the backbone and functional groups of the molecule which results in characteristic and reproducible absorption bands in the IR spectrum of the compound [449]. The IR spectrum also permits identification of the presence of specific unsaturated bonds and/or aromatic rings and functional groups including their orientation and location in molecules [450].

The characterisation of EFV, potential excipients and mixtures of EFV and excipients was investigated using FTIR. The infrared (IR) absorption spectrum of EFV and 1:1 mixtures of EFV and flaxseed, olive, grapeseed, soybean, sunflower and sesame seed oils, Span[®] 20 and Tween[®] 80 were generated using a Spectrum 100 FTIR attenuated total reflectance spectrometer (Perkin Elmer[®] Ltd, Beaconsfield, United Kingdom) over the wave number range 650-4000 cm⁻¹. The mixtures and samples were mounted onto a diamond crystal using an applied force of approximately 100 N, the spectral data collected and subsequently were processed using FT-IR Spectrum version 10.5.4 software (PerkinElmer[®], Inc Pty Ltd, Beaconsfield, United Kingdom).

4.4.4 X-ray diffraction (XRD)

XRD may be used to characterise SEDDS and facilitates identification of the state of an API in a lipid matrix, degree and type of polymorphism and phase behaviour of the components of the SEDDS, in this case [451,452]. X-ray diffractometers are comprised of an X-ray tube, sample holder and X-ray detector. Detailed X-rays are generated in a cathode ray tube by heating a filament to produce electrons, accelerating the electrons towards a target with the aid of an applied voltage and bombarding the target material with the electrons [453]. When electrons have enough energy to dislodge inner shell electrons in the target material, characteristic X-ray spectra are produced.

The characterisation of EFV, potential excipients mixtures of API and excipient was investigated using XRD. Powder XRD patterns were generated using a Bruker D8 Discover diffractometer (Billerica, Massachusetts, USA) with a proportional counter and Cu-K α radiation and a nickel filter of 1.5405 Å. The voltage and current used for the experiments were

30 kV and 40 mA respectively. The data was collected in the $2\theta = 10^\circ$ to 100° angle range at a scanning rate of $1.5^\circ/\text{min}$ with a filter time constant of 0.38 s and a slit width of 6 mm. Samples were placed onto a silicon wafer and the generated data treated and analysed using Version 14.0 EVA (evaluation curve fitting) XRD Commander Version 2.61 software (Bruker-AXS GmbH, Karlsruhe, Germany) with baseline correction performed by subtracting a spline function fitted to the curved background.

4.4.5 Raman spectroscopy

Raman spectroscopy generates useful structural and property information of molecules from vibrational transitions [454]. Raman spectra are generated by focusing monochromatic radiation onto a sample and analysing the resultant scattered light as a function of frequency and relies primarily on inelastic scattering of electromagnetic radiation by a molecular system with the scattering effects providing a structural fingerprint which can be used to identify molecules [455–458]. In general strong FTIR bands are related to polar functional groups whereas strong Raman bands are a consequence of non-polar functional groups and vibrational changes in the spectra of molecules serve as probe for potential intermolecular interactions between the components of a mixture [459].

Raman spectroscopy was used to characterise EFV, excipients and EFV excipient mixtures to determine if interaction between EFV and components of the emulsion occurred. A Bruker Vertex 70-Ram II Raman spectrometer (Bruker Optics Inc., Billerica, Massachusetts, United States of America) equipped with a 1064 nm Nd: YAG laser for excitation in the region of $3400\text{--}80\text{ cm}^{-1}$ and liquid nitrogen cooled germanium detector was used to generate Raman spectra that were acquired at 300 scans per minute. The instrument was set at 300 mW and the sample was placed in a hemispheric bore of an aluminium sample holder. The spectral resolution was 4 cm^{-1} and the spectra were processed using OPUS version 6.5 spectroscopy software (Bruker Optics Inc., Billerica, Massachusetts United States of America).

4.4.6 Differential scanning calorimetry (DSC)

Characterisation of EFV and potential interactions between the API and excipients were investigated using DSC studies conducted using a Model 6000 Perkin Elmer[®] DSC (Beaconsfield, England) fitted with an RCS 90 refrigerated cooling system (New Castle, DE, USA). Approximately 2.5-5 mg of EFV, pure and in 1:1 m/m mixtures of EFV and each

excipient namely, flaxseed oil, Tween[®] 80 and Span[®] 20 and a ternary mixture including ethanol. These samples were weighed using a Mettler AG 135 top loading balance (Mettler Instruments, Zurich, Switzerland). An aliquot of the mixtures was placed into a 40 μ L aluminium pan that was covered and placed onto a disc inside the DCS cell of the instrument. The studies were performed by heating the samples from 30 to 300 $^{\circ}$ C at a rate of 10 $^{\circ}$ C/ min while purging the system with liquid nitrogen at 20 $^{\circ}$ C/min. The resultant data was analysed using PyrisTM 6000 Manager Software for Windows (Perkin-Elmer[®] Ltd, Connecticut, USA).

4.5 Results and discussion

4.5.1 Solubility studies

The results of solubility studies are summarized in Table 4.3.

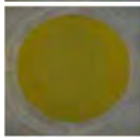
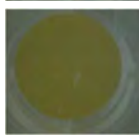
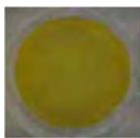
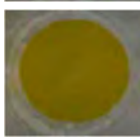
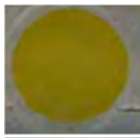
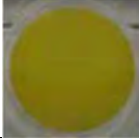
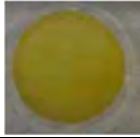
Table 4.63 Saturation solubility of EFV in vegetable oils.

Vegetable Oil	Mean solubility (n=3) \pm SD mg/ml
Flaxseed	89.41 \pm 0.12
Soybean	81.53 \pm 0.18
Macadamia	71.31 \pm 0.12
Grapeseed	69.83 \pm 0.16
Olive	69.55 \pm 0.09
Sunflower	55.99 \pm 0.87

The highest solubility of 89.41 mg/ml for EFV was observed in flaxseed oil which was therefore used as the oil phase for constructing pseudo-ternary phase diagrams for a self-emulsifying nano-emulsion. In addition to the physicochemical properties of EFV the molecular volume, polarity of the oil, chain length and saturation or unsaturation of triglyceride chains of the vegetable oils also influence solubility [460]. Medium chain triglyceride (MCT) containing oils are best for LBDDS as they are resistant to oxidation and exhibit high solvent capacity when compared to long chain triglycerides (LCT) oils due to the high effective concentration of ester functional groups in the oil [149]. However, most of the vegetable oils selected for this study LCT and C₁₈ chains. As the proportion of the unsaturated component C_{18:3} component or n-3 poly-unsaturated fatty acids of the vegetable oils increase so the solubility of EFV increases. Flaxseed oil has approximately 50 % C_{18:3} soybean oil approximately 9.5 % C_{18:3}, grapeseed, sunflower and olive oils contain < 2 % C_{18:3} as reported earlier in section 4.2.1.

4.5.2 Pseudo-ternary phase diagram construction

Binary solutions of surfactant and oil in all ratios for the surfactant mixtures for dilution line 1 to dilution line 8 exhibited two phases which exhibited Winsor I type phase behaviour on standing for 30 minutes but formed turbid mixtures following vortex mixing for 30 seconds at 800 rpm. Dilution line 9 or ratio 9 resulted in formation of a transparent and kinetically stable, isotropic system which exhibited Winsor IV type behaviour for up to 12 months at room temperature (22°C). The droplet sizes of these ratio mixtures gradually increased as the proportion of flaxseed oil increased and surfactant content decreased. The surfactant to oil ratio for the 9:1 pseudo-binary solution resulted in emulsions with the smallest droplet size and lowest PDI of all ratios tested. A micro- and nano-emulsion region was observed along dilution line 9 for all three surfactant mixtures tested. The scanned image of binary mixtures of flaxseed oil and surfactant mixture are depicted in Figure 4.6 with their associated droplet sizes (DS), PDI and Zeta Potential. The 9:1 ratio mixture is clear and transparent, while the rest of the ratios form turbid mixtures on vortexing and therefore Winsor type I behavior on standing for >30 minutes.

Ratio S _{mix} : Oil m/m	S1	CQA	S2	CQA	S3	CQA
9:1		DS: 185.1 nm PDI: 0.408 ZP: -35.4 mV		DS: 190.3 nm PDI: 0.207 ZP: -34.4 mV		DS: 156.8 nm PDI: 0.266 ZP: -43.9 mV
4:1		DS: 287.2 nm PDI: 0.407 ZP: -35.4 mV		DS: 209.1 nm PDI: 0.305 ZP: -35.3 mV		DS: 519.7 nm PDI: 0.307 ZP: -31.0 mV
7:3		DS: 322.9 nm PDI: 0.412 ZP: -40.3 mV		DS: 350.7 nm PDI: 0.72 ZP: -29.9 mV		DS: 1402 nm PDI: 0.58 ZP: -33.1 mV
3:2		DS: 327.2 nm PDI: 0.277 ZP: -34.9 mV		DS: 804.7 nm PDI: 0.682 ZP: -33.5 mV		DS: 829.7 nm PDI: 0.26 ZP: -41.9 mV
1:1		DS: 436.6 nm PDI: 0.214 ZP: -35.0 mV		DS: 860.5 nm PDI: 0.782 ZP: -32.2 mV		DS: 844.3 nm PDI: 0.38 ZP: -43.8 mV
2:3		DS: 295.9 nm PDI: 0.316 ZP: -45.8 mV		DS: 1441 nm PDI: 0.343 ZP: -37.8 mV		DS: 774.7 nm PDI: 0.22 ZP: -40.7 mV

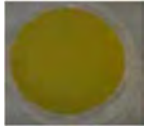
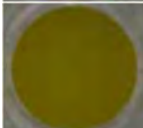
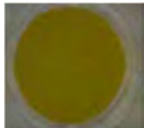
3:7		DS: 451.9 nm PDI: 0.363 ZP: -41.0 mV		DS: 2380.7 nm PDI: 0.308 ZP: -37 mV		DS: 667.2 nm PDI: 0.69 ZP: -40.4 mV
1:4		DS: 906.7 nm PDI: 0.236 ZP: -47.8 mV		DS: 1617.7 nm PDI: 0.411 ZP: -35 mV		DS: 1253 nm PDI: 0.40 ZP: -28.7 mV
1:9		DS: 1149.0 nm PDI: 0.201 ZP: -38.7 mV		DS: 1023.1 nm PDI: 0.709 ZP: -41.7 mV		DS: 1204 nm PDI: 0.68 ZP: -41.7 mV

Figure 4.6. Scanned image investigation of turbidity and transparency for phase identification studies and critical quality attributes (CQA) droplet size (DS), polydispersity index (PDI) and Zeta Potential (ZP).

Five distinct regions were identified in the phase diagram including a nano-emulsion that is transparent resembling Winsor IV behaviour, a milky Winsor IV or cloudy isotropic mixture, a translucent Winsor I, II and III area, a milky Winsor I, II and III and a gel or semi-solid region. Dilution line 9 formed clear isotropic and transparent nano-emulsions up to 35% v/v water inclusion until turbidity was reached for surfactant mixture 1 as depicted in Figure 4.7.

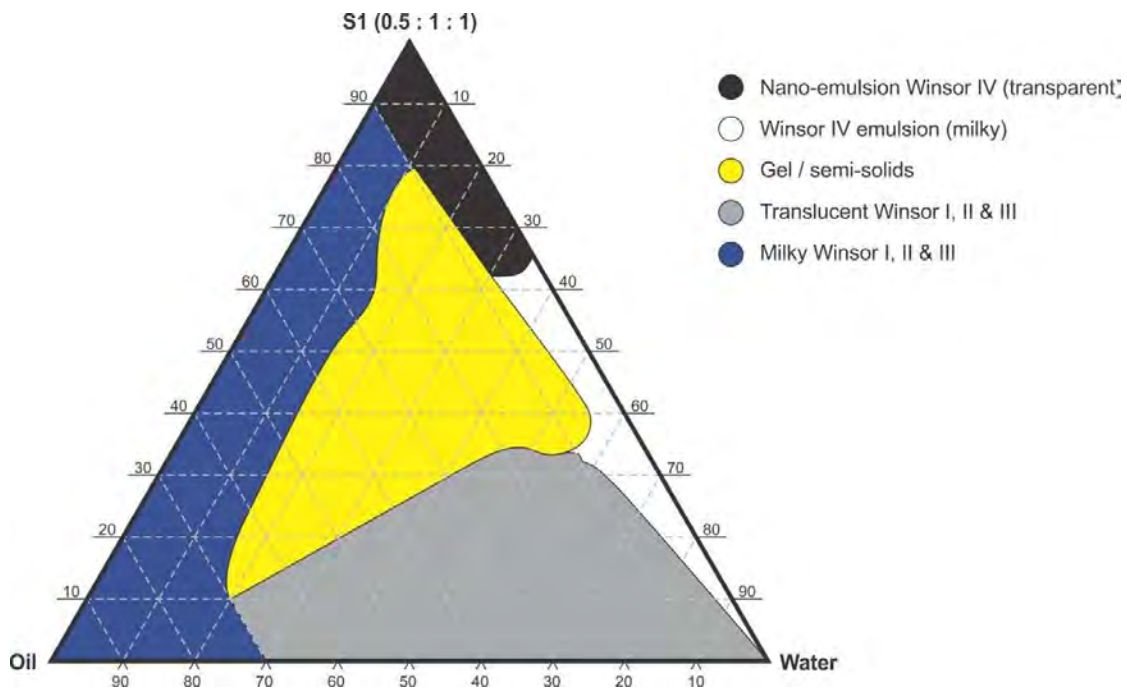


Figure 4.712. Pseudo-ternary phase diagram of flaxseed oil with surfactant mixture S1 in which a (0.5: 1: 1 m/m ratio of ethanol: Tween[®] 80: Span[®] 20 is used.

Water was added up to 20% v/v for surfactant mixture 2 as depicted in Figure 4.8 and up to 5% v/v for surfactant mixture 3 as depicted in Figure 4.9. Whilst the area of the nano-emulsion

decreases as ethanol content of the surfactant mixture increases, the milky isotropic and two or three-phase regions of the o/w emulsion exhibited an increased area whereas the gel region decreased in size with an increase in ethanol content more than likely due to the flexibility of interfacial film resulting on disruption of solid structure with an increase in the dimensions of the area of the fluid phase. The dilute aqueous isotropic regions of cloudy o/w emulsions may be appropriate for achieving an immediate release effect, due to the ease of dispersion of this phase in aqueous media [461]. Electrical conductivity measurements along dilution line nine suggest that phase-inversion of system from a w/o to an o/w micro- or nano-emulsion occurs at a specific point if not over a range of values as summarized in the titration chart used. The surfactant mixture for the S1 mixture exhibited the largest nano-emulsion region in the phase diagram and resulted in the production of the largest number of kinetically stable nano-emulsions following addition of water.

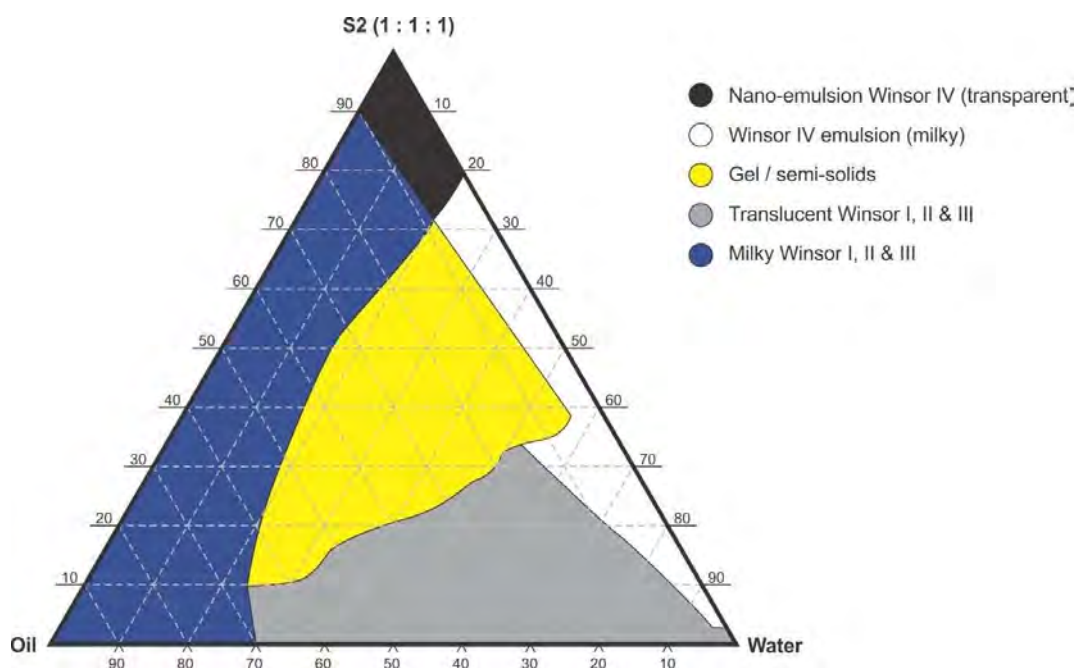


Figure 4.813. Pseudo-ternary phase diagram of flaxseed oil with surfactant mixture S2 in which a (1: 1: 1 m/m of Ethanol: Tween® 80: Span® 20).

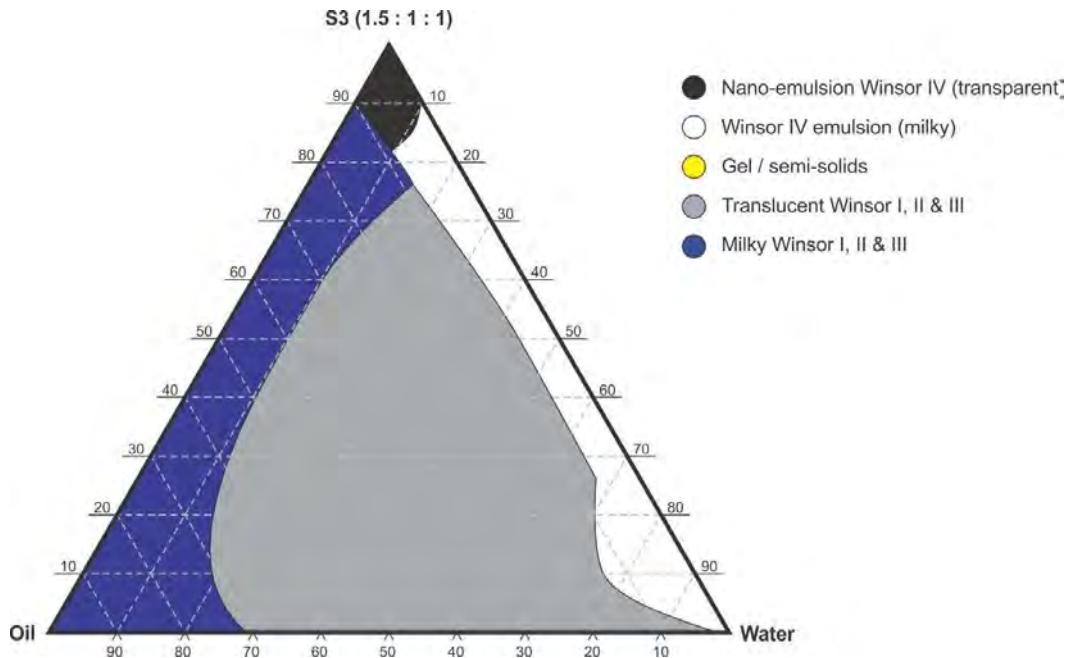


Figure 4.914. Pseudo-ternary phase diagram of flaxseed oil with surfactant mixture S3 in which a (1.5: 1: 1 m/m of Ethanol: Tween[®] 80: Span[®] 20).

4.5.3 Fourier Transform Infrared Spectroscopy (FTIR)

The spectrum for EFV is depicted in Figure 4.10 and the data agrees with previously reported data and a summary of the band assignments is listed in Table 4.4.

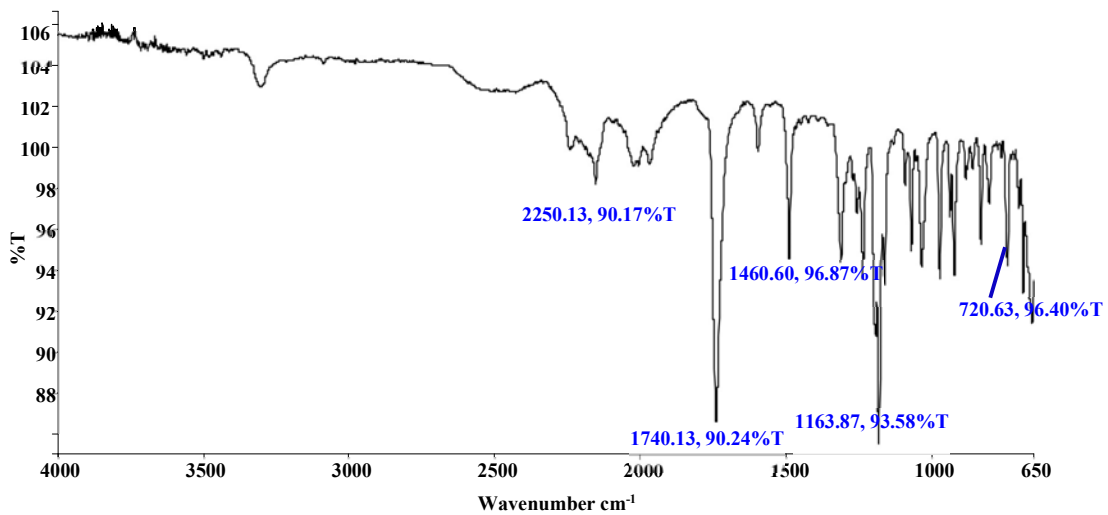


Figure 4.1015. FTIR spectrum of EFV.

Table 4.4 Observed and reported FTIR signals for EFV [462].

Reported cm ⁻¹	Observed cm ⁻¹	Functional group
3097	3095	-CH (Aryl)
2247	2250	C triple bond C
1741	1740	-C=O
1602	1600	
1495	1500	-C-F
1396	1400	-CHN (ring)
1362	1362	
1317	1318	-CO
1242	1241	-CF
1163	1163	-CF ₃
1039	1037	-C-Cl
978	976	-CF
923	919	-CCH
889	877	-CCC
850	848	HCCH

The FTIR spectrum for EFV revealed the characteristic signals of the drug with an intense band due to C=O stretching vibration of the amide group at 1740 cm⁻¹ and CF₃ stretching band at 1163 cm⁻¹, alkyne C≡C at 2250 cm⁻¹ with a relatively small intensity relative to other peaks, in addition, to solvent bands in the 1003 to 720 cm⁻¹ region [463,464].

The FTIR spectra of 1:1 m/m binary mixtures of EFV and flaxseed, soybean and macadamia oil are depicted in Figures 4.11, 4.12 and 4.13 respectively.

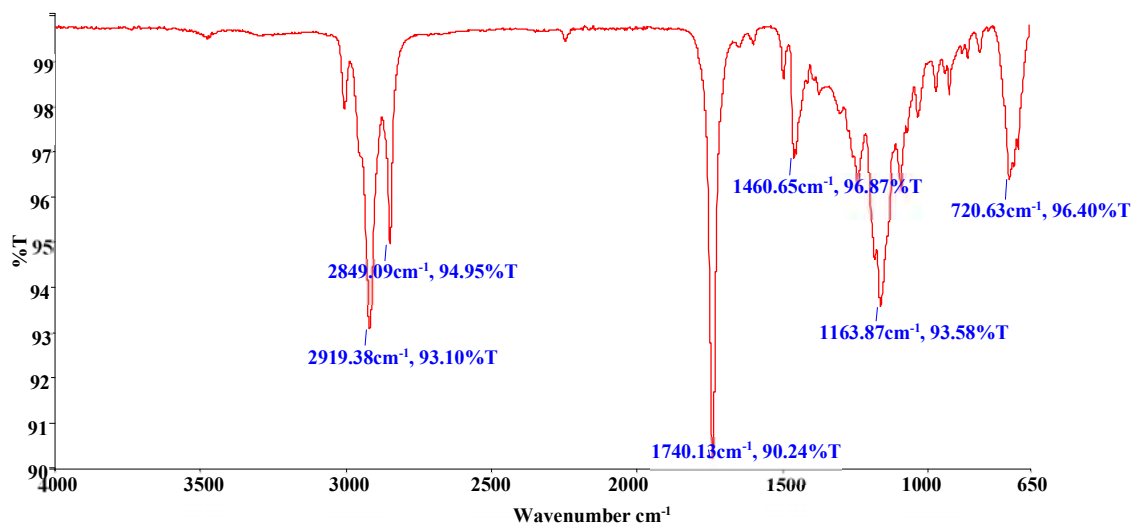


Figure 4.1116. FTIR spectrum a of 1:1 m/m mixture of EFV and flaxseed oil.

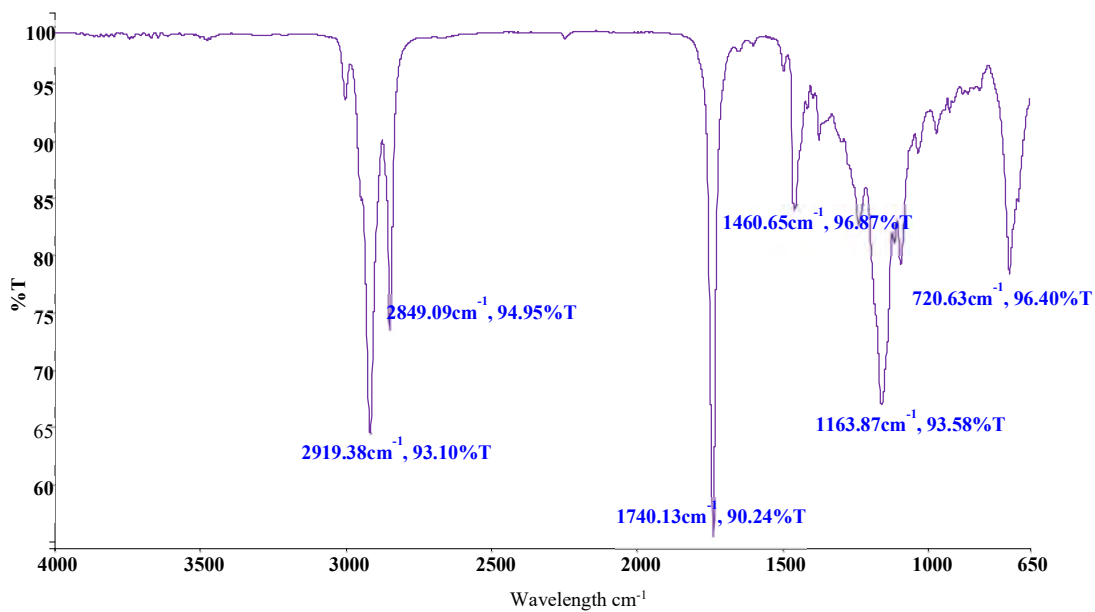


Figure 4.1217. FTIR spectrum of 1:1 m/m mixture of EFV and soybean oil.

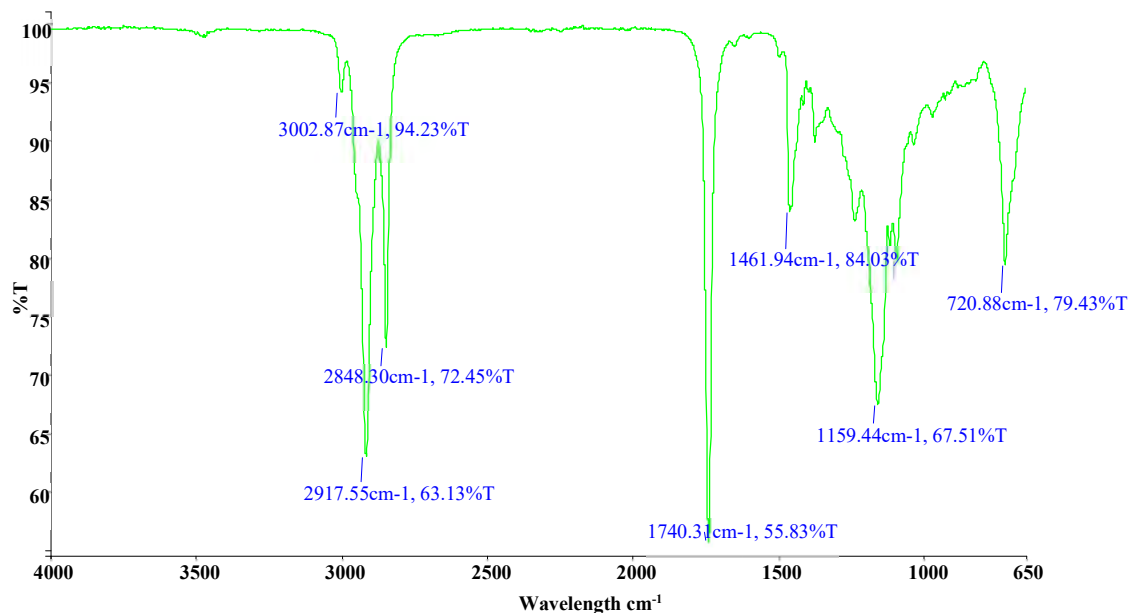


Figure 4.1318. FTIR spectrum a of 1:1 m/m mixture of EFV and macadamia oil.

FTIR spectra of 1:1 m/m binary mixture of EFV in vegetable oils revealed the presence of the characteristic peaks of EFV in the same spectral regions for C=O stretching of the amide group at 1740 cm^{-1} , a CF_3 stretching band at 1163 cm^{-1} , the alkyne $\text{C}\equiv\text{C}$ bond at 2250 cm^{-1} was diminished probably due to encapsulation of EFV resulting in obscured peaks of the molecular drug. Triglyceride functional groups from the oil revealed peaks appearing at 2848 cm^{-1} and 2917.38 cm^{-1} for alkane $-\text{CH}_2$ stretches, asymmetrical and symmetrical and the $-\text{CH}=\text{CH}-$ bending at 720 cm^{-1} which is characteristic of vegetable oils [465–467]. The vegetable oils have similar functional groups although a different composition of triglycerides, consequently, it is difficult to detect differences in composition of the oils in this class using FTIR. The spectra for mixtures of EFV and grapeseed, olive and sunflower oils used are reported in Appendix 2 in Figure 7.9, 7.10 and 7.11 respectively. No interaction between EFV and the vegetable oils is evident, and all functional groups are present in all spectra.

The FT-IR spectra of 1:1 mixture of EFV with Span[®] 20 and with Tween[®] 80 are depicted in Figures 4.14 and 4.15 respectively.

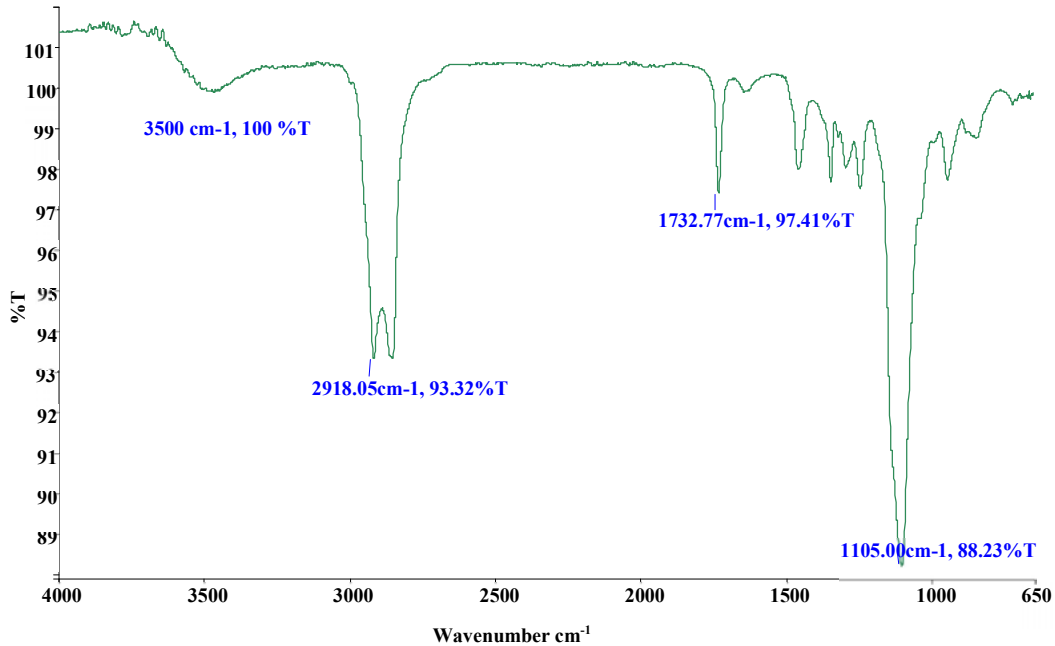


Figure 4.1419. FTIR spectrum of 1:1 m/m mixture of EFV and Span[®] 20.

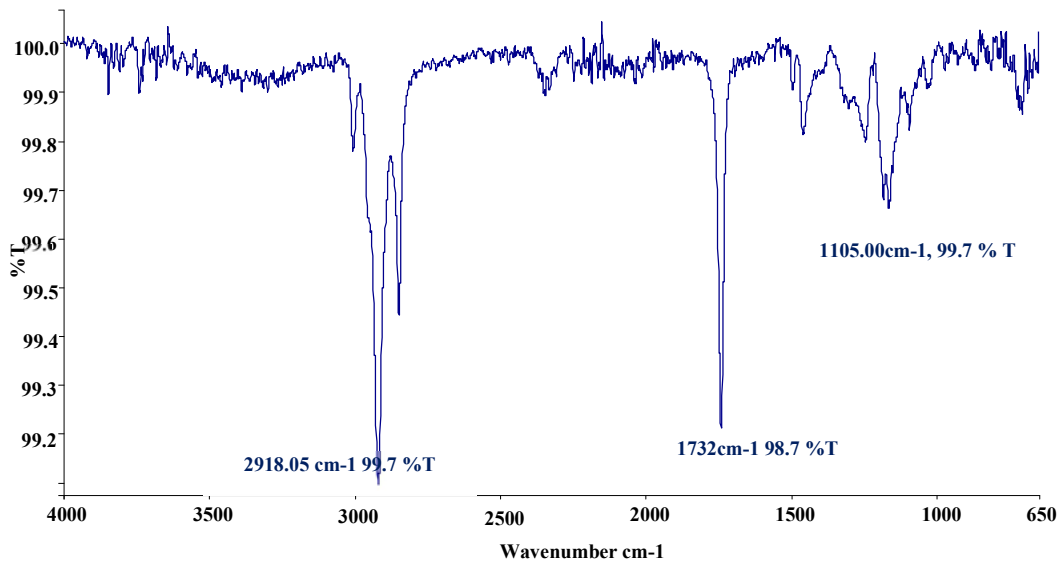


Figure 4.1520. FTIR spectrum of a 1:1 m/m mixture of EFV and Tween[®] 80.

The FTIR of 1:1 binary mixture of EFV on solution of Span[®] 80 and of Tween[®] 20 revealed the peaks for EFV were present in the molecular state and decreased in intensity and slightly obscured by the excipients. A reduction in peak intensity is an indication of reduced

crystallinity, studies were further confirmed by XRD and DSC in section 4.5.5 and section 4.5.6. The spectrum for Span[®] 20 exhibits a broad peak at 3500 cm⁻¹ due to OH groups, at 2918 cm⁻¹ for carboxylic acids, at 1732 cm⁻¹ for an aldehyde functional group and 1461 cm⁻¹ for alkane and aromatic ring stretches [468]. The spectrum for Tween[®] 80 reveals the presence of a number of intense, sharp peaks re due to the a methyl group –CH₃ at 2918 cm⁻¹, at 1740 cm⁻¹ attributed to a C=O and the peak at 1105 cm⁻¹ due to stretching of C–O–C bond [469].

Although EFV peaks were reduced in intensity in 1:1 m/m combinations with Span[®] 20 and with Tween[®] 80, the peaks were presently more intense when EFV was mixed with the ternary mixture that contained ethanol, this suggests that the ethanolic solution of EFV emulsion resulted in a predominantly crystalline form of EFV signals seen in XRD and FTIR, this could possibly be due to predominantly EFV partitioning into the ethanol phase of the mixture with higher solubility capacity and EFV existing mostly as a crystalline form. The FTIR spectrum of EFV in a complete mixture with all excipients is depicted in Figure 4.16 and the molecular peaks of the known and expected EFV functional groups with no shifting of peaks, no formation of new peak or unexpected functional group was observed indicating that no chemical interaction occurred between EFV and vegetable oils which suggests stable formulations can be produced.

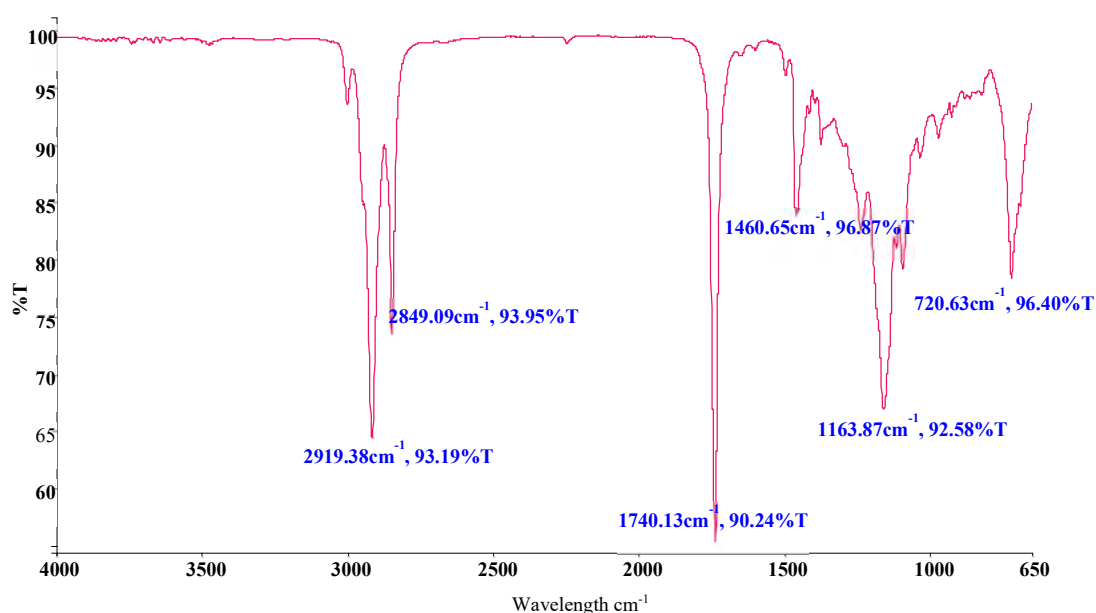


Figure 4.1621. FTIR spectrum of a 1:1 m/m mixture of EFV and a ternary emulsion mixture (1:1:1 m/m of Tween[®] 80, Span[®] 20 and ethanol).

4.5.4 Raman Spectroscopy

The Raman spectrum for EFV is reported in Figure 4.17. The functional groups for EFV detected using Raman spectroscopy revealed that all expected signals for pure efavirenz and blank nano-emulsions were present and are in agreement with previously reported spectral data [65]. The signal for the -CH_2 functional group at 3093 cm^{-1} , the $\text{C}\equiv\text{C}$ bond at 2252 cm^{-1} , the $\text{C}=\text{O}$ bond at 1656 cm^{-1} reflect the presence of EFV [470,471]. A comparison of experimentally determined vibrational wavenumbers to reported data for EFV is listed in Table 4.5.

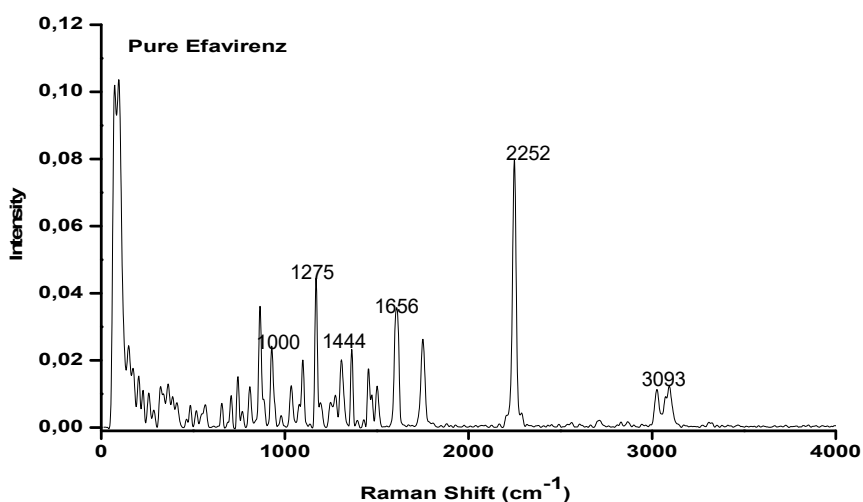


Figure 4.17. Raman spectrum for pure EFV

Table 4.5 Theoretical (reported) and experimental vibrational wavenumbers for Raman spectrum of EFV [472].

Reported cm^{-1}	Observed cm^{-1}	Functional group
3093	3093	-CH_2
3071	3072	-CH
3027	3022	-CH
2250	2252	$\text{C}=\text{C}$
1752	1750	$\text{C}=\text{O}$
1655	1656	$\text{-C}=\text{C-}$
1615	1614	Cyclic ring
1602	1606	Cyclic ring
1500	1504	$(\text{-CH}) + \text{Ring}$
1455	1454	-NH
1445	1444	

1364	1367	(-CCH) + (-CH ₂)
1306	1307	Ring
1275	-	
1170	1170	(-CCH)
1098	1099	-CCI
1032	1039	(HCCH) or (-COC)
977	931	-CCH, -C-C-C
565	564	C triple bond C
543	542	CF ₃

The Raman spectrum for EFV in flaxseed oil is depicted in Figure 4.18 and reveals the presence of well-defined bands for EFV circled at 3093 cm⁻¹, 2252 cm⁻¹, 1656 cm⁻¹ and 1444 cm⁻¹ indicating that the molecular backbone of EFV remains unchanged in this mixture. Additional peaks typical of the -CH₂ group at 2854 cm⁻¹ bonded to an unsaturated carbon atom -CH₂-CH=CH- and 1656 cm⁻¹ for -C=C- bond are common in unsaturated fatty acid chains and are possibly due to the flaxseed oil [473].

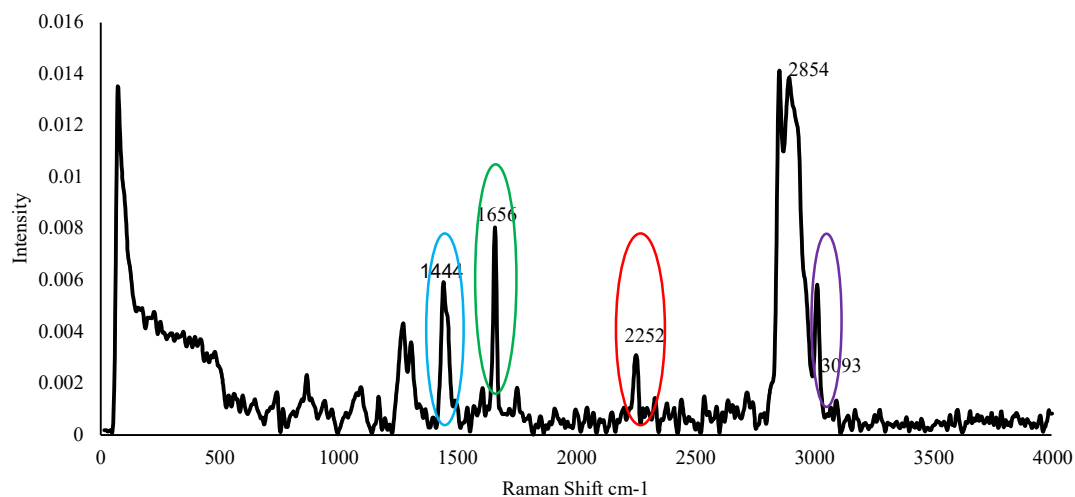


Figure 4.1822. Raman spectrum of a 1:1 m/m mixture EFV and flaxseed oil

Binary mixtures of EFV and each of the surfactants tested are depicted in Figures 4.19 and 4.20 with Span[®] 20 and with Tween[®] 80. The characteristic peaks for EFV at 3093 cm⁻¹, 1444 cm⁻¹

¹ and 1656 cm⁻¹ were not present in the spectrum except the signal at 2252 cm⁻¹. This may indicate once again that EFV has been solubilized or encapsulated.

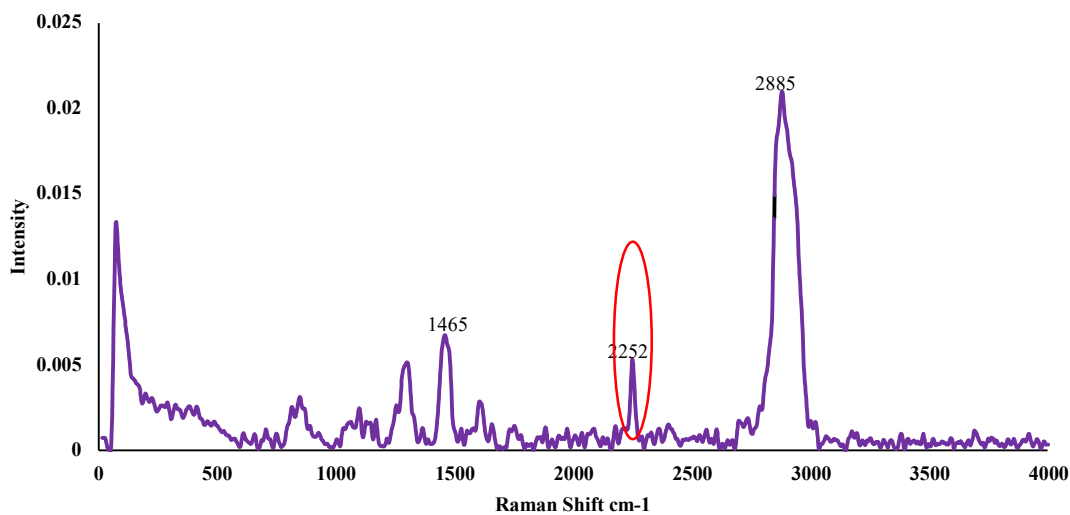


Figure 4.1923. Raman spectrum of a 1:1 m/m mixture of EFV and Span® 20

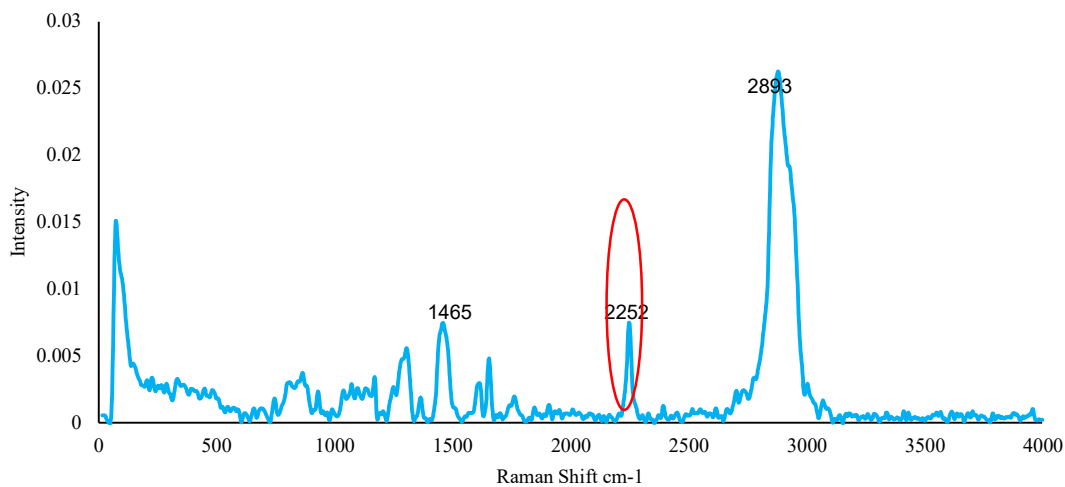


Figure 4.2024. Raman spectrum of a 1:1 m/m mixture of EFV efavirenz and Tween® 80

The spectrum of EFV and ternary mixtures of emulsion components depicted in Figure 4.21 exhibits all expected peaks of crystalline EFV and the excipients with no shift or formation any new peaks implying no interaction between EFV and the lipids to use in the formulation. Similarly, EFV 1:1 m/m mixtures with ternary mixtures of 1:1:1 of Tween® 80, Span® 20 and ethanol showed the existence of the crystalline form of EFV.

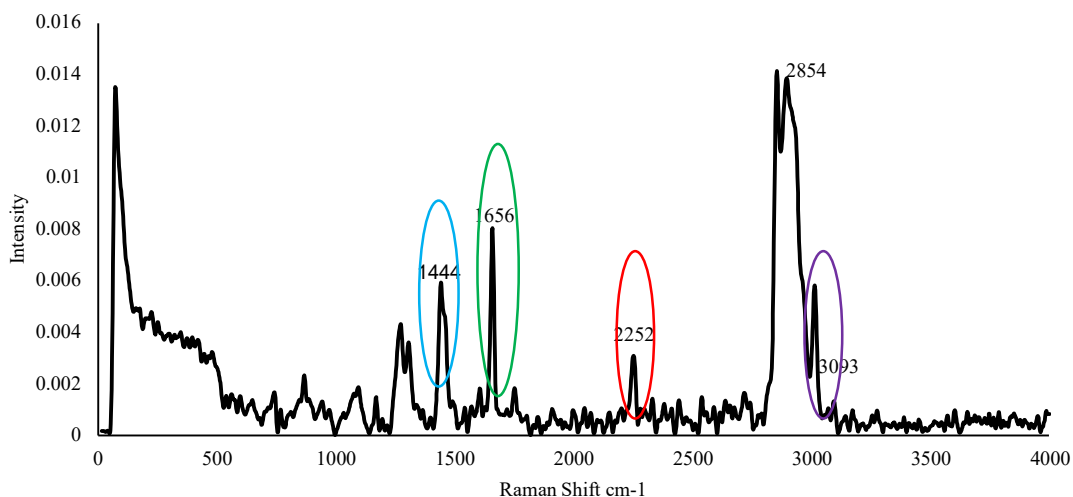


Figure 4.2125. Raman spectrum of 1:1 m/m mixture of EFV and components of a ternary emulsion mixture i.e. 1:1:1 m/m of Tween® 80, Span® 20 and ethanol.

4.5.5 X-ray diffraction (XRD)

Crystalline material has well-defined edges and tend to have sharp melting points. In contrast, amorphous material has irregular or curved surfaces, do not give well-resolved x-ray diffraction patterns, and melt over a wide range of temperatures. EFV exists as Form I and Form II polymorphs and the patent literature reveals that all polymorphs revert to Form 1 which is considered the most stable form [64]. The diffraction pattern for efavirenz depicted in Figure 4.22 reveals the present of peaks at 21.8°, 25.1°, 27.8°, 31.9°, 43.9°, and 54.0° that correspond to the diffraction pattern of the stable crystalline Form I polymorph of efavirenz [464,474].

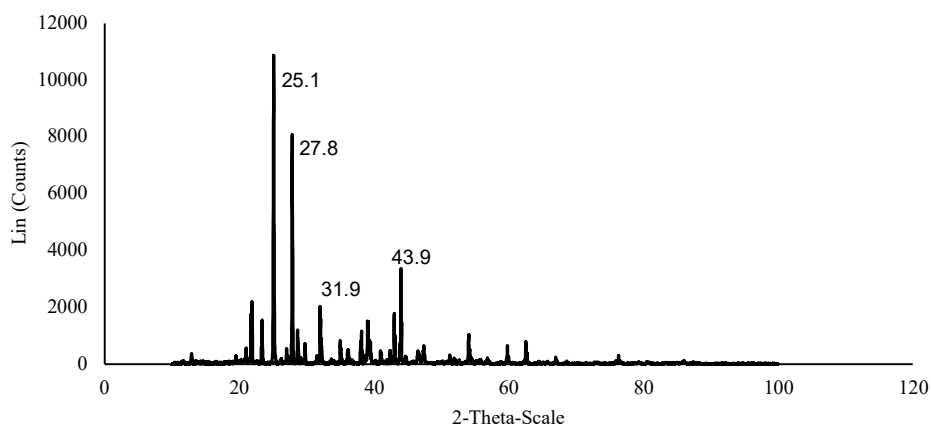


Figure 4.22. XRD pattern of pure EFV

The XRD of EFV in 1:1 binary mixtures with flaxseed oil and each surfactant revealed none of the Form 1 signals, resulting in a single fused peak observed at 20.1° confirming complete encapsulation of EFV into the molecular state or a possible change from crystalline to an amorphous state [475]. Depicted in Figures 4.23, 4.24 and 4.25 are the spectra in 1:1 m/m combination with flaxseed oil, Tween® 80 and Span® 20 respectively. The disappearance of all EFV crystalline peaks maybe a result of the EFV being in solution and molecular state or indicate that an amorphous nature of the drug is present in the mixture, other reports have suggested this may also mask the bitter taste of EFV [476].

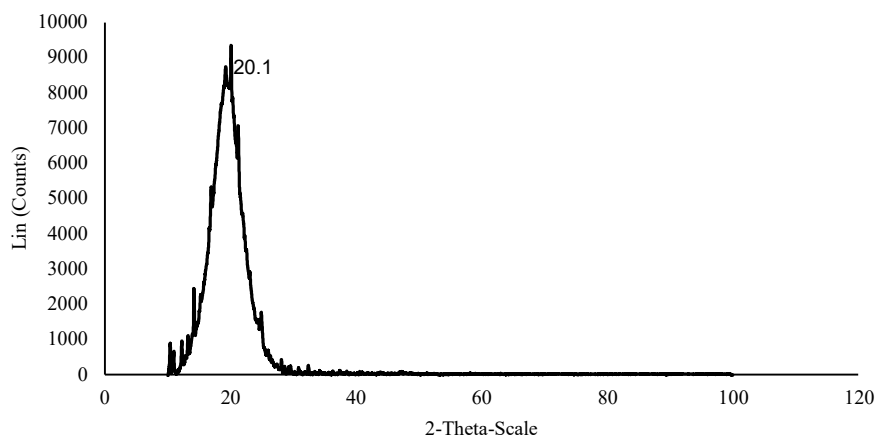


Figure 4.2326. XRD pattern of 1:1 m/m mixture of EFV and flaxseed oil.

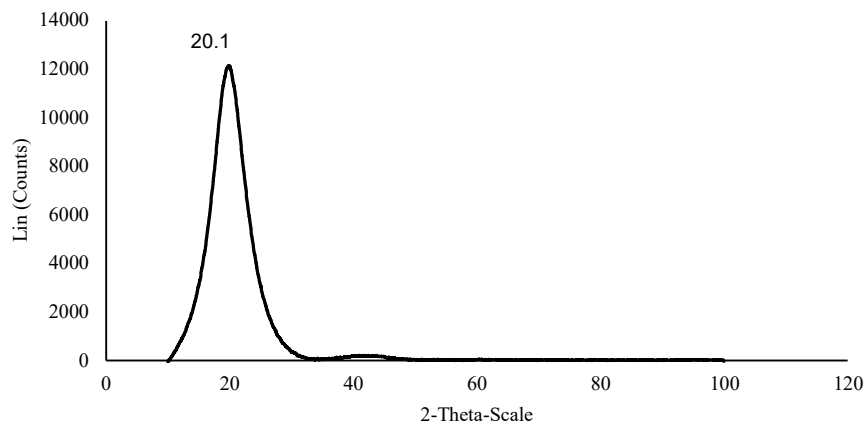


Figure 4.2427. XRD pattern of 1:1 m/m mixture of EFV Tween® 80.

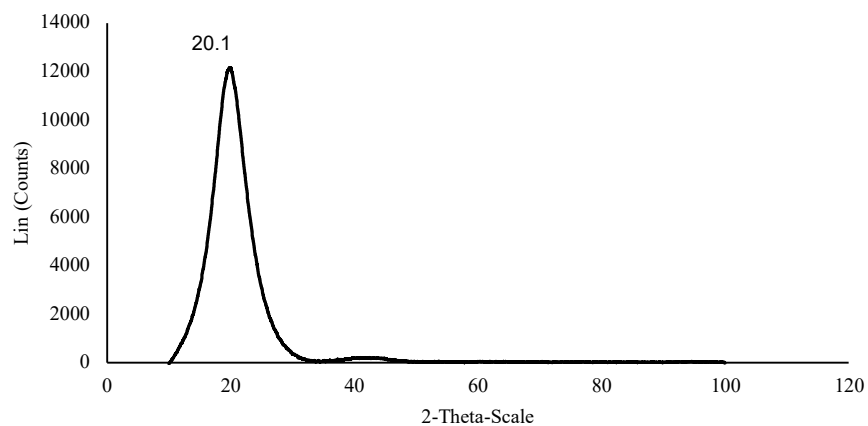


Figure 4.285. XRD pattern of 1:1 m/m mixture of EFV Span® 20.

The XRD spectrum of EFV in a ternary mixture of surfactants and co-solvent is depicted in Figure 4.26 reveals the presence of an x-ray pattern for crystalline efavirenz in the ternary mixture of excipients. X-ray diffraction measurements reveal no evidence of any other contaminants, phases or existence of different polymorphs within the emulsion mixture. The X-ray diffraction pattern of EFV in ternary mixtures of API, surfactant and co-solvent reveals multiple sharp peaks, indicating the presence of the crystalline form I stable polymorph of EFV [477].

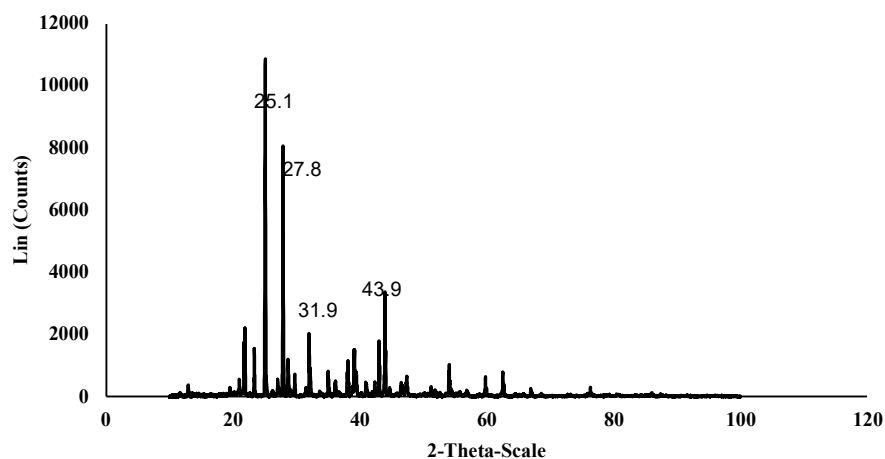


Figure 4.2629. XRD pattern of 1:1 m/m mixture of EFV and ternary mixture of excipients (1:1:1 m/m of Tween® 80, Span® 20 and ethanol).

4.5.6 Differential scanning calorimetry (DSC)

The melting behaviour, crystalline and polymorphic nature of EFV and its mixtures with excipients was evaluated using DSC. The DSC data generated in these studies are depicted in Figures 4.27 and Figure 4.28 which was identical in all binary mixtures of EFV and Tween[®] 80, EFV and Span[®] 20, EFV and surfactant mixture with ethanol (ternary mixtures). The Form 1 crystalline EFV exhibits a single and sharp endothermic peak onset at 136 °C and peak temperature of 140 °C with an enthalpy approximately equal to 124 J/g, this peak is associated with the melting point of the compound. After melting, an exothermic event is observed at about 263 °C, characteristic of EFV decomposition [464,536].

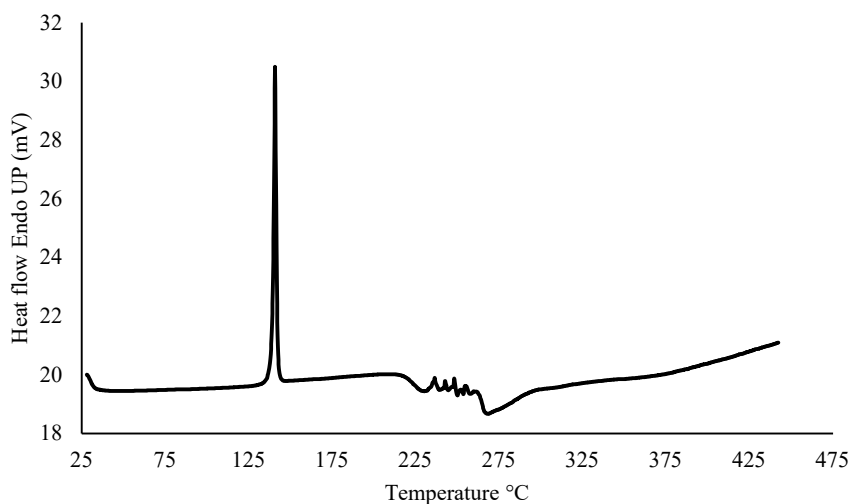


Figure 30.27. DSC thermogram of pure EFV.

The DSC thermogram of 1:1 m/m mixtures of EFV and ternary surfactant mixture of Tween[®] 80, Span[®] 20 and ethanol is shown in Figure 4.28, the peak for EFV melting almost disappeared. This could be a result of interaction that may occur in the form of partial amorphization, i.e., part of the drug loses crystallinity under analysis conditions or through the emulsion carrier interacting with the drug, possibly solubilizing EFV with analysis heating or as the system suffers degradation [537]. As the sample received heat, ethanol in the mixture evaporated and EFV solubilized partition which is predominantly amorphous is detected by DSC with result of no sharp peak as see with pure EFV.

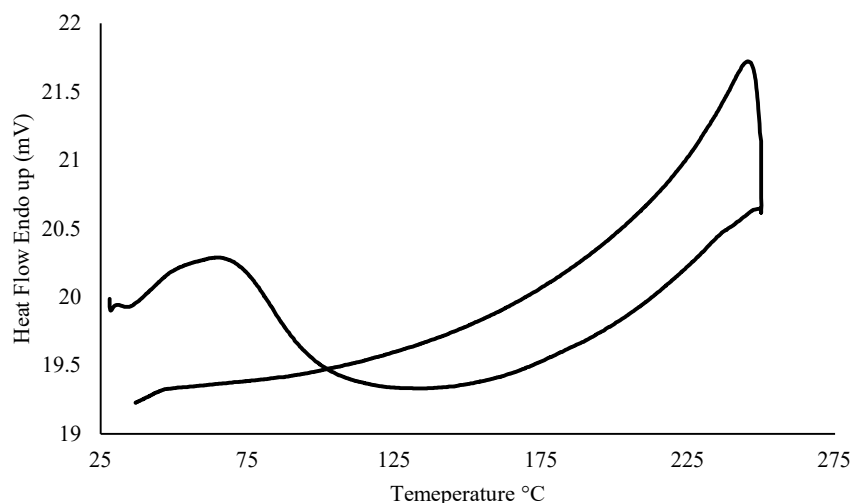


Figure 4.2831. DSC thermogram of 1:1 m/m mixtures of EFV and mixture of (Tween[®] 80, Span[®] 20, and ethanol)

4.6 Conclusions

Pre-formulation studies were conducted to characterize and determine the properties of EFV and excipients that would facilitate the manufacture of SEDDS. The selection of an appropriate oil, surfactant and co-surfactant for formulation activities was based on the results of solubility studies conducted with EFV using different vegetable oils and surfactants. EFV exhibited the greatest solubility in flaxseed oil which was selected as the vegetable oil component of the SNEDDS formulations to be developed in combination non-ionic Tween[®] 80 and Span[®] 20 surfactants.

Pseudo-ternary phase diagrams with flaxseed oil and different combinations of Tween[®] 80, Span[®] 20 and ethanol surfactant mixtures (S_{mix}) were constructed to guide the selection of oil and S_{mix} ratios to be used to ensure that nano-emulsions would form in situ when the formulations were exposed to water. The pseudo-ternary phase diagrams suggest that low amounts of the oil and high levels of surfactant would ensure the production of clear emulsions in situ which are indicative of SEDDS of droplet size < 100 nm.

Phase behaviour investigations of component mixtures LBDDS are useful for optimization of formulations and pre-formulation studies assist in defining appropriate proportions of each component to use, in addition to facilitation decision making in relation to manufacturing processes. In this case there is a need to determine whether high pressure or high shear homogenization can be used. Such decisions are required to ensure that an optimum product

with pre-defined quality attributes will be produced. The phase behaviour of crude cold pressed flaxseed oil with non-ionic surfactants revealed an area within the pseudo-ternary phase diagrams for surfactant mixtures S1 and S2 that formed gels/semi-solid structures which can be exploited for other drug delivery strategies such as topical application. Extensive pre-formulation studies are necessary to identify potential excipients for use in SEDDS to ensure the most suitable excipients for optimum product performance. Complementary analytical tools and their appropriate application will ensure complete characterisation of appropriate raw materials and proportions thereof to use for the successful formulation manufacturing investigated and described in Chapter 5 of this thesis.

The FTIR analysis of 1:1 binary mixture of EFV in solution of Span[®] 80 and of Tween[®] 20 revealed the peaks for EFV were present in the molecular state and decreased in intensity and slightly obscured by the excipients. A reduction in peak intensity maybe an indication of reduced crystallinity [479]. XRD data revealed that 1:1 m/m binary mixtures of EFV and each excipient except for ethanol resulted in complete disappearance of the signals for the EFV for XRD possibly due to a change of crystalline EFV to an amorphous form or the formation of a complete molecular dispersion of the API in the lipids investigated [478]. The DSC thermograms of 1:1 m/m mixtures of EFV and ternary surfactant mixture of Tween[®] 80, Span[®] 20 and ethanol resulted with the peak for EFV melting almost disappearing which could be a result of interaction that may occur in the form of partial amorphization to confirm the XRD result and also possibly due to improved solubility through functionality of self-emulsifying systems that are readily dispersible in aqueous and/or physiological media [479].

CHAPTER 5

FORMULATION DESIGN, OPTIMISATION AND CHARACTERISATION OF EFAVIRENZ LOADED FLAXSEED OIL SEDDS

5.1 Introduction

Pharmaceutical formulation development studies are aimed at facilitating the design of a high performance and quality product. A simple, adaptable and scalable manufacturing process is desirable to ensure sustainable production of a stable dosage form that exhibits consistent in vitro and in vivo performance [480,481]. The information and knowledge generated during pharmaceutical development activities and manufacture provides a rational scientific basis and understanding to support the establishment of a design space, use clinically relevant specifications and manufacturing controls for a particular product [482]. While the aqueous solubility of an API presents formulation challenges as discussed in Chapter 2 once an API is matched with compatible excipients in which the API is soluble, the proportions of each excipient required become crucial to ensure the stability, in vitro and in vivo performance of a SEDDS. Formulation development studies are aimed at producing a pharmaceutical product with the optimum composition to ensure therapeutic outcomes are achieved [422,483].

The components of SEDDS are selected to achieve maximum API loading that small or controlled droplet sizes form in the gastrointestinal tract to ensure maximal absorption. Consequently API loading and droplet size are Critical Quality Attributes (CQA) that for this formulation development process of SEDDS [150,484]. Other CQA of nano-emulsions include the droplet size, polydispersity index (PDI) and Zeta Potential (ZP). For optimised drug delivery, there is a need to understand physiological processes such as hepatic uptake and accumulation, tissue diffusion, tissue extravasation and renal excretion as a function of droplet size and/or other CQA.

Reports have shown that nano-carriers in the range 10 nm to 500 nm in size generate a greater fold increase in surface area to volume ratio and show higher trans epithelial transport and oral bioavailability compared to other formulation technologies with greater size particles [153,485]. Mono-disperse nano-carriers of PDI < 0.7 were desired. The ZP has an impact of particle stability, cellular uptake and intracellular trafficking of emulsion droplets [487]. therefore nano-emulsions with a high positive or negative ZP that are electrically stabilized are

desired whereas those with a low ZP tend to coagulate or flocculate leading to poor physical stability of emulsions, hydrophilic and negatively charged nano-carriers permeate rapidly through the mucus barrier, whereas hydrophobic and less negatively or preferably positively charged nano-carriers interact much more efficiently with the absorption membrane [253].

5.1.1 Design of experiments and mixtures designs

The optimization of emulsion mixtures to produce a product with predefined target specifications through estimation of the effects of formulation components on performance of the mixture can be achieved using a Design of Experiments (DoE) approach. Experimental designs such as a Box-Behnken or D-optimal mixture design in combination with Response Surface Methodology (RSM) has been applied to product formulation development activities in the food, pharmaceutical and cosmeceutical industries since a reduced number of experiments are used to generate data for which interactions between input variables can be identified using statistical tools thereby avoiding the shortcomings of using the traditional one factor at a time approaches [488–490]. Since the introduction of concepts of Quality-by-Design (QbD) the maxim that quality of pharmaceutical products should be designed and built into a product during the development process rather than testing it into the product has been the approach used for product development [359]. A factorial approach using a CCD was used to optimize an HPLC method for the analysis of EFV (§ 3.5 in Chapter 3), However since we need to define a design space mixed experimental designs are required to construct that design space. The design space of a mixtures design experiment is essentially the set of possible combinations of the relative proportion of each component in a formulation which must add to a total of one [491,492]. The design space of a factorial experiment is a set of possible combinations of independent input variables or components [493]. When the components of a mixture to be produced are constrained that they must total 1 in a 3-component mixture, then a standard mixture design is formed and it is depicted as a triangular design space in Figure 5.1.

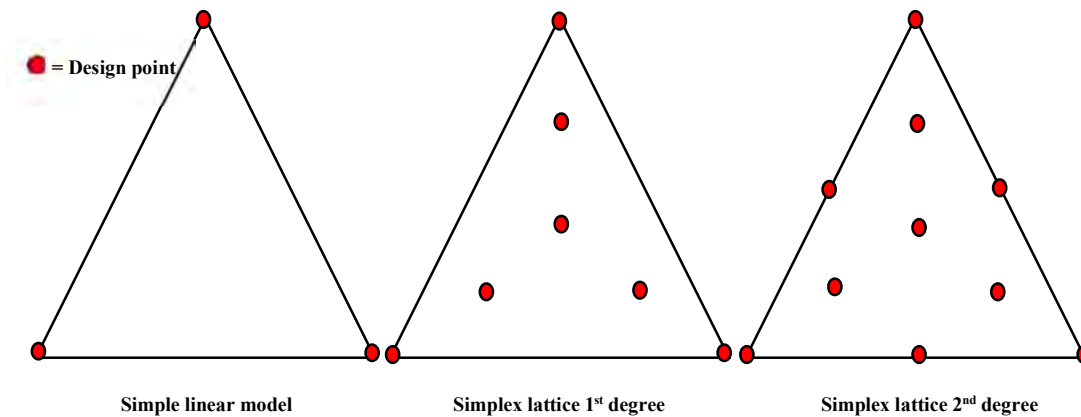


Figure 5.132. Schematic representation of standard simple linear and simplex lattice designs.

Simple linear, simplex-lattice and simplex centroid designs are the standard approaches used for fitting data for mixtures and there is an increase in number of design points and complexity progressing from simple linear to simplex lattice 2nd degree models [494]. When the components of a mixture are subjected to additional constraints, such as requiring they fall between a minimum and maximum for each component, designs other than the standard mixture design or constrained mixture designs are constructed [495,496].

5.1.2 Surfactant mixture optimization

By way of example for a three-component surfactant mixture prepared using Span[®] 20 (A) Tween[®] 80 (B), and ethanol (C) the input variables for optimization would be the proportion of each of the components. Consequently, when using statistical modelling for data analysis the input variables in a surfactant mixture can be considered the vertices of the triangular design space. Reducing the terms to A, B and C, changing the composition would produce terms that describe effects of a model viz., A, B, C, AB, AC, BC, A²BC, AB²C, ABC² which are subsequently tested to identify which term(s) have a coefficient which is significantly different from 0, in other words is > 0 and can be used to produce information relating to of the correlation of predicted and observed responses [353]. The largest positive coefficient for a model term(s) represents those terms that exert the largest effect on a specific response monitored. The most common empirical models to which experimental data are fitted are linear, quadratic or cubic models of which the linear model is the simplest and complexity of the polynomial increased from 1st, 2nd, to 3rd degree respectively [366]. A 4th degree

polynomial for systems involving composition, with the sum of the proportions by volume and weight has also been applied and reported in when using mixture design of experiments [497].

5.1.3 Phase behaviour and exploitation of design spaces

Phase behaviour studies to investigate emulsion formation types for compositions containing flaxseed oil, Tween[®] 80, Span[®] 20 and ethanol. Screening studies were undertaken to identify points or regions of phase diagrams where emulsions with physicochemical properties such as isotropy and transparency were produced and the associated droplet size and polydispersity index were important parameters in formulation development activities, in this context. The identified regions can be further exploited to produced products with appropriate characteristics for routes of administration such as topical delivery, where gel regions were observed [498]. When < 10 % w/w flaxseed oil was used along dilution line 9 (Figure 5.2) the region in which points marked in red fall from P1 to P20 was observed to be where transparent isotropic emulsions formed.

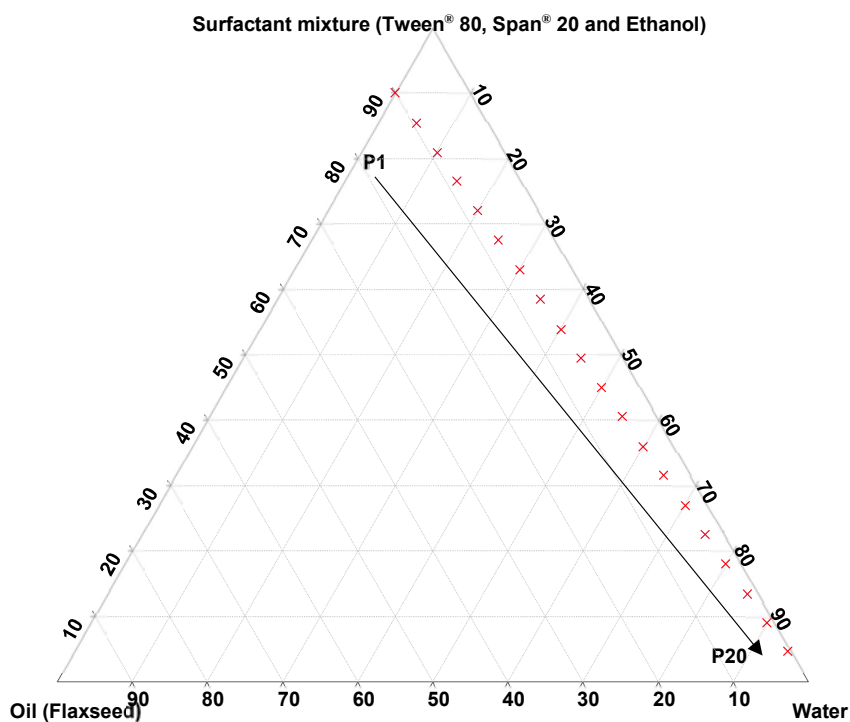


Figure 5.233. Phase diagram for screening for emulsion regions.

The region defines the optimum area for the facile production of transparent micro and nano-emulsions with droplet sizes ranging between 10 nm and 500 nm with low energy use. By

saturating nano-emulsions with EFV, the nano-emulsions remained isotropic and transparent in nature and exhibited sufficient loading capacity for EFV so as enable the manufacture of small dose units of 1.15 g formulation containing 600 mg of EFV. This dose unit size is lower than that of 1.3 g of commercially available EFV tablet whilst still delivering 600 mg EFV. This is particularly advantageous as there is the potential to produce child size SNEDDS products for paediatric patients and enhance the ease of administration.

Following phase identification and location of an appropriate emulsion region, further optimization of the composition of the surfactant mixture viz., Span[®] 20, Tween[®] 80 and ethanol in nano-emulsions with 10 % w/w flaxseed oil was undertaken using a D-optimum simplex constrained mixture design space. The actual contour polygonal area in the triangular space is depicted in Figure 5.3. The design set the levels of Span[®] 20 (A) and Tween[®] 80 (B) at a minimum of 5 % w/w and maximum of 90 % w/w with ethanol (C) content set to a maximum of 20 % w/w. The minimum composition of each component was set at 5 % w/w to ensure that the effects of ternary surfactant mixtures and not binary mixtures where non-isotropic phase behaviour was observed.

Component Coding: Actual

● Design Points

Std Error Shading

0.500 1.500

X1 = A: Span 20

X2 = B: Tween 80

X3 = C: Ethanol

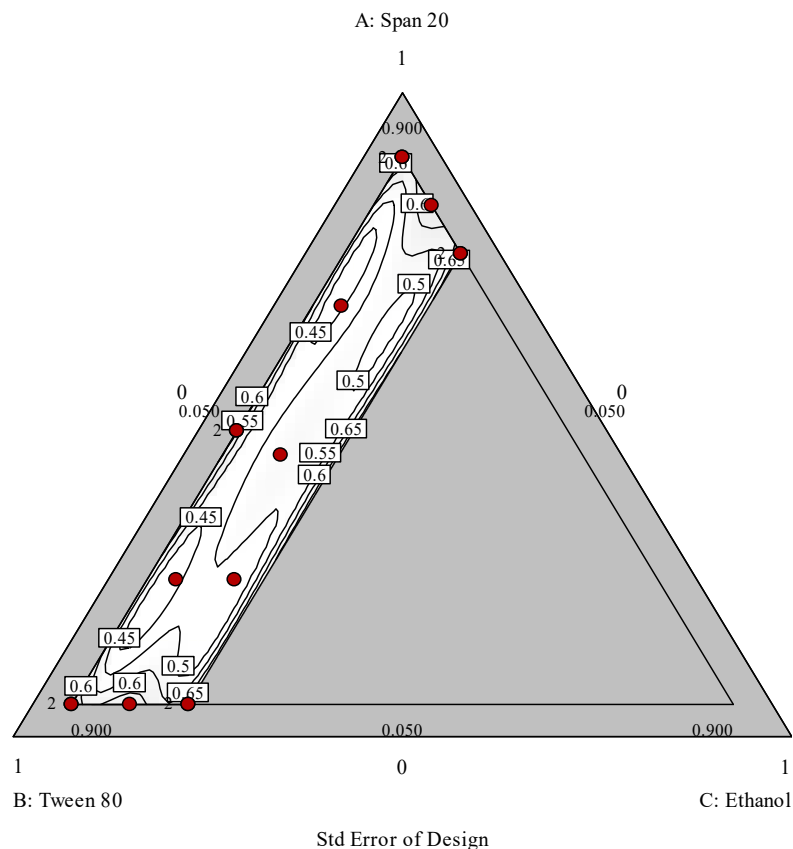


Figure 5.334. Real contour plot of the simplex lattice design applied to surfactant mixture optimization

5.2 Experimental (manufacture and characterisation of SEDDS)

5.2.1 Materials

Cold pressed flaxseed, soybean, sunflower, olive, grapeseed and macadamia oils were purchased from Escentia products (Johannesburg, Gauteng, South Africa). Span[®] 20 and Tween[®] 80 were purchased from Merck (Johannesburg, Gauteng, South Africa). HPLC grade acetonitrile from Burdick and Jackson[™] and ethanol were purchased from Anatech (Olivedale, Gauteng, South Africa). EFV was donated by Adcock Ingram[®] Limited (Wadeville, Gauteng, South Africa). HPLC-grade water was produced using a RephiLe Bioscience Direct-Pure[®] Ultrapure RO water system, (Boston, MA, United States of America) which was purchased from Microsep (Pty) Ltd, Johannesburg, South Africa).

5.2.2 Preparation of nano-emulsions

Nano-emulsions were manufactured by initially placing approximately adding 1.2 g of excess EFV into a test tube containing 1 g the nano-emulsion and stirring at 100 rpm with the aid of an FMH-STR magnetic stirrer (Lasec[®], Cape Town, South Africa) at a laboratory temperature of $22 \pm 2^\circ \text{C}$ for 48 hours. The saturated nano-emulsions were centrifuged at 3000 rpm for 15 minutes using a Model HN-SII IEC centrifuge (Thermo Scientific, Waltham, MA, United State of America) to separate excess EFV from the nano-emulsion.

5.2.3 Droplet size and polydispersity index

The PDI and droplet size of the SEDDS a was determined using a Nano-ZS Malvern Zetasizer (Malvern Instruments, Malvern, Worcester, United Kingdom) set in the Dynamic Light Scattering (DLS) mode. The sample was prepared for analysis by dispersing a 500 μL aliquot of the nano-emulsion prepared as described in § 5.4 in 50 mL HPLC grade water and placed into a $12.5 \times 12.5 \times 45$ mm BRAND[®] disposable cuvette (BRAND GMBH + CO KG, Wertheim, Germany). The sample was analysed at a scattering angle of 90° at 25°C and light scattering data analysed using Mie theory, with real and imaginary refractive indices set at 1.456 and 0.01 respectively [499].

5.2.4 Zeta Potential

The Zeta Potential (ZP) of each dispersion was determined using a Nano-ZS Malvern Zetasizer (Malvern Instruments, Malvern, Worcester, United Kingdom) set in the Laser Doppler Anemometry (LDA) mode. The sample was prepared by dispersing a 500 μL aliquot of the nano-emulsion with 50 mL HPLC grade water in A-grade volumetric flasks which were sonicated using a Model B12 Branson[®] ultrasonic bath (Branson Inc., Shelton, Conn, USA) for 5 minutes. Samples were then transferred into a folded capillary cell using a glass pipette for ZP measurements. All samples were prepared and analysed in triplicate ($n = 3$) at an applied field strength of 20 V/cm and the Helmholtz-Smoluchowsky equation used to calculate the ZP for each sample [500,501].

5.2.5 Transmission electron microscopy

Transmission Electron Microscopy (TEM) was used to visualise the shape and surface morphology of the nano-emulsion droplets in aqueous dispersions. Briefly, a drop of the

aqueous nano-emulsion dispersion was placed onto a 3.05 mm copper grid fitted with a FORMVAR/Carbon support 300 mesh film (TAAB Laboratories Equipment Ltd, Alderson, Berks, RG7 8NA, United Kingdom). Excess liquid was removed using Whatman® 110 hydrophilic filter paper (Whatman® International Ltd, Maidstone, United Kingdom) after which the sample was allowed to dry at room temperature (22 °C) for 24 h. The sample was visualized using a Zeiss® Libra Model 120 TEM (Zeiss, GmbH, Germany) operated at an accelerating voltage of 80 kV.

5.2.6 Fourier Transform Infrared Spectroscopy (FTIR)

The FTIR spectrum of the EFV loaded nano-emulsion was captured using a Spectrum 100 Fourier transform-infrared attenuated total reflectance spectrometer (Perkin Elmer® Ltd, Beaconsfield, United Kingdom) over the wave number range 650-4000 cm⁻¹. A sample of nano-emulsion samples were mounted onto a diamond crystal using an applied force of approximately 100 N and spectral data was processed using FT-IR Spectrum version 10.5.4 software (PerkinElmer®, Inc Pty Ltd, Beaconsfield, United Kingdom). Manufactured samples were characterised at the same time as EFV loaded nano-emulsions that were harvested after in vitro dissolution testing and left to dry in an open petri dish at room temperature for 72 hours.

5.2.7 Raman spectroscopy

Raman spectroscopy was used to characterise loaded and blank nano-emulsions to determine if the spectra signals were altered due to interaction of the components used in the EFV loaded nano-emulsions. A Bruker Vertex 70-Ram II Raman spectrometer from (Bruker Optics, Inc., Billerica, MA, USA) equipped with a 1064 nm Nd: YAG laser for excitation in the region of 3400–80 cm⁻¹ and liquid nitrogen cooled germanium detector was used to generate spectra that were acquired at 300 scans per minute. The instrument was set at 300 mW and the sample was placed in a hemispheric bore of an aluminium sample holder. The spectral resolution was 4 cm⁻¹ and the spectra were processed using OPUS version 6.5 spectroscopy software (Bruker Optics, Inc., Billerica, MA, USA).

5.2.8 X-ray diffraction

X-ray diffractograms of EFV loaded nano-emulsions were generated using a Bruker D8 Discover diffractometer (Billerica, Massachusetts, USA) with a proportional counter, Cu-Ka

radiation and 1.5405 Å nickel filter. The voltage and current used for data generation were 30 kV and 40 mA, respectively in the $2\theta = 10^\circ$ to 100° angle range at a scanning rate of 1.5 $^\circ/\text{min}$ with a filter time constant of 0.38 s and slit width of 6 mm. Samples were placed onto a silicon wafer slide and diffractogram data treated and analysed using Version 14.0 EVA (evaluation curve fitting) XRD Commander Version 2.61 software (Bruker- AXS GmbH, Karlsruhe, Germany) with baseline correction performed by subtracting a spline function fitted to the curved background.

5.2.9 EFV loading capacity

The loading capacity of SEDDS was established for each batch of nano-emulsion produced. Approximately 100 mg of each SEDDS formulation was weighed using a Mettler Toledo analytical balance (Mettler[®] Instruments Inc, Zurich, Switzerland) dispersed and dissolved in mixture of 3/2 v/v ethanol and water in a 10 mL A-grade volumetric flask. The samples were then sonicated using a Model B12 Branson[®] ultrasonic bath (Branson Inc., Shelton, Conn, USA) for 5 minutes. The amount of EFV in each formulation was determined using the validated RP-HPLC method described in 3.5.2 in Chapter 3. The amount of API in each batch was interpolated from standard calibration curve for EFV produced on a daily basis.

5.2.10 In-vitro EFV release

In-vitro testing to characterise EFV release from SNEDDS were undertaken using USP II apparatus. The in-house method developed was initially based on the previously reported methods summarised in Table 5.1 and the available dissolution apparatus in our laboratory.

Table 5.7. Published methods for in-vitro EFV release testing

Dosage form	Apparatus	Dissolution medium	% EFV released	Reference
Capsules	USP II	1 % m/v SLS	98.39 % at 4 hours	[502]
Tablets	USP II	0.1 M HCl + 0.5 % m/v SLS	100 % at 60 mins	[503]
Solid lipid nanoparticles (SLN)	Dialysis tube	Phosphate buffer pH 7.4	60.6 – 98.22% at 24 hours	[504]
Capsules	USP II	0.1% m/v Tween [®] 80	70 % at 100 mins	[505]
Tablets	USP II	0.5 %, 1.0 %, and 2.0 % m/v SLS s	Up to 87.51% at 60 mins	[506]
Polymeric nanoparticles	USP II	Phosphate buffer pH 7.4	69.05 % over 24 hours.	[507]
Lipid liquid solutions	USP II	1% m/v SLS	Up to 90.2% over 60 mins	[508]
Suspension	Dialysis tube	0.1 M HCl pH 1.2	91.21% at 24 hours	[509]
Polymeric solid dispersions	USP II	0.25 % m/v SLS in FeSSIF pH 5.0	> 87 % at 120 minutes	[510]

The most common approach involves the use of sodium lauryl sulphate (SLS) in 0.5 - 2 % m/v concentrations in acidic conditions. The FDA suggests the use of 1 % w/v SLS when testing drug release testing of sparingly soluble compounds in capsules with a sinker with justification if necessary [511]. Therefore a 0.1 M HCl with 1 % m/v SLS was used as the dissolution medium in this research. On interaction with 1% m/v SLS in 0.1M (HCl) dissolution medium, the nano-emulsion formulations formed a white edged crystalline semi-solid which sank in the dissolution vessel. The dissolution time of nano-emulsion filled capsules (n = 6) at 37 ± 1 °C was approximately 8 ± 1.03 min and the first sample was pulled at 15 minutes therefore, sinkers were not necessary in this study. A 300 μ L aliquot of EFV loaded nano-emulsion was transferred into a size 00 hard gelatine capsule using a Gilson PIPETMAN[®] electronic micropipette prior to in vitro EFV release studies. Such as a small amount was used so as to maintain sink conditions with the 900 mL dissolution medium.

In vitro dissolution studies were conducted using a Hanson Vision[®] G2 Elite 8 USP apparatus II dissolution bath fitted with a Vision AutoPlus and DissoScan[™] auto sampler (Teledyne Hanson Research, Chatsworth, LA, United States of America). Testing was conducted at a rotation speed of 50 rpm in 900 mL 0.1M hydrochloric acid pH 1.2 with 1 % w/v SLS at 37 ± 1 °C. A 10mL sample was withdrawn at 15, 30, 60, 120, 390 and 720 minutes with replacement after sampling. Studies were performed in triplicate (n=3) and EFV determined using the validated HPLC method described in Chapter 3 of this thesis.

5.2.11 Comparison of release profiles

EFV release following in vitro release testing of oral formulations were compared using the f2 similarity factor [512]. It is a logarithmic transformation of the sum-squared error difference between a test and reference product at all-time points and is calculated using Equation 5.1. The value of f2 may lie between 0 and 100, however the closer the value to 100 the more similar the profiles are [513].

$$f2 = 50 * \log\left\{1 + \left(\frac{1}{n}\right) \sum_{t=1}^n (R_t - T_t)^2\right\}^{-0.5} * 100\}$$

Equation 5.20

Where,

R_t = cumulative percent EFV released for the reference product (F5)

T_t = cumulative percent EFV released for the test product (F3)

n = number of time points

5.2.12 Stability

Short term stability evaluation of nano-emulsions was undertaken using under different conditions viz., phase separation, heat cool cycles, storage at room temperature (22°C) and 4 °C for 28 days. The droplet size, PDI and ZP were determined in triplicate (n=3) every week over and the data compared °C o the data generate immediately after manufacture (T₀) [514]. Formulations were manufactured and tested on the day of manufacture and then packed prior to storage in tightly sealed 50 g clear glass jars.

5.2.12.1 Phase separation

The nano-emulsions were tested for phase separation by centrifuging at 3500 rpm at room temperature (22 °C) for 30 minutes at using an IEC Model HN-SII centrifuge (Damon, Needham HTS, MA, USA). After centrifugation, the nano-emulsions were visually assessed for any phase separation (formation of immiscible phases or sedimentation) as this is maybe a manifestation of instability [515]. Samples were stored at various conditions for 28 days and centrifuged each 7 days.

5.2.12.2 Heat cool cycles

Samples of EFV loaded SEDDS stored for 28 days at 22 °C were then assessed against heat cool cycles after the whole period. The formulations were subjected to six cooling and heating cycles between storage in a Fuchsware refrigerator (Fuchsware, Midrand, Gauteng, South Africa) refrigerator at 4 °C and a Gallenkamp® Hotbox size one oven (Weiss Gallenkamp Limited, Leicestershire, UK) set at 45 °C. The samples were stored at each temperature for 48 hours [516].

5.3 Results and discussion

5.3.1 Statistical design and analysis

A single block D-optimal mixture design was launched using the constraints summarized in Table 5.2 with the aid of Design expert software version 12.0 software (Stat-Ease Inc., Minneapolis, MN, United States of America).

Table 5.8. Input variable constraints for D-optimal design.

Lower Limit %		Component		Upper Limit %
5	≤	Span [®] 20 (A)	≤	90
5	≤	Tween [®] 80 (B)	≤	90
5	≤	Ethanol (C)	≤	20
		Total: A+B+C	=	100

The purpose of the study was to evaluate the impact of Span[®] 20 (A), Tween[®] 80 (B) and ethanol (C) content on emulsion behaviour. The constraints for the surfactants were set at a minimum of 5 % minimum and maximum of 90 % maxima while ethanol (C) constraints were set to between 5 and 20 %. The minimum composition of each component was set at 5 % in order to assess the effects of a ternary surfactant mixture and avoid the use of binary mixtures which resulted in non-isotropic emulsions in phase behaviour studies in (§ 4.4.2 in Chapter 4).

The design was a single block simplex-lattice design for which the composition of the surfactant mixture viz., $A + B + C = 1$ and were used for the manufacture of 10 % m/m flaxseed oil nano-emulsions. The design required 16 experimental runs to evaluate the impact of surfactant on emulsion formation and the runs which are reported in Table 5.3.

Table 5.3. Surfactant mixture composition for the D-optimal design and actual experimental responses for 10 % m/m flaxseed oil nano-emulsions.

Run	Input variables % m/m			Responses		
	Span [®] 20 A	Tween [®] 80 B	Ethanol C	Droplet size nm	PDI	Zeta Potential mV
1	47.5	47.5	5	88.43	0.75	-23.85
2	66.875	24.375	8.75	408.25	0.332	-22.8
3	24.375	66.875	8.75	68.9	0.461	-21.9
4	5	82.5	12.5	173.4	0.176	-16.5
5	7.5	5	20	507.2	0.26	-23.2
6	7.5	5	20	404.4	0.324	-23
7	47.5	47.5	5	138.7	0.587	-18.8
8	5	75.0	20	180.56	0.481	-25.5
9	24.375	59.375	16.25	92.5	0.51	-18.6
10	5	90	5	70.5	0.12	-14.7
11	90.00	5	5	362.6	0.265	-21.4
12	5	75	20	58.1	0.412	-17.2
13	90	5	5	364.6	0.285	-21.9
14	43.75	43.75	12.5	441.1	0.365	-23.4
15	82.5	5	12.5	290.1	0.214	-23.4
16	5	90	5	70.75	0.119	-16.8

The experimental data were automatically fitted to models by the software to linear, quadratic, cubic, special cubic, quartic and special quartic models. The best fit mathematical model was

identified based on the comparison of statistical parameters of R^2 , adjusted R^2 and PRESS. The PRESS values of each tested model are listed in Table 5.4.

Table 5.4 PRESS statistic values for each applied and Sum of squares for all models applied to the data.

Model	PRESS value for responses monitored		
	Droplet size	Polydispersity	Zeta Potential
Linear	1.601E +05	5.43	138.58
Quadratic	2.480E +05	0.551	187.28
Cubic	6.933E +09	4612.21	1.349E +06
Special cubic	3.536E +05	0.5776	226.48
Special quartic	1.002E +06	0.2666	558.01
Sum of squares of suggested model	3.484E +05	3.97	68.8

The predicted residual sum of squares (PRESS) was used to establish the suitability of each model in respect of data fitting and the model with the lowest PRESS was identified as suitable for that response. The PRESS value analyses the prediction ability of models and the model with the minimum PRESS is usually considered the best predictive model for a set of data [368,517]. The recommended models therefore were, a special quartic model for both droplet size and PDI and a linear model for ZP.

The R^2 value is a measure of the variance of the response variables and the closer the R^2 value is to one viz., > 0.9 and the smaller the standard deviation therefore the more accurate the response predicted by the model [518]. A negative value for predicted R^2 implies that the overall mean is a better predictor of the response. However, adequate precision measures the signal to noise ratio and values > 4 indicate an adequate signal [519]. The ratio of Adjusted R^2 to R^2 is a measure of model fit when the model is applied to new data and ratios $> 20\%$ difference between R^2 and adjusted R^2 , indicate that the model contains a substantial number of predictors, relative to the amount of data used. When applied to new data sets the model is not reliable and is compromised further as the number of predictors increases which is an indication of a possible problem with the model due to a large block effect or data used by the model [520].

ANOVA analysis data were generated following fitting of the data to the suggested models are reported in detail in s Sections 5.5.1, 5.5.2 and 5.5.3 for droplet size, PDI and ZP, respectively. It was observed that the R^2 of droplet size and PDI were at least > 0.9 and the adjusted R^2 values of both were in close agreement with those of R^2 with a difference < 0.2 suggesting model adequacy as reported in the fit statistics summary in Table 5.5. The R^2 for Zeta Potential was low and not close to 0.9 and the difference between the R^2 and adjusted R^2 was > 0.2 which is possibly indicative of a large block effect or problem with the model. However, the adequate

precision was > 4 for all responses and was desirable showing that an adequate signal was observed and that the model could be used to navigate the design space. Consequently, a detailed analysis of each model was performed and is reported in the relevant sections.

Table 5.5. Fit statistics for responses using suggested models.

Response	Predicted model	f-value	Degrees of freedom	p-value	R ²	Adjusted R ²	Predicted R ²	Adequate precision
Droplet size	Special quartic	8.91	8	0.0046	0.910	0.908	-1.618	7.205
Polydispersity Index	Special quartic	86.11	8	0.0001	0.9899	0.9789	0.8335	29.195
Zeta Potential	Linear	5.09	2	0.0233	0.439	0.353	0.115	5.982

Following regression analysis and identification of suitable models using PRESS values additional evaluation is required to establish if the data fits the model fits adequately. Residuals may be used to establish if the model is able to predict and/or fit the data [366]. Residuals are essential remainders of the response following fitting of data to a model and are used to identify unexplained patterns in the data when fitted to a model [521]. Prior to point predicting using a design space, composition residual analysis was undertaken to confirm that the assumptions for Analysis of Variance (ANOVA) had been met. For this purpose, diagnostic plots viz., Box Cox plots of residuals were plotted for all three responses monitored and it was confirmed that data transformation was not required for droplet size, ZP and PDI and are depicted in Figures 5.4, 5.5 and 5.6 respectively.

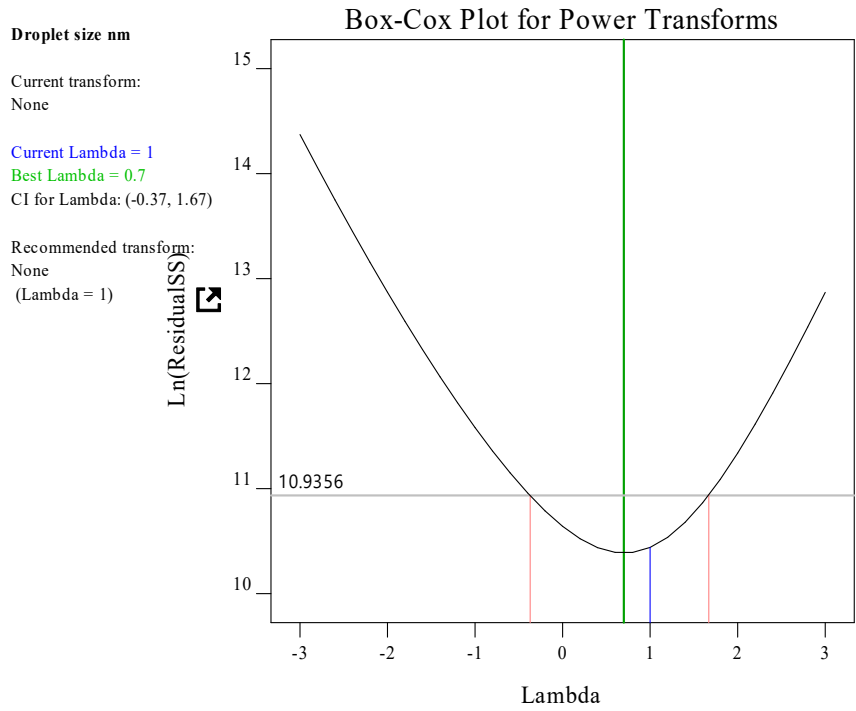


Figure 5.35. Diagnostic Box-Cox plot non-transformed for the special quartic model for droplet size

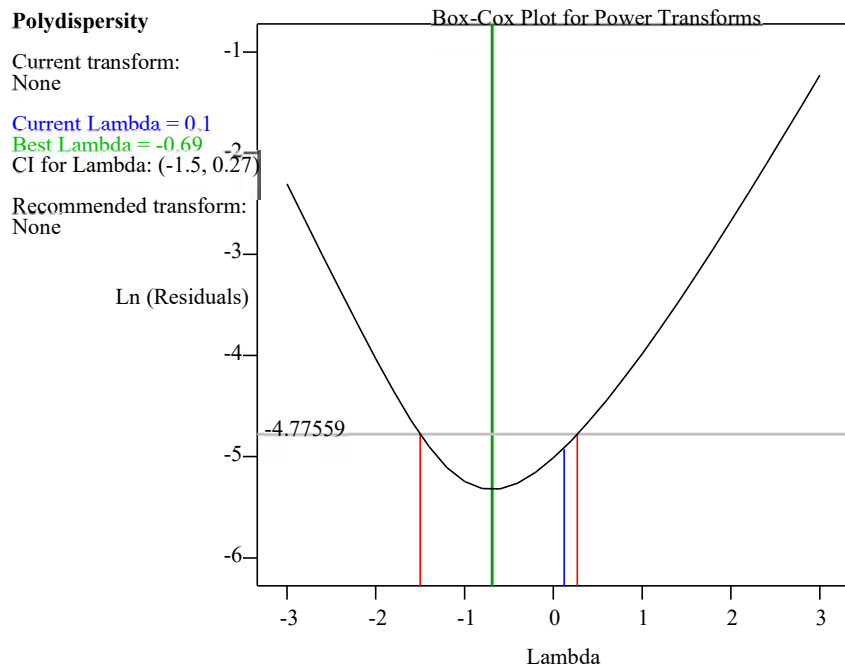


Figure 5.36. Diagnostic Box-Cox plot for non-transformed for the special quartic model for PDI

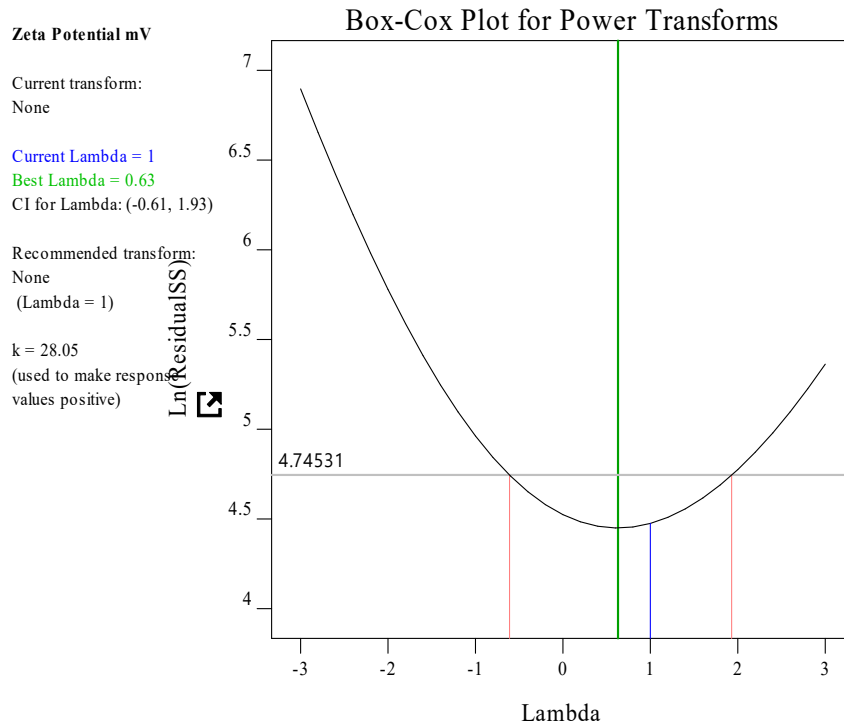


Figure 5.637. Diagnostic Box-Cox plot for non-transformed for the linear model for ZP.

To determine if power transformations were required, the Box-Cox plot depicted in Figure 5.4 were reviewed at $\lambda = 1$ (Lambda=1). The $\lambda = 1$ is depicted by the blue line and falls within the 95 % confidence interval (red lines) which is the optimum range of the parabola and therefore the untransformed model could be used to navigate the design space. At $\lambda=1$ for PDI and Zeta Potential, the blue line also fell within the 95 % confidence interval indicating the untransformed was suitable for use to navigate the design space [522].

Normal probability plots of residuals and plots of residuals versus predicted responses were also used to establish model adequacy [523]. For a model to be deemed adequate, all data points should fall on a relatively straight line in a normal probability plot and should be scattered in the residuals versus predicted response plot [524,525]. The residuals versus predicted response plots was structure less and independent with almost equal scatter of data above and below the zero-line of the plot. Implying that the proposed models are adequate and the variance of experimental measurements is constant for all values of responses monitored [526]. The normal plots of residuals in all cases were observed to fall along the trend line as depicted in Figures 5.7, 5.9 and 5.11 for droplet size, PDI and ZP.

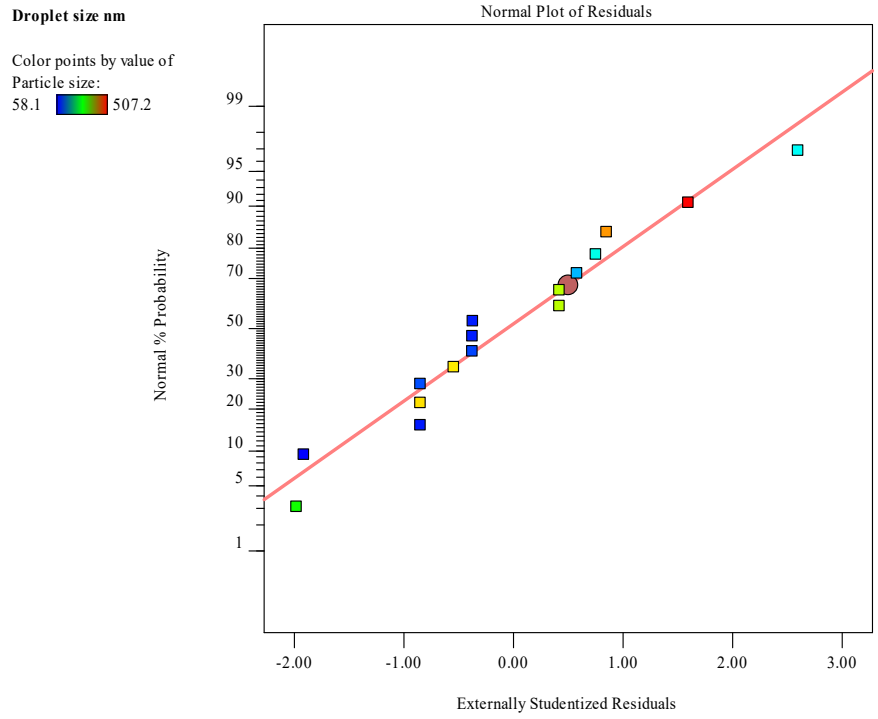


Figure 5.738. Normal plot of residuals for the special quartic model for droplet size.

The plots of residuals versus predicted reveal that the models were adequate, as the data meet the criteria as can be observed in Figures 5.8, 5.10 and 5.12 in which the residuals versus predicted plots for droplet size, PDI and ZP are depicted.

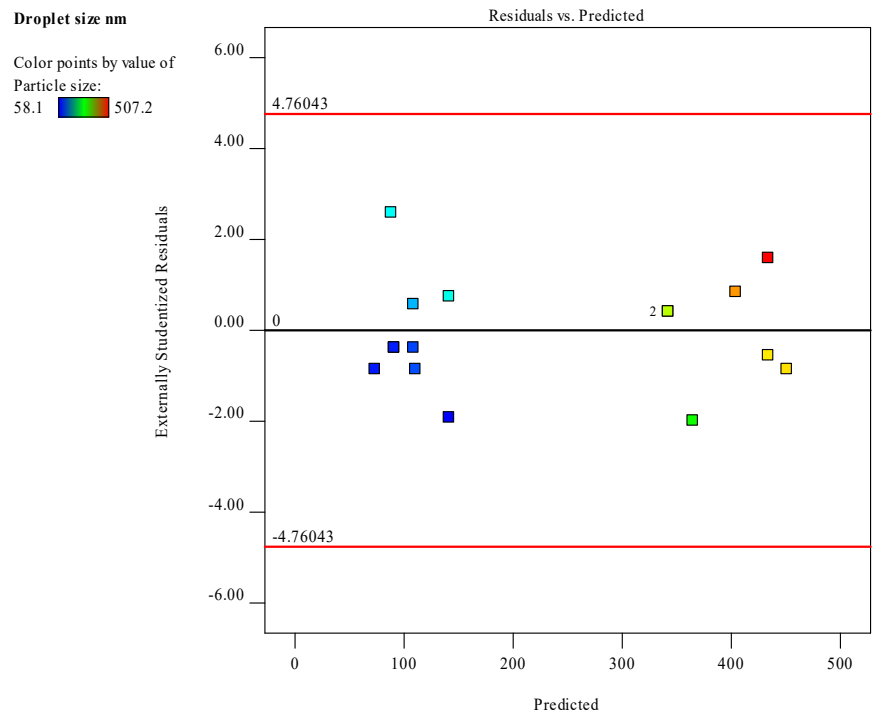


Figure 5.839. Residuals vs predicted plot for the special quartic model for droplet size.

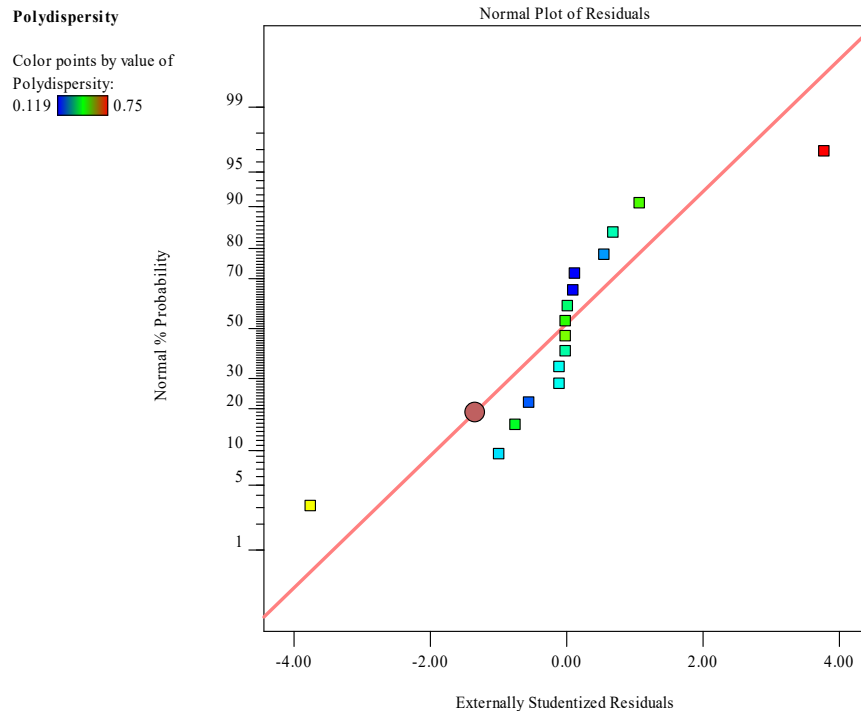


Figure 5.940. Normal plot of residuals for the special quartic model for PDI.

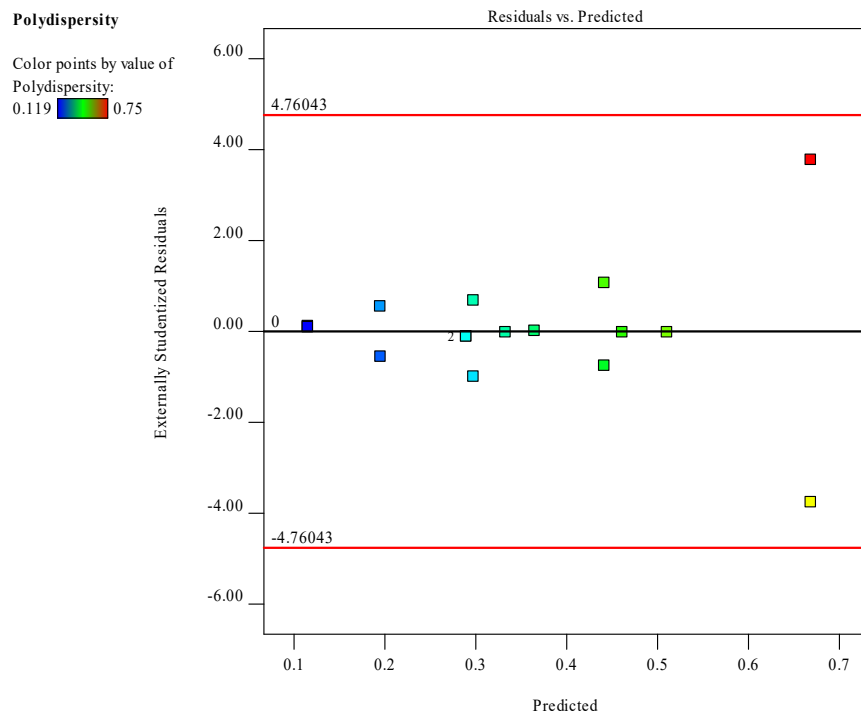


Figure 5.10. Predicted vs actual diagnostic plot for the special quartic model for PDI

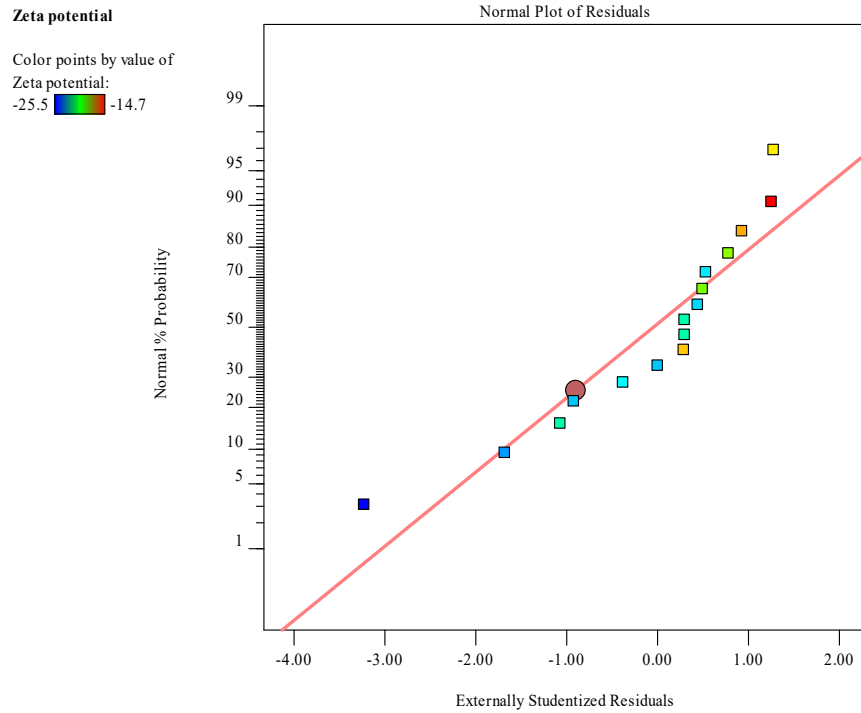


Figure 5.11. Normal plot of residuals for the linear model for ZP.

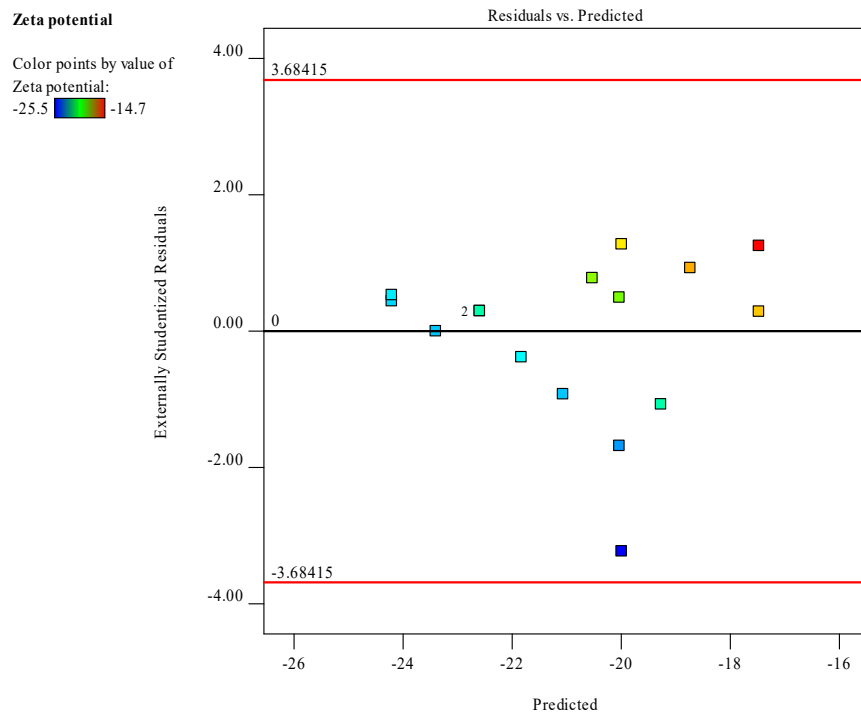


Figure 5.1241. Predicted vs actual diagnostic plot for the linear for ZP.

5.3.1.1 Droplet size

The resultant droplet size of the dispersed phase ranged between 58.1 nm and 507.2 nm with the smallest droplet sizes observed when Tween[®] 80 was used at the maximum level of 90 % in the surfactant mixture whereas in contrast the droplet size increased as the Span[®] 20 content was increased. A sharp increase in particle size was observed as the ethanol content was increased in the region of the Span[®] 20 and ethanol vertices and can be observed as the red region in the contour plot depicted in Figure 5.13. The 3D surface response is given in Figure 8 of Appendix 2.

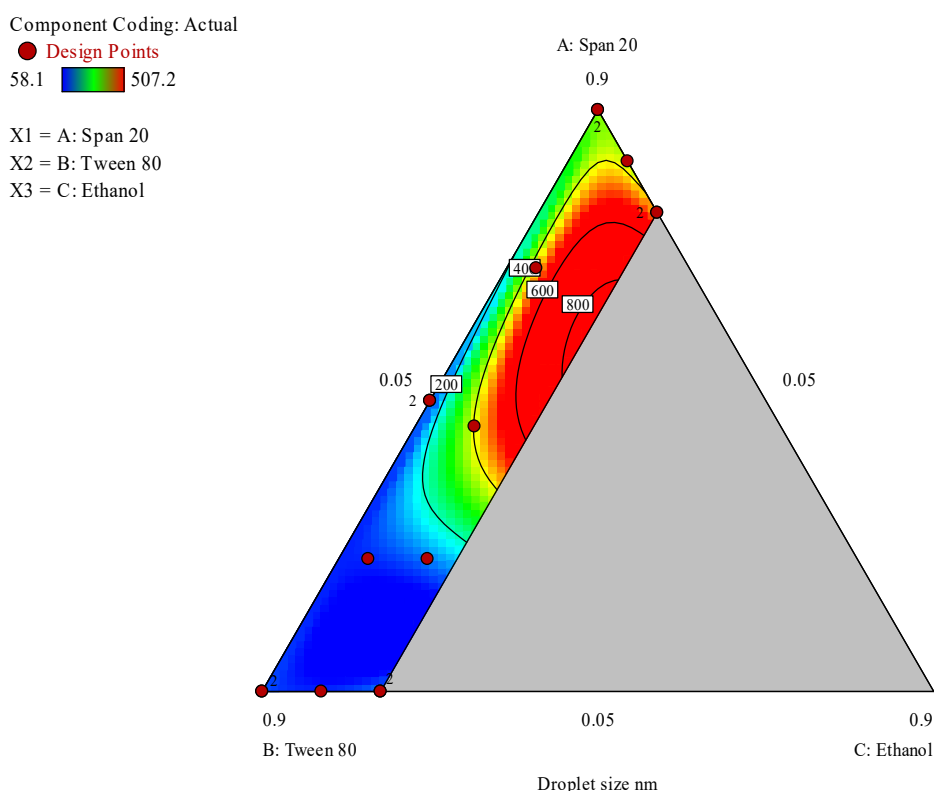


Figure 5.1342. Contour plot depicting the impact of surfactant mixture content on droplet size

The model F-value of 8.91 (Table 5.6) indicates that the special quartic model for droplet size was significant and that there is only a 0.46 % chance that a model F-value this large is due to noise. A p-value < 0.05 implies that the coefficients of the model terms were significantly different from zero or that the effect of the model terms or combination of terms exerts an effect that can be estimated from the formulation composition. The model terms for the mixture A, B, C and A²BC were significant. The terms AB, AC, BC, AB²C and ABC² were not significant. i.e. Span 20 (A), Tween 80 (B) and ethanol (C) in combinations as in each term had significant

influence on the resulting droplet size. From the model equation obtained in terms of coded factors for droplet size reported as Equation 5.2., the coefficients of each mixture terms would be able to suggest the largest negative effects or positive effects. By way of example for droplet size, The first three terms of Equation 5.2 A, B and C are in indication that as single excipients Span[®] 20, Tween[®] 80 and Ethanol all had a significant effect on droplet size with ethanol (C) having the largest positive effect.

$$\text{Droplet size} = 342.00A + 90.75B + 3328.66C - 530.59AB - 2941.83AC - 3530.63BC + 52488.71A^2BC - 11742.82AB^2C - 32873.13ABC^2$$

Equation 5.21

Table 5.6. ANOVA data for the special quartic model for droplet size, df = degrees of freedom.

Source	Sum of Squares	df	Mean Square	F-value	p-value	
Model	3.618E+05	8	45222.05	8.91	0.0046	significant
^Q Linear Mixture	2.675E+05	2	1.337E+05	28.89	0.0004	significant
AB	23590.52	1	23590.52	5.10	0.0586	significant
AC	845.21	1	845.21	0.1825	0.6820	significant
BC	1219.23	1	1219.23	0.2633	0.6236	significant
A ² BC	75719.26	1	75719.26	16.35	0.0049	significant
AB ² C	1434.95	1	1434.95	0.3099	0.5951	Not significant
ABC ²	457.54	1	457.54	0.0988	0.7624	Not significant
Residual	32410.38	7	4630.05			
Lack of Fit	19627.96	2	9813.98	3.59	0.0977	Not significant
Pure Error	12782.42	5	2556.48			
Cor Total	3.942E+05	15				

The lack of fit F-value of 3.59 implies that lack of fit was not significant. The predicted R² for droplet size was negative implying that the mean data might be a better predictor for this response than using the model. However, adequate precision was > 4 and was desirable indicating that an adequate signal was observed and that the model could be used to navigate the design space.

5.3.1.2 Polydispersity Index

The contour plot for the PDI of all the emulsions in the design space ranged between 0.119 and 0.75 in the design space with the lowest value for PDI observed at around the upper limit of ethanol and Span[®] 20 in region in blue had very low PDI values close to 0.119. The equation

in terms of coded terms shows that ethanol as single excipient (C) had the largest positive effect on PDI, however the rest of the region showed no particular pattern with the 3D response surface plot reported in Figure 7.9 of Appendix 3. As the amount of ethanol in the mixture increases, it is expected that the solvent capacity of the system also increases therefore sufficiently breaking down emulsion micelles into smaller mono-disperse droplets. The highest PDI values of undesirable polydispersity > 0.7 was observed on the minim point of ethanol and about 50 % of both Span[®] 20 and Tween[®] 80 shown as the almost yellow/orange region in the contour plot depicted in Figure 5.14.

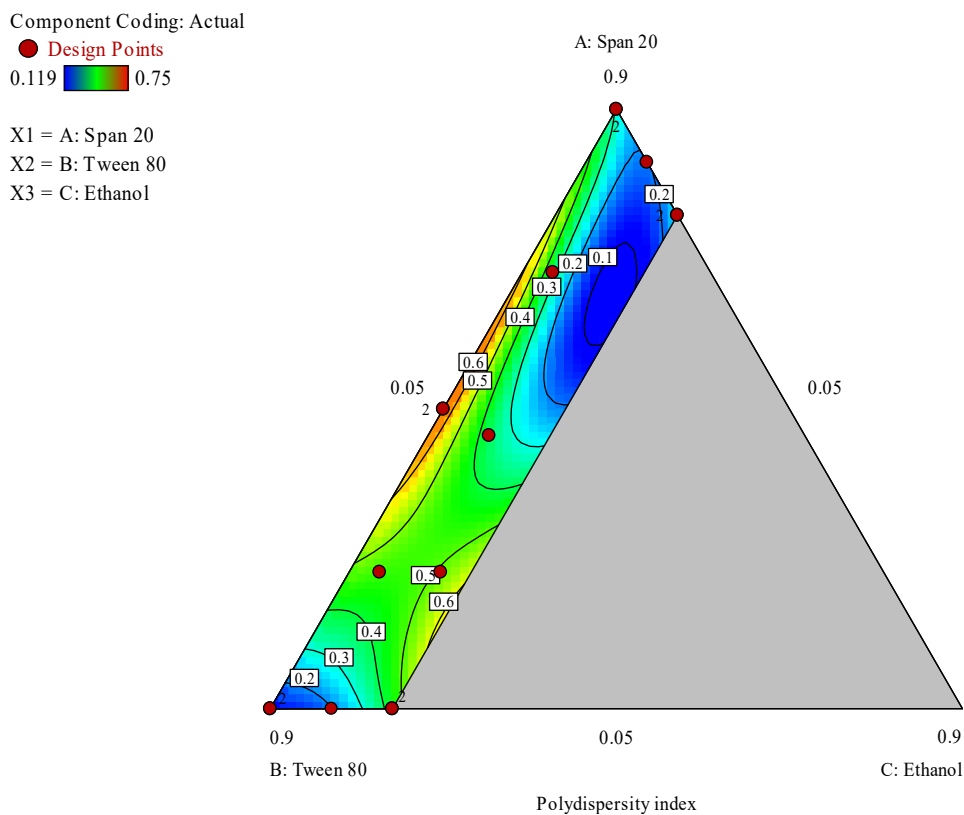


Figure 5.14. Contour plot depicting the impact of surfactant mixture content on PDI.

The model F-value of 86.11 (Table 5.8) indicates that the special quartic model for PDI was significant and that there is only a 0.01% chance that a model F-value this large is due to noise. A p-value of probability $> F < 0.05$ implies that the coefficients of effect and relationship of the model terms A, B, C, AB, AC, BC, A²BC, AB²C and ABC² were significantly different from zero and can be estimated and ANOVA data and results for this special quartic model are listed in Table 5.7. This information indicates that the amount of Tween[®] 80, Span[®] 20 and ethanol used in the surfactant mixture has an effect on the PDI for all polynomial model terms listed. The model equation in terms of coded factors for PDI is reported as Equation 5.3.

The predicted R^2 0.8335 is in reasonable agreement with the adjusted R^2 0.9789. The lack of fit F-value 0.08 implies that lack of fit was not significant for the model and that there is a 56.02% chance that the lack of fit F-value this large is due to noise.

$$\text{Polydispersity index} = 0.2868A + 0.1155B + 10.85C + 2.19AB - 12.93AC - 10.78BC - 43.34A^2BC + 1.016AB^2C + 37.74ABC^2$$

Equation 5.22

Table 5.7. ANOVA data for special quartic model for Polydispersity index, *df* = degrees of freedom.

Source	Sum of Squares	df	Mean Square	F-value	p-value	
Model	0.5429	8	0.0679	86.11	< 0.0001	significant
⁽¹⁾ Linear Mixture	0.0004	2	0.0002	0.2235	0.8052	
AB	0.4020	1	0.4020	503.39	< 0.0001	
AC	0.0158	1	0.0158	19.84	0.0030	
BC	0.0114	1	0.0114	14.22	0.0070	significant
A ² BC	0.0510	1	0.0510	63.83	< 0.0001	
AB ² C	0.0000	1	0.0000	0.0133	0.9115	
ABC ²	0.0006	1	0.0006	0.7551	0.4137	
Residual	0.0056	7	0.0008			
Lack of Fit	0.0012	2	0.0006	0.6522	0.5602	not significant
Pure Error	0.0044	5	0.0009			
Cor Total	0.5485	15				

5.3.1.3 Zeta Potential

All the three components of the surfactant mixture have an effect on the ZP of the dispersion according to the linear relationship described mathematically in equation 5.4.

$$\text{Zeta Potential} = -23.10A - 17.08B - 29.48C$$

Equation 5.23

The amount of ethanol used in the surfactant mixture has the largest effect on the ZP as indicated by the large absolute value for the coefficient for (C) in the equation and the contour plot depicted in Figure 5.15 when 20 % ethanol (C) exhibits largest ZP. The contour plot reveals the presence of significant region in blue indicating that as the concentration of Span[®] 20 in the surfactant mixture increases the ZP decreases and becomes more negative with the lowest negative point occurring when ethanol is used at the upper limit tested and Tween[®] 80 at the lowest level.

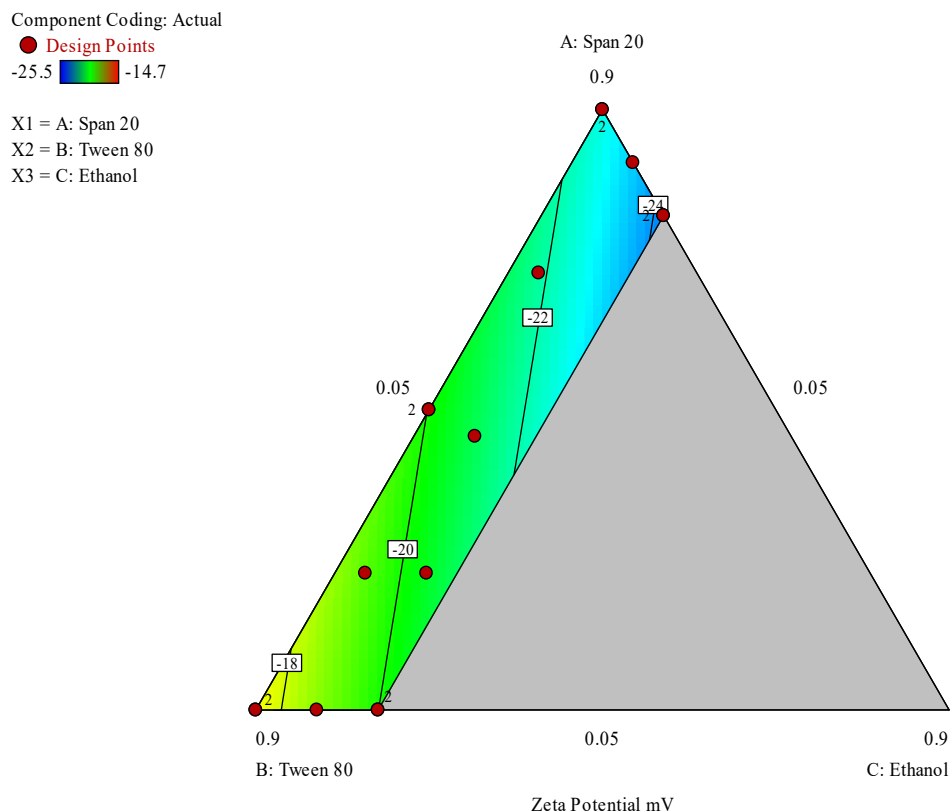


Figure 5.15. Contour plot depicting the impact of surfactant mixture composition on ZP

The model F-value of 5.09 reported in Table 5.8 implies that the linear model for ZP is significant and that there is only a 2.33% chance that a model F-value this large is due to noise. The probability p-value < 0.05 implies the model terms are significant and the coefficients of the effect of each model term is significantly different from zero and can be estimated for this linear model. Only the model terms A (Span[®] 20), B (Tween[®] 80) and C (ethanol) are significant within the formulation composition of these nano-emulsions. The predicted R^2 value of 0.1152 is not in close agreement with the adjusted R^2 of 0.3530 suggesting a large block effect or possible problem with the model although, the adequate precision > 4 is desirable and this adequate signal indicates that the model can be used to navigate the design space. The lack of fit F-value 0.49 implies that lack of fit is not significant for the model and there is an 82.64% chance that a lack of fit F-value this large is due to noise.

Table 5.8. ANOVA data for a linear model of Zeta Potential, *df* = degrees of freedom.

Source	Sum of Squares	df	Mean Square	F-value	p-value	
Model	63.33	2	31.66	5.09	0.0233	significant
^o Linear Mixture	63.33	2	31.66	5.09	0.0233	
Residual	92.11	13	7.09			
Lack of Fit	54.93	8	6.87	0.9237	0.5628	not significant
Pure Error	37.17	5	7.43			
Cor Total	155.43	15				

5.3.1.4 Statistical optimization

The optimization function was used to predict the levels for each of the components of the surfactant mixture based on criteria and the specific constraints listed in Table 5.9.

Table 5.9. Constraints used for identifying the optimized composition.

Name	Goal	Lower Limit	Upper Limit	Lower Weight	Upper Weight	Importance
Span® 20 (A)	is in range	0.05	0.9	1	1	3
Tween® 80 (B)	is in range	0.05	0.9	1	1	3
Ethanol ©	minimize	0.05	0.2	1	1	3
Droplet size	is in range	100	150	1	1	3
Polydispersity index	minimize	0.119	0.75	1	1	3
Zeta Potential	minimize	-25.5	-14.7	1	1	3

The primary criterion used for the optimization process was that the amount of ethanol used in the surfactant mixture should be as low as possible from a regulatory and safety perspective. The second criterion used required that the emulsion droplet size be between 100 and 150 nm. The e third and fourth criteria required that the PDI be as low and ZP as high as possible. Two optimized surfactant solutions were produced based on the desirability function and the formulation composition for the two solutions are reported as batches F4 and F5 in Table 5.10. The desirability of significantly less than 1 show that the point prediction of the region in the optimized criteria is very small in proportion to the region of non-conforming in the design space.

Table 5.10. Solutions for specified optimization criteria.

Number/Formulation	Span® 20 %	Tween® 80 %	Ethanol %	Droplet Size nm	PDI	ZP mV	Desirability
1/F4	58.1	36.0	6.0	198	0.641	-21.320	0.463
2/F5	32.2	58.3	9.5	159	0.484	-20.204	0.531

The overlay plot that shows a yellow area in which the desired optimization criteria are met is depicted Figure 5.16. Following manufacture and assessment of the batch F4 and F5 product the percent prediction error for the D-optimum design was calculated using Equation 5.5.

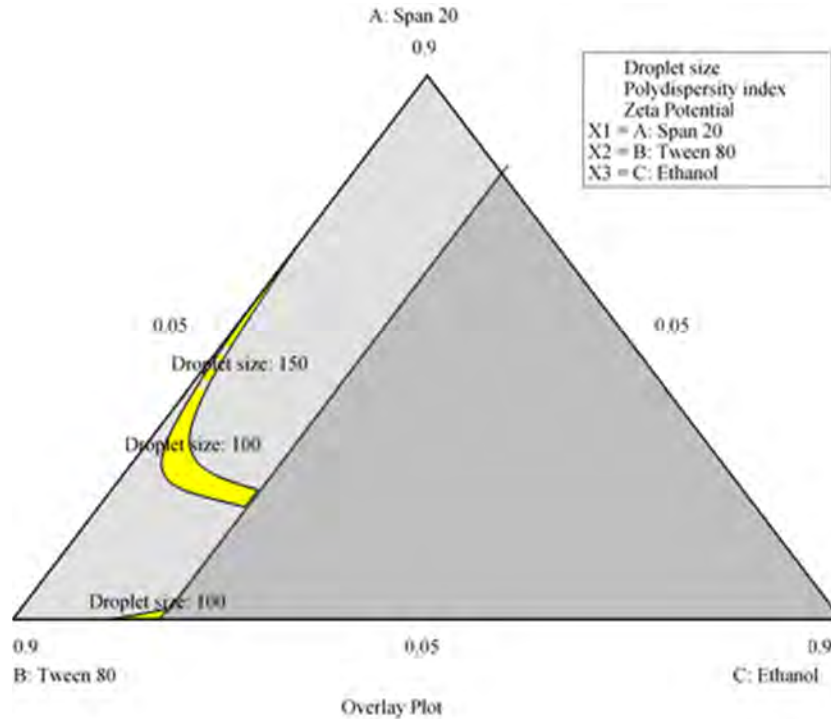


Figure 5.16. Overlay plot of the desirable area (yellow) derived using the specified criteria listed in Table 5.10.

$$\text{Prediction error} = \left[\left(\frac{V_e - V_p}{V_e} \right) \times 100 \right]$$

Equation 24.5

Where,

V_e = experimental value

V_p = predicted value

The prediction error for droplet size was 12 % for batch F4 and 8.33% for batch F5 revealing that this experimental design was the best predictor for droplet size whereas the prediction error for PDI was 31.6 % for batch F4 and -16.94% for batch F5. The model was not able to predict ZP adequately with prediction errors of 249 % and 219% for batches F4 and F5, respectively. As seen the overlay plot the region of optimization is narrow with respect to the design space suggesting that optimization of this system using a D-optimal design may not be possible as

relatively good predictability was only observed for droplet size. It is therefore necessary to evaluate alternate experimental designs for future optimization investigations.

5.4.2 Characterization and in vitro assessment of optimized nano-emulsions

The five surfactant mixtures viz., batches F1, F2, F3, F4 and F5 the composition of which is reported in Table 5.11 were evaluated. Three compositions were identified from phase diagrams in Figure 4.7, 4.8 and 4.9 in section 4.5.2, and two were derived following numerical optimization using the D-optimal design. Batches F1, F2 and F3 were nano-emulsion formulations made using arbitrary surfactant mixture compositions identified when assessing the phase behaviour for S1, S2 and S3 surfactant mixtures at point P1 point along dilution line 9 for each surfactant mixture in the phase diagram described in section 4.5.2. Batches F4 and F5 were identified as solutions 1 and 2 from the statistical optimization data reported in section 5.7.4.

Table 5.9. Compositions of surfactant mixtures used for the manufacture and characterization of 10 % w/w EFV loaded flaxseed nano-emulsions

Formulation	Span® 20 % m/m	Tween® 80 % m/m	Ethanol % m/m	Droplet size nm	PDI	ZP mV	EFV content mg/mL
F1	40	40	20	185.1 ± 0.7	0.444 ± 0.003	-35.4 ± 0.9	377 ± 4.9
F2	33.3	33.3	33.3	190.3 ± 2.0	0.387 ± 0.016	-34.4 ± 0.7	437 ± 13.1
F3	28.5	28.5	42.8	156.8 ± 23.4	0.342 ± 0.048	-41.0 ± 0.9	571 ± 18.7
F4	58.1	36.0	6.0	225.6 ± 16.8	0.487 ± 0.003	-31.9 ± 3.12	329 ± 9.45
F5	32.2	58.3	9.5	146.7 ± 25.3	0.402 ± 0.012	-24.1 ± 2.33	334 ± 11.2

5.4.2.1 EFV loading

The ethanol content in the surfactant solution had the greatest effect on the EFV loading of the nano-emulsions. The largest concentration of EFV of 571 mg/mL was observed for batch F3 indicating high ethanol levels enhance the solubility of EFV in the nano-emulsion. A decrease in EFV loading was observed as the amount of ethanol used, decreased. To administer the recommended maximum adult dose of 600 mg 1.09 g of the batch F3 nano-emulsion formulation would need to be administered. The total mass of product required is considerably less and more convenient than that of commercially available 600 mg EFV tablets produced by Cipla, Erige, Adco and Aspen weighed 1.34 ± 0.09 , 1.25 ± 0.11 g, 1.20 ± 0.08 g and 1.106 ± 0.045 g (n=20), respectively suggesting that the nano-emulsion may be a more convenient dosage form size for patients to use.

5.4.2.2 Droplet size and PDI

The droplet size distributions of the five nano-emulsions ranged from 146 nm for batch F5 to 225 nm for batch F4 with results depicted in Figure 5.17. No obvious trend with regards to surfactant mixture composition and droplet size was observed although a sharp increase in particle size was observed as the amount of ethanol used increased in the region of the Span[®] 20 and ethanol vertices in the contour plot in Figure 5.13 in section 5.7.1. All batches except for batch F4 exhibited mono-modal droplet size distributions which exhibited a bimodal size distribution. The PDI for of the nano-emulsions for all batches ranged from a minimum 0.342 (F3) to a maximum 0.487 (F4). Batches F3 and F4 were manufactured using the extreme low (5 %) and high (20 %) ethanol content. As the amount of ethanol used in the nano-emulsion a more homogenous droplet size of the dispersed phase was observed with a corresponding low PDI. All formulations exhibited values for PDI < 0.7 and were therefore considered mono-disperse [527].

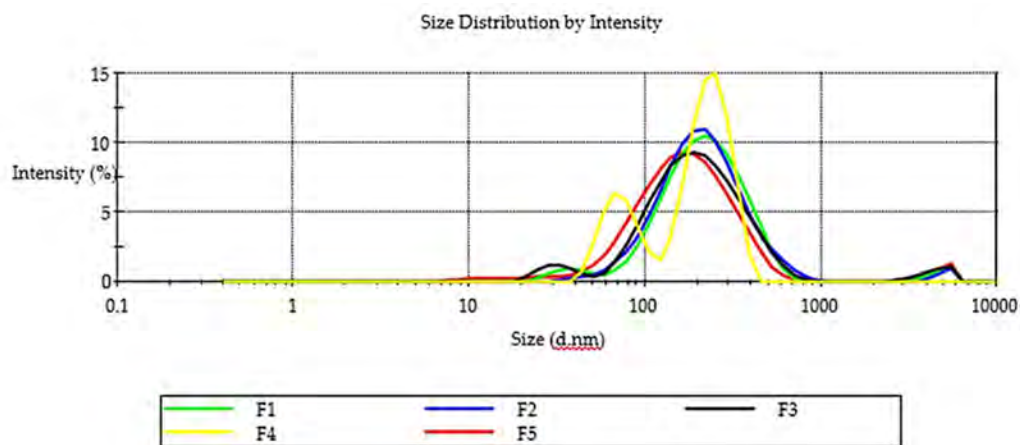


Figure 5.1743. Droplet size distribution for batches F1 - F5.

The bimodal droplet PS distribution observed for batch F4 may, in part, be due to the surfactant mixture. Ethanol content had the largest effect on solvent capacity of the mixture for both surfactants, the oil phase and EFV. Therefore, the bimodal distribution observed for batch F4 may be due to the solvent capacity of the system for the lipophilic phase Span[®] 20 which was at its highest concentration, As batch F4 was manufactured with the lowest composition of ethanol and the highest amount of Span[®] 20 (lipophilic) including the fixed 10 % flaxseed oil which may have formed large agglomerates of their HLB of different sizes within the nano-

emulsion due to the very low solvent capacity of the surfactant mixture [528]. In contrast high concentration of ethanol used in batch F3 result in a more unimodal droplet size as agglomeration in the nano-emulsion is minimized. Confirmed by D-Optimal analysis of PDI in section 5.7.2, ethanol (as a single excipient) content had the largest effect on the solvent capacity and miscibility of the mixture for both surfactants, the oil phase and the drug. The more ethanol in the system, the more flexible the interfacial film between the immiscible phases and rigid interfacial film has been reported to give rise to bimodal distributions [529].

5.4.2.3 Zeta Potential (ZP)

Although the surfactants used in these studies are non-ionic and do not ionize, changes in polarity as adsorption of the surfactant molecules onto charged water molecules may lead to the formation of an electric double layer similar to that observed when ionic surfactants are used [122,207]. Ethanol as a component which is polar may have been the reason for a negative Zeta Potential of the emulsion mixtures. For all batches, F5 which had the least amount of ethanol had the largest value of ZP. F1, F2, F3 and F4 had ZP values more negative than -30 mV suggesting that the composition used may produce stable nano-emulsions over the long term. Emulsion droplets with a ZP of approximately ± 20 mV exhibit only short-term stability, with the tendency for the droplets to flocculate and coalesce [530]. However, all five batches produced in these studies exhibited ZP values < -20 mV (Table 5.12) suggesting the nano-emulsions produced were likely to be stable [531-532].

5.4.2.4 Transmission electron microscopy

Transmission electron microscopy revealed the presence of largely spherical lipid droplets as depicted in Figure 5.18 for F5. TEM images for F4, F3, F2 and F1 are given in appendix 3 in Figures 7.15, 7.16, 7.17 and 7.18 respectively.

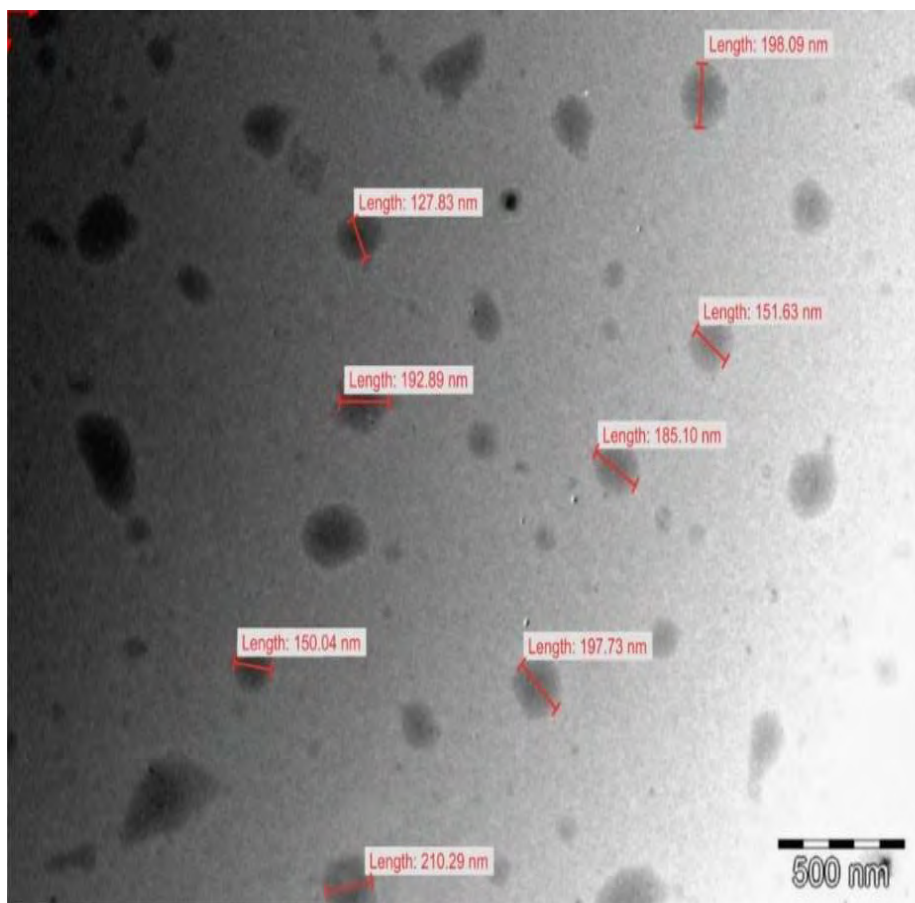


Figure 5.18. Transmission electron micrograph of nano-emulsion F5.

The average droplet size determined using TEM data was in close agreement with that determined using dynamic light scattering (Table 5.12). Some droplets in the size range 20–100 nm was observed in the nano-emulsion dispersion albeit in low numbers as reflected in the droplet size distribution [533].

5.8.5 FTIR

The FTIR spectrum of EFV loaded nano-emulsions depicted in Figure 5.19 reveals the characteristic signals for EFV viz., an intense band due to the stretching vibration of the –C–F bonds at 1196 cm^{-1} , C=O stretching of the amide group at 1740 cm^{-1} , CF_3 stretching band at 1163 cm^{-1} and C-C stretching due to an alkyne $\text{C}\equiv\text{C}$ at 2250 cm^{-1} [462,534]. The spectral data is in agreement with previously reported data and a summary of the band assignments observed are listed in the discussion of pre-formulation studies in § 4.4.2 of this thesis. The

spectra still contained all the expected bands and peaks of the reported EFV crystalline polymorph.

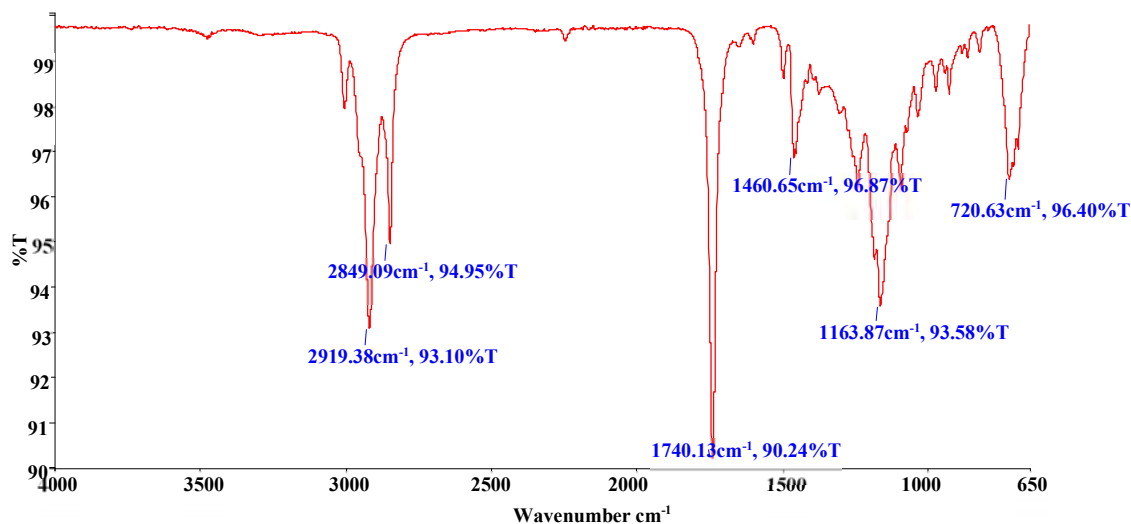


Figure 5.1944. FTIR spectrum of EFV loaded nano-emulsions.

5.4.2.5 Raman spectroscopy

The Raman spectra of EFV loaded nano-emulsion F1 is depicted in Figure 5.20, those of F2, F3, F4 and F5 were completely identical to Figure 5.20. The stretching vibrations of EFV remain unchanged and are were unaffected when loaded into the nano-emulsion indicating no interaction between EFV and the excipients used in the formulation. However long-term real-time stability studies will be required to ensure the system is indeed stable. Raman spectroscopic spectrum reveals all expected signals for EFV present and were in agreement with previously reported data with a table of comparisons of experimental vibrational wavenumbers spectra as described in pre-formulation studies in Table 4.5 in section 4.5.4 of this thesis [470]. The signal for the $-\text{CH}_2$ group at 3093 cm^{-1} , the $\text{C}\equiv\text{C}$ bond at 2250 cm^{-1} , the $\text{C}=\text{O}$ bond at 1750 cm^{-1} and the $\text{C}-\text{H}$ stretch at approximately 1000 cm^{-1} reflect that EFV is present in crystalline form [463].

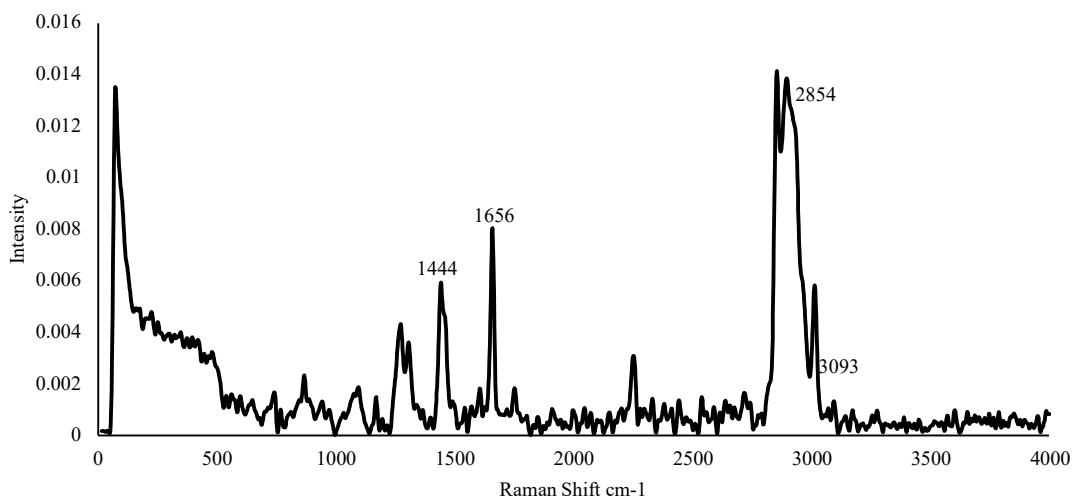


Figure 5.2045. Raman spectrum of EFV loaded nano-emulsion F1.

5.4.2.6 X-ray diffraction

The X-ray diffraction pattern for an EFV loaded nano-emulsion F1 is depicted in Figure 5.21 reveals the presence of peaks at 21.8°, 25.1°, 27.8°, 31.9°, 43.9° and 54.0° that correspond to the diffraction pattern of the stable crystalline form I polymorph of EFV [64,474]. The diffractogram for F2, F3, F4 and F5 were completely identical to that of F1.

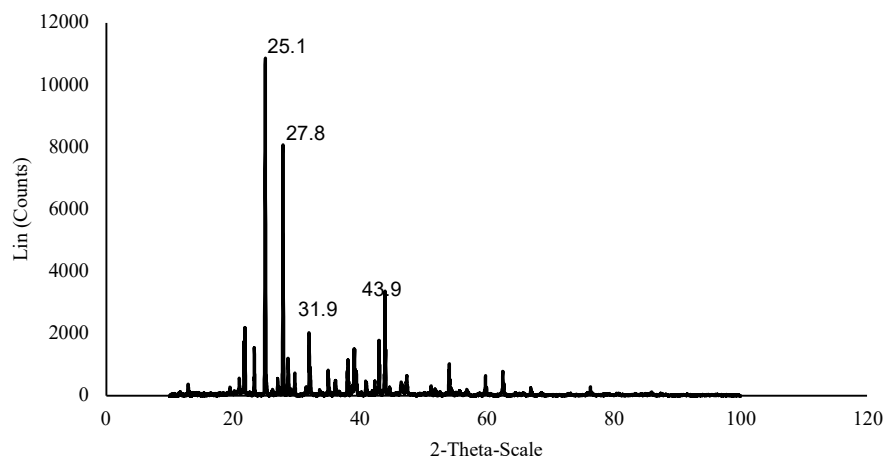


Figure 5.2146. XRD signal of pure EFV loaded nano-emulsion F1-F5.

5.4.2.7 In vitro EFV release

Dissolution testing was conducted over 12 hours with samples pulled at 15, 30, 60, 120, 390 and 720 minutes and analysed by HPLC. A 0.1M HCl solution of 1 % w/v SLS was used with a volume of 900 mL added to the vessels. An aliquot of 1.25 mL of the dissolution medium was withdrawn at the specified time intervals and was replaced with fresh medium of similar volume. Size 00 hard gelatine capsules were filled with 300 μ L of each formulation tested, this corresponded to HPLC determined EFV in each formulation approximately 113.1, 131.1, 171.3, 98.7, 100.2 μ g/mL of EFV in F1, F2, F3, F4 and F5 capsules respectively tested in the dissolution media if 100 % EFV was released. To ensure the same sink conditions (ultimate EFV concentration was three times lower than the equilibrium concentration of the drug in the dissolution media which was determined to be 683.3 μ g/mL), The cumulative drug release profile of the nano-emulsions was produced and reported in Figure 5.22.

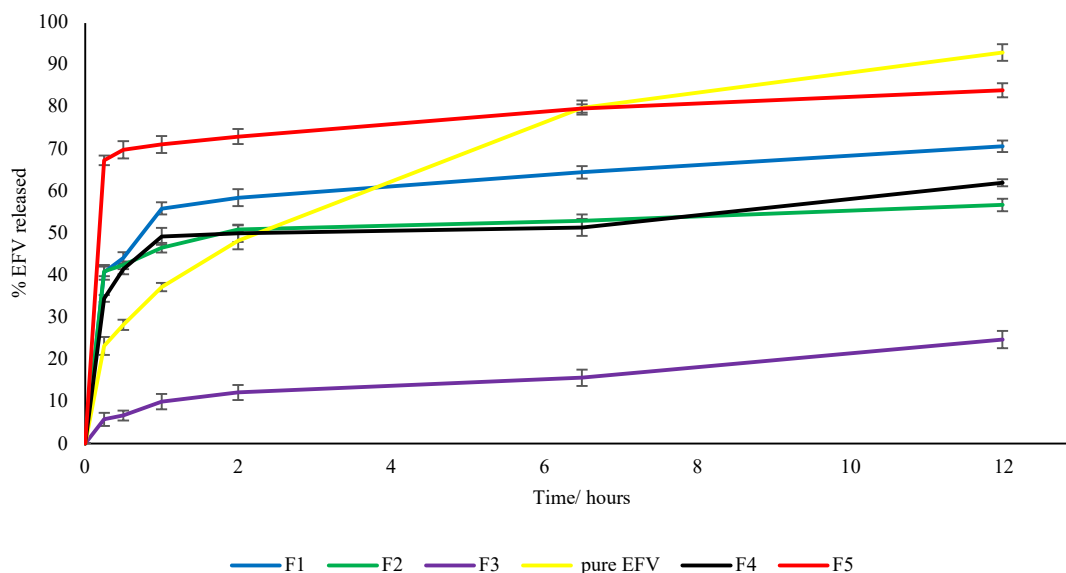


Figure 5.2247. Mean \pm SD ($n = 3$) dissolution profiles for batches F1, F2, F3, F4 and F5 and EFV powder.

In vitro release testing revealed that there was an initial burst of EFV released from batches F1, F2, F4, F5 and when EFV raw material was tested within the first hour of commencement of testing. The initial burst may suggest the presence of an EFV rich region in the exterior lipid layer of the nano-emulsion. Batch F5 exhibited the greatest extent of EFV release at 12 hours

whereas batches F1, F4, F5 and F3 exhibited a slower rate and lower extent of release as can be observed in Figure 5.22. As the proportion of ethanol in the formulation is increased, the percent EFV released at 12 hours decreased. As interaction of the nano-emulsion with the 1% m/v SLS in 0.1M HCl dissolution medium occurred crystallization (formation of a semi-solid) which had white edges that sank to the bottom of the dissolution vessel was observed. The F4 and F5 batches of nano-emulsion were prepared using the same amount of ethanol but different proportions of Tween[®] 80 and Span[®] 20. The extent of EFV release from batch F5 was greater than that for batch F4 at 12 hours possibly due to the different hydrophilic lipophilic balance (HLB) value of the surfactants used. Tween[®] 80 is soluble in an aqueous environment, whereas Span[®] 20 is not and therefore Tween[®] 80 interacts with the dissolution medium and contributes to improved dissolution of EFV [535].

It is well known that API may precipitate in vitro and in vivo due to sharp changes in pH, dilution with body fluids or digestion of solubilizing excipients resulting in low API concentrations in the aqueous phase and more drug trapped in the crystal structure consequently, the saturation method of manufacture of these nano-emulsions may result in nucleation which promotes crystallization once saturation of the system has been achieved [536]. On visual observation, nano-emulsion F3 on contact with dissolution media formed a semi-solid structure at a faster rate than F5 and to a lesser extent F2. This may be a manifestation of crystallization or precipitation was observed for all batches tested and was greatest for batch F3. Alternatively, EFV release from nano-emulsion F3 may be attributed to solubilisation of EFV in the nano-emulsions droplets which retards release. Drug precipitation described as crystallization that may occur during dissolution studies may be undesirable as the compound is expelled from solution when entrapped in micelles before absorption, this may reduce the extent of drug distribution immediately after administration, however in some cases a drug release profile such as F3 may be useful for the reduction of the dose dumping effect and the adverse effects thereof of EFV by providing more controlled drug release however the eventual release of the drug may be aided by the presence of enzymes and digestion of the lipids in the formulation.

5.4.2.8 Stability studies

These SEDDS were developed with the perspective of encapsulated oral dosage forms usually stored at room temperature, stability samples were therefore focused on weekly migration of samples at 22 °C for 28 days. Samples stored at 4 °C were sampled once at 4 weeks and samples

for heat cool cycles were processed after 28 days of storage at 22°C and also assed for EFV content. Samples stored at 22 °C were pooled each week and assessed for droplet size, PDI and Zeta Potential. Some of the critical quality attributes (CQA) following stability studies results are reported in Table 5.12 and reveal that the formulations were relatively stable at 4 °C were CQA remained relatively constant when compared to those at T0 measured immediately following manufacture.

Table 5.12. CQA results of formulations assessed after various stability conditions.

CQA	T0 22° C	T1 week 22° C	T2weeks 22 °C	T3weeks 22 °C	T4weeks 22° C	T 4weeks 4° C	T(HTC)	Sample
Droplet size nm	146.6	150	151.67	160.54	198.72	148.90	182.40	F5
PDI	0.40	0.41	0.40	0.42	0.417	0.39	0.79	
ZP mV	-24.1	-26.0	-25.89	-25.05	-26.07	-244	-22.31	
EFV content mg/ml	334					299		
Droplet size nm	225.6	233.7	250.1	267.8	287.5	232.4	389.6	F4
PDI	0.487	0.457	0.415	0.47	0.42	0.46	0.81	
ZP mV	-31.9	-32.4	-30.8	-29.77	-29.01	-30.3	-24.2	
EFV content mg/ml	329					320		
Droplet size nm	156.8	175.05	174.5	168.9	157	194.05	216.5	F3
PDI	0.34	0.41	0.39	0.44	0.42	0.33	0.63	
ZP mV	-41.0	-38.6	-39.3	-36.7	-29.1	-42.3	-19.5	
EFV content mg/ml	571							
Droplet size nm	190.3	194.8	210.1	217.6	225.9	198.5	300	F2
PDI	0.38	0.36	0.41	0.39	0.44	0.407	0.65	
ZP mV	-34.4	-30	-32.6	-28.7	-29.8	-37.9	-16.4	
EFV content mg/ml	437						429	
Droplet size nm	185.1	178.6	195.8	207.5	219.4	194.7	287.1	F1
PDI	0.44	0.39	0.40	0.46	0.47	0.507	0.70	
ZP mV	-35.4	-36.3	-35.9	-33.6	-31.5	-37.8	-29.6	
EFV content mg/ml	377						363	

Generally, the nano-emulsions showed a droplet size and PDI increase over time. Samples that were exposed to heat cycling (T_{HTC}) exhibited the largest droplet size and PDI increases with PDI values which were greater than 0.7 showing that the formulations became polydisperse over time. The migration of Zerta potential over time did not show any specific pattern or trend.

The least stable nano-emulsions were observed to be the ones exposed to heat cool heat cycles, followed by those stored at 22 °C for 4 weeks then 3 weeks all the way to those on the day of manufacture. At T_{4weeks}, the nano-emulsions kept at 4 °C had a smaller increase of droplet size compared to the formulation kept at 22 °C. Higher temperatures have been shown to increase the kinetic energy of particles which in turn leads to collisions between particles and thus particle size increase from particle agglomeration [122]. However, these formulations were considered suitable and stable in enough in the short term for oral administration as they did not present with any phase, separation, colour change or significant changes in CQA assessed after 28 days of storage at 22 °C which is their expected storage conditions.

5.5 Conclusions

Kinetically stable (low energy nano-emulsions produced using flaxseed oil, Tween[®] 80 and Span[®] 20 and ethanol were successfully manufactured. The EFV release profiles observed from different nano-emulsions can be exploited for further optimization to produce formulations suitable for undertaking in vivo pharmacokinetic studies. The side effects of EFV associated with dose dumping may be reduced by using nano-emulsions to modulate release. The nano-emulsion approach is promising however the stability of formulations in gelatine or other encapsulated forms in which crystallization of EFV from solution is minimized, should be explored. The use of flaxseed oil in dosage forms intended for oral delivery may be beneficial to patients as there are health benefits associated with use of polyunsaturated fatty acids containing oils. Furthermore, flaxseed oil is relatively economic and is a sustainable raw material for dosage forms [425].

The recommended dose of EFV in adults is 600 mg administered once daily and the most common dosage form available is a tablet, which is inconveniently large that may negatively affect patient adherence. The design of LBDDS focused on making the release characteristics independent of the gastro-intestinal physiology, the fed/fasted state of the patient and focussed on producing a small dosage form convenient for the patient to use. The negative ZP observed suggest the technology would be useful for macrophage targeting since macrophages identify and take up negatively charged particles. Macrophages are key cells in HIV infection and are significant reservoirs of the virus. The results of these studies reveal there is potential to use a SEDDS as a carrier system for EFV that may exhibit increased bioavailability and may modulate delivery. Furthermore, the dose and frequency of dosing may be reduced thereby enhancing patient adherence. The method of manufacture used to manufacture the SEDDS is

simple can be scaled for industrial production however scale up manufacture and proof of in-vivo performance must be undertaken as the next phase of this research process.

CHAPTER SIX

CONCLUSIONS

HIV is a disease prevalent in many countries around the globe with the highest mortality observed in developing countries. In efforts to improve access to HIV drugs, simplification of process chemistry, reformulation, dose reduction, inclusion of new drug classes and new therapeutic strategies have been developed and used as tools to contribute to the reduction of the HIV burden. Currently, there are several NNRTIs approved for use in HIV treatment, with EFV being one of the most prescribed drug of this class.

The bioavailability of EFV is however very low due to poor aqueous solubility and as a result current dosage forms may not perform with the best possible therapeutic outcomes. SEDDS have recently been the focus as an approach for overcoming the poor solubility and oral bioavailability of API particularly those classified as BCS II and IV compounds. SEDDS approach may ensure a consistent temporal profile with reduced frequency of dosing and dose levels which is of particular importance for the use of combination formulations of ART to promote adherence and patient outcomes. Furthermore, reduced frequency of dosing may play role in mitigating for the shortcoming of a low genetic barrier to resistance of EFV. Consequently, it was deemed appropriate to attempt to develop, manufacture and assess the release of EFV through self-emulsifying drug delivery system (SEDDS) formulations using sustainable vegetable oils to mitigate for some of the challenges associated with the performance of EFV dosage forms.

Different analytical techniques have been used for the characterisation of SEDDS. The loading capacity (LC) and in-vitro release of EFV from SEDDS was monitored using a RP-HPLC method developed and validated for use in these studies. This method was also used to determine the solubility of EFV in several vegetable oils with highest solubility of EFV observed in flaxseed oil. Future work could also examine the solubility of EFV in surfactants to establish if the triglyceride or the surfactant is a dominant solubilizing factor although ethanol was observed to have the highest impact on solubility of EFV.

Pseudo-ternary phase diagrams and Winsor phase behaviour were used for identification of formulation phases that assisted in defining appropriate proportions of each component to use and the facilitation of decisions in relation to manufacturing processes such as whether high or low energy methods were suitable for combinations of flaxseed oil, Tween[®] 80, Span[®] 20 and

ethanol co-solvent. Distinct regions of the phase diagrams revealed transparent isotropic regions, gel regions and other Winsor I, II and III with phases separated (non-isotropic) regions. The transparent isotropic region proportions were chosen as an area of interest and further analysed and optimized using statistical DoE due to their low energy formation and high solubility capacity of EFV.

Particle size and PDI analysis was performed using a Nano-ZS Zetasizer and surface morphology of the nano-dispersions was generated using transmission electron microscopy (TEM). Crystallization and polymorphic transitions of SEDDS were investigated using DSC, FT-IR, XRD and Raman spectroscopy. XRD data revealed that 1:1 m/m binary mixtures of EFV and each excipient except for ethanol resulted in complete disappearance of the signals for the EFV for XRD possibly due to a change of crystalline EFV to an amorphous form or the formation of a complete molecular dispersion of the API in the lipids investigated. The FTIR and Raman spectra revealed the disappearance of EFV in the presence of surfactants due to EFV existing in the molecular state in the SEDDS dispersions with improved solubility through functionality of self-emulsifying systems that are readily dispersible in aqueous and/or physiological media. The data generated in these studies revealed no serious incompatibility between the API and excipients.

The use of statistical design of experiments (DoE) was successfully applied on the development and optimization of a RP-HPLC method using a CCD experimental design and the optimization of formulation mixtures was done using a D-optimal mixtures design. Kinetically stable (low energy nano-emulsions produced using flaxseed oil, Tween[®] 80 and Span[®] 20 and ethanol were successfully manufactured. Desired and DoE optimized formulations based on CQA were produced and characterized in terms of in vitro release of efavirenz, physical and chemical stability. Stable nano-emulsions under the tested conditions containing 10% m/m flaxseed oil were successfully manufactured. Droplet sizes ranged between 156 and 225 nm, zeta potential between -24 and -41 mV and all formulations were found to be monodisperse with polydispersity indices ≤ 0.487 . The EFV release profiles observed from different nano-emulsions can be exploited for further optimization to produce formulations suitable for undertaking in vivo pharmacokinetic studies. The nano-emulsion approach is promising and appears to be a possible vehicle for the enhancement of solubility dissolution of EFV however, further development and evaluation of the SEDDS formulation produced in these studies is required including assessment of the short and long-term stability of the dosage form to establish a shelf-life for the optimised formulation. The stability of formulations in gelatine or

other encapsulated forms in which crystallization of EFV from solution is minimized, should be explored.

There are underutilized opportunities that may assist and promote the development of pharmaceutical manufacturing on the continent. For example, Trade Related Aspects of Intellectual Property Rights (TRIPS) flexibilities are a step in this direction. These flexibilities include the fact that most products on the Essential Medicines List (EML) are no longer protected by patents and generic versions can be produced without the need for voluntary licences from originator companies. National Medicines Regulatory Authorities (NMRA) such as the International Conference on Harmonisation (ICH), the U.S. Food and Drug Administration (FDA), the European Medicines Agency (EMA) and the South African Health Products Regulatory Authority (SAHPRA) play a crucial role in the registration of medicines and the promotion of and compliance to cGMP in the pharmaceutical development and manufacturing process. However, the capacity of such regulatory authorities, especially in Africa, still needs to be continuously developed through research into technical aspects and analytical methods in research and manufacturing to ensure high quality, safe and effective medicines are independently brought to market.

References

1. UNAIDS. Global HIV & AIDS statistics — 2019 fact sheet [Internet]. 2020 [cited 2020 Mar 8]. Available from: <https://www.unaids.org/en/resources/fact-sheet>
2. World Health Organization. HIV/AIDS Key Facts [Internet]. 2020 [cited 2020 Sep 6]. Available from: <https://www.who.int/news-room/fact-sheets/detail/hiv-aids>
3. National Department of Health. South Africa's National Strategic Plan on HIV/Aids, TB and STI's 2017-2022: Summary [Internet]. Vol. 1, South African National AIDS Council. 2017. Available from: https://www.gov.za/sites/default/files/gcis_document/201705/nsp-hiv-tb-stia.pdf
<http://www.thepresidency.gov.za/MediaLib/Downloads/Home/Publications/SANACCallforNominations/A5summary12-12.pdf>
4. Avert. HIV AND AIDS in South Africa [Internet]. 2020 [cited 2020 Dec 20]. p. 1. Available from: <https://www.avert.org/professionals/hiv-around-world/sub-saharan-africa/south-africa>
5. Bradshaw D, Steyn K. Poverty and chronic diseases in South Africa. Tygerberg, South Africa: Burden of Diseases Research Unit. 2001.
6. Oleribe OO, Momoh J, Uzochukwu BSC, Mbofana F, Adebisi A, Barbera T, et al. Identifying key challenges facing healthcare systems in Africa and potential solutions. *Int J Gen Med*. 2019;12:395–403.
7. Vitoria M, Rangaraj A, Ford N, Doherty M. Current and future priorities for the development of optimal HIV drugs. *Curr Opin HIV AIDS*. 2019;14(2):143–159.
8. Chiu IM, Yaniv A, Dahlberg JE, Gazit A, Skuntz SF, Tronick SR, et al. Nucleotide sequence evidence for relationship of AIDS retrovirus to lentiviruses. *Nature*. 1985 Sep;317(6035):366–388.
9. Reeves JD, Doms RW. Human immunodeficiency virus type 2. *J Gen Virol*. 2002;83(6):1253–1265.
10. Klimas N, Koneru AOB, Fletcher MA. Overview of HIV. *Psychosom Med*. 2008;70(5):523–530.
11. Grossman Z, Meier-Schellersheim M, Paul WE, Picker LJ. Pathogenesis of HIV infection: what the virus spares is as important as what it destroys. *Nat Med* [Internet]. 2006;12(3):289–295. Available from: <https://doi.org/10.1038/nm1380>
12. Workowski KA, Bolan GA, Prevention C for DC and. Sexually transmitted diseases treatment guidelines, 2015. *MMWR Recomm reports Morb Mortal Wkly report Recomm reports* [Internet]. 2015 Jun 5;64(RR-03):1–137. Available from: <https://pubmed.ncbi.nlm.nih.gov/26042815>
13. Tsegaye A, Wolday D, Otto S, Petros B, Assefa T, Alebachew T, et al. Immunophenotyping of blood lymphocytes at birth, during childhood, and during adulthood in HIV-1-uninfected Ethiopians. *Clin Immunol* [Internet]. 2003;109(3):338–346. Available from: <http://www.sciencedirect.com/science/article/pii/S1521661603002390>
14. Luckheeram RV, Zhou R, Verma AD, Xia B. CD4⁺T cells: differentiation and functions.

- Clin Dev Immunol [Internet]. 2012/03/14. 2012;2012:925135. Available from: <https://pubmed.ncbi.nlm.nih.gov/22474485>
15. Shete A, Thakar M, Abraham PR, Paranjape R. A review on peripheral blood CD4+ T lymphocyte counts in healthy adult Indians. *Indian J Med Res* [Internet]. 2010 Dec;132(6):667–675. Available from: <https://pubmed.ncbi.nlm.nih.gov/21245613>
 16. Kaplan JE, Hanson DL, Cohn DL, Karon J, Buskin S, Thompson M, et al. When to Begin Highly Active Antiretroviral Therapy? Evidence Supporting Initiation of Therapy at CD4+ Lymphocyte Counts \geq 350 cells/ μ L. *Clin Infect Dis* [Internet]. 2003 Oct 1;37(7):951–968. Available from: <https://doi.org/10.1086/377606>
 17. Mair C, Hawes SE, Agne HD, Sow PS, N'doye I, Manhart LE, et al. Factors associated with CD4 lymphocyte counts in HIV-negative Senegalese individuals. *Clin Exp Immunol* [Internet]. 2008/01/10. 2008 Mar;151(3):432–440. Available from: <https://pubmed.ncbi.nlm.nih.gov/18190600>
 18. Arts EJ, Hazuda DJ. HIV-1 antiretroviral drug therapy. *Cold Spring Harb Perspect Med* [Internet]. 2012 Apr;2(4):321–339. Available from: <https://pubmed.ncbi.nlm.nih.gov/22474613>
 19. Johnson LF, Mossong J, Dorrington RE, Schomaker M, Hoffmann CJ, Keiser O, et al. Life Expectancies of South African Adults Starting Antiretroviral Treatment: Collaborative Analysis of Cohort Studies. *PLOS Med* [Internet]. 2013 Apr 9;10(4):e1001418. Available from: <https://doi.org/10.1371/journal.pmed.1001418>
 20. Meintjes G, Moorhouse MA, Carmona S, Davies N, Dlamini S, Van Vuuren C, et al. Adult antiretroviral therapy guidelines 2017. *South Afr J HIV Med*. 2017;18(1):1–24.
 21. Health NI of. HIV Treatment [Internet]. 2020. p. 1. Available from: <https://hivinfo.nih.gov/understanding-hiv/fact-sheets/what-start-choosing-hiv-regimen>
 22. CHAN KC. Antiretroviral therapy [Internet]. [cited 2020 Sep 6]. Available from: <https://www.aids.gov.hk/pdf/g190htm/11.htm>
 23. Apostolova N, Funes HA, Blas-Garcia A, Galindo MJ, Alvarez A, Esplugues J V. Efavirenz and the CNS: What we already know and questions that need to be answered. *J Antimicrob Chemother*. 2015;70(10):2693–2708.
 24. Nastri BM, Zannella C, Folliero V, Rinaldi L, Restivo L. Role of Highly Active Antiretroviral Therapy (HAART) for the COVID-19 treatment. *Eur Rev Med Pharmacol Sci*. 2020;(24):11982–11994.
 25. Saag MS, Benson CA, Gandhi RT, Hoy JF, Landovitz RJ, Mugavero MJ, et al. Antiretroviral drugs for treatment and prevention of HIV infection in adults: 2018 recommendations of the international antiviral society-USA panel. *JAMA - J Am Med Assoc*. 2018;320(4):379–396.
 26. Hirasen K, Evans D, Maskew M, Sanne IM, Shearer K, Govathson C, et al. The right combination - treatment outcomes among HIV-positive patients initiating first-line fixed-dose antiretroviral therapy in a public sector HIV clinic in Johannesburg, South Africa. *Clin Epidemiol* [Internet]. 2017 Dec 18;10:17–29. Available from: <https://pubmed.ncbi.nlm.nih.gov/29296098>
 27. de Béthune M-P. Non-nucleoside reverse transcriptase inhibitors (NNRTIs), their discovery, development, and use in the treatment of HIV-1 infection: A review of the

- last 20 years (1989–2009). *Antiviral Res* [Internet]. 2010;85(1):75–90. Available from: <http://www.sciencedirect.com/science/article/pii/S0166354209004616>
28. Kirtane AR, Langer R, Traverso G. Past, Present, and Future Drug Delivery Systems for Antiretrovirals. *J Pharm Sci* [Internet]. 2016;105(12):3471–3482. Available from: <http://www.sciencedirect.com/science/article/pii/S0022354916417090>
 29. Lindenberg M, Kopp S, Dressman JB. Classification of orally administered drugs on the World Health Organization Model list of Essential Medicines according to the biopharmaceutics classification system. *Eur J Pharm Biopharm* [Internet]. 2004;58(2):265–278. Available from: <http://www.sciencedirect.com/science/article/pii/S0939641104000438>
 30. Papich MG, Martinez MN. Applying Biopharmaceutical Classification System (BCS) Criteria to Predict Oral Absorption of Drugs in Dogs: Challenges and Pitfalls. *AAPS J* [Internet]. 2015/04/29. 2015 Jul;17(4):948–964. Available from: <https://pubmed.ncbi.nlm.nih.gov/25916691>
 31. Date AA, Destache CJ. A review of nanotechnological approaches for the prophylaxis of HIV/AIDS. *Biomaterials* [Internet]. 2013/05/28. 2013 Aug;34(26):6202–6228. Available from: <https://pubmed.ncbi.nlm.nih.gov/23726227>
 32. Agency EM. Atazanavir Mylan assessment report [Internet]. London; 2016. Available from: https://www.ema.europa.eu/en/documents/assessment-report/atazanavir-mylan-epar-public-assessment-report_en.pdf
 33. Ghadi R, Dand N. BCS class IV drugs: Highly notorious candidates for formulation development. *J Control Release*. 2017 Feb;248:71–95.
 34. Lenić I, Blake K, Garcia-Arieta A, Potthast H, Welink J. Overview of the European Medicines Agency’s Experience With Biowaivers in Centralized Applications. *Clin Transl Sci* [Internet]. 2019/05/27. 2019 Sep;12(5):490–496. Available from: <https://pubmed.ncbi.nlm.nih.gov/31046182>
 35. The International Council for Harmonisation of Technical Requirements for Pharmaceuticals for Human Use. ICH harmonised guideline. Biopharmaceutics Classification System-Based Biowaivers. M9 [Internet]. 2019. p. 16. Available from: https://database.ich.org/sites/default/files/M9_Guideline_Step4_2019_1116.pdf
 36. Madgulkar AR, Bhalekar MR, Kadam AA. Improvement of Oral Bioavailability of Lopinavir Without Co-administration of Ritonavir Using Microspheres of Thiolated Xyloglucan. *AAPS PharmSciTech*. 2018 Jan;19(1):293–302.
 37. Ruela Corrêa JC, D’Arcy DM, Dos Reis Serra CH, Nunes Salgado HR. Darunavir: A critical review of its properties, use and drug interactions. *Pharmacology*. 2012;90(1–2):102–109.
 38. Arali B, Kumar A, - MS, 2018 U. Physicochemical characterization and dissolution properties of efavirenz- β cyclodextrin solid binary systems. *Int J Pharm Sci Res* [Internet]. 2018;9(12):5350–5356. Available from: <https://ijpsr.com/bft-article/physicochemical-characterisation-and-dissolution-properties-of-efavirenz-beta-cyclodextrin-solid-binary-systems/?view=fulltext#:~:text=Efavirenz is practically insoluble in,and low solubility 14%2C 15>
 39. Info D. Efavirenz | C14H9ClF3NO2 - PubChem

- <https://pubchem.ncbi.nlm.nih.gov/compound/efavirenz#section=Top>. 2018;1–49.
40. Alves LDS, de La Roca Soares MF, de Albuquerque CT, da Silva ER, Vieira ACC, Fontes DAF, et al. Solid dispersion of efavirenz in PVP K-30 by conventional solvent and kneading methods. *Carbohydr Polym*. 2014 Apr;104:166–174.
 41. Taneja S, Shilpi S, Khatri K. Formulation and optimization of efavirenz nanosuspensions using the precipitation-ultrasonication technique for solubility enhancement. *Artif Cells, Nanomedicine Biotechnol*. 2016;44(3):978–984.
 42. Babić S, Horvat AJM, Mutavdžić Pavlović D, Kaštelan-Macan M. Determination of pKa values of active pharmaceutical ingredients. *TrAC - Trends Anal Chem*. 2007;26(11):1043–1061.
 43. Manallack DT. The pK(a) Distribution of Drugs: Application to Drug Discovery. *Perspect Medicin Chem* [Internet]. 2007 Sep 17;1:25–38. Available from: <https://pubmed.ncbi.nlm.nih.gov/19812734>
 44. Gallicano K. Antiretroviral-drug concentrations in semen. *Antimicrob Agents Chemother* [Internet]. 2000 Apr;44(4):1117–1128. Available from: <https://pubmed.ncbi.nlm.nih.gov/10799009>
 45. Ozdemir I A, * SS, Sanli N, Barış Sardogan. A New Method for Determination of Efavirenz and pKa by Using LC-UV. *Int J Pharm Res Allied Sci* [Internet]. 2018;7(4):120–126. Available from: <https://ijpras.com/storage/models/article/ilhOnNRE3uTR6YHZZI8qWDZzFWNxJ4EmxqxI1FAHGwX1FTliWUMtHjiC71tMM/a-new-method-for-determination-of-efavirenz-and-pka-by-using-lc-uv.pdf>
 46. Habyalimana V, Mbinze JK, Yemoa AL, Waffo C, Diallo T, Tshilombo NK, et al. Application of design space optimization strategy to the development of LC methods for simultaneous analysis of 18 antiretroviral medicines and 4 major excipients used in various pharmaceutical formulations. *J Pharm Biomed Anal* [Internet]. 2017;139(April 2018):8–21. Available from: <http://dx.doi.org/10.1016/j.jpba.2017.02.040>
 47. Bannan CC, Calabró G, Kyu DY, Mobley DL. Calculating Partition Coefficients of Small Molecules in Octanol/Water and Cyclohexane/Water. *J Chem Theory Comput* [Internet]. 2016/08/01. 2016 Aug 9;12(8):4015–4024. Available from: <https://pubmed.ncbi.nlm.nih.gov/27434695>
 48. Ibarra-Escutia A, Rojas-Hernández A, Galano A, Ángeles E, Martínez-Mendoza D, Moya-Hernández R. Determination of acidity constants, partition coefficients between water and 1-octanol, and deprotonation route of 4-tert-butyl-bis-(2,6-thiomorpholin-4-ylmethyl)-1-phenol and 4-hydroxy-3,5-bis(morpholin-1-ylmethyl)benzotriazole; compounds with antihypert. *J Mex Chem Soc*. 2016;60(3):152–162.
 49. Cairns D. *Essentials of Pharmaceutical Chemistry* [Internet]. Aberdeen: Pharmaceutical Press; 2008. 297 p. Available from: http://doi.wiley.com/10.1002/bmb.2004.494032039997%5Cnhttp://books.google.com/books?hl=en&lr=&id=KxqwWWSbDRYC&oi=fnd&pg=PR9&dq=Chemistry+and+Molecular+Aspects+of+Drug+Design+and+Action&ots=_kzBAh8UTY&sig=NZjM1Hrz18a92vofFVL1scw4lqY
 50. Patel P. *Preformulation Studies: An Integral Part of Formulation Design* [Internet]. Intech. Mehemdabad; 2012. p. 38. Available from:

<http://dx.doi.org/10.1039/C7RA00172J><https://www.intechopen.com/books/advanced-biometric-technologies/liveness-detection-in-biometrics><http://dx.doi.org/10.1016/j.colsurfa.2011.12.014>

51. Apley M, Crist GB, Fellner V, Gonzalez MA, Hunter RP, Martinez MN, et al. Determination of thermodynamic solubility of active pharmaceutical ingredients for veterinary species: A new USP general chapter. *Dissolution Technol.* 2017;24(1):36–39.
52. Duwal S, Seeler D, Dickinson L, Khoo S, Von Kleist M. The utility of efavirenz-based prophylaxis against HIV infection. A systems pharmacological analysis. *Front Pharmacol.* 2019;10(Mar):1–13.
53. Rabel SR, Maurin MB, Rowe SM, Hussain M. Determination of the pK(a) and pH-solubility behavior of an ionizable cyclic carbamate, (S)-6-chloro-4-(cyclopropylethynyl)-1,4-dihydro-4-(trifluoromethyl)-2H-3,1-benzoxazin-2-one (DMP 266). *Pharm Dev Technol.* 1996;1(1):91–95.
54. Aungst BJ. P-glycoprotein, secretory transport, and other barriers to the oral delivery of anti-HIV drugs [Internet]. Vol. 39, *Advanced Drug Delivery Reviews*. Elsevier; 1999 [cited 2018 Jun 13]. p. 105–116. Available from: <https://www.sciencedirect.com/science/article/pii/S0169409X99000228>
55. Aziz SB, Brza MA, Nofal MM, Abdulwahid RT, Hussien SA, Hussein AM, et al. A comprehensive review on optical properties of polymer electrolytes and composites. *Materials (Basel).* 2020;13(17).
56. Howell JA, Sutton RE. Ultraviolet and Absorption Light Spectrometry. *Anal Chem* [Internet]. 1998 Jun 1;70(12):107–118. Available from: <https://doi.org/10.1021/a19800040>
57. Kumar YA, Rao NR. Development of Rapid UV Spectrophotometric Method for the Estimation of Efavirenz in Formulations. 2010;7(3):856–860.
58. Ramaswamy A, Arul Gnana Dhas AS. Development and validation of analytical method for quantitation of Emtricitabine, Tenofovir, Efavirenz based on HPLC. *Arab J Chem* [Internet]. 2018 Feb 1 [cited 2018 Apr 23];11(2):275–281. Available from: <https://www.sciencedirect.com/science/article/pii/S1878535214001695>
59. Kumar A M, Mahesh N, Diwan PV, Prasad VVL., Sandhya BN. Development and validation of UV Spectrophotometric method for simultaneous estimation of Lamivudine and Efavirenz in the Pharmaceutical dosage form. *J Adv Pharm Educ Res.* 2012;2(4):210–214.
60. Fandaruff C, Araya-Sibaja AM, Pereira RN, Hoffmeister CRD, Rocha HVA, Silva MAS. Thermal behavior and decomposition kinetics of efavirenz under isothermal and non-isothermal conditions. *J Therm Anal Calorim.* 2014;115(3):2351–2356.
61. S. Kumar PJB and BR. Simultaneous HPLC Determination of Efavirenz, 8-hydroxy Efavirenz, Neostigmine and Comparison of their Separation Using a C18 and Biphenyl Column through Pharmacological Evaluation. *Indian J Pharm Sci.* 2017;79(3):353–360.
62. Raza K. Polymorphism: The Phenomenon Affecting the Performance of Drugs. *SOJ Pharm Pharm Sci.* 2014;
63. Chistyakov D, Sergeev G. The Polymorphism of Drugs: New Approaches to the

- Synthesis of Nanostructured Polymorphs. *Pharmaceutics* [Internet]. 2020 Jan 1;12(1):1–34. Available from: <https://pubmed.ncbi.nlm.nih.gov/31906357>
64. Mahapatra S, Thakur TS, Joseph S, Varughese S, Desiraju GR. New solid state forms of the anti-HIV drug efavirenz. Conformational flexibility and high Z' issues. *Cryst Growth Des.* 2010;10(7):3191–3202.
 65. Suendo YWWSNSV. Observation of Polymorphic Transition of Efavirenz during Heating by Raman Spectroscopy. *Int J Sci Res* [Internet]. 2018;7(7):724–727. Available from: <https://www.ijsr.net/archive/v7i7/ART201941.pdf>
 66. Adkins JC, Noble S. Efavirenz. *Drugs.* 1998 Dec;56(6):1055–1056.
 67. Fandaruff C, Rauber GS, Araya-Sibaja AM, Pereira RN, De Campos CEM, Rocha HVA, et al. Polymorphism of anti-HIV drug efavirenz: Investigations on thermodynamic and dissolution properties. *Cryst Growth Des.* 2014;14(10):4968–4975.
 68. Rawal RK, Murugesan V, Katti SB. Structure-Activity Relationship Studies on Clinically Relevant HIV-1 NNRTIs. *Curr Med Chem.* 2012;19(31):5364–5380.
 69. Song Y, Fang Z, Zhan P, Liu X. Recent advances in the discovery and development of novel HIV-1 NNRTI platforms (Part II): 2009-2013 update. *Curr Med Chem.* 2014;21(3):329–355.
 70. Bastos MM, Costa CCP, Bezerra TC, da Silva F de C, Boechat N. Efavirenz a nonnucleoside reverse transcriptase inhibitor of first-generation: Approaches based on its medicinal chemistry. *Eur J Med Chem* [Internet]. 2016;108:455–465. Available from: <http://www.sciencedirect.com/science/article/pii/S0223523415303627>
 71. Romero DL. Advances in the Development of HIV Reverse Transcriptase Inhibitors. In: Bristol JABT-AR in MC, editor. MI: Academic Press; 1994. p. 123–132. Available from: <https://www.sciencedirect.com/science/article/pii/S0065774308607265>
 72. Okusu S, Kawai H, Yasuda Y, Sugita Y, Kitayama T, Tokunaga E, et al. Asymmetric synthesis of efavirenz via organocatalyzed enantioselective trifluoromethylation. *Asian J Org Chem.* 2014;3(4):449–452.
 73. Williams AL, Dandepally SR, Kotturi S V. A p-methoxybenzyl (PMB) protection/deprotection approach toward the synthesis of 5-phenoxy-4-chloro-N-(aryl/alkyl) thiophene-2-sulfonamides. *Mol Divers.* 2010;14(4):697–707.
 74. Yasuda N, Tan L. Inhibitor (NNRTI), and a Previous Structurally Related Development Candidate. Yasuda N, editor. Weinheim: Wiley; 2011. 1–43 p.
 75. von Moltke LL, Greenblatt DJ, Granda BW, Giancarlo GM, Duan SX, Daily JP, et al. Inhibition of human cytochrome P450 isoforms by nonnucleoside reverse transcriptase inhibitors. *J Clin Pharmacol.* 2001;41(1):85–91.
 76. Elizabeth D. Hermsen, Pharm.D., M.B.A., BCPS, Courtney V. Fletcher, Pharm.D., Michael Para, M.D., Susan Swindells M. Nonnucleoside Analogues (Delavirdine, Efavirenz, Etravirine, Nevirapine) [Internet]. 2017. Available from: <http://www.airida.cn/d50.asp>
 77. Dellamonica P, Di Perri G, Garraffo R. NNRTIs: Pharmacological data. *Médecine Mal Infect* [Internet]. 2012;42(7):287–295. Available from: <https://www.sciencedirect.com/science/article/pii/S0399077X12001114>

78. Vrouenraets SME, Wit FWNM, van Tongeren J, Lange JMA. Efavirenz: A review. Vol. 8, Expert Opinion on Pharmacotherapy. 2007. p. 851–871.
79. Eckhardt BJ, Gulick RM. Drugs for HIV Infection. In: Cohen J, Powderly WG, Opal SMBT-ID (Fourth E, editors. Elsevier; 2017. p. 1293-1308.e2. Available from: <http://www.sciencedirect.com/science/article/pii/B9780702062858001520>
80. World Health Organization. Prescribing Information and Weight-Based Dosing of Available ARV Formulations for Infants and Children [Internet]. [cited 2020 Dec 15]. p. 101–157. Available from: https://www.who.int/hiv/pub/paediatric/paediatric_arv_dosing.pdf
81. Denic A, Glasscock RJ, Rule AD. Structural and Functional Changes With the Aging Kidney. Adv Chronic Kidney Dis [Internet]. 2016 Jan;23(1):19–28. Available from: <https://pubmed.ncbi.nlm.nih.gov/26709059>
82. Burgess MJ, Zeuli JD, Kasten MJ. Management of HIV/AIDS in older patients-drug/drug interactions and adherence to antiretroviral therapy. HIV AIDS (Auckl) [Internet]. 2015 Oct 27;7:251–264. Available from: <https://pubmed.ncbi.nlm.nih.gov/26604826>
83. Nazziwa R, Sekadde M, Kanyike F, Wobudeya E, Nabukeera-Barungi N. Efavirenz poisoning in a 12 year old HIV negative African boy. Pan Afr Med J [Internet]. 2012/07/26. 2012;12:86. Available from: <https://pubmed.ncbi.nlm.nih.gov/23077707>
84. Dong BJ. Efavirenz DuPont Pharmaceuticals Co. IDrugs. 1998 Oct;1(6):700–711.
85. Blanch J, Corbella B. Associated with Efavirenz Overdose. Clin Infect Dis. 2001;33(2):270–271.
86. Zhou S-F. Drugs Behave as Substrates, Inhibitors and Inducers of Human Cytochrome P450 3A4. Curr Drug Metab. 2008;9(4):310–322.
87. Kenedi CA, Goforth HW. A systematic review of the psychiatric side-effects of efavirenz. AIDS Behav. 2011 Nov;15(8):1803–1818.
88. Rice Jr DP, Faragon JJ, Banks S, Chirch LM. HIV/HCV Antiviral Drug Interactions in the Era of Direct-acting Antivirals. J Clin Transl Hepatol [Internet]. 2016/09/25. 2016 Sep 28;4(3):234–240. Available from: <https://pubmed.ncbi.nlm.nih.gov/27777891>
89. Gaida R, Truter I, Grobler C. Efavirenz: A review of the epidemiology, severity and management of neuropsychiatric side-effects. South African J Psychiatry. 2015;21(3):94–97.
90. Mugundu G, Hariparsad N, Desai P. Impact of Ritonavir, Atazanavir and Their Combination on the CYP3A4 Induction by Efavirenz in Primary Human Hepatocytes. Drug Metab Lett. 2010;4(1):45–50.
91. Hariparsad N, Nallani SC, Sane RS, Buckley DJ, Buckley AR, Desai PB. Induction of CYP3A4 by efavirenz in primary human hepatocytes: comparison with rifampin and phenobarbital. J Clin Pharmacol. 2004 Nov;44(11):1273–1281.
92. Pedral-Sampaio DB, Alves CR, Netto EM, Brites C, Oliveira AS, Badaro R. Efficacy and safety of Efavirenz in HIV patients on Rifampin for tuberculosis . Vol. 8, Brazilian Journal of Infectious Diseases . scielo ; 2004. p. 211–216.

93. Ogburn ET, Jones DR, Masters AR, Xu C, Guo Y, Desta Z. Efavirenz primary and secondary metabolism in vitro and in vivo: Identification of novel metabolic pathways and cytochrome P450 2A6 as the principal catalyst of efavirenz 7-hydroxylation. *Drug Metab Dispos*. 2010;38(7):1218–1229.
94. Robertson SM, Penzak SR, Lane J, Pau AK, Mican JM. A Potentially Significant Interaction between Efavirenz and Phenytoin: A Case Report and Review of the Literature. *Clin Infect Dis* [Internet]. 2005 Jul 15;41(2):e15–18. Available from: <https://doi.org/10.1086/431208>
95. Rathbun RC, Liedtke MD. Antiretroviral drug interactions: Overview of interactions involving new and investigational agents and the role of therapeutic drug monitoring for management. *Pharmaceutics*. 2011;3(4):745–781.
96. Inc AP. Auro-efavirenz Product monograph [Internet]. 2017. p. 1–54. Available from: https://pdf.hres.ca/dpd_pm/00040742.PDF
97. Segamwenge IL, Bernard MK. Acute Liver Failure among Patients on Efavirenz-Based Antiretroviral Therapy. *Case reports Hepatol* [Internet]. 2018 May 10;2018:1270716. Available from: <https://pubmed.ncbi.nlm.nih.gov/29862098>
98. Knapp KM, Brogly SB, Muenz DG, Spiegel HML, Conway DH, Scott GB, et al. Prevalence of congenital anomalies in infants with in utero exposure to antiretrovirals. *Pediatr Infect Dis J* [Internet]. 2012 Feb;31(2):164–170. Available from: <https://pubmed.ncbi.nlm.nih.gov/21983213>
99. Law R, Bozzo P, Koren G, Einarson A. FDA pregnancy risk categories and the CPS: do they help or are they a hindrance? *Can Fam Physician* [Internet]. 2010 Mar;56(3):239–241. Available from: <https://pubmed.ncbi.nlm.nih.gov/20228306>
100. Chersich MF, Urban MF, Venter FWD, Wessels T, Krause A, Gray GE, et al. Efavirenz use during pregnancy and for women of child-bearing potential. *AIDS Res Ther*. 2006;3(1):1–6.
101. Pillay P, Black V. Safety, strength and simplicity of efavirenz in pregnancy. *South Afr J HIV Med* [Internet]. 2012;13(1):164–178. Available from: <https://sajhivmed.org.za/index.php/hivmed/article/view/157/263>
102. le Roux SM, Abrams EJ. Efavirenz in pregnancy. *Lancet HIV* [Internet]. 2020;7(1):e6–8. Available from: [http://dx.doi.org/10.1016/S2352-3018\(19\)30330-3](http://dx.doi.org/10.1016/S2352-3018(19)30330-3)
103. Ford N, Mofenson L, Shubber Z, Calmy A, Andrieux-Meyer I, Vitoria M, et al. Safety of efavirenz in the first trimester of pregnancy: An updated systematic review and meta-analysis. *Aids*. 2014;28(SUPPL. 2).
104. Olagunju A, Bolaji O, Amara A, Waitt C, Else L, Adejuyigbe E, et al. Breast milk pharmacokinetics of efavirenz and breastfed infants' exposure in genetically defined subgroups of mother-infant pairs: an observational study. *Clin Infect Dis an Off Publ Infect Dis Soc Am*. 2015 Aug;61(3):453–463.
105. (US) NL of M. Drugs and Lactation Database [Internet]. 2020. Available from: <https://www.ncbi.nlm.nih.gov/books/NBK501534/#:~:text=Efavirenz is excreted into breastmilk,their HIV-negative breastfed infants.>
106. Colebunders R, Hodossy B, Burger D, Daems T, Roelens K, Coppens M, et al. The effect of highly active antiretroviral treatment on viral load and antiretroviral drug levels

- in breast milk. *AIDS*. 2005 Nov;19(16):1912–195.
107. Slater M, Stringer EM, Stringer JSA. Breastfeeding in HIV-positive women: What can be recommended? *Paediatr Drugs*. 2010;12(1):1–9.
 108. Olagunju A, Rajoli RKR, Atoyebi SA, Khoo S, Owen A, Siccardi M. Physiologically-based pharmacokinetic modelling of infant exposure to efavirenz through breastfeeding. *AAS Open Res*. 2018;1(May):16.
 109. Mirochnick M, Thomas T, Capparelli E, Zeh C, Holland D, Masaba R, et al. Antiretroviral Concentrations in Breast-Feeding Infants of Mothers Receiving Highly Active Antiretroviral Therapy. *Antimicrob Agents Chemother* [Internet]. 2009 Mar 1;53(3):1170 LP – 1176. Available from: <http://aac.asm.org/content/53/3/1170.abstract>
 110. McLaughlin MM, Guerrero AJ, Merker A. Renal effects of non-tenofovir antiretroviral therapy in patients living with HIV. *Drugs Context* [Internet]. 2018 Mar 21;7:212519. Available from: <https://pubmed.ncbi.nlm.nih.gov/29623097>
 111. Boswell MT, Rossouw TM. Approach to acute kidney injury in HIV-infected patients in South Africa. *South Afr J HIV Med*. 2017;18(1):1–7.
 112. Angel-Moreno-Maroto A, Suárez-Castellano L, Hernández-Cabrera M, Pérez-Arellano J-L. Severe efavirenz-induced hypersensitivity syndrome (not-DRESS) with acute renal failure. *J Infect* [Internet]. 2006;52(2):39–40. Available from: <https://www.sciencedirect.com/science/article/pii/S0163445305001489>
 113. Apostolova N, Ballesteros D, Monleo D, Morales JM, Blas-garcı A, Rocha M, et al. Inhibition of Mitochondrial Function by Efavirenz Increases Lipid Content in Hepatic Cells. 2010;115–125.
 114. Neukam K, Mira JA, Ruiz-Morales J, Rivero A, Collado A, Torres-Cornejo A, et al. Liver toxicity associated with antiretroviral therapy including efavirenz or ritonavir-boosted protease inhibitors in a cohort of HIV/hepatitis C virus co-infected patients. *J Antimicrob Chemother* [Internet]. 2011 Nov 1;66(11):2605–2614. Available from: <https://doi.org/10.1093/jac/dkr357>
 115. Pinillos F, Dandara C, Swart M, Strehlau R, Kuhn L, Patel F, et al. Case report: Severe central nervous system manifestations associated with aberrant efavirenz metabolism in children: The role of CYP2B6 genetic variation. *BMC Infect Dis* [Internet]. 2016;16(1):1–7. Available from: <http://dx.doi.org/10.1186/s12879-016-1381-x>
 116. Curley P, Rajoli RKR, Moss DM, Liptrott NJ, Letendre S, Owen A, et al. Efavirenz is predicted to accumulate in brain tissue: An in silico, in vitro, and in vivo investigation. *Antimicrob Agents Chemother*. 2017;61(1):1–10.
 117. Preuss. JYC V. Efavirenz [Internet]. StatPearls Publishing LLC. 2020 [cited 2020 Sep 11]. Available from: <https://www.ncbi.nlm.nih.gov/books/NBK542316/>
 118. Robarge JD, Metzger IF, Lu J, Thong N, Skaar TC, Desta Z, et al. Population Pharmacokinetic Modeling To Estimate the Contributions of Genetic and Nongenetic Factors to Efavirenz Disposition. *Antimicrob Agents Chemother* [Internet]. 2017 Jan 1;61(1):13–16. Available from: <http://aac.asm.org/content/61/1/e01813-16.abstract>
 119. Tsibris AMN, Hirsch MS. Antiretroviral Therapy for Human Immunodeficiency Virus Infection. In: Bennett JE, Dolin R, Blaser Douglas, and Bennett’s Principles and Practice of Infectious Diseases (Eighth Edition) MJBT-M, editors. Philadelphia: Content

- Repository Only!; 2015. p. 1622-1641.e6. Available from: <http://www.sciencedirect.com/science/article/pii/B9781455748013001302>
120. Information G. Efavirenz. *Meyler's Side Eff Drugs*. 2016;25–31.
 121. Max B, Sherer R. Management of the Adverse Effects of Antiretroviral Therapy and Medication Adherence. *Clin Infect Dis* [Internet]. 2000 Jun 1;30(Supplement_2):S96–116. Available from: <https://doi.org/10.1086/313859>
 122. Makoni PA, Kasongo KW, Walker RB. Short term stability testing of efavirenz-loaded solid lipid nanoparticle (SLN) and nanostructured lipid carrier (NLC) dispersions. *Pharmaceutics*. 2019;11(8).
 123. Maggiolo F. Efavirenz: A decade of clinical experience in the treatment of HIV. Vol. 64, *Journal of Antimicrobial Chemotherapy*. 2009. p. 910–928.
 124. Patel M, Sawant* RS and K. Recent Advances in Drug Delivery Strategies for Improved Therapeutic Efficacy of Efavirenz [Internet]. Vol. 14, *Recent Patents on Nanotechnology*. 2020. p. 119–127. Available from: <http://www.eurekaselect.com/node/175882/article>
 125. Oswald S, Meyer zu Schwabedissen HE, Nassif A, Modess C, Desta Z, Ogburn ET, et al. Impact of efavirenz on intestinal metabolism and transport: insights from an interaction study with ezetimibe in healthy volunteers. *Clin Pharmacol Ther* [Internet]. 2012/02/01. 2012 Mar;91(3):506–513. Available from: <https://pubmed.ncbi.nlm.nih.gov/22297387>
 126. Dooley KE, Denti P, Martinson N, Cohn S, Mashabela F, Hoffmann J, et al. Pharmacokinetics of efavirenz and treatment of HIV-1 among pregnant women with and without tuberculosis coinfection. *J Infect Dis* [Internet]. 2014/07/31. 2015 Jan 15;211(2):197–205. Available from: <https://pubmed.ncbi.nlm.nih.gov/25081933>
 127. Rakhmanina NY, van den Anker JN. Efavirenz in the therapy of HIV infection. *Expert Opin Drug Metab Toxicol*. 2010;6(1):95–103.
 128. Avery LB, VanAusdall JL, Hendrix CW, Bumpus NN. Compartmentalization and antiviral effect of efavirenz metabolites in blood plasma, seminal plasma, and cerebrospinal fluid. *Drug Metab Dispos* [Internet]. 2012/11/19. 2013 Feb;41(2):422–429. Available from: <https://pubmed.ncbi.nlm.nih.gov/23166317>
 129. Csajka C, Marzolini C, Fattinger K, Décosterd LA, Fellay J, Telenti A, et al. Population pharmacokinetics and effects of efavirenz in patients with human immunodeficiency virus infection. *Clin Pharmacol Ther*. 2003 Jan;73(1):20–30.
 130. Mahabadi. AMN. Volume of Distribution [Internet]. StatPearls Publishing, Treasure Island (FL). 2021 [cited 2021 Jan 16]. Available from: <https://www.ncbi.nlm.nih.gov/books/NBK545280/>
 131. McDonagh EM, Lau JL, Alvarellos ML, Altman RB, Klein TE. PharmGKB summary: Efavirenz pathway, pharmacokinetics. *Pharmacogenet Genomics* [Internet]. 2015 Jul;25(7):363–376. Available from: <https://pubmed.ncbi.nlm.nih.gov/25966836>
 132. Aouri M, Barcelo C, Ternon B, Cavassini M, Anagnostopoulos A, Yerly S, et al. In vivo profiling and distribution of known and novel phase I and phase II metabolites of efavirenz in plasma, urine, and cerebrospinal fluid. *Drug Metab Dispos*. 2016;44(1):151–161.

133. Ward BA, Gorski JC, Jones DR, Hall SD, Flockhart DA, Desta Z. The Cytochrome P450 2B6 (CYP2B6) Is the Main Catalyst of Efavirenz Primary and Secondary Metabolism: Implication for HIV/AIDS Therapy and Utility of Efavirenz as a Substrate Marker of CYP2B6 Catalytic Activity. *J Pharmacol Exp Ther* [Internet]. 2003 Jul 1;306(1):287 LP – 300. Available from: <http://jpet.aspetjournals.org/content/306/1/287.abstract>
134. Desta Z, Saussele T, Ward B, Bliedernicht J, Li L, Klein K, et al. Impact of CYP2B6 polymorphism on hepatic efavirenz metabolism in vitro. *Pharmacogenomics* [Internet]. 2007 Jun 1;8(6):547–558. Available from: <https://doi.org/10.2217/14622416.8.6.547>
135. Mutlib AE, Chen H, Nemeth GA, Markwalder JA, Seitz SP, Gan LS, et al. Identification and characterization of efavirenz metabolites by liquid chromatography/mass spectrometry and high field NMR: Species differences in the metabolism of efavirenz. *Drug Metab Dispos.* 1999;27(11):1319–1333.
136. Kalepu S, Nekkanti V. Insoluble drug delivery strategies: Review of recent advances and business prospects. *Acta Pharm Sin B* [Internet]. 2015;5(5):442–453. Available from: <http://dx.doi.org/10.1016/j.apsb.2015.07.003>
137. Boyd BJ, Bergström CAS, Vinarov Z, Kuentz M, Brouwers J, Augustijns P, et al. Successful oral delivery of poorly water-soluble drugs both depends on the intraluminal behavior of drugs and of appropriate advanced drug delivery systems. *Eur J Pharm Sci* [Internet]. 2019;137:104967. Available from: <http://www.sciencedirect.com/science/article/pii/S0928098719302301>
138. Chatterjee B, Hamed Almurisi S, Ahmed Mahdi Dukhan A, Mandal UK, Sengupta P. Controversies with self-emulsifying drug delivery system from pharmacokinetic point of view. *Drug Deliv.* 2016;23(9):3639–3652.
139. Savjani KT, Gajjar AK, Savjani JK. Drug Solubility: Importance and Enhancement Techniques. *ISRN Pharm.* 2012;2012(100 mL):1–10.
140. Matić J, Paudel A, Bauer H, Garcia RAL, Biedrzycka K, Khinast JG. Developing HME-Based Drug Products Using Emerging Science: a Fast-Track Roadmap from Concept to Clinical Batch. *AAPS PharmSciTech.* 2020;21(5).
141. Mohsin K, Alamri R, Ahmad A, Raish M, Alanazi FK, Hussain MD. Development of self-nanoemulsifying drug delivery systems for the enhancement of solubility and oral bioavailability of fenofibrate, A poorly water-soluble drug. *Int J Nanomedicine.* 2016;11:2829–2838.
142. Kalepu S, Manthina M, Padavala V. Oral lipid-based drug delivery systems – an overview. *Acta Pharm Sin B* [Internet]. 2013 Dec 1 [cited 2018 Apr 20];3(6):361–372. Available from: <https://www.sciencedirect.com/science/article/pii/S2211383513000919>
143. Krstić M, Medarević Đ, Đuriš J, Ibrić S. Self-nanoemulsifying drug delivery systems (SNEDDS) and self-microemulsifying drug delivery systems (SMEDDS) as lipid nanocarriers for improving dissolution rate and bioavailability of poorly soluble drugs. *Lipid Nanocarriers Drug Target* [Internet]. 2018 Jan 1 [cited 2019 Jul 17];473–508. Available from: <https://www.sciencedirect.com/science/article/pii/B9780128136874000128>
144. Shrestha H, Bala R, Arora S. Lipid-Based Drug Delivery Systems. *J Pharm* [Internet]. 2014;2014:1–10. Available from:

<http://www.hindawi.com/journals/jphar/2014/801820/>

145. van Staden D, du Plessis J, Viljoen J. Development of topical/transdermal self-emulsifying drug delivery systems, not as simple as expected. *Sci Pharm*. 2020;88(2).
146. Alskär LC. Improved Molecular Understanding of Lipid-Based Formulations for Enabling Oral Delivery of Poorly Water-Soluble Drugs. Uppsala; 2018.
147. Poovi G, Damodharan N. Lipid nanoparticles: A challenging approach for oral delivery of BCS Class-II drugs. *Futur J Pharm Sci* [Internet]. 2018;4(2):191–205. Available from: <http://www.sciencedirect.com/science/article/pii/S2314724517301656>
148. Kadam RS, Bourne DWA, Kompella UB. Nano-advantage in enhanced drug delivery with biodegradable nanoparticles: contribution of reduced clearance. *Drug Metab Dispos* [Internet]. 2012/04/12. 2012 Jul;40(7):1380–1388. Available from: <https://pubmed.ncbi.nlm.nih.gov/22498894>
149. Gurram AK, Deshpande PB, Kar SS, Nayak UY, Udupa N, Reddy MS. Role of Components in the Formation of Self-microemulsifying Drug Delivery Systems. *Indian J Pharm Sci* [Internet]. 2015;77(3):249–257. Available from: <https://pubmed.ncbi.nlm.nih.gov/26180269>
150. Kovvasu SP, Kunamaneni P, Joshi R. Self-emulsifying Drug Delivery Systems and their Marketed Products: A Review. *Asian J Pharm*. 2019;13(2):73–84.
151. Aswathanarayan JB, Vittal RR. Nanoemulsions and Their Potential Applications in Food Industry. *Front Sustain Food Syst*. 2019;3(November):1–21.
152. Gupta A, Eral HB, Hatton TA, Doyle PS. Nanoemulsions: Formation, properties and applications. *Soft Matter* [Internet]. 2016;12(11):2826–2841. Available from: <http://dx.doi.org/10.1039/C5SM02958A>
153. Humberstone AJ, Charman WN. Lipid-based vehicles for the oral delivery of poorly water soluble drugs. *Adv Drug Deliv Rev*. 1997;25(1):103–128.
154. Pehlivanov I. Self-Emulsifying Drug Delivery Systems As an Approach To Improve Therapeutic Effectiveness of Orally Administrated Drugs. *J IMAB - Annu Proceeding (Scientific Pap)*. 2019;25(2):2575–2582.
155. Alskär LC, Porter CJH, Bergström CAS. Tools for Early Prediction of Drug Loading in Lipid-Based Formulations. *Mol Pharm*. 2016;13(1):251–261.
156. Pavoni L, Perinelli DR, Bonacucina G, Cespi M, Palmieri GF. An Overview of Micro- and Nanoemulsions as Vehicles for Essential Oils: Formulation, Preparation and Stability. *Nanomater (Basel, Switzerland)* [Internet]. 2020 Jan 12;10(1):135. Available from: <https://pubmed.ncbi.nlm.nih.gov/31940900>
157. Kawakatsu T, Trägårdh G, Trägårdh C. Production of W/O/W emulsions and S/O/W pectin microcapsules by microchannel emulsification. *Colloids Surfaces A Physicochem Eng Asp* [Internet]. 2001;189(1):257–264. Available from: <http://www.sciencedirect.com/science/article/pii/S0927775701005088>
158. Leal-Calderon F, Homer S, Goh A, Lundin L. W/O/W emulsions with high internal droplet volume fraction. *Food Hydrocoll* [Internet]. 2012;27(1):30–41. Available from: <http://www.sciencedirect.com/science/article/pii/S0268005X11002608>

159. Tarun Kumar Guleri *, Loveleen Preet Kaur, Paras Bedi DS. Micro emulsion: a promising approach for controlled drug release. *Int Res J Pharm Appl Sci* [Internet]. 2013;3(1):109–116. Available from: [http://www.irjpas.com/File_Folder/3\(1\)109-116.pdf](http://www.irjpas.com/File_Folder/3(1)109-116.pdf)
160. Polizelli MA, Telis VRN, Amaral LQ, Feitosa E. Formation and characterization of soy bean oil/surfactant/water microemulsions. *Colloids Surfaces A Physicochem Eng Asp* [Internet]. 2006 Jun 15 [cited 2019 Apr 15];281(1–3):230–236. Available from: <https://www.sciencedirect.com/science/article/pii/S0927775706001816>
161. Senthil Kumar K, Dhachinamoorthi D, Saravanan R, Gopal UK, Shanmugam V. Microemulsions as carrier for novel drug delivery: A review. *Int J Pharm Sci Rev Res*. 2011;10(2):37–45.
162. Solans C, Izquierdo P, Nolla J, Azemar N, Garcia-Celma MJ. Nano-emulsions [Internet]. Vol. 10, *Current Opinion in Colloid and Interface Science*. Elsevier; 2005 [cited 2019 Sep 6]. p. 102–110. Available from: <https://www.sciencedirect.com/science/article/pii/S1359029405000348>
163. McClements DJ. Nanoemulsions versus microemulsions: terminology, differences, and similarities. *Soft Matter* [Internet]. 2012;8(6):1719–1729. Available from: <http://dx.doi.org/10.1039/C2SM06903B>
164. Gonçalves A, Nikmaram N, Roohinejad S, Estevinho BN, Rocha F, Greiner R, et al. Production, properties, and applications of solid self-emulsifying delivery systems (S-SEDS) in the food and pharmaceutical industries. Vol. 538, *Colloids and Surfaces A: Physicochemical and Engineering Aspects*. 2018. p. 108–126.
165. Kale SN, Deore SL. Emulsion micro emulsion and nano emulsion: A review. *Syst Rev Pharm*. 2016;8(1):39–47.
166. Agrawal OP, Agrawal S. An overview of new drug delivery system: microemulsion quaternary phase diagrams can describe the phase. *Asian J Pharm Sci Technol*. 2012;2(1):5–12.
167. Tartaro G, Mateos H, Schirone D, Angelico R, Palazzo G. Microemulsion microstructure(s): A tutorial review. *Nanomaterials*. 2020;10(9):1–40.
168. Sharma AK, Garg T, Goyal AK, Rath G. Role of microemulsions in advanced drug delivery. *Artif Cells, Nanomedicine Biotechnol*. 2016;44(4):1177–1185.
169. Chen L, Ao F, Ge X, Shen W. Food-grade pickering emulsions: Preparation, stabilization and applications. *Molecules*. 2020;25(14):3202–3223.
170. Rocha JA, Baydak EN, Yarranton HW, Sztukowski DM, Ali-Marcano V, Gong L, et al. Role of Aqueous Phase Chemistry, Interfacial Film Properties, and Surface Coverage in Stabilizing Water-in-Bitumen Emulsions. *Energy and Fuels*. 2016;30(7):5240–5252.
171. El-Hamidi M, Zaher FA. Production of vegetable oils in the world and in Egypt: an overview. *Bull Natl Res Cent*. 2018;42(19):1–17.
172. Dasgupta N, Ranjan S, Gandhi M. Nanoemulsion ingredients and components. *Environ Chem Lett* [Internet]. 2019;17(2):917–928. Available from: <https://doi.org/10.1007/s10311-018-00849-7>
173. Garti N, Yaghmur A, Leser ME, Clement V, Watzke HJ. Improved oil solubilization in

- oil/water food grade microemulsions in the presence of polyols and ethanol. *J Agric Food Chem.* 2001;49(5):2552–2562.
174. Do LD, Withayyapayanon A, Harwell JH, Sabatini DA. Environmentally Friendly Vegetable Oil Microemulsions Using Extended Surfactants and Linkers. *J Surfactants Deterg* [Internet]. 2009;12(2):91–99. Available from: <https://doi.org/10.1007/s11743-008-1096-0>
 175. St-Onge M-P, Bosarge A, Goree LLT, Darnell B. Medium chain triglyceride oil consumption as part of a weight loss diet does not lead to an adverse metabolic profile when compared to olive oil. *J Am Coll Nutr* [Internet]. 2008 Oct;27(5):547–552. Available from: <https://pubmed.ncbi.nlm.nih.gov/18845704>
 176. Deng L, Que F, Wei H, Xu G, Dong X, Zhang H. Solubilization of tea seed oil in a food-grade water-dilutable microemulsion. *PLoS One.* 2015;10(5):1–12.
 177. Edris AE. Pharmaceutical and therapeutic potentials of essential oils and their individual volatile constituents: A review. *Phyther Res.* 2007;21(4):308–323.
 178. Poyato C, Navarro-Blasco I, Calvo MI, Cavero RY, Astiasarán I, Ansorena D. Oxidative stability of O/W and W/O/W emulsions: Effect of lipid composition and antioxidant polarity. *Food Res Int* [Internet]. 2013;51(1):132–140. Available from: <http://www.sciencedirect.com/science/article/pii/S0963996912005017>
 179. Mugao LG, Gichimu BM, Muturi PW, Mukono ST. Characterization of the Volatile Components of Essential Oils of Selected Plants in Kenya. Zheng D, editor. *Biochem Res Int* [Internet]. 2020;2020:1–8. Available from: <https://doi.org/10.1155/2020/8861798>
 180. Lombardo D, Kiselev MA, Magazù S, Calandra P. Amphiphiles self-assembly: Basic concepts and future perspectives of supramolecular approaches. *Adv Condens Matter Phys.* 2015;2015:1–22.
 181. Wennerström H, Lindman B. Micelles. *Physical chemistry of surfactant association.* *Phys Rep* [Internet]. 1979;52(1):1–86. Available from: <http://www.sciencedirect.com/science/article/pii/0370157379900875>
 182. Ramanathan M, Shrestha LK, Mori T, Ji Q, Hill JP, Ariga K. Amphiphile nanoarchitectonics: from basic physical chemistry to advanced applications. *Phys Chem Chem Phys* [Internet]. 2013;15(26):10580–10611. Available from: <http://dx.doi.org/10.1039/C3CP50620G>
 183. De Angelis P, Cardellini A, Asinari P. Exploring the Free Energy Landscape to Predict the Surfactant Adsorption Isotherm at the Nanoparticle-Water Interface. *ACS Cent Sci.* 2019;5(11):1804–1812.
 184. Azum N, Rub MA, Asiri AM, Bawazeer WA. Micellar and interfacial properties of amphiphilic drug–non-ionic surfactants mixed systems: Surface tension, fluorescence and UV–vis studies. *Colloids Surfaces A Physicochem Eng Asp* [Internet]. 2017;522:183–192. Available from: <http://www.sciencedirect.com/science/article/pii/S0927775717302352>
 185. Tehrani-Bagha AR, Holmberg K. Solubilization of hydrophobic dyes in surfactant solutions. *Materials (Basel).* 2013;6(2):580–608.
 186. Sachin KM, Karpe SA, Singh M, Bhattarai A. Self-assembly of sodium dodecylsulfate

- and dodecyltrimethylammonium bromide mixed surfactants with dyes in aqueous mixtures. *R Soc Open Sci.* 2019;6(3):1–23.
187. Mohajeri E, Noudeh GD. Effect of temperature on the critical micelle concentration and micellization thermodynamic of nonionic surfactants: Polyoxyethylene sorbitan fatty acid esters. *E-Journal Chem.* 2012;9(4):2268–2274.
 188. Burlatsky SF, Atrazhev V V., Dmitriev D V., Sultanov VI, Timokhina EN, Ugolkova EA, et al. Surface tension model for surfactant solutions at the critical micelle concentration. *J Colloid Interface Sci.* 2013;393(1):151–160.
 189. Azum N, Kumar D. Kinetic study of the metal-dipeptide complex with ninhydrin facilitated by gemini (m-s-m) surfactant micelles. *Sci Rep [Internet].* 2020;10(1):1–13. Available from: <http://dx.doi.org/10.1038/s41598-020-61001-6>
 190. Resende KX, Corrêa MA, De Oliveira AG, Scarpa MV. Effect of cosurfactant on the supramolecular structure and physicochemical properties of non-ionic biocompatible microemulsions. *Rev Bras Ciencias Farm J Pharm Sci.* 2008;44(1):35–42.
 191. Yang J, Xu H, Wu S, Ju B, Zhu D, Yan Y, et al. Preparation and evaluation of microemulsion-based transdermal delivery of *Cistanche tubulosa* phenylethanoid glycosides. *Mol Med Rep.* 2017;15(3):1109–1116.
 192. Tadros T. Surfactants BT - Encyclopedia of Colloid and Interface Science. In: Tadros T, editor. Berlin, Heidelberg: Springer Berlin Heidelberg; 2013. p. 1242–1290. Available from: https://doi.org/10.1007/978-3-642-20665-8_40
 193. Zakharova LY, Pashirova TN, Doktorovova S, Fernandes AR, Sanchez-Lopez E, Silva AM, et al. Cationic surfactants: Self-assembly, structure-activity correlation and their biological applications. Vol. 20, *International Journal of Molecular Sciences.* 2019. 1–31 p.
 194. Madhav S, Gupta D. A review on microemulsion based system. *Int J Pharm Sci Res.* 2011;2(8):1888–1899.
 195. Phan CM. Dissociation of Ionic Surfactants at the Air/Water Interface: Complete or Partial? *J Phys Chem B.* 2016;120(31):7681–7686.
 196. Panchal K, Desai A, Nagar T. Physicochemical behavior of mixed nonionic-ionic surfactants in water and aqueous salt solutions. *J Dispers Sci Technol.* 2006;27(1):33–38.
 197. Durkee J. 2 - US and global environmental regulations. In: Durkee JBT-M of ICT and P, editor. Oxford: Elsevier Science; 2006. p. 43–98. Available from: <http://www.sciencedirect.com/science/article/pii/B9780080448886500168>
 198. Wakerly MG, Pouton CW, Meakin BJ, Morton FS. Self-Emulsification of Vegetable Oil-Nonionic Surfactant Mixtures. In: *Phenomena in Mixed Surfactant Systems [Internet].* Washington: American Chemical Society; 1986. p. 18–242. (ACS Symposium Series; vol. 311). Available from: <https://doi.org/10.1021/bk-1986-0311.ch018>
 199. Jiao J. Polyoxyethylated nonionic surfactants and their applications in topical ocular drug delivery. *Adv Drug Deliv Rev [Internet].* 2008;60(15):1663–1673. Available from: <http://www.sciencedirect.com/science/article/pii/S0169409X08002299>

200. McLachlan A, Singh K, McAlduff M, Marangoni DG, Shortall S, Wettig SD. M-s-m cationic gemini and zwitterionic surfactants-a thermodynamic analysis of their mixed micelle formation. *RSC Adv.* 2020;10(6):3221–3232.
201. Souza FD, Souza BS, Tondo DW, Leopoldino EC, Fiedler HD, Nome F. Imidazolium-Based Zwitterionic Surfactants: Characterization of Normal and Reverse Micelles and Stabilization of Nanoparticles. *Langmuir* [Internet]. 2015 Mar 31;31(12):3587–3595. Available from: <https://doi.org/10.1021/la504802k>
202. Zieba M, Wiczorek D, Klimaszewska E, Malysa A, Kwasniewska D. Application of new synthesized zwitterionic surfactants as hair shampoo components. *J Dispers Sci Technol* [Internet]. 2019;40(8):1189–1196. Available from: <https://doi.org/10.1080/01932691.2018.1503545>
203. Azeem A, Rizwan M, Ahmad FJ, Iqbal Z, Khar RK, Aqil M, et al. Nanoemulsion components screening and selection: A technical note. *AAPS PharmSciTech.* 2009;10(1):69–76.
204. Effendy I, Maibach HI. Surfactants and experimental irritant contact dermatitis. *Contact Dermatitis.* 1995 Oct;33(4):217–225.
205. Garg V, Gupta R, Kapoor B, Singh SK, Gulati M. 14 - Application of self-emulsifying delivery systems for effective delivery of nutraceuticals. In: Grumezescu AM, editor. *Emulsions* [Internet]. Academic Press; 2016. p. 479–518. Available from: <http://www.sciencedirect.com/science/article/pii/B9780128043066000143>
206. Komaiko JS, McClements DJ. Formation of Food-Grade Nanoemulsions Using Low-Energy Preparation Methods: A Review of Available Methods. *Compr Rev Food Sci Food Saf.* 2016;15(2):331–352.
207. Rahmah Elfiyani, Anisa Amalia SYP. Effect of Using the Combination of Tween 80 and Ethanol on the Forming and Physical Stability of Microemulsion of Eucalyptus Oil as Antibacterial. *J Young Pharm.* 2017;9(1):118–121.
208. van der Vossen AC, van der Velde I, Smeets OSNM, Postma DJ, Eckhardt M, Vermes A, et al. Formulating a poorly water soluble drug into an oral solution suitable for paediatric patients; lorazepam as a model drug. *Eur J Pharm Sci* [Internet]. 2017;100:205–210. Available from: <http://www.sciencedirect.com/science/article/pii/S0928098717300490>
209. Marek E, Kraft WK. Ethanol Pharmacokinetics in Neonates and Infants. *Curr Ther Res - Clin Exp* [Internet]. 2014;76:90–97. Available from: <http://dx.doi.org/10.1016/j.curtheres.2014.09.002>
210. Gadhawe A. Determination of Hydrophilic-Lipophilic Balance Value. 2014;3(4):573–585.
211. Miller R. Emulsifiers: Types and Uses. In: Caballero B, Finglas PM, Toldrá F, editors. *Encyclopedia of Food and Health* [Internet]. Oxford: Academic Press; 2015. p. 498–502. Available from: <http://www.sciencedirect.com/science/article/pii/B978012384947200249X>
212. Ng N, Rogers MA. Surfactants. In: Melton L, Shahidi F, Varelis PBT-E of FC, editors. *Oxford: Academic Press; 2019. p. 276–282.* Available from: <https://www.sciencedirect.com/science/article/pii/B9780081005965215989>

213. Premlal Ranjith HM, Wijewardene U. 16 - Lipid emulsifiers and surfactants in dairy and bakery products. In: Gunstone FDBT-ML for U in F, editor. Woodhead Publishing Series in Food Science, Technology and Nutrition [Internet]. Woodhead Publishing; 2006. p. 393–428. Available from: <https://www.sciencedirect.com/science/article/pii/B9781855739710500161>
214. Yuan Liu Z-CW 1, 1 Y-YD, 3 HD, 1 YZ, 1 X-JT, 1 PL, et al. Comparison of the Effects of Different Food-Grade Emulsifiers on the Properties and Stability of a Casein-Maltodextrin-Soybean Oil Compound Emulsion. *Molecules*. 2020;1–16.
215. Pant A, Jha K, Singh M. Role of Excipient's HLB Values in Microemulsion System. *IOSR J Pharm Biol Sci (IOSR-JPBS)* [Internet]. 2019;14(2):1–19. Available from: www.Iosrjournals.Org
216. Dixit GR, Mathur VB. Microemulsions: Platform for improvement of solubility and dissolution of poorly soluble drugs. *Asian J Pharm Clin Res*. 2015;8(5):7–17.
217. Ruckenstein E. Microemulsions, Macroemulsions, and the Bancroft Rule. *Langmuir* [Internet]. 1996 Jan 1;12(26):6351–6363. Available from: <https://doi.org/10.1021/la960849m>
218. Davis HT. Factors determining emulsion type: Hydrophile-lipophile balance and beyond. *Colloids Surfaces A Physicochem Eng Asp* [Internet]. 1994;91:9–24. Available from: <http://www.sciencedirect.com/science/article/pii/0927775794029296>
219. Dhoot AS, Naha A, Priya J, Xalxo N. Phase diagrams for three component mixtures in pharmaceuticals and its applications. *J Young Pharm*. 2018;10(2):132–147.
220. Prince LM. Micellization, Solubilization, and Microemulsions. Vol. 2, Micellization, Solubilization, and Microemulsions. New York: Springer, Boston, MA; 1977. 45–54 p.
221. M.L. R. Theory for the Phase Behavior of Microemulsions. In: Mittal K.L. (eds) *Micellization, Solubilization, and Microemulsions*. Massachusetts; 1977.
222. Mahdi ES, Sakeena MH, Abdulkarim MF, Abdullah GZ, Sattar MA, Noor AM. Effect of surfactant and surfactant blends on pseudoternary phase diagram behavior of newly synthesized palm kernel oil esters. *Drug Des Devel Ther*. 2011;5:311–3123.
223. Mishra A, Panola R, Rana AC. Microemulsions: As drug delivery system. *J Sci Innov Res*. 2014;3(4):467–474.
224. Payyal SP, Rompicherla NC, Sathyanarayana SD, Shriram RG, Vadakkepushpakath AN. Microemulsion Based Gel of Sulconazole Nitrate for Topical Application. *Turkish J Pharm Sci* [Internet]. 2020/06/22. 2020 Jun;17(3):259–264. Available from: <https://pubmed.ncbi.nlm.nih.gov/32636702>
225. Karamustafa F, Çelebi N. Development of an oral microemulsion formulation of alendronate: Effects of oil and co-surfactant type on phase behaviour. *J Microencapsul* [Internet]. 2008 Jan 1;25(5):315–323. Available from: <https://doi.org/10.1080/02652040801977045>
226. Aveyard R, Binks BP, Esquena J, Fletcher PDI, Buscall R, Davies S. Flocculation of Weakly Charged Oil–Water Emulsions. *Langmuir* [Internet]. 1999 Feb 1;15(4):970–980. Available from: <https://doi.org/10.1021/la981099e>
227. Sadurní N, Solans C, Azemar N, García-Celma MJ. Studies on the formation of O/W

- nano-emulsions, by low-energy emulsification methods, suitable for pharmaceutical applications. *Eur J Pharm Sci* [Internet]. 2005;26(5):438–445. Available from: <http://www.sciencedirect.com/science/article/pii/S0928098705002460>
228. Mehrnia MA, Jafari SM, Makhmal-Zadeh BS, Maghsoudlou Y. Crocin loaded nano-emulsions: Factors affecting emulsion properties in spontaneous emulsification. *Int J Biol Macromol* [Internet]. 2016;84:261–277. Available from: <http://www.sciencedirect.com/science/article/pii/S014181301530221X>
 229. Ee SL, Duan X, Liew J, Nguyen QD. Droplet size and stability of nano-emulsions produced by the temperature phase inversion method. *Chem Eng J* [Internet]. 2008;140(1–3):626–631. Available from: <http://www.sciencedirect.com/science/article/pii/S1385894707008054>
 230. Perazzo A, Preziosi V, Guido S. Phase inversion emulsification: Current understanding and applications. *Adv Colloid Interface Sci* [Internet]. 2015;222:581–599. Available from: <http://europepmc.org/abstract/MED/25632889>
 231. Förster T, Schambil F TH. Emulsification by the phase inversion temperature method: the role of self-bodying agents and the influence of oil polarity. *Int J Cosmet Sci.* 1990;12(5):217–227.
 232. Pathak M. Nanoemulsions and Their Stability for Enhancing Functional Properties of Food Ingredients. In: Oprea AE, Grumezescu AMBT-NA in F, editors. Bihar: Academic Press; 2017. p. 87–106. Available from: <http://www.sciencedirect.com/science/article/pii/B9780128119426000054>
 233. Kumar M, Bishnoi RS, Shukla AK, Jain CP. Techniques for formulation of nanoemulsion drug delivery system: A review. *Prev Nutr Food Sci.* 2019;24(3):225–234.
 234. Gall V, Runde M, Schuchmann HP. Extending applications of high-pressure homogenization by using simultaneous emulsification and mixing (SEM) - An overview. *Processes.* 2016;4(4).
 235. Calligaris S, Plazzotta S, Bot F, Grasselli S, Malchiodi A, Anese M. Nanoemulsion preparation by combining high pressure homogenization and high power ultrasound at low energy densities. *Food Res Int* [Internet]. 2016;83:25–30. Available from: <http://www.sciencedirect.com/science/article/pii/S0963996916300321>
 236. Vladisavljević GT. Preparation of microemulsions and nanoemulsions by membrane emulsification. *Colloids Surfaces A Physicochem Eng Asp.* 2019;579(August).
 237. Qin D, Liu Z, Bai H, Sun DD, Song X. A new nano-engineered hierarchical membrane for concurrent removal of surfactant and oil from oil-in-water nanoemulsion. *Sci Rep* [Internet]. 2016;6(April):1–12. Available from: <http://dx.doi.org/10.1038/srep24365>
 238. Spyropoulosa F, Hancocks RD, Norton IT. Food-grade emulsions prepared by membrane emulsification techniques. *Procedia Food Sci* [Internet]. 2011;1:920–926. Available from: <http://dx.doi.org/10.1016/j.profoo.2011.09.139>
 239. Charcosset C, Limayem I, Fessi H. The membrane emulsification process - A review. *J Chem Technol Biotechnol.* 2004;79(3):209–218.
 240. Azmi NAN, Elgharbawy AAM, Motlagh SR, Samsudin N, Salleh HM. Nanoemulsions: Factory for food, pharmaceutical and cosmetics. *Processes.* 2019;7(9).

241. Bucci AJ, Van Hekken DL, Tunick MH, Renye JA, Tomasula PM. The effects of microfluidization on the physical, microbial, chemical, and coagulation properties of milk. *J Dairy Sci* [Internet]. 2018;101(8):6990–7001. Available from: <https://www.sciencedirect.com/science/article/pii/S0022030218304922>
242. Sarheed O, Dibi M, Ramesh KVRNS. Studies on the effect of oil and surfactant on the formation of alginate-based O/W lidocaine nanocarriers using nanoemulsion template. *Pharmaceutics*. 2020;12(12):1–21.
243. Prá VD, Pires FB, Dolwitsch CB, Lazzaretti AP, Roggia I, Mortari SR, et al. Formulation and characterization of ultrasound-assisted nanoemulsions containing palm oil (*Elaeis guineensis* Jacq) in water. *Brazilian J Chem Eng*. 2019;36(2):941–947.
244. Ahmad N, Ahmad R, Alam MA, Ahmad FJ, Amir M. Impact of ultrasonication techniques on the preparation of novel Amiloride-nanoemulsion used for intranasal delivery in the treatment of epilepsy. *Artif Cells, Nanomedicine Biotechnol* [Internet]. 2018;46(sup3):S192–207. Available from: <https://doi.org/10.1080/21691401.2018.1489826>
245. Hashtjin AM, Abbasi S. Optimization of ultrasonic emulsification conditions for the production of orange peel essential oil nanoemulsions. *J Food Sci Technol*. 2015;52(5):2679–2689.
246. Stetefeld J, McKenna SA, Patel TR. Dynamic light scattering: a practical guide and applications in biomedical sciences. *Biophys Rev* [Internet]. 2016;8(4):409–427. Available from: <http://dx.doi.org/10.1007/s12551-016-0218-6>
247. Uskoković V. Dynamic Light Scattering Based Microelectrophoresis: Main Prospects and Limitations. *J Dispers Sci Technol*. 2012;33(12):1762–1786.
248. Carvalho PM, Felício MR, Santos NC, Gonçalves S, Domingues MM. Application of light scattering techniques to nanoparticle characterization and development. *Front Chem*. 2018;6(June):1–17.
249. Smith DJ. Characterization of Nanomaterials Using Transmission Electron Microscopy. In: *Nanoscience & Nanotechnology Series* [Internet]. Washington DC: The Royal Society of Chemistry; 2015. p. 1–29. Available from: <http://dx.doi.org/10.1039/9781782621867-00001>
250. Asadi Asadabad M, Jafari Eskandari M. Transmission Electron Microscopy as Best Technique for Characterization in Nanotechnology. *Synth React Inorganic, Met Nano-Metal Chem* [Internet]. 2015 Mar 4;45(3):323–326. Available from: <https://doi.org/10.1080/15533174.2013.831901>
251. Danaei M, Dehghankhold M, Ataei S, Hasanzadeh Davarani F, Javanmard R, Dokhani A, et al. Impact of particle size and polydispersity index on the clinical applications of lipidic nanocarrier systems. *Pharmaceutics*. 2018;10(2):1–17.
252. Sopyan I, Gozali D, Paramudya E. Formulation and Stability Testing of Microemulsion Griseovulfin. *Indones J Pharm*. 2020;2(2):32.
253. Gumustas M, Sengel-Turk CT, Gumustas A, Ozkan SA, Uslu B. Effect of Polymer-Based Nanoparticles on the Assay of Antimicrobial Drug Delivery Systems. In: *Multifunctional Systems for Combined Delivery, Biosensing and Diagnostics* [Internet]. Elsevier; 2017 [cited 2019 Apr 19]. p. 67–108. Available from:

<https://www.sciencedirect.com/science/article/pii/B9780323527255000058>

254. Silva HD, Cerqueira MA, Vicente AA. Influence of surfactant and processing conditions in the stability of oil-in-water nanoemulsions. *J Food Eng* [Internet]. 2015;167:89–98. Available from: <http://dx.doi.org/10.1016/j.jfoodeng.2015.07.037>
255. Uner M. Preparation, characterization and physico-chemical properties of solid lipid nanoparticles (SLN) and nanostructured lipid carriers (NLC): their benefits as colloidal drug carrier systems. *Pharmazie*. 2006 May;61(5):375–386.
256. MA H. The formulation, manufacture and evaluation of capsules containing freeze-dried aqueous extracts of *leonotis leonorus* or *mentha longifolia*. [Internet]. University of the Western Cape; 2006. Available from: https://etd.uwc.ac.za/bitstream/handle/11394/1925/Ma_MPHARM_2006.pdf?sequence=1&isAllowed=y
257. Shen S, Wu Y, Liu Y, Wu D. High drug-loading nanomedicines: Progress, current status, and prospects. *Int J Nanomedicine*. 2017;12:4085–4109.
258. Sarkar P, Bhattacharya S, Pal TK. Application of statistical design to evaluate critical process parameters and optimize formulation technique of polymeric nanoparticles. *R Soc Open Sci*. 2019;6(7).
259. Çalış S, Öztürk Atar K, Arslan FB, Eroğlu H, Çapan Y. Chapter 4 - Nanopharmaceuticals as Drug-Delivery Systems: For, Against, and Current Applications. In: Mohapatra SS, Ranjan S, Dasgupta N, Mishra RK, Thomas SBT-N for DD, editors. *Micro and Nano Technologies* [Internet]. Elsevier; 2019. p. 133–154. Available from: <http://www.sciencedirect.com/science/article/pii/B9780128140338000047>
260. Krstić M, Medarević Đ, Đuriš J, Ibrić S. Chapter 12 - Self-nanoemulsifying drug delivery systems (SNEDDS) and self-microemulsifying drug delivery systems (SMEDDS) as lipid nanocarriers for improving dissolution rate and bioavailability of poorly soluble drugs. In: Grumezescu AM, editor. *Lipid Nanocarriers for Drug Targeting* [Internet]. William Andrew Publishing; 2018. p. 473–508. Available from: <http://www.sciencedirect.com/science/article/pii/B9780128136874000128>
261. Klein S, Shah VP. A standardized mini paddle apparatus as an alternative to the standard paddle. *AAPS PharmSciTech*. 2008;9(4):1179–1184.
262. D’Souza S. A Review of In Vitro Drug Release Test Methods for Nano-Sized Dosage Forms. *Adv Pharm*. 2014;2014:1–12.
263. Puri A, Loomis K, Smith B, Lee JH, Yavlovich A, Heldman E, et al. Lipid-based nanoparticles as pharmaceutical drug carriers: From concepts to clinic. *Crit Rev Ther Drug Carrier Syst*. 2009;26(6):523–580.
264. Sirotti C, Cocceani N, Colombo I, Lapasin R, Grassi M. Modeling of drug release from microemulsions: A peculiar case. *J Memb Sci*. 2002 Jul 1;204:401–412.
265. Rawal SU, Patel MM. Chapter 2 - Lipid nanoparticulate systems: Modern versatile drug carriers. In: Grumezescu AMBT-LN for DT, editor. New York: William Andrew Publishing; 2018. p. 49–138. Available from: <http://www.sciencedirect.com/science/article/pii/B9780128136874000025>
266. Patra JK, Das G, Fraceto LF, Campos EVR, Rodriguez-Torres MDP, Acosta-Torres LS,

- et al. Nano based drug delivery systems: Recent developments and future prospects 10 Technology 1007 Nanotechnology 03 Chemical Sciences 0306 Physical Chemistry (incl. Structural) 03 Chemical Sciences 0303 Macromolecular and Materials Chemistry 11 Medical and He. *J Nanobiotechnology* [Internet]. 2018;16(1):1–33. Available from: <https://doi.org/10.1186/s12951-018-0392-8>
267. Shen J, Burgess DJ. In Vitro Dissolution Testing Strategies for Nanoparticulate Drug Delivery Systems: Recent Developments and Challenges. *Drug Deliv Transl Res*. 2013 Oct;3(5):409–415.
 268. B. Deepika, Juveria Tasleem, Kandukoori Naga Raju, S. Sarojini KSS. Dissolution: a predictive tool for conventional and novel dosage forms. *J Pharma Res* [Internet]. 2018;7(6). Available from: <file:///C:/Users/Administrator/Downloads/JPR-7-6-113-119.PDF>
 269. Sievens-Figueroa L, Pandya N, Bhakay A, Keyvan G, Michniak-Kohn B, Bilgili E, et al. Using USP I and USP IV for discriminating dissolution rates of nano- and microparticle-loaded pharmaceutical strip-films. *AAPS PharmSciTech* [Internet]. 2012/10/23. 2012 Dec;13(4):1473–1482. Available from: <https://pubmed.ncbi.nlm.nih.gov/23090112>
 270. Chanamai R, McClements DJ. Creaming Stability of Flocculated Monodisperse Oil-in-Water Emulsions. *J Colloid Interface Sci* [Internet]. 2000;225(1):214–218. Available from: <http://www.sciencedirect.com/science/article/pii/S0021979700967663>
 271. Bibette J. Flocculation and Coalescence of Oil-in-Water Emulsions. *MRS Proc* [Internet]. 2011/02/25. 1991;248:303. Available from: <https://www.cambridge.org/core/article/flocculation-and-coalescence-of-oil-in-water-emulsions/FE919040FC7A06E54FE109B3ABCA0730>
 272. Goodarzi F, Zendehboudi S. A Comprehensive Review on Emulsions and Emulsion Stability in Chemical and Energy Industries. *Can J Chem Eng*. 2019;97(1):281–309.
 273. Robins MM. Emulsions - Creaming phenomena. *Curr Opin Colloid Interface Sci*. 2000;5(5–6):265–272.
 274. Pons R. Polymeric Surfactants as Emulsion Stabilizers. In: Alexandridis P, Lindman BBT-ABC, editors. Amsterdam: Elsevier Science B.V.; 2000. p. 409–422. Available from: <http://www.sciencedirect.com/science/article/pii/B9780444824417500189>
 275. Pinfield VJ, Dickinson E, Povey MJW. Modeling of Combined Creaming and Flocculation in Emulsions. *J Colloid Interface Sci* [Internet]. 1997;186(1):80–89. Available from: <http://europemc.org/abstract/MED/9056306>
 276. Journal B, Souza WJ, Santos KMC, Cruz AA, Franceschi E, Dariva C, et al. Effect of Water Content, Temperature and Average Droplet Size on the Settling Velocity of Water-in-Oil-Emulsions. *Brazilian J Chem Eng*. 2015;32(02):455–464.
 277. Panagiotou T, Fisher R. Improving Product Quality with Entrapped Stable Emulsions: From Theory to Industrial Application. *Challenges*. 2012;3(2):84–113.
 278. Schramm LL. Emulsions, Foams, and Suspensions: Fundamentals and Applications. *Emulsions, Foams, and Suspensions: Fundamentals and Applications*. Verlag: Wiley; 2006. 1–448 p.
 279. Khan MF, Sheraz MA, Ahmed S, Kazi SH, Ahmad I. Emulsion Separation ,

- Classification and Stability Assessment. *J Pharm Pharm Sci.* 2014;2(2):56–62.
280. Vippagunta SR, Brittain HG, Grant DJW. Crystalline solids. *Adv Drug Deliv Rev* [Internet]. 2001;48(1):3–26. Available from: <https://www.sciencedirect.com/science/article/pii/S0169409X01000977>
 281. Borka L. Review on crystal polymorphism of substances in the European pharmacopoeia. *Pharm Acta Helv.* 1991;66(1):16–22.
 282. Giron D. Thermal analysis and calorimetric methods in the characterisation of polymorphs and solvates. *Thermochim Acta* [Internet]. 1995;248:1–59. Available from: <https://www.sciencedirect.com/science/article/pii/004060319401953E>
 283. Censi R, Di Martino P. Polymorph Impact on the Bioavailability and Stability of Poorly Soluble Drugs. *Molecules* [Internet]. 2015 Oct 15;20(10):18759–18776. Available from: <https://pubmed.ncbi.nlm.nih.gov/26501244>
 284. Hilfiker R, Raumer M Von. *Polymorphism in the Pharmaceutical.* Weinheim: Wiley-VCH Verlag; 2019. 485 p.
 285. Xiao L, Wang B, Yang G, Gauthier M. Poly (Lactic Acid) -Based Biomaterials : Synthesis , Modification and Applications. In: Ghista DN, editor. *InTech*; 1012. p. 247–282. Available from: <https://cdn.intechweb.org/pdfs/26368.pdf>
 286. Segall AI. Preformulation: The use of FTIR in compatibility studies. *J Innov Appl Pharm Sci.* 2019;4(3):1–6.
 287. Hait SK, Moulik SP, Rodgers MP, Burke SE, Palepu R. Physicochemical studies on microemulsions. 7. Dynamics of percolation and energetics of clustering in water/AOT/isooctane and water/AOT/decane w/o microemulsions in presence of hydrotopes (sodium salicylate, α -naphthol, β -naphthol, resorcinol, catechol, h. *J Phys Chem B.* 2001;105(29):7145–7154.
 288. Kalaitzaki A. Biocompatible microemulsions : Formulation encapsulation of bioactive compounds and their potential applications [Internet]. Orebro; 2014. Available from: <https://www.diva-portal.org/smash/get/diva2:717555/FULLTEXT02>
 289. Yoshida MI, Gomes ECL, Soares CDV, Cunha AF, Oliveira MA. Thermal analysis applied to verapamil hydrochloride characterization in pharmaceutical formulations. *Molecules.* 2010;15(4):2439–2452.
 290. Malviya R, Bansal V, Pal O, Sharma P. High performance liquid chromatography: A short review. *J Glob Pharma Technol.* 2010 Jun;2:22–26.
 291. Sankar R, Snehathatha K, Firdose S, Babu P. applications in HPLC in pharmaceutical analysis. *Int J Pharm Sci Rev Res.* 2019 Dec;59:117–124.
 292. D’Atri V, Fekete S, Clarke A, Veuthey JL, Guillarme D. Recent Advances in Chromatography for Pharmaceutical Analysis. *Anal Chem.* 2019;91(1):210–239.
 293. Hong P, Koza S, Bouvier ESP. A review size-exclusion chromatography for the analysis of protein biotherapeutics and their aggregates. Vol. 35, *Journal of Liquid Chromatography and Related Technologies.* 2012. p. 2923–2950.
 294. Buszewski B, Noga S. Hydrophilic interaction liquid chromatography (HILIC)-a powerful separation technique. Vol. 402, *Analytical and Bioanalytical Chemistry.* 2012.

- p. 231–247.
295. Eksteen R, Pardue K. Modified Silica-Based Packing Materials for Size Exclusion Chromatography. In: Handbook Of Size Exclusion Chromatography And Related Techniques [Internet]. 2003. Available from: <https://www.researchgate.net/publication/274073908>
 296. Ettre LS. Nomenclature for chromatography (iupac recommendations 1993). *Pure Appl Chem.* 1993;65(4):819–872.
 297. El Hage K, Bemish RJ, Meuwly M. From in silica to in silico: retention thermodynamics at solid-liquid interfaces. *Phys Chem Chem Phys.* 2018;20(27):18610–18622.
 298. Hanai T. HPLC A Practical guide. Smith RM, editor. The Royal Society of Chemistry; 1999. 99 p.
 299. LoBrutto YK and R. Stationary Phases. In: HPLC for Pharmaceutical Scientists. John Wiley & Sons, Inc.; 2007. p. 75–137.
 300. Jandera P. Comparison of various modes and phase systems for analytical HPLC. In: Valkó KBT-H of AS, editor. Separation Methods in Drug Synthesis and Purification [Internet]. Elsevier Science B.V.; 2000. p. 1–71. Available from: <https://www.sciencedirect.com/science/article/pii/S1567719200800042>
 301. Hong P, Koza S, Bouvier ESP. Size-Exclusion Chromatography for the Analysis of Protein Biotherapeutics and their Aggregates. *J Liq Chromatogr Relat Technol* [Internet]. 2012/11/30. 2012 Nov;35(20):2923–2950. Available from: <https://pubmed.ncbi.nlm.nih.gov/23378719>
 302. Scott RPW. Mechanisms : Normal Phase. *Langmuir.* 2000;706–711.
 303. Jandera P. Comparison of various modes and phase systems for analytical HPLC. *Handb Anal Sep.* 2020;8:1–91.
 304. Yoshida T, Okada T. Peptide separation in normal-phase liquid chromatography. Study of selectivity and mobile phase effects on various columns. *J Chromatogr A.* 1999;840(1):1–9.
 305. Hayes R, Ahmed A, Edge T, Zhang H. Core-shell particles: Preparation, fundamentals and applications in high performance liquid chromatography. Vol. 1357, *Journal of Chromatography A.* Elsevier; 2014. p. 36–52.
 306. Haddad PR, Jackson PE, -Boston -Heidelberg -London -New York -Oxford Paris -San Diego -San Francisco -Singapore -Sydney -Tokyo A. ion chromatography principles and applications Elsevier. Vol. 46, *Journal Of Chromatography Library.*
 307. DeStefano JJ, Schuster SA, Lawhorn JM, Kirkland JJ. Performance characteristics of new superficially porous particles. *J Chromatogr A.* 2012 Oct 5;1258:76–83.
 308. Dores-Sousa JL, De Vos J, Eeltink S. Resolving power in liquid chromatography: A trade-off between efficiency and analysis time. Vol. 42, *Journal of Separation Science.* Wiley-VCH Verlag; 2019. p. 38–50.
 309. Martin-Villacorta J, Méndez R. Effect of temperature and mobile phase composition on rp-hplc separation of cephalosporins. *J Liq Chromatogr.* 1990;13(16):3269–3288.
 310. McNeff C V., Yan B, Stoll DR, Henry RA. Practice and theory of high temperature

- liquid chromatography. *J Sep Sci.* 2007;30(11):1672–1685.
311. Schmidt Aus Berlin AH. Innovative hplc method design (development & understanding). 2017.
 312. Stauffer E, Dolan JA, Newman R. Chapter 8 - Gas Chromatography and Gas Chromatography—Mass Spectrometry. In: Stauffer E, Dolan JA, Newman RBT-FDA, editors. Burlington: Academic Press; 2008. p. 235–293.
 313. Center for Drug Evaluation and Research (CDER) Reviewer Guidance' Validation of Chromatographic Methods. 1994;
 314. Webster GK, Diaz AR, Seibert DS, Weekley BS, Jackson JD. Plate number requirements for establishing method suitability. *J Chromatogr Sci.* 2005;43(2):67–72.
 315. Kelly M. Chromatography today. Vol. 664, *Journal of Chromatography A.* 1994. 135–137 p.
 316. Gjerde DT, Hoang L, Hornby D. Appendix 1: Chromatographic Separation Equations and Principles for RNA Separation. *RNA Purif Anal.* 2009;147–158.
 317. Jaroniec M. Partition and displacement models in reversed-phase liquid chromatography with mixed eluents [Internet]. Vol. 656, *Journal of Chromatography A.* 1993. p. 37–50. Available from: <http://www.sciencedirect.com/science/article/pii/002196739380796B>
 318. Jeansonne MS. Chromatographic Peak Shape Analysis and Modeling. [Internet]. Available from: https://digitalcommons.lsu.edu/gradschool_disstheses
 319. Hansen S, Pedersen-Bjergaard S, Rasmussen K. Introduction to Pharmaceutical Analysis. In: Introduction to Pharmaceutical Chemical Analysis. John Wiley & Sons Inc; 2011. p. 1–11.
 320. Pápai Z, Pap TL. Analysis of peak asymmetry in chromatography. *J Chromatogr A* [Internet]. 2002;953(1):31–38. Available from: <https://www.sciencedirect.com/science/article/pii/S0021967302001218>
 321. Beer M De. Development of Gradient Stationary Phase Optimized Selectivity Approaches for Improved Method Development in High Performance Liquid Chromatography Maarten De Beer. Gent; 2015.
 322. Swartz M. HPLC detectors: A brief review. Vol. 33, *Journal of Liquid Chromatography and Related Technologies.* 2010. p. 1130–1150.
 323. Es'haghi Z. Photodiodes - Communications, Bio-Sensings, Measurements and High-Energy Physics. In: Photodiodes [Internet]. IntechOpen; 2011. Available from: <https://www.intechopen.com/books/advanced-biometric-technologies/liveness-detection-in-biometrics>
 324. González-Morales D, Valencia A, Díaz-Nuñez A, Fuentes-Estrada M, López-Santos O, García-Beltrán O. Development of a Low-Cost UV-Vis Spectrophotometer and Its Application for the Detection of Mercuric Ions Assisted by Chemosensors. Vol. 20, *Sensors* . 2020.
 325. He J, Cheung AP, Wang E, Fang K, Liu P. High-performance liquid chromatographic analysis for a non- chromophore-containing phosphatidyl inositol analog , 1- [(1-O-inositol , using indirect UV detection. *J Chromatogr A.* 2001;913:355–363.

326. Ghassabian SMM and S. Linearity of Calibration Curves for Analytical Methods: A Review of Criteria for Assessment of Method Reliability. Intech. 2018;
327. Eshaghi Z. Photodiode Array Detection in Clinical Applications; Quantitative Analyte Assay Advantages, Limitations and Disadvantages. In: Photodiodes - Communications, Bio-Sensings, Measurements and High-Energy Physics [Internet]. 2011. Available from: www.intechopen.com
328. Agrahari V, Bajpai M, Nanda S. Essential concepts of mobile phase selection for Reversed phase HPLC. Res J Pharm Technol [Internet]. 2013;6(5):459–464. Available from: www.rjptonline.org
329. Welch CJ, Brkovic T, Schafer W, Gong X. Performance to burn? Re-evaluating the choice of acetonitrile as the platform solvent for analytical HPLC. Green Chem. 2009;11(8):1232–1238.
330. Dembek M, Bocian S. Pure water as a mobile phase in liquid chromatography techniques. TrAC - Trends Anal Chem. 2020;123.
331. Yabré M, Ferey L, Somé IT, Gaudin K. Greening reversed-phase liquid chromatography methods using alternative solvents for pharmaceutical analysis. Molecules. 2018;23(5).
332. Sadek PC. The HPLC Solvent Guide, 2nd Edition. 2nd Editio. New Jersey, United States: Wiley; 2002. 664 p.
333. Bruno TJ. Instability of HPLC Solvents. In: CRC Handbook of Chemistry and Physics. 96th ed. Florida: CRC Press, Boca Raton, FL; 2015.
334. Lupo S. New Advice on an Old Topic: Buffers in Reversed-Phase HPLC. LCGC North Am. 2017;35(7):424–433.
335. Espinosa S, Bosch E, Rosés M. Retention of ionizable compounds on HPLC. 12. The properties of liquid chromatography buffers in acetonitrile-water mobile phases that influence HPLC retention. Anal Chem. 2002;74(15):3809–3918.
336. Dolan J. A Guide to HPLC and LC-MS Buffer Selection. WwwAce-HplcCom [Internet]. 2012; Available from: www.ace-hplc.com
337. Cristofolletti R, Nair A, Abrahamsson B, Groot DW, Kopp S, Langguth P, et al. Biowaiver Monographs for Immediate Release Solid Oral Dosage Forms: Efavirenz. J Pharm Sci. 2013;102(2):318–329.
338. Montgomery ER, Edmanson AL, Cook SC, Hovsepian PK. Development and validation of a reverse-phase HPLC method for analysis of efavirenz and its related substances in the drug substance and in a capsule formulation. J Pharm Biomed Anal [Internet]. 2001 May 1 [cited 2018 Sep 3];25(2):267–284. Available from: <https://www.sciencedirect.com/science/article/pii/S0731708500004957?via%3Dihub>
339. Karyn M. Usher, Steven W. Hansen, Jennifer S. Amoo, Allison P. Bernstein MEPM. Precision of Internal Standard and External Standard Methods in High Performance Liquid Chromatography. LCGC [Internet]. 2015;33(4):40–46. Available from: <http://www.chromatographyonline.com/precision-internal-standard-and-external-standard-methods-high-performance-liquid-chromatography>
340. Wang M, Wang C, Han X. Selection of internal standards for accurate quantification of complex lipid species in biological extracts by electrospray ionization mass

- spectrometry-What, how and why? *Mass Spectrom Rev* [Internet]. 2016/01/15. 2017 Nov;36(6):693–714. Available from: <https://pubmed.ncbi.nlm.nih.gov/26773411>
341. Bakshi M, Singh S. Development of validated stability-indicating assay methods—critical review. *J Pharm Biomed Anal* [Internet]. 2002;28(6):1011–1040. Available from: <http://www.sciencedirect.com/science/article/pii/S073170850200047X>
 342. Bienvenu E, Hoffmann KJ, Ashton M, Kayumba PC. A rapid and selective HPLC-UV method for the quantitation of efavirenz in plasma from patients on concurrent HIV/AIDS and tuberculosis treatments. *Biomed Chromatogr*. 2013;27(11):1554–1559.
 343. Gaur PK, Mishra S, Bajpai M, Mishra A. Enhanced Oral Bioavailability of Efavirenz by Solid Lipid Nanoparticles: In Vitro Drug Release and Pharmacokinetics Studies. 2014;2014.
 344. Gupta S, Kesarla R, Chotai N, Omri A. Development and validation of reversed-phase HPLC gradient method for the estimation of efavirenz in plasma. *PLoS One*. 2017;1–12.
 345. Makoni P, Khamanga S, Kasongo K, Walker R. The use of experimental design for the development and validation of an HPLC-ECD method for the quantitation of efavirenz. *Pharmazie*. 2018 Oct;73:570–578.
 346. de Sá Viana O, Medeiros FPM, Grangeiro-Júnior S, Albuquerque MM, La Roca Soares MF, Soares-Sobrinho JL, et al. Development and validation of a HPLC analytical assay method for efavirenz tablets: A medicine for HIV infections. *Brazilian J Pharm Sci*. 2011;47(1):97–102.
 347. Surve DH, Jindal AB. Development and validation of reverse-phase high-performance liquid chromatographic (RP-HPLC) method for quantification of Efavirenz in Efavirenz-Enfuvirtide co-loaded polymer-lipid hybrid nanoparticles. *J Pharm Biomed Anal* [Internet]. 2019;175:112765. Available from: <https://doi.org/10.1016/j.jpba.2019.07.013>
 348. Administration F and D. Guidance for Industry Q2B Validation of Analytical Procedures: Methodology. 1996;(November):301–827. Available from: <http://www.fda.gov/cder/guidance/index.htm%5Cnhttp://www.fda.gov/cber/guidelines.htm>
 349. Marson BM, Concentino V, Junkert AM, Fachi MM, Vilhena RO, Pontarolo R. Validation of analytical methods in a pharmaceutical quality system: an overview focused on HPLC methods. *Quim Nova*. 2020;43(8):1190–1203.
 350. Çoruh S, Eleveli S, Geyikçi F. Statistical evaluation and optimization of factors affecting the leaching performance of copper flotation waste. *Sci World J*. 2012;2012.
 351. Kalariya PD, Namdev D, Srinivas R, Gananadhamu S. Application of experimental design and response surface technique for selecting the optimum RP-HPLC conditions for the determination of moxifloxacin HCl and ketorolac tromethamine in eye drops. *J Saudi Chem Soc* [Internet]. 2017 Jan 1 [cited 2018 Sep 3];21:S373–82. Available from: <https://www.sciencedirect.com/science/article/pii/S131961031400060X>
 352. Commerce. USD of. NIST/SEMATECH e-Handbook of Statistical Methods. U.S. Department of Commerce.; 2012.
 353. Guthrie WF. NIST/SEMATECH e-Handbook of Statistical Methods (NIST Handbook

- 151). 2020.
354. Bezerra MA, Santelli RE, Oliveira EP, Villar LS, Escaleira LA. Response surface methodology (RSM) as a tool for optimization in analytical chemistry. *Talanta*. 2008;76(5):965–977.
 355. Anitha G, Pandey VP. Review on: Statistical designs and response surface methodology (RSM) as a tool for the optimization of HPLC Methods [Internet]. Vol. 5, and Analytical Research. Available from: www.ijpar.com
 356. Bowden GD, Pichler BJ, Maurer A. A Design of Experiments (DoE) Approach Accelerates the Optimization of Copper-Mediated ¹⁸F-Fluorination Reactions of Arylstannanes. *Sci Rep*. 2019;9(1):1–10.
 357. Bai Y, Saren G, Huo W. Response surface methodology (RSM) in evaluation of the vitamin C concentrations in microwave treated milk. *J Food Sci Technol*. 2014;52(7):4647–4651.
 358. Bayuo J, Abukari MA, Pelig-Ba KB. Optimization using central composite design (CCD) of response surface methodology (RSM) for biosorption of hexavalent chromium from aqueous media. *Appl Water Sci* [Internet]. 2020;10(6):1–12. Available from: <https://doi.org/10.1007/s13201-020-01213-3>
 359. Fukuda IM, Pinto CFF, Moreira CDS, Saviano AM, Lourenço FR. Design of experiments (DoE) applied to pharmaceutical and analytical quality by design (QbD). Vol. 54, *Brazilian Journal of Pharmaceutical Sciences*. Faculdade de Ciências Farmaceuticas (Biblioteca); 2018.
 360. Che Sulaiman IS, Basri M, Fard Masoumi HR, Ashari SE, Ismail M. Design and development of a nanoemulsion system containing extract of: *Clinacanthus nutans* (L.) leaves for transdermal delivery system by D-optimal mixture design and evaluation of its physicochemical properties. *RSC Adv* [Internet]. 2016;6(71):67378–67388. Available from: <http://dx.doi.org/10.1039/C6RA12930G>
 361. Ribeiro-Oliveira JP, de Santana DG, Pereira VJ, dos Santos CM. Data transformation: an underestimated tool by inappropriate use. *Acta Sci - Agron*. 2018;40(1):1–11.
 362. Henley SS, Golden RM, Kashner TM. Statistical modeling methods: challenges and strategies. *Biostat Epidemiol*. 2020;4(1):105–139.
 363. Jayaraman K. *A Statistical Manual For Forestry Research*. Fao. 1999;(May):231.
 364. Nakagawa S, Johnson PCD, Schielzeth H. The coefficient of determination R² and intra-class correlation coefficient from generalized linear mixed-effects models revisited and expanded. *J R Soc Interface*. 2017;14(134).
 365. Skrypnik L, Novikova A. Response surface modeling and optimization of polyphenols extraction from apple pomace based on nonionic emulsifiers. *Agronomy*. 2020;10(1).
 366. Faraway JJ. *Practical Regression and Anova using R* [Internet]. Vol. 1. 1999. 1–213 p. Available from: <https://cran.r-project.org/doc/contrib/Faraway-PRA.pdf>
 367. Shishovska MA, Stefova MT. Fast and universal HPLC method for determination of permethrin in formulations using 1.8- μ m particle-packed column and performance comparison with other column types. *J Chromatogr Sci*. 2012;50(1):43–50.

368. National Research Council. Assessing the reliability of complex models: Mathematical and statistical foundations of verification, validation, and uncertainty quantification. *Assessing the Reliability of Complex Models: Mathematical and Statistical Foundations of Verification, Validation, and Uncertainty Quantification*. 2012. 1–144 p.
369. Mohamad Zen NI, Abd Gani SS, Shamsudin R, Fard Masoumi HR. The use of D-optimal mixture design in optimizing development of okara tablet formulation as a dietary supplement. *Sci World J*. 2015;2015.
370. Hou Q, Mahnken JD, Gajewski BJ, Dunton N. The Box-Cox power transformation on nursing sensitive indicators: Does it matter if structural effects are omitted during the estimation of the transformation parameter? *BMC Med Res Methodol*. 2011;11(118):1471–2288.
371. Thomas DR and YJD. Point Estimates and Confidence Intervals for Variable Importance in Multiple Linear Regression. *J Educ Behav Stat*. 2007;32(1):61–91.
372. Khalil NY, Darwish IA, Alshammari MF, Wani TA. ICH guidelines-compliant HPLC-UV method for pharmaceutical quality control and therapeutic drug monitoring of the multi-targeted tyrosine kinase inhibitor pazopanib. *South African J Chem*. 2017;70:60–66.
373. Ben-Haim Y, Hemez FM. Robustness, fidelity and prediction-looseness of models. In: *Proceedings of the Royal Society A: Mathematical, Physical and Engineering Sciences*. 2012. p. 227–244.
374. Chan CC. Principles and practices of analytical method validation: Validation of analytical methods is time-consuming but essential. *Qual Assur J*. 2011 Jul;14(3–4):61–74.
375. Peris-Vicente J, Esteve-Romero J, Carda-Broch S. Validation of Analytical Methods Based on Chromatographic Techniques: An Overview. In: *Analytical Separation Science*. 2015. p. 1757–1808.
376. Naseef H, Moqadi R, Qurt M. Development and validation of an HPLC method for determination of antidiabetic drug alogliptin benzoate in bulk and tablets. *J Anal Methods Chem*. 2018;2018.
377. Raposo F. Evaluation of analytical calibration based on least-squares linear regression for instrumental techniques: A tutorial review. 2016;77(March):167–185.
378. Broadhurst D, Goodacre R, Reinke SN, Kuligowski J, Wilson ID, Lewis MR, et al. Guidelines and considerations for the use of system suitability and quality control samples in mass spectrometry assays applied in untargeted clinical metabolomic studies. *Metabolomics*. 2018;14(6):1–17.
379. Xiong Y, Xiao KP, Rustum AM. Development and validation of a stability-indicating RP-HPLC method to separate low levels of dexamethasone and other related compounds from betamethasone. *J Pharm Biomed Anal*. 2009 Apr;49(3):646–654.
380. Space JS, Opio AM, Nickerson B, Jiang H, Dumont M, Berry M. Validation of a dissolution method with HPLC analysis for lasofoxifene tartrate low dose tablets. *J Pharm Biomed Anal* [Internet]. 2007;44(5):1064–1071. Available from: <http://europepmc.org/abstract/MED/17560750>
381. Gedawy A, Al-Salami H, Dass CR. Development and validation of a new analytical

- HPLC method for simultaneous determination of the antidiabetic drugs, metformin and gliclazide. *J Food Drug Anal* [Internet]. 2019;27(1):315–322. Available from: <http://www.sciencedirect.com/science/article/pii/S1021949818301121>
382. Tiwari G, Tiwari R. Bioanalytical method validation: An updated review. *Pharm Methods*. 2010 Oct;1(1):25–38.
 383. Chesher D. Evaluating assay precision. *Clin Biochem Rev*. 2008 Aug;29(1):23–26.
 384. Bartlett JW, Frost C. Reliability, repeatability and reproducibility: Analysis of measurement errors in continuous variables. *Ultrasound Obstet Gynecol*. 2008;31(4):466–475.
 385. Lawson GM. Defining limit of detection and limit of quantitation as applied to drug of abuse testing: striving for a consensus. Vol. 40, *Clinical Chemistry*. 1994. p. 1218–1219.
 386. Alankar Shrivastava VBG. Methods for the determination of limit of detection and limit of quantitation of the analytical methods. *Chronicles Young Sci*. 2011;2(1).
 387. Saadati N, Abdullah MP, Zakaria Z, Sany SBT, Rezayi M, Hassonizadeh H. Limit of detection and limit of quantification development procedures for organochlorine pesticides analysis in water and sediment matrices. *Chem Cent J*. 2013;7(1):1–10.
 388. Honeycutt WT, Ley MT, Materer NF. Precision and limits of detection for selected commercially available, low-cost carbon dioxide and methane gas sensors. *Sensors (Switzerland)*. 2019;19(14).
 389. Şengül Ü. Comparing determination methods of detection and quantification limits for aflatoxin analysis in hazelnut. *J Food Drug Anal*. 2016;24(1):56–62.
 390. Sharma MK, Murugesan M. Forced Degradation Study an Essential Approach to Develop Stability Indicating Method. *J Chromatogr Sep Tech*. 2017;08(01).
 391. Baber N. International conference on harmonisation of technical requirements for registration of pharmaceuticals for human use (ICH). *Br J Clin Pharmacol*. 1994;37(5):401–404.
 392. Hamrapurkar P, Patil P, Desai M, Phale M, Pawar S. Stress degradation studies and development of a validated stability-indicating-assay-method for determination of diacerein in presence of degradation products. *Pharm Methods*. 2011 Jan;2(1):30–35.
 393. Blessy M, Patel RD, Prajapati PN, Agrawal YK. Development of forced degradation and stability indicating studies of drugs—A review. *J Pharm Anal* [Internet]. 2014;4(3):159–165. Available from: <http://www.sciencedirect.com/science/article/pii/S2095177913001007>
 394. Bajaj S, Singla D, Sakhuja N. Stability testing of pharmaceutical products. *J Appl Pharm Sci*. 2012;2(3):129–138.
 395. Devrukhakar PS, Borkar R, Shastri N, Surendranath K V. A Validated Stability-Indicating RP-HPLC Method for the Simultaneous Determination of Tenofovir, Emtricitabine, and a Efavirenz and Statistical Approach to Determine the Effect of Variables. Akbay C, Remsberg CM, Jayaprakasha GK, editors. *ISRN Chromatogr* [Internet]. 2013;2013:878295. Available from: <https://doi.org/10.1155/2013/878295>
 396. Article R, Kulkarni S V, Damle MC. Development and validation of Stability Indicating

- HPLC method for estimation of Embelin in *Embelia tjeriam* cottam(Vidanga). *Int J Ayurvedic Med* [Internet]. 2015;6(3):243–249. Available from: <http://ijam.co.in>
397. Jones TM. Preformulation Studies , in *Pharmaceutical Formulation: The Science and Technology of Dosage Forms*,. In: *Drug Discovery* [Internet]. The Royal Society of Chemistry; 2018. p. 1–41. Available from: <http://dx.doi.org/10.1039/9781782620402-00001>
 398. Fathima N, Mamatha T, Qureshi HK, Anitha N, Venkateswara Rao J. Drug-excipient interaction and its importance in dosage form development. *J Appl Pharm Sci*. 2011;1(6):66–71.
 399. Filipe D, Ferreira L. ICH Q8/Q9/Q10 Guidelines: Changing Paradigm in Pharmaceutical Development [Internet]. University of Coimbra; 2014. Available from: https://estudogeral.sib.uc.pt/bitstream/10316/28095/1/EN_Diogo_Ferreira_ICH_Q8%2C_Q9_and_Q10_Changing_Paradigm_in_Pharmaceutical_Development_08-2014.pdf
 400. Yu LX, Akseli I, Allen B, Amidon G, Bizjak TG, Boam A, et al. Advancing Product Quality: a Summary of the Second FDA/PQRI Conference. *AAPS J*. 2016;18(2):528–543.
 401. Alsante KM, Huynh-Ba K, Baertschi SW, Reed RA, Landis MS, Kleinman MH, et al. Recent trends in product development and regulatory issues on impurities in active pharmaceutical ingredient (API) and drug products. Part 1: Predicting degradation related impurities and impurity considerations for pharmaceutical dosage forms. *AAPS PharmSciTech* [Internet]. 2013/11/27. 2014 Feb;15(1):198–212. Available from: <https://pubmed.ncbi.nlm.nih.gov/24281749>
 402. Lee EH. A practical guide to pharmaceutical polymorph screening & selection. *Asian J Pharm Sci* [Internet]. 2014;9(4):163–175. Available from: <http://www.sciencedirect.com/science/article/pii/S1818087614000245>
 403. Ribeiro APB, Masuchi MH, Miyasaki EK, Domingues MAF, Stroppa VLZ, de Oliveira GM, et al. Crystallization modifiers in lipid systems. *J Food Sci Technol*. 2015 Jul;52(7):3925–3946.
 404. Jendrzejewska I, Zajdel P, Pietrasik E, Barsova Z, Goryczka T. Application of X-ray powder diffraction and differential scanning calorimetry for identification of counterfeit drugs. *Monatshefte fur chemie* [Internet]. 2018/04/10. 2018;149(5):977–985. Available from: <https://pubmed.ncbi.nlm.nih.gov/29720770>
 405. Bharate SS, Vishwakarma RA. Impact of preformulation on drug development. *Expert Opin Drug Deliv* [Internet]. 2013 Sep 1;10(9):1239–1257. Available from: <https://doi.org/10.1517/17425247.2013.783563>
 406. Veras KS, Fachel FNS, Pittol V, Garcia KR, Bassani VL, Dos Santos V, et al. Compatibility study of rosmarinic acid with excipients used in pharmaceutical solid dosage forms using thermal and non-thermal techniques. *Saudi Pharm J SPJ Off Publ Saudi Pharm Soc* [Internet]. 2019/09/25. 2019 Dec;27(8):1138–1145. Available from: <https://pubmed.ncbi.nlm.nih.gov/31885473>
 407. Pani NR, Nath LK, Acharya S. Compatibility studies of nateglinide with excipients in immediate release tablets. *Acta Pharm*. 2011;61(2):237–247.
 408. Bruni G, Berbenni V, Milanese C, Girella A, Marini A. Drug-excipient compatibility

- studies in binary and ternary mixtures by physico-chemical techniques. *J Therm Anal Calorim.* 2010;102(1):193–201.
409. Blagden N, de Matas M, Gavan PT, York P. Crystal engineering of active pharmaceutical ingredients to improve solubility and dissolution rates. Vol. 59, *Advanced Drug Delivery Reviews.* 2007. p. 617–630.
 410. Ribeiro LNM, Franz-Montan M, Breikreitz MC, Alcântara ACS, Castro SR, Guilherme VA, et al. Nanostructured lipid carriers as robust systems for topical lidocaine-prilocaine release in dentistry. *Eur J Pharm Sci.* 2016;93:192–202.
 411. Litteer B, Beckers D. Increasing application of x-ray powder diffraction in the pharmaceutical industry. *American Laboratory* [Internet]. 2005 Jun;22. Available from: [http://old.vscht.cz/clab/RTG/dokumenty/panalytical/xrd/Increasing application of X-ray powder diffraction in the pharmaceutical industry.pdf](http://old.vscht.cz/clab/RTG/dokumenty/panalytical/xrd/Increasing%20application%20of%20X-ray%20powder%20diffraction%20in%20the%20pharmaceutical%20industry.pdf)
 412. Katdare A, Chaubal M V. Excipient development for pharmaceutical, biotechnology, and drug delivery systems. *Excipient Development for Pharmaceutical, Biotechnology, and Drug Delivery Systems.* 2006. 1–452 p.
 413. Dhiman M, Yedurkar P, Sawant KK. Formulation, characterization, and in vitro evaluation of bioadhesive gels containing 5-Fluorouracil. *Pharm Dev Technol.* 2008;13(1):15–25.
 414. Osterberg RE, DeMerlis CC, Hobson DW, McGovern TJ. Trends in excipient safety evaluation. Vol. 30, *International Journal of Toxicology.* 2011. p. 600–610.
 415. Magnuson B, Munro I, Abbot P, Baldwin N, Lopez-Garcia R, Ly K, et al. Review of the regulation and safety assessment of food substances in various countries and jurisdictions. *Food Addit Contam Part A Chem Anal Control Expo Risk Assess* [Internet]. 2013/06/20. 2013;30(7):1147–1220. Available from: <https://pubmed.ncbi.nlm.nih.gov/23781843>
 416. Constable A, Mahadevan B, Pressman P, Garthoff JA, Meunier L, Schrenk D, et al. An integrated approach to the safety assessment of food additives in early life. *Toxicol Res Appl* [Internet]. 2017 Jan 1;1:2397847317707370. Available from: <https://doi.org/10.1177/2397847317707370>
 417. Jimmy B, Jose J. Patient medication adherence: measures in daily practice. *Oman Med J* [Internet]. 2011 May;26(3):155–159. Available from: <https://pubmed.ncbi.nlm.nih.gov/22043406>
 418. Plöger GF, Hofsäss MA, Dressman JB. Solubility Determination of Active Pharmaceutical Ingredients Which Have Been Recently Added to the List of Essential Medicines in the Context of the Biopharmaceutics Classification System–Biowaiver. Vol. 107, *Journal of Pharmaceutical Sciences.* 2018. p. 1478–1488.
 419. Savjani KT, Gajjar AK, Savjani JK. Drug solubility: importance and enhancement techniques. *ISRN Pharm* [Internet]. 2012/07/05. 2012;2012:195727. Available from: <https://pubmed.ncbi.nlm.nih.gov/22830056>
 420. Raymond C Rowe PJS, Owen and SC. *Handbook of Pharmaceutical Excipients* [Internet]. Fifth. Rowe RC, editor. *AusIMM Bulletin.* London: Pharmaceutical Press; 2006. Available from: [https://gmpua.com/RD/RD/HandbookPharmaceutical Excipients.pdf](https://gmpua.com/RD/RD/HandbookPharmaceuticalExcipients.pdf)

421. Batchelor HK, Marriott JF. Formulations for children: problems and solutions. *Br J Clin Pharmacol* [Internet]. 2015 Mar;79(3):405–418. Available from: <https://pubmed.ncbi.nlm.nih.gov/25855822>
422. van der Merwe J, Steenekamp J, Steyn D, Hamman J. The role of functional excipients in solid oral dosage forms to overcome poor drug dissolution and bioavailability. Vol. 12, *Pharmaceutics*. 2020.
423. Manea AM, Ungureanu C, Meghea A. Effect of vegetable oils on obtaining lipid nanocarriers for sea buckthorn extract encapsulation. *Comptes Rendus Chim* [Internet]. 2014 Sep 1 [cited 2018 Apr 23];17(9):934–943. Available from: <https://www.sciencedirect.com/science/article/pii/S1631074813003585>
424. Rodriguez-Leyva D, Dupasquier CMC, McCullough R, Pierce GN. The cardiovascular effects of flaxseed and its omega-3 fatty acid, alpha-linolenic acid. *Can J Cardiol* [Internet]. 2010 Nov;26(9):489–496. Available from: <https://pubmed.ncbi.nlm.nih.gov/21076723>
425. Mazza G. Health benefits of phytochemicals from selected Canadian crops. *Trends Food Sci Technol* [Internet]. 1999 Jun 1 [cited 2019 May 14];10(6–7):193–198. Available from: <https://www.sciencedirect.com/science/article/pii/S0924224499000552>
426. Ander BP, Dupasquier CMC, Prociuk MA, Pierce GN. Polyunsaturated fatty acids and their effects on cardiovascular disease. *Exp Clin Cardiol*. 2003;8(4):164–172.
427. Whelan J, Fritsche K. Linoleic acid. *Adv Nutr* [Internet]. 2013 May 1;4(3):311–322. Available from: <https://pubmed.ncbi.nlm.nih.gov/23674797>
428. Orsavova J, Misurcova L, Ambrozova JV, Vicha R, Mlcek J. Fatty Acids Composition of Vegetable Oils and Its Contribution to Dietary Energy Intake and Dependence of Cardiovascular Mortality on Dietary Intake of Fatty Acids. *Int J Mol Sci* [Internet]. 2015 Jun 5;16(6):12871–12890. Available from: <https://pubmed.ncbi.nlm.nih.gov/26057750>
429. Oi LE, Choo M-Y, Lee HV, Rahman NA, Juan JC. Chapter 9 - Mesoporous and other types of catalysts for conversion of non-edible oil to biogasoline via deoxygenation. In: Rai M, Ingle APBT-SB, editors. Elsevier; 2019. p. 257–281. Available from: <http://www.sciencedirect.com/science/article/pii/B9780128176542000095>
430. Garavaglia J, Markoski MM, Oliveira A, Marcadenti A. Grape Seed Oil Compounds: Biological and Chemical Actions for Health. *Nutr Metab Insights* [Internet]. 2016 Aug 16;9:59–64. Available from: <https://pubmed.ncbi.nlm.nih.gov/27559299>
431. Bayrak A, Kiralan M, Ipek A, Arslan N, Cosge B, Khawar KM. Fatty acid compositions of linseed (*Linum Usitatissimum* L.) genotypes of different origin cultivated in Turkey. *Biotechnol Biotechnol Equip*. 2010;24(2):1836–1842.
432. Aquino-Bolaños EN, Mapel-Velazco L, Martín-del-Campo ST, Chávez-Servia JL, Martínez AJ, Verdalet-Guzmán I. Fatty acids profile of oil from nine varieties of *Macadamia nut*. *Int J Food Prop* [Internet]. 2017 Jun 3;20(6):1262–1269. Available from: <https://doi.org/10.1080/10942912.2016.1206125>
433. Clemente TE, Cahoon EB. Soybean oil: genetic approaches for modification of functionality and total content. *Plant Physiol* [Internet]. 2009/09/25. 2009 Nov;151(3):1030–1040. Available from: <https://pubmed.ncbi.nlm.nih.gov/19783644>
434. Boskou D, Blekas G, Tsimidou M. Olive Oil Composition. In: *Olive Oil: Chemistry and*

- Technology: Second Edition [Internet]. Second Edi. Urbana: AOCS Press; 2006. p. 41–72. Available from: <http://dx.doi.org/10.1016/B978-1-893997-88-2.50008-0>
435. List GR. Oilseed Composition and Modification for Health and Nutrition. *Funct Diet Lipids* [Internet]. 2016 Jan 1 [cited 2020 Mar 12];23–46. Available from: <https://www.sciencedirect.com/science/article/pii/B9781782422471000028>
 436. Raß M, Schein C, Matthäus B. Virgin sunflower oil. Vol. 110, *European Journal of Lipid Science and Technology*. 2008. p. 618–624.
 437. Bandyopadhyay S, Prakash O, Singh B. Optimized self nano-emulsifying systems of ezetimibe with enhanced bioavailability potential using long chain and medium chain triglycerides. *Colloids Surf B Biointerfaces*. 2012 May 24;100:50–61.
 438. Kamal-Eldin A. Minor Components of Fats and Oils [Internet]. *Bailey's Industrial Oil and Fat Products*. 2005. (Major Reference Works). Available from: <https://doi.org/10.1002/047167849X.bio012>
 439. Chen B. Minor components and their roles on lipid oxidation in bulk oil that contains association colloids [Internet]. ProQuest Dissertations and Theses. University of Massachusetts Amherst; 2012. Available from: <https://search.proquest.com/docview/1034279122?accountid=27575>
 440. Prieto C, Calvo L. Performance of the Biocompatible Surfactant Tween 80, for the Formation of Microemulsions Suitable for New Pharmaceutical Processing. Dinarvand R, editor. *J Appl Chem* [Internet]. 2013;2013:930356. Available from: <https://doi.org/10.1155/2013/930356>
 441. Taymouri S, Varshosaz J. Effect of different types of surfactants on the physical properties and stability of carvedilol nano-niosomes. *Adv Biomed Res* [Internet]. 2016 Mar 16;5:48. Available from: <https://pubmed.ncbi.nlm.nih.gov/27110545>
 442. Juárez-Osornio C, Gracia-Fadrique J. Structures similar to lipid emulsions and liposomes. Dipalmitoylphosphatidylcholine, cholesterol, Tween 20–Span 20 or Tween 80–Span 80 in aqueous media. *J Liposome Res* [Internet]. 2017 Apr 3;27(2):139–150. Available from: <https://doi.org/10.1080/08982104.2016.1174944>
 443. Valeur KS, Hertel SA, Lundstrøm KE, Holst H. The Cumulative Daily Tolerance Levels of Potentially Toxic Excipients Ethanol and Propylene Glycol Are Commonly Exceeded in Neonates and Infants. *Basic Clin Pharmacol Toxicol*. 2018;122(5):523–530.
 444. Maher S, Ryan B, Duffy A, Brayden DJ. Formulation strategies to improve oral peptide delivery. *Pharm Pat Anal*. 2014;3(3):313–336.
 445. Syed HK, Peh KK. Identification of phases of various oil, surfactant/co-surfactants and water system by ternary phase diagram. *Acta Pol Pharm - Drug Res*. 2014;71(2):301–309.
 446. Cartón A, González G, Torre AID La, Cabezas JL. Separation of ethanol-water mixtures using 3A molecular sieve. *J Chem Technol Biotechnol*. 1987;39(2):125–32.
 447. Banat F, Al-lagtah N, Al-sheh S. Separation of ethanol–water mixtures using molecular sieves and biobased adsorbents. *Chem Eng Res Des*. 2004;82(A7):855–864.
 448. Colucci G, Santamaria-Echart A, Silva SC, Fernandes IPM, Sipoli CC, Barreiro MF. Development of water-in-oil emulsions as delivery vehicles and testing with a natural

- antimicrobial extract. *Molecules*. 2020;25(9):5–7.
449. Coates J. *Encyclopedia of Analytical Chemistry -Interpretation of Infrared Spectra, A Practical Approach*. *Encycl Anal Chem* [Internet]. 2004;1–23. Available from: <http://www3.uma.pt/jrodrigues/disciplinas/QINO-II/Teorica/IR.pdf>
 450. Ertl P. An algorithm to identify functional groups in organic molecules. *J Cheminform* [Internet]. 2017 Jun 7;9(1):36. Available from: <https://pubmed.ncbi.nlm.nih.gov/29086048>
 451. Lu Y-Y, Dai W-B, Wang X, Wang X-W, Liu J-Y, Li P, et al. Effects of crystalline state and self-nanoemulsifying drug delivery system (SNEDDS) on oral bioavailability of the novel anti-HIV compound 6-benzyl-1-benzoyloxymethyl-5-iodouracil in rats. *Drug Dev Ind Pharm*. 2018 Feb;44(2):329–337.
 452. Bunjes H, Unruh T. Characterization of lipid nanoparticles by differential scanning calorimetry, X-ray and neutron scattering. *Adv Drug Deliv Rev*. 2007 Jul;59(6):379–402.
 453. Igwebike-Ossi CD. *X-Ray Techniques*. Intech [Internet]. 2017; Available from: <https://www.intechopen.com/books/advanced-biometric-technologies/liveness-detection-in-biometrics>
 454. Kim H, Kosuda KM, Van Duyne RP, Stair PC. Resonance Raman and surface- and tip-enhanced Raman spectroscopy methods to study solid catalysts and heterogeneous catalytic reactions. *Chem Soc Rev* [Internet]. 2010;39(12):4820–4844. Available from: <http://dx.doi.org/10.1039/C0CS00044B>
 455. Jones RR, Hooper DC, Zhang L, Wolverson D, Valev VK. Raman Techniques: Fundamentals and Frontiers. *Nanoscale Res Lett* [Internet]. 2019 Jul 12;14(1):231. Available from: <https://pubmed.ncbi.nlm.nih.gov/31300945>
 456. Mitsutake H, Poppi RJ, Breitreitz MC. Raman imaging spectroscopy: history, fundamentals and current of the technique. *J Braz Chem Soc*. 2019;30(11):2243–2258.
 457. Hu R, He T, Zhang Z, Yang Y, Liu M. Safety analysis of edible oil products via Raman spectroscopy. *Talanta* [Internet]. 2019;191:324–332. Available from: <http://www.sciencedirect.com/science/article/pii/S0039914018308853>
 458. Carmona MA, Lafont F, Jiménez-Sanchidrián C, Ruiz JR. Raman spectroscopy study of edible oils and determination of the oxidative stability at frying temperatures. *Eur J Lipid Sci Technol*. 2014;116(11):1451–6.
 459. Wartewig S, Neubert RHH. Pharmaceutical applications of Mid-IR and Raman spectroscopy. *Adv Drug Deliv Rev*. 2005 Jun;57(8):1144–1170.
 460. Chudasama AS, Patel V V, Nivsarkar M, Vasu KK, Shishoo CJ. In vivo Evaluation of Self Emulsifying Drug Delivery System for Oral Delivery of Nevirapine. *Indian J Pharm Sci* [Internet]. 2014 May;76(3):218–224. Available from: <https://pubmed.ncbi.nlm.nih.gov/25035533>
 461. Szumała P. Structure of Microemulsion Formulated with Monoacylglycerols in the Presence of Polyols and Ethanol. *J Surfactants Deterg*. 2015;18(1):97–106.
 462. Reddy NP, Padmavathi Y, Mounika P, Anjali A. FTIR spectroscopy for estimation of efavirenz in raw material and tablet dosage form. *Int Curr Pharm J*. 2015;4(6):390–395.

463. Marques MM, Rezende CA, Lima GC, Marques ACS, Prado LD, Leal KZ, et al. New solid forms of efavirenz: Synthesis, vibrational spectroscopy and quantum chemical calculations. *J Mol Struct* [Internet]. 2017 Jun 5 [cited 2019 Nov 14];1137:476–484. Available from: <https://www.sciencedirect.com/science/article/pii/S002228601730220X>
464. De Gomes ECL, Mussel WN, Resende JM, Fialho SL, Barbosa J, Yoshida MI. Chemical interactions study of antiretroviral drugs efavirenz and lamivudine concerning the development of stable fixed-dose combination formulations for AIDS treatment. *J Braz Chem Soc*. 2013;24(4):573–579.
465. Liang P, Wang H, Chen C, Ge F, Liu D, Li S, et al. The Use of Fourier Transform Infrared Spectroscopy for Quantification of Adulteration in Virgin Walnut Oil. Culea E, editor. *J Spectrosc* [Internet]. 2013;2013:305604. Available from: <https://doi.org/10.1155/2013/305604>
466. Rohman A, Man YBC. Fourier transform infrared (FTIR) spectroscopy for analysis of extra virgin olive oil adulterated with palm oil. *Food Res Int* [Internet]. 2010;43(3):886–892. Available from: <http://dx.doi.org/10.1016/j.foodres.2009.12.006>
467. Vlachos N, Skopelitis Y, Psaroudaki M, Konstantinidou V, Chatzilazarou A, Tegou E. Applications of Fourier transform-infrared spectroscopy to edible oils. *Anal Chim Acta*. 2006;573–574:459–465.
468. Balan V, Mihai C-T, Cojocaru F-D, Uritu C-M, Dodi G, Botezat D, et al. Vibrational Spectroscopy Fingerprinting in Medicine: from Molecular to Clinical Practice. *Mater (Basel, Switzerland)* [Internet]. 2019 Sep 6;12(18):2884. Available from: <https://pubmed.ncbi.nlm.nih.gov/31489927>
469. Ur Rehman M, Rasul A, Khan MI, Hanif M, Aamir MN, Waqas MK, et al. Development of niosomal formulations loaded with cyclosporine a and evaluation of its compatibility. *Trop J Pharm Res*. 2018;17(8):1457–1464.
470. Mishra S, Tandon P, Ayala AP. Study on the structure and vibrational spectra of efavirenz conformers using DFT: Comparison to experimental data. *Spectrochim Acta - Part A Mol Biomol Spectrosc* [Internet]. 2012 Mar 1 [cited 2019 Nov 28];88:116–123. Available from: <https://www.sciencedirect.com/science/article/pii/S1386142511010791?via%3Dihub>
471. Wardhana YW, Hardian A, Chaerunisa AY, Suendo V, Soewandhi SN. Kinetic estimation of solid state transition during isothermal and grinding processes among efavirenz polymorphs. *Heliyon* [Internet]. 2020;6(5):e03876. Available from: <http://www.sciencedirect.com/science/article/pii/S2405844020307210>
472. Ramkumaar GR, Bhoopathy TJ, Gunasekaran S, Gokilan C, Srinivasan S, Charles J. Experimental and theoretical investigation and NBO analysis on the structure of efavirenz HIV drug. *Int J ChemTech Res*. 2013;5(5):2563–2574.
473. Dongye G, Zhou Q, Sun S, Hu G, Wang Q, Hu X. The analysis of linseed oil by FTIR and FT-Raman. *Guang Pu Xue Yu Guang Pu Fen Xi*. 2000 Dec;20(6):836–837.
474. Gorain B, Choudhury H, Pandey M, Madheswaran T, Kesharwani P, Tekade RK. and Incompatibilities [Internet]. *Dosage Form Design Parameters*. Elsevier Inc.; 2018. 363–402 p. Available from: <http://dx.doi.org/10.1016/B978-0-12-814421-3.00011-7>

475. Sathigari SK. Amorphous-State Characterization of Efavirenz—Polymer Hot-Melt Extrusion Systems for Dissolution Enhancement. *J Pharm Sci.* 2012;
476. Verma U, Mujumdar A, Naik J. Preparation of Efavirenz resinate by spray drying using response surface methodology and its physicochemical characterization for taste masking. *Dry Technol* [Internet]. 2020;38(5–6):793–805. Available from: <https://doi.org/10.1080/07373937.2019.1590845>
477. Dash RN, Mohammed H, Humaira T. Design, optimization, and evaluation of ezetimibe solid supersaturatable self-nanoemulsifying drug delivery for enhanced solubility and dissolution. *J Pharm Investig.* 2016;46(2):153–168.
478. Janssens S, Van den Mooter G. Review: physical chemistry of solid dispersions. *J Pharm Pharmacol.* 2009 Dec;61(12):1571–1586.
479. Rahman MA, Hussain A, Hussain MS, Mirza MA, Iqbal Z. Role of excipients in successful development of self-emulsifying/microemulsifying drug delivery system (SEDDS/SMEDDS). *Drug Dev Ind Pharm.* 2013 Jan;39(1):1–19.
480. Namjoshi S, Dabbaghi M, Roberts MS, Grice JE, Mohammed Y. Quality by design: Development of the quality target product profile (QTPP) for semisolid topical products. *Pharmaceutics.* 2020;12(3).
481. Pramod K, Tahir MA, Charoo NA, Ansari SH, Ali J. Pharmaceutical product development: A quality by design approach. *Int J Pharm Investig* [Internet]. 2016;6(3):129–138. Available from: <https://pubmed.ncbi.nlm.nih.gov/27606256>
482. Sangshetti JN, Deshpande M, Zaheer Z, Shinde DB, Arote R. Quality by design approach: Regulatory need. *Arab J Chem* [Internet]. 2017;10:S3412–425. Available from: <http://www.sciencedirect.com/science/article/pii/S1878535214000288>
483. Chakraborty S, Shukla D, Mishra B, Singh S. Lipid--an emerging platform for oral delivery of drugs with poor bioavailability. *Eur J Pharm Biopharm Off J Arbeitsgemeinschaft fur Pharm Verfahrenstechnik eV.* 2009 Sep;73(1):1–15.
484. Thakare P, Mogal V, Borase P, Dusane J, Kshirsagar S. A review on self-emulsified drug delivery system self-emulsifying. *Pharm Biol Eval.* 2016;3(2):140–153.
485. Khan AA, Mudassir J, Mohtar N, Darwis Y. Advanced drug delivery to the lymphatic system: Lipid-based nanoformulations. *Int J Nanomedicine.* 2013;8:2733–2744.
486. Lu GW, Gao P. Emulsions and Microemulsions for Topical and Transdermal Drug Delivery. In: *Handbook of Non-Invasive Drug Delivery Systems* [Internet]. William Andrew Publishing; 2010 [cited 2019 Apr 25]. p. 59–94. Available from: <https://www.sciencedirect.com/science/article/pii/B9780815520252100034>
487. Kong WY, Salim N, Masoumi HRF, Basri M, da Costa SS, Ahmad N. Optimization of hydrocortisone-loaded nanoemulsion formulation using D-optimal mixture design. *Asian J Chem.* 2018;30(4):853–858.
488. N. Politis S, Colombo P, Colombo G, M. Rekkas D. Design of experiments (DoE) in pharmaceutical development. *Drug Dev Ind Pharm* [Internet]. 2017 Jun 3;43(6):889–901. Available from: <https://doi.org/10.1080/03639045.2017.1291672>
489. Singh B, Kapil R, Nandi M, Ahuja N. Developing oral drug delivery systems using formulation by design: Vital precepts, retrospect and prospects. *Expert Opin Drug Deliv.*

- 2011;8(10):1341–1360.
490. Darroch JN, Waller J. Additivity and interaction in three-component experiments with mixtures. *Biometrika*. 1985;72(1):153–163.
 491. Dal Bello LHA, de Castro Vieira AF. Tutorial for mixture-process experiments with an industrial application. *Pesqui Operacional*. 2011;31(3):543–564.
 492. Collins LM, Dziak JJ, Li R. Design of experiments with multiple independent variables: a resource management perspective on complete and reduced factorial designs. *Psychol Methods* [Internet]. 2009 Sep;14(3):202–224. Available from: <https://pubmed.ncbi.nlm.nih.gov/19719358>
 493. Wang P-S, Fang J-J. The Optimization of Medicine Formulation Using Mixture Experiments. In. Available from: <https://www.semanticscholar.org/paper/The-Optimization-of-Medicine-Formulation-Using-Wang-Fang/f3decc321f28e0327d765d9b7562831d292cf5c4?p2df>
 494. Ferryanto L. Designing and analyzing experiments with mixtures [Internet]. [cited 2020 Nov 4]. Available from: <https://www.isixsigma.com/tools-templates/design-of-experiments-doe/designing-and-analyzing-experiments-mixtures/>
 495. Jeirani Z, Mohamed Jan B, Si Ali B, Mohd. Noor I, Chun Hwa S, Saphanuchart W. The optimal mixture design of experiments: Alternative method in optimizing the aqueous phase composition of a microemulsion. *Chemom Intell Lab Syst* [Internet]. 2012;112:1–7. Available from: <http://dx.doi.org/10.1016/j.chemolab.2011.10.008>
 496. Gorman JW, Hinman JE. Simplex Lattice Designs for Multicomponent Systems. *Technometrics*. 1962;4(4):463–487.
 497. Muta T, Parikh A, Kathawala K, Haidari H, Song Y, Thomas J, et al. Quality-by-design approach for the development of nano-sized tea tree oil formulation-impregnated biocompatible gel with antimicrobial properties. *Pharmaceutics*. 2020;12(11):1–16.
 498. Fan X, Zheng W, Singh DJ. Light scattering and surface plasmons on small spherical particles. Vol. 3, *Light: Science and Applications*. 2014. p. 1–14.
 499. Iqbala N, , Carla Vitorino*, b, c KMG. How lipid nanocarriers improve transdermal delivery of olanzapine Nimra Iqbal [Internet]. 2019 [cited 2020 Dec 16]. p. 1–21. Available from: <https://core.ac.uk/download/pdf/79515929.pdf>
 500. Sze A, Erickson D, Ren L, Li D. Zeta-potential measurement using the Smoluchowski equation and the slope of the current-time relationship in electroosmotic flow. *J Colloid Interface Sci*. 2003;261(2):402–410.
 501. Kamble RN, Mehta PP, Kumar A. Efavirenz Self-Nano-Emulsifying Drug Delivery System: In Vitro and In Vivo Evaluation. *AAPS PharmSciTech* [Internet]. 2016;17(5):1240–1247. Available from: <http://link.springer.com/10.1208/s12249-015-0446-2>
 502. Jaydip B, Dhaval M, Soniwala MM, Chavda J. Formulation and optimization of liquisolid compact for enhancing dissolution properties of efavirenz by using DoE approach. *Saudi Pharm J* [Internet]. 2020;28(6):737–745. Available from: <http://www.sciencedirect.com/science/article/pii/S131901642030102X>
 503. Gaur PK, Mishra S, Bajpai M, Mishra A. Enhanced oral bioavailability of Efavirenz by

- solid lipid nanoparticles: In vitro drug release and pharmacokinetics studies. *Biomed Res Int.* 2014;2014.
504. Madhavi BB, Kusum B, Chatanya CK, Madhu MN, Harsha VS, Banji D. Dissolution enhancement of efavirenz by solid dispersion and PEGylation techniques. *Int J Pharm Investig* [Internet]. 2011 Jan;1(1):29–34. Available from: <https://pubmed.ncbi.nlm.nih.gov/23071917>
 505. Honório T da S, Pinto EC, Rocha HVA, Esteves VSD, dos Santos TC, Castro HCR, et al. In vitro-in vivo correlation of efavirenz tablets using GastroPlus®. *AAPS PharmSciTech* [Internet]. 2013/08/14. 2013 Sep;14(3):1244–1254. Available from: <https://pubmed.ncbi.nlm.nih.gov/23943401>
 506. Rozana R, Yulizar Y, Saefumillah A, Apriandanu DOB. Synthesis, characterization and in vitro release study of efavirenz-loaded chitosan nanoparticle. *AIP Conf Proc.* 2020;2242(June).
 507. Kumar Sahoo S, Sankar Dash G, Biswal S, Kumar Biswal P, Chandra Senapati P. Fabrication and evaluation of self-nanoemulsifying oil formulations (SNEOFs) of Efavirenz. *J Dispers Sci Technol* [Internet]. 2019 Mar 4;40(3):464–475. Available from: <https://doi.org/10.1080/01932691.2018.1472008>
 508. Gurumukhi VC, Bari SB. Fabrication of efavirenz loaded nano-formulation using quality by design (QbD) based approach: Exploring characterizations and in vivo safety. *J Drug Deliv Sci Technol* [Internet]. 2020;56:101545. Available from: <http://www.sciencedirect.com/science/article/pii/S1773224719314005>
 509. Lavra ZMM, Pereira de Santana D, Ré MI. Solubility and dissolution performances of spray-dried solid dispersion of Efavirenz in Soluplus. *Drug Dev Ind Pharm* [Internet]. 2017 Jan 2;43(1):42–54. Available from: <https://doi.org/10.1080/03639045.2016.1205598>
 510. (CDER) C for DE and R. FDA guidance for industry 1 dissolution testing of immediate release solid oral dosage forms [Internet]. *Dissolution Technologies.* 1997 [cited 2020 Dec 16]. p. 1–17. Available from: <https://www.fda.gov/media/70936/download>
 511. Flanner JWM and HH. Mathematical comparison of curves with an emphasis on in vitro dissolution profiles. *Pharm Technol.* 1996;20:64–74.
 512. Shah VP, Tsong Y, Sathe P, Liu J-P. In Vitro Dissolution Profile Comparison—Statistics and Analysis of the Similarity Factor, f_2 . *Pharm Res* [Internet]. 1998;15(6):889–896. Available from: <https://doi.org/10.1023/A:1011976615750>
 513. Jianxian C, Saleem K, Ijaz M, Ur-Rehman M, Murtaza G, Asim MH. Development and in vitro Evaluation of Gastro-protective Aceclofenac-loaded Self-emulsifying Drug Delivery System. *Int J Nanomedicine* [Internet]. 2020 Jul 23;15:5217–5226. Available from: <https://pubmed.ncbi.nlm.nih.gov/32801687>
 514. Khatri P, Shao J. Separation of external aqueous phase from o/w nanoemulsions. *Eur J Pharm Sci Off J Eur Fed Pharm Sci.* 2017 Jan;96:171–175.
 515. Jumaryatno P, Chabib L, Hayati F, Awaluddin R. Stability study of Ipomoea reptans extract self-nanoemulsifying drug delivery system (SNEDDS) as anti-diabetic therapy. *J Appl Pharm Sci.* 2018;8(9):11–14.
 516. Borhan FP, Abd Gani SS, Shamsuddin R. The use of D-optimal mixture design in

- optimising okara soap formulation for stratum corneum application. *Sci World J.* 2014 Dec 8;2014.
517. Nyberg J. Practical Optimal Experimental Design in Drug Development and treatment using Non Linear mixed effects models [Internet]. UPPSALA; 2011. Available from: <http://www.diva-portal.org/smash/get/diva2:451173/FULLTEXT01.pdf>
 518. Pregartner G. Design-of-Experiment Statistical Modeling of Large Scale Lithium Ion Cells. Graz University of Technology; 2012.
 519. Varshosaz J, Ghaffari S, Khoshayand MR, Atyabi F, Azarmi S, Kobarfard F. Development and optimization of solid lipid nanoparticles of amikacin by central composite design. *J Liposome Res.* 2010 Jun;20(2):97–104.
 520. Martin J, de Adana DDR, Asuero AG. Fitting Models to Data: Residual Analysis, a Primer. In: Hessling JP, editor. Uncertainty Quantification and Model Calibration [Internet]. Rijeka: IntechOpen; 2017. Available from: <https://doi.org/10.5772/68049>
 521. Lawson J. Design and Analysis of Experiments with R [Internet]. Boca Raton: Taylor & Francis Group; 2015. Available from: <http://library1.nida.ac.th/termpaper6/sd/2554/19755.pdf>
 522. University TPS. Applied Regression Analysis [Internet]. 2018 [cited 2020 Dec 23]. Available from: <https://online.stat.psu.edu/stat462/node/117/>
 523. Hill WJ, Hunter WG. A Review of Response Surface Methodology: A Literature Survey. *Technometrics* [Internet]. 1966 Nov 1;8(4):571–590. Available from: <https://www.tandfonline.com/doi/abs/10.1080/00401706.1966.10490404>
 524. Noordin MY, Venkatesh VC, Sharif S, Elting S, Abdullah A. Application of response surface methodology in describing the performance of coated carbide tools when turning AISI 1045 steel. *J Mater Process Technol.* 2004;145(1):46–58.
 525. Montgomery DC. Design and Analysis of Experiments. 8th ed. Catalysis from A to Z. Massachusetts: John Wiley & Sons, Inc; 2013.
 526. Gurpreet K, Singh SK. Review of nanoemulsion formulation and characterization techniques. *Indian J Pharm Sci.* 2018;80(5):781–789.
 527. Koroleva M, Nagovitsina T, Yurtov E. Nanoemulsions stabilized by non-ionic surfactants: Stability and degradation mechanisms. *Phys Chem Chem Phys.* 2018;20(15):10369–10377.
 528. Tojo C, de Dios M, Barroso F. Surfactant effects on microemulsion-based nanoparticle synthesis. *Materials (Basel).* 2010;4(1):55–72.
 529. Samimi S, Maghsoudnia N, Eftekhari RB, Dorkoosh F. Chapter 3 - Lipid-Based Nanoparticles for Drug Delivery Systems. In: Mohapatra SS, Ranjan S, Dasgupta N, Mishra RK, Thomas SBT-C and B of N for DD, editors. *Micro and Nano Technologies* [Internet]. Elsevier; 2019. p. 47–76. Available from: <http://www.sciencedirect.com/science/article/pii/B9780128140314000039>
 530. Kelly C, Jefferies C, Cryan S-A. Targeted Liposomal Drug Delivery to Monocytes and Macrophages. *J Drug Deliv.* 2011;2011:1–11.
 531. Berger E, Breznan D, Stals S, Jasinghe VJ, Gonçalves D, Girard D, et al. Cytotoxicity

- assessment, inflammatory properties, and cellular uptake of Neutraplex lipid-based nanoparticles in THP-1 monocyte-derived macrophages. *Nanobiomedicine*. 2017 Dec 20;4:1–14.
532. Marban C, Forouzanfar F, Ait-Ammar A, Fahmi F, El Mekdad H, Daouad F, et al. Targeting the brain reservoirs: Toward an HIV cure. *Front Immunol*. 2016;7(SEP):1–13.
533. Pokharkar V, Patil-Gadhe A, Palla P. Efavirenz loaded nanostructured lipid carrier engineered for brain targeting through intranasal route: In-vivo pharmacokinetic and toxicity study. *Biomed Pharmacother* [Internet]. 2017 Oct 1 [cited 2018 Apr 25];94:150–164. Available from: <https://www.sciencedirect.com/science/article/pii/S0753332217313173>
534. Dai W-G. In vitro methods to assess drug precipitation. *Int J Pharm* [Internet]. 2010;393(1):1–16. Available from: <http://www.sciencedirect.com/science/article/pii/S0378517310002140>
535. Gao P, Shi Y. Characterization of supersaturatable formulations for improved absorption of poorly soluble Drugs. *AAPS J*. 2012;14(4):703–713.
536. Fandaruff C, Araya-Sibaja AM, Pereira RN, Cuffini SL, de Campos CEM, Hoffmeister CRD, et al. Interaction and compatibility studies of efavirenz with pharmaceutical excipients. *J Excipients Food Chem*. 2014;5(3):152–160.
537. da Costa MA, Seiceira RC, Rodrigues CR, Hoffmeister CRD, Cabral LM, Rocha HVA. Efavirenz dissolution enhancement I: Co-micronization. *Pharmaceutics*. 2013;5(1):1–22.

APPENDIX 1

ANOVA, diagnostic and response surface plots for responses monitored following use of CCD experimental design for optimization.

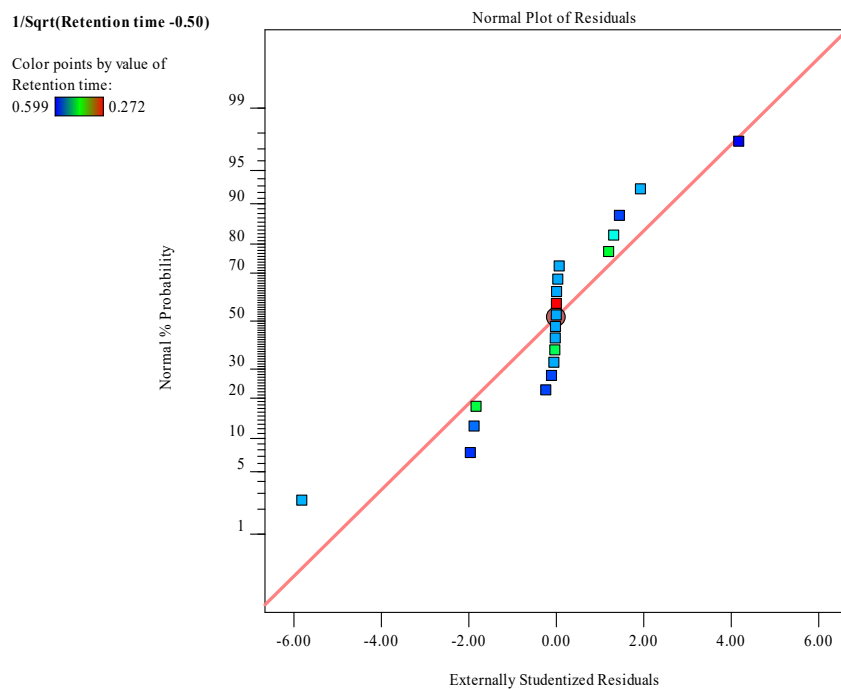


Figure 7.48. Diagnostic Normal plot of residuals for the inverse transformed quadratic model for retention time.

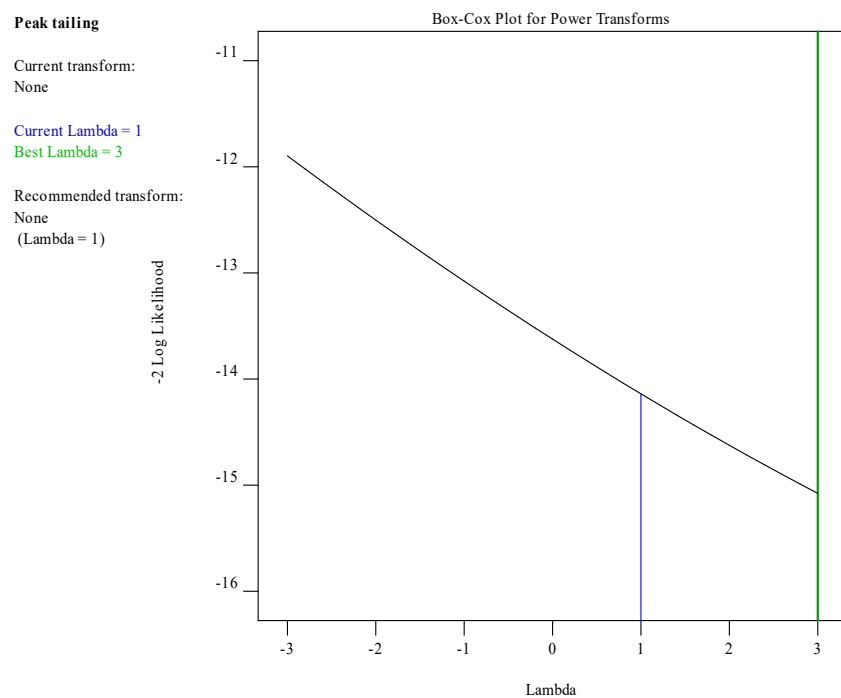


Figure 7.49. Diagnostic Box-Cox plot for peak tailing mean model.

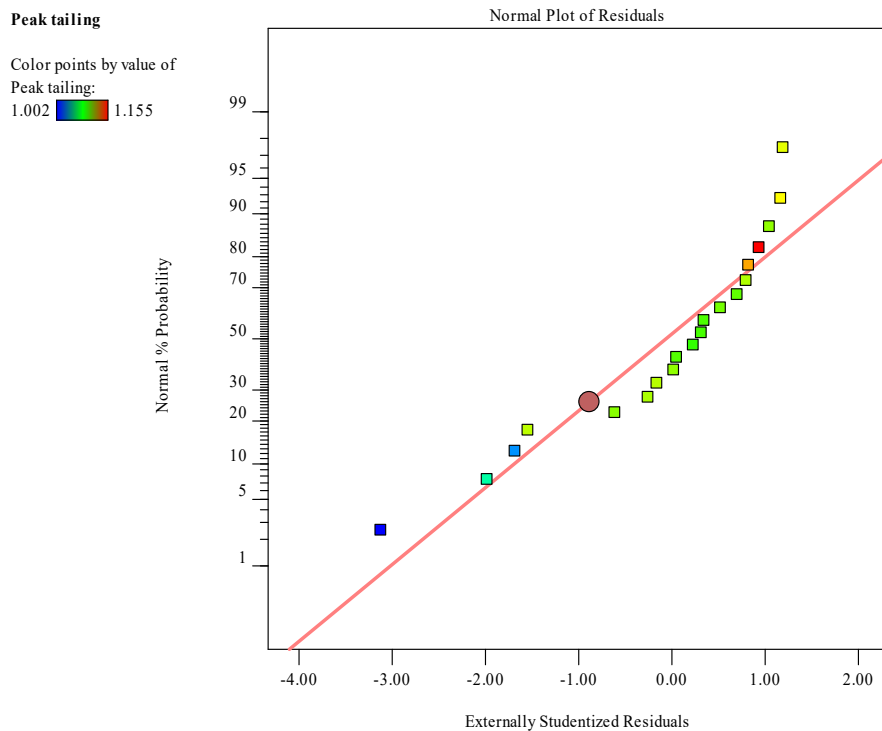


Figure 7.50. Diagnostic normal plot of residuals for peak tailing mean model.

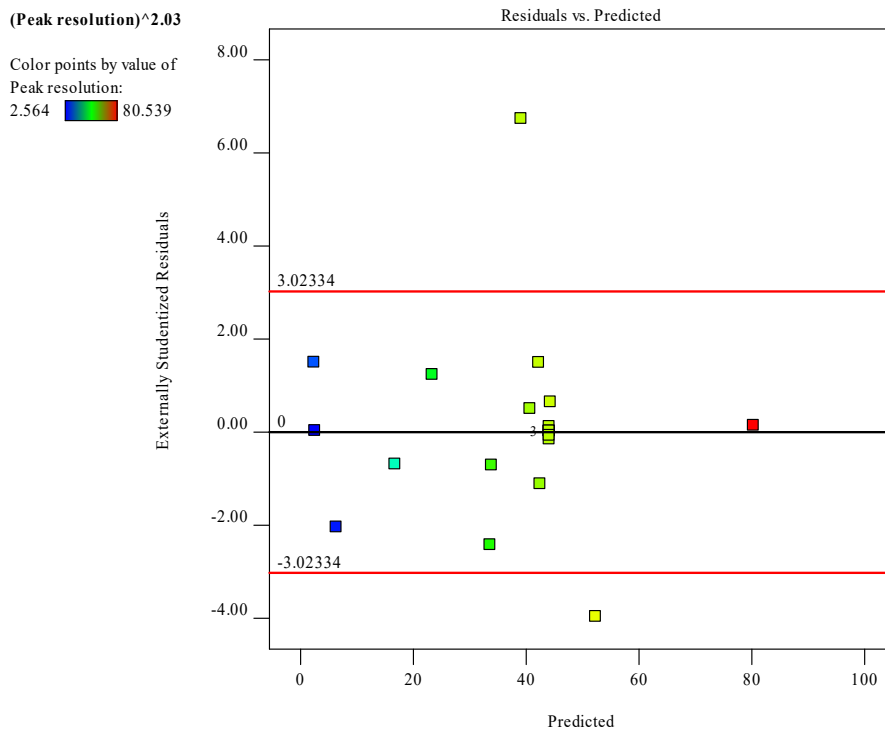


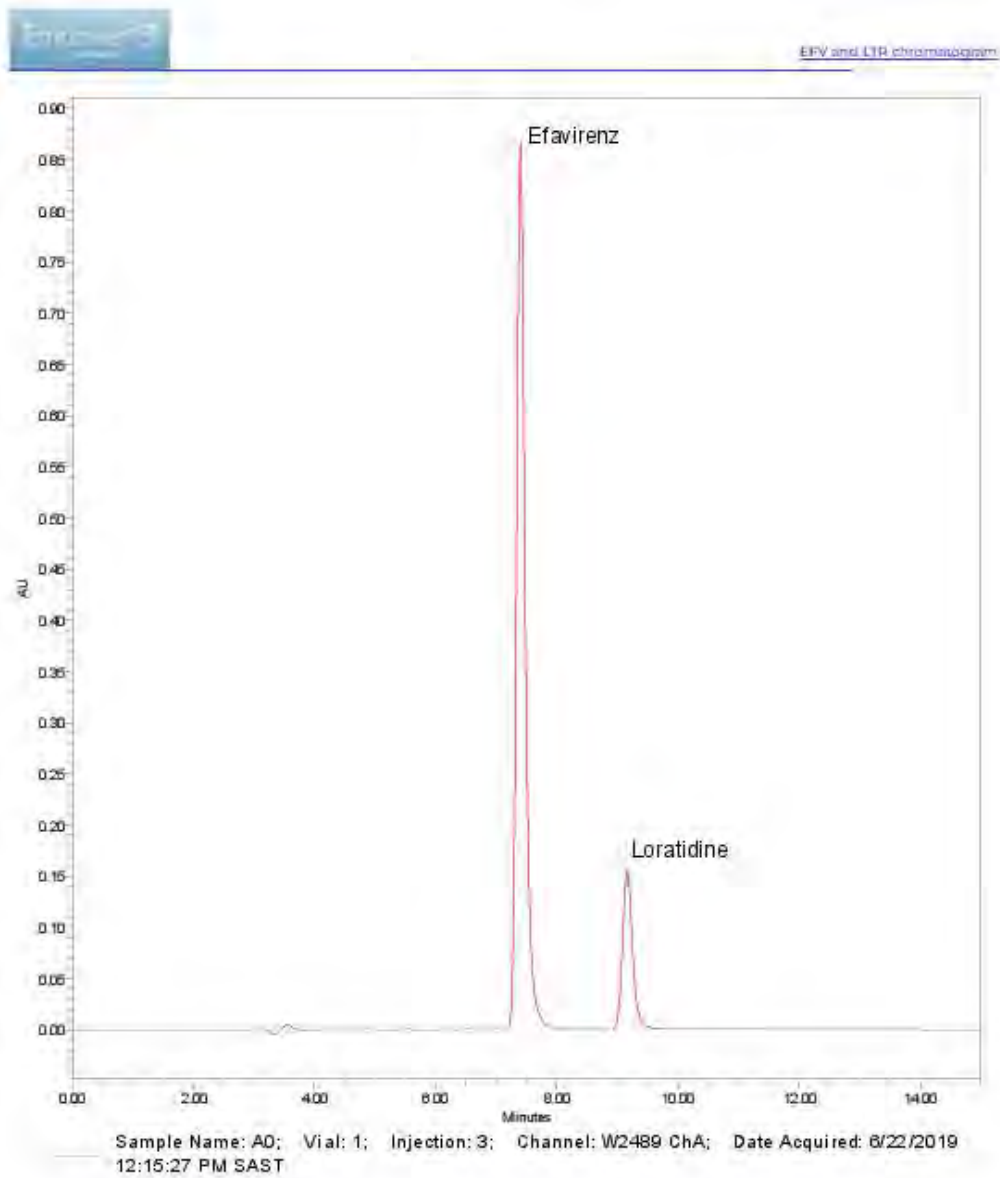
Figure 7.51. Diagnostic plot of residual versus predicted and externally studentized residuals for the transformed quadratic model for peak resolution.

Table 7.10. Solutions produced by CCD optimization criteria in section 3.5.2 to produce the selected conditions solution 3.

Number	ACN	Column temperature	pH of buffer	Retention time	Peak tailing	Peak resolution	Desirability	
1	85.412	40.000	4.483	4.769	1.093	7.890	0.691	
2	85.154	49.999	4.476	4.769	1.093	7.888	0.691	
3	80.187	40.998	4.471	4.874	1.093	7.888	0.691	Selected
4	72.040	50.000	5.499	5.769	1.093	7.892	0.691	
5	71.966	49.999	5.456	5.769	1.093	7.886	0.691	
6	72.076	50.000	5.519	5.769	1.093	7.894	0.691	
7	72.163	50.000	5.569	5.769	1.093	7.899	0.691	
8	71.793	49.993	5.357	5.769	1.093	7.869	0.691	
9	72.214	50.000	5.580	5.763	1.093	7.897	0.691	
10	72.291	50.000	5.623	5.763	1.093	7.900	0.690	
11	71.595	50.000	5.243	5.769	1.093	7.845	0.690	
12	72.642	50.000	5.842	5.769	1.094	7.910	0.688	
13	71.196	49.999	5.013	5.769	1.093	7.779	0.686	
14	73.161	50.000	5.671	5.624	1.092	7.815	0.682	
15	73.258	49.999	5.863	5.666	1.094	7.843	0.682	
16	70.888	49.994	4.834	5.769	1.093	7.711	0.681	
17	73.561	49.999	5.941	5.639	1.094	7.819	0.678	
18	73.927	50.000	5.962	5.584	1.093	7.777	0.674	
19	74.045	49.999	6.000	5.576	1.093	7.767	0.673	
20	75.033	49.997	6.000	5.421	1.092	7.643	0.661	
21	72.867	25.000	5.628	5.769	1.085	6.221	0.607	

Table 7.11. Table of results obtained for producing the calibration curve using the optimized HPLC conditions.

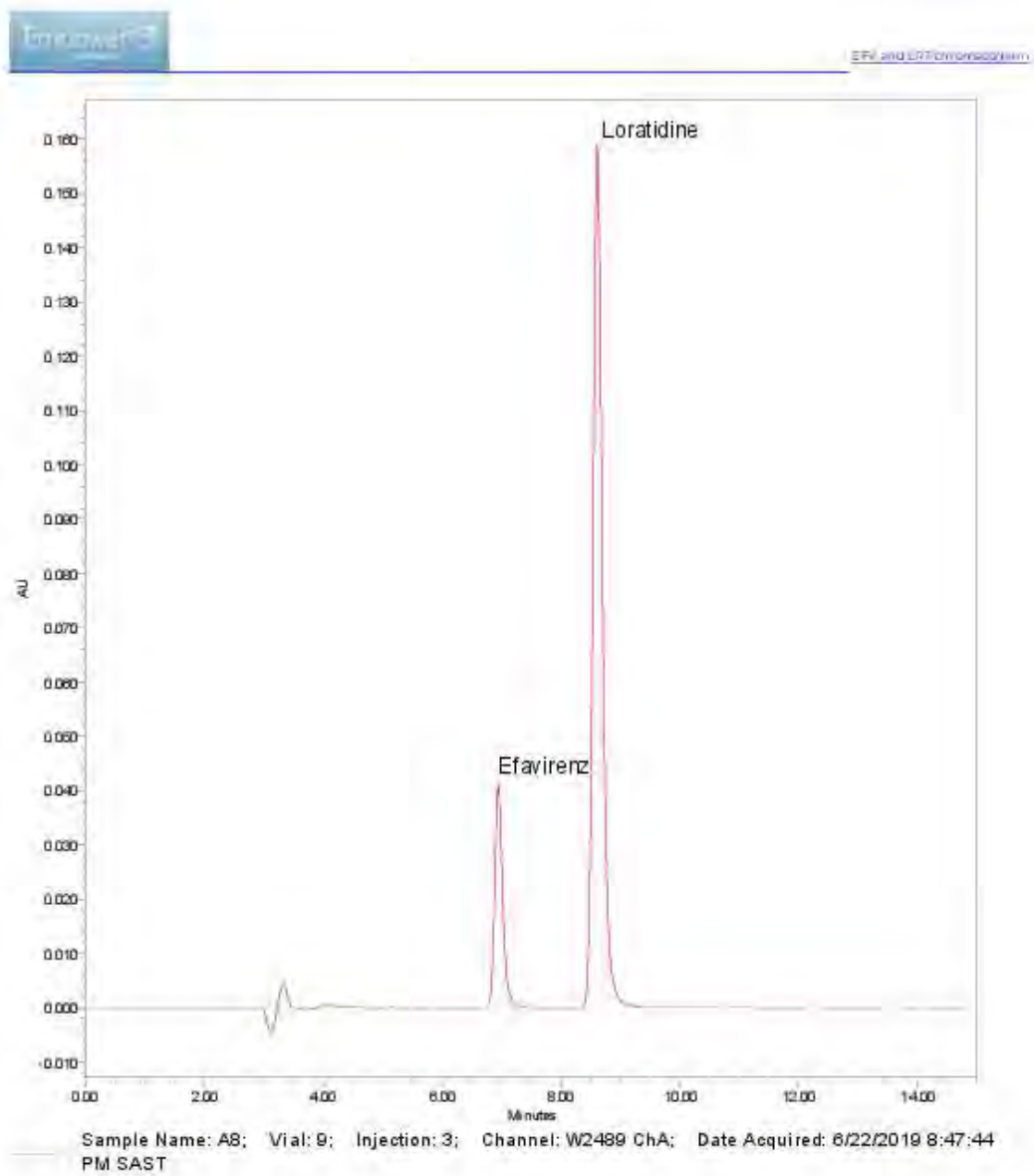
Sample conc µg/ml	sample #	Peak area EFV	Peak area LRT	Peak area ratio (EFV/LRT)	Mean peak area ratio	SD	% RSD
17.5	1	381062	1738290	0,21921656	0,219205471	0,000254	0,11606
	2	382305	1742068	0,21945469			
	3	382977	1749183	0,21894621			
35	1	793942	1758078	0,45159657	0,451204901	0,000342	0,07577
	2	788173	1747451	0,45104154			
	3	784734	1740090	0,45097322			
70	1	1571105	1746095	0,89978208	0,899393541	0,000762	0,084729
	2	1570239	1744932	0,89988549			
	3	1575270	1753189	0,89851693			
105	1	2312929	1742792	1,32714001	1,326738571	0,000564	0,042515
	2	2313089	1743118	1,32698360			
	3	2319006	1748749	1,32609425			
140	1	3460761	1741541	1,98718319	1,987976355	0,000903	0,045442
	2	3488900	1754134	1,98895865			
	3	3477603	1749490	1,98778101			
175	1	4823622	1728132	2,79123469	2,798837231	0,009675	0,345782
	2	4943656	1762496	2,80491757			
	3	4874296	1740678	2,80022841			
227.5	1	5759447	1781114	3,23362064	3,236496572	0,000672	0,020785
	2	5686648	1758084	3,23457127			
	3	5660919	1746460	3,24136768			
280	1	6488366	1762217	3,68193361	3,682111508	0,002909	0,078959
	2	6483890	1759036	3,68604735			
	3	6459178	1756000	3,67834738			



Reported by User: BRG_Analyst2 (BRG_Analyst2)
Report Method: Untitled
Report Method IC110
Page: 1 of 1

Project Name: BRG\Privilege
Date Printed: 8/2/2021
10:19:11 AM Africa/Johannesburg

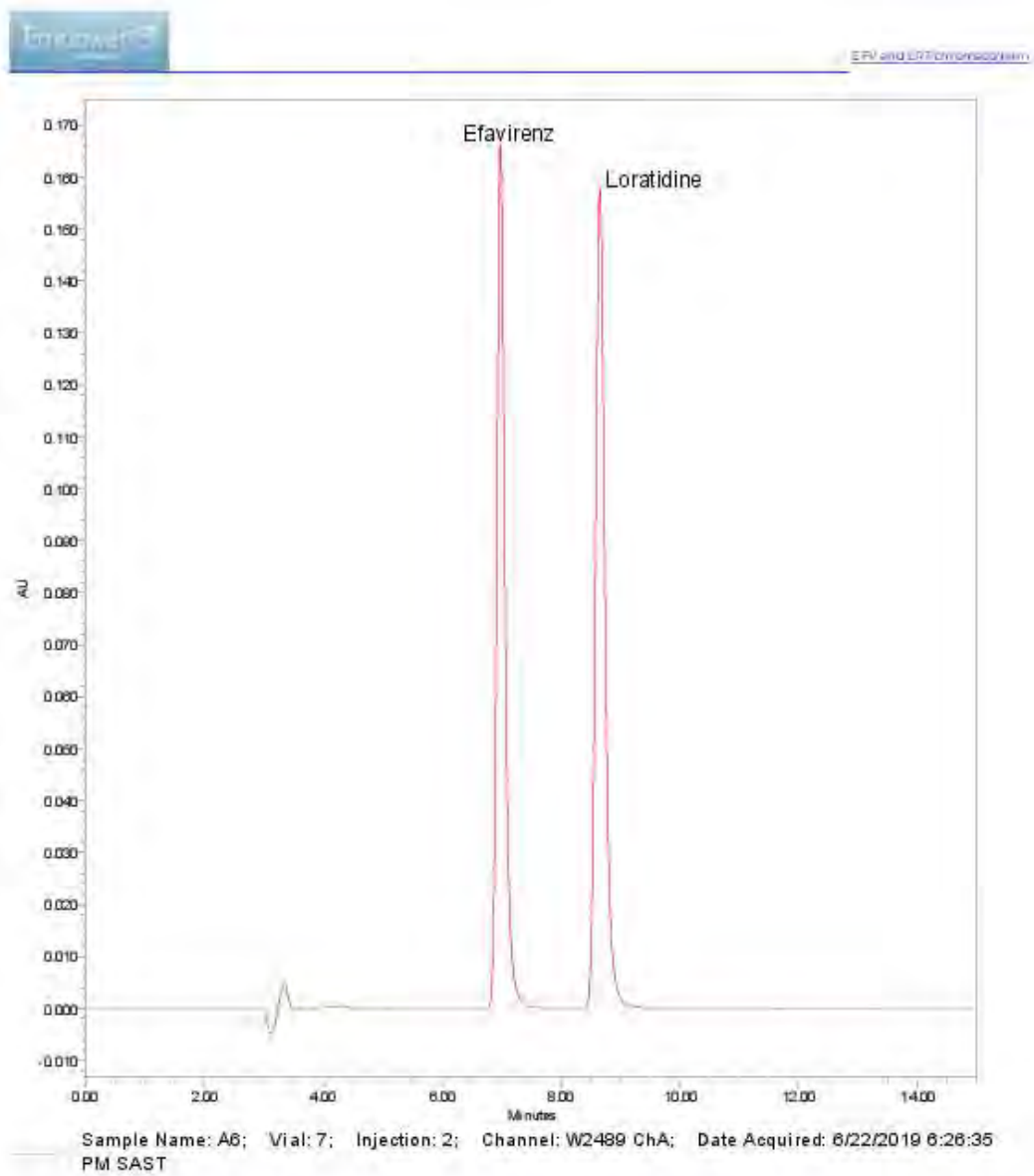
Figure 7.52. HPLC chromatogram of 250 µg/mL EFV and 15 µg/mL LRT, concentrations depicts 100 % of pure EFV sample.



Reported by User: BRG_Analyst2 (BRG_Analyst2)
 Report Method: Untitled
 Report Method IC110
 Page: 1 of 1

Project Name: BRG\Privilege
 Date Printed: 8/2/2021
 10:22:05 AM Africa/Johannesburg

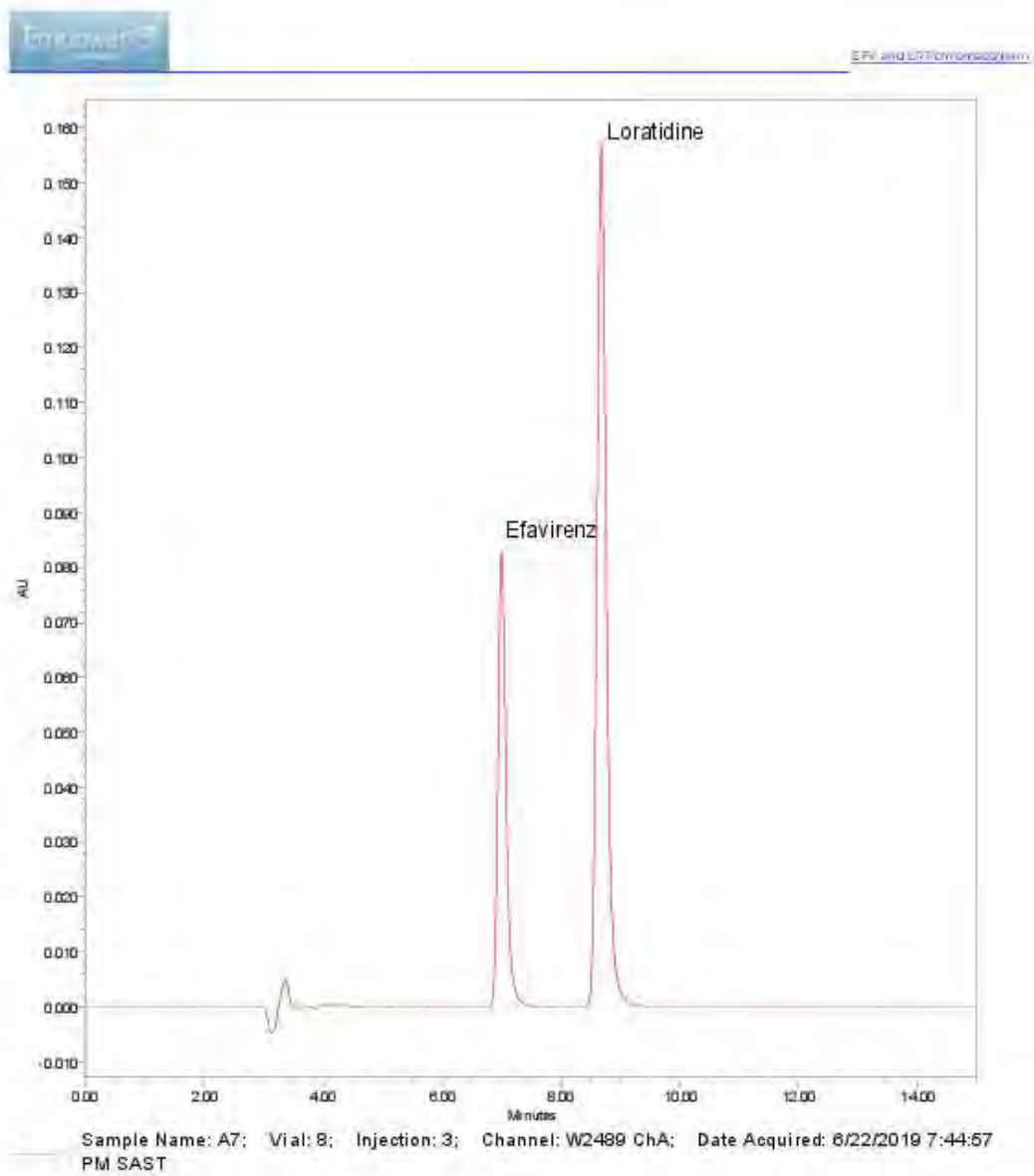
Figure 7.53. Chromatogram of alkali degradation of efavirenz at T0, only 8 % EFV recovered.



Reported by User: BRG_Analyst2 (BRG_Analyst2)
 Report Method: Untitled
 Report Method IC110
 Page: 1 of 1

Project Name: BRG\Privilege
 Date Printed: 8/2/2021
 10:21:19 AM Africa/Johannesburg

Figure 7.54. HPLC chromatogram of temperature stress studies of EFV, with 46 % of EFV recovered.



Reported by User: BRG_Analyst2 (BRG_Analyst2)
 Report Method: Untitled
 Report Method IC110
 Page: 1 of 1

Project Name: BRG\Privilege
 Date Printed: 8/2/2021
 10:21:40 AM Africa/Johannesburg

Figure 7.55. HPLC chromatogram of oxidative degradation of EFV, with 38 % of EFV recovered.

APPENDIX 2

FTIR, Raman and XRD spectra and signals following pre-formulation studies

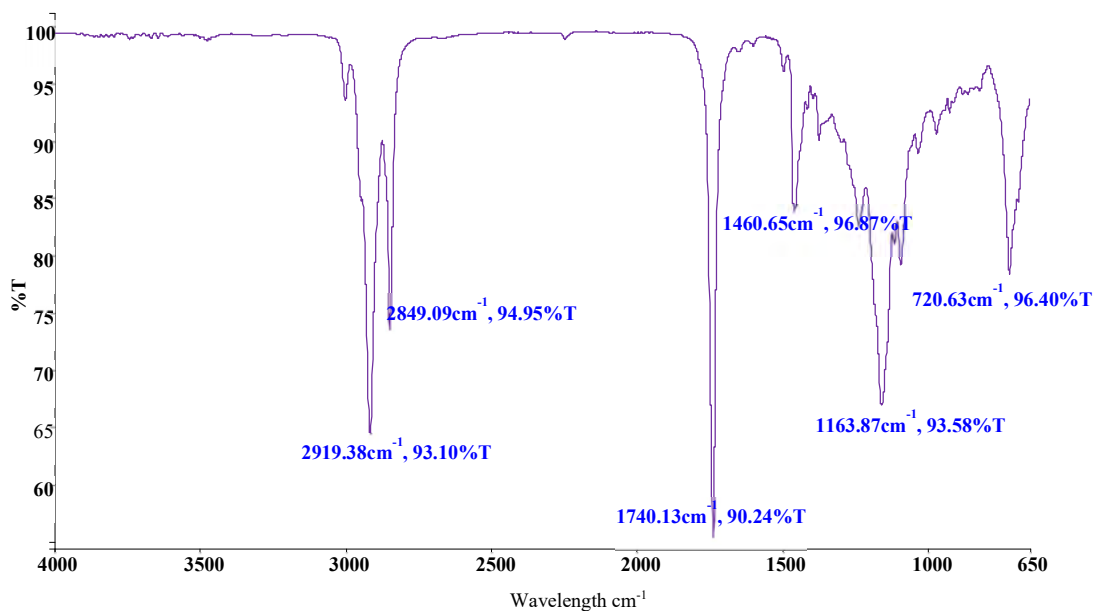


Figure 7.56. FTIR Spectra of 1:1 m/m mixtures of EFV and grapeseed oil.

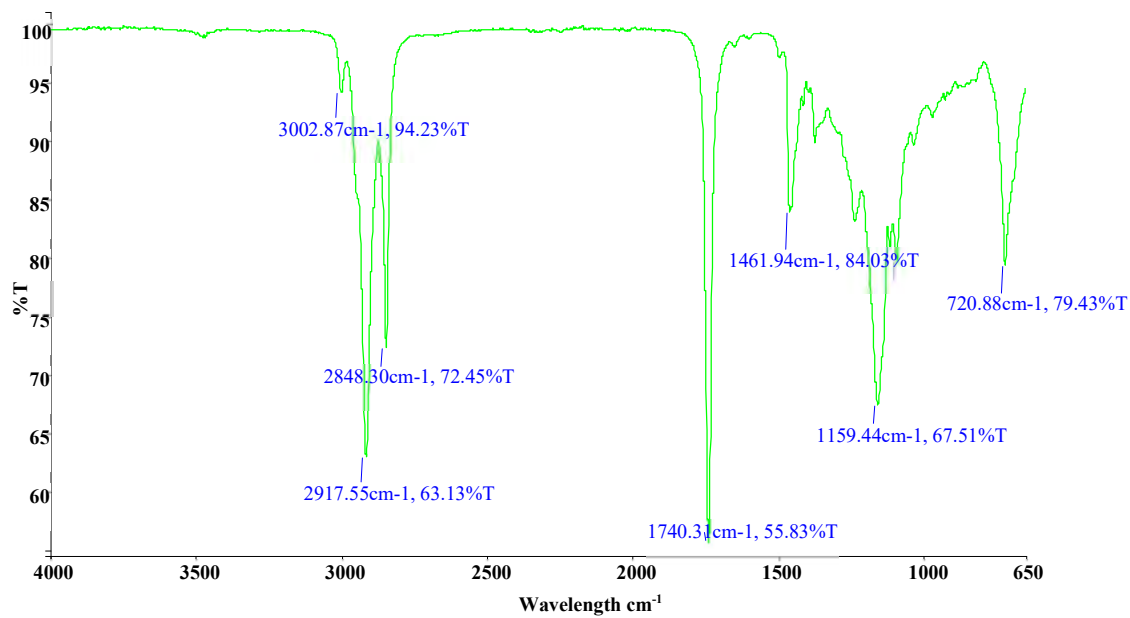


Figure 7.57. FTIR Spectra of 1:1 m/m mixtures of EFV and olive oil.

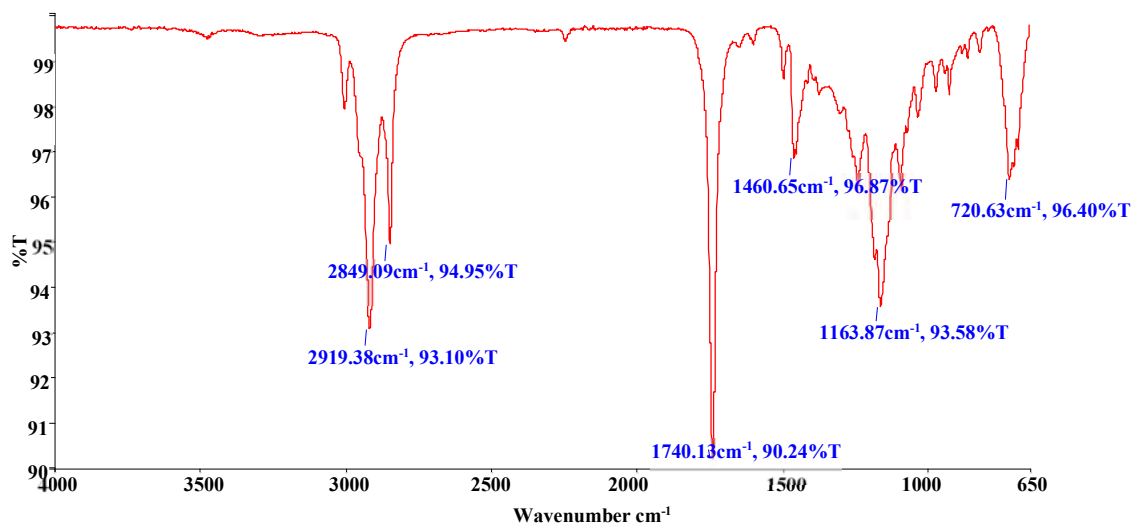


Figure 7.58. FTIR Spectra of 1:1 m/m mixtures of EFV and sunflower oil.

APPENDIX 3

Response surface plots for responses monitored following use of D-optimal experimental design for optimization.

Component Coding: Actual

Design Points:

● Above Surface

○ Below Surface

58.1  507.2

X1 = A: Span 20

X2 = B: Tween 80

X3 = C: Ethanol

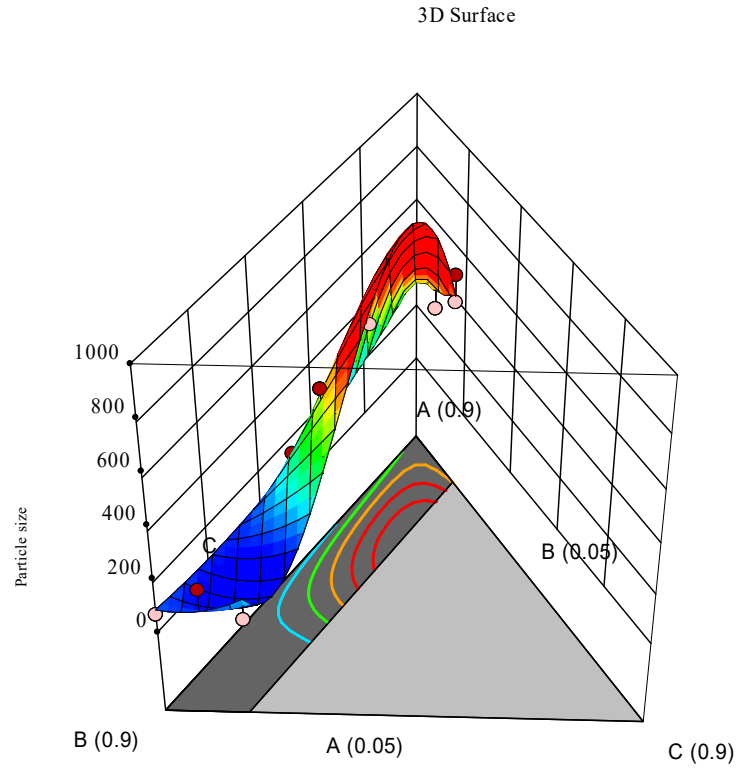


Figure 7.1259. 3D Response surface showing the effect of the concentration of Span[®] 20, Tween[®] and Ethanol on droplet size.

Component Coding: Actual

Design Points:

● Above Surface

○ Below Surface

0.119  0.75

X1 = A: Span 20

X2 = B: Tween 80

X3 = C: Ethanol

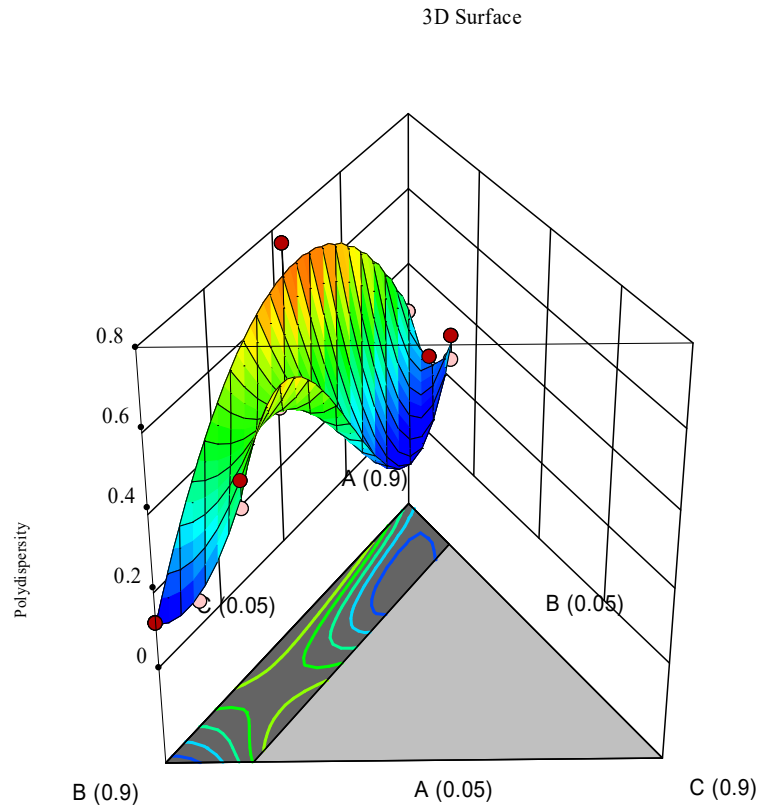


Figure 7.1360. 3D response surface plot for PDI showing the effect of surfactant concentrations.

Component Coding: Actual

Design Points:

● Above Surface

○ Below Surface

-25.5  -14.7

X1 = A: Span 20

X2 = B: Tween 80

X3 = C: Ethanol

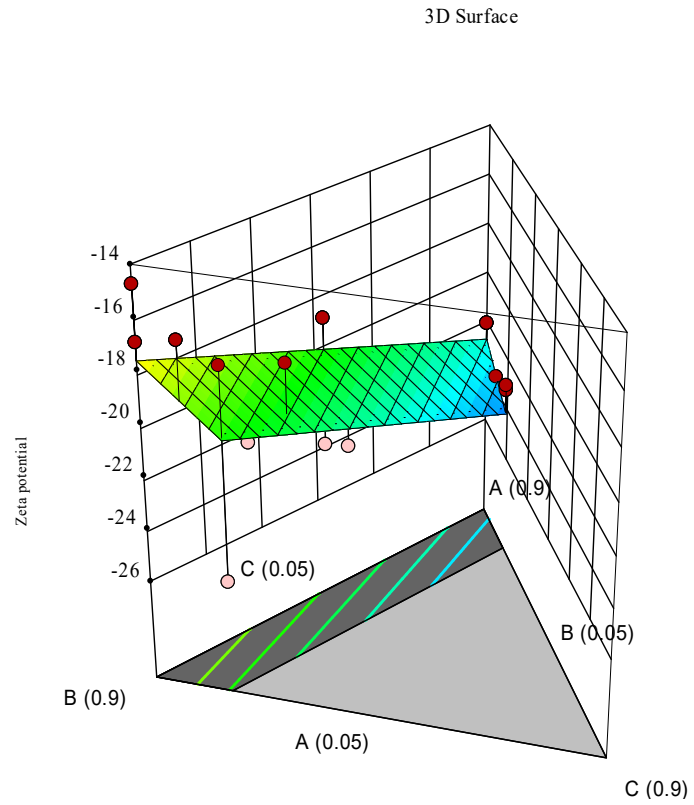


Figure 7.14. 3D Response surface plot for Zeta potential.

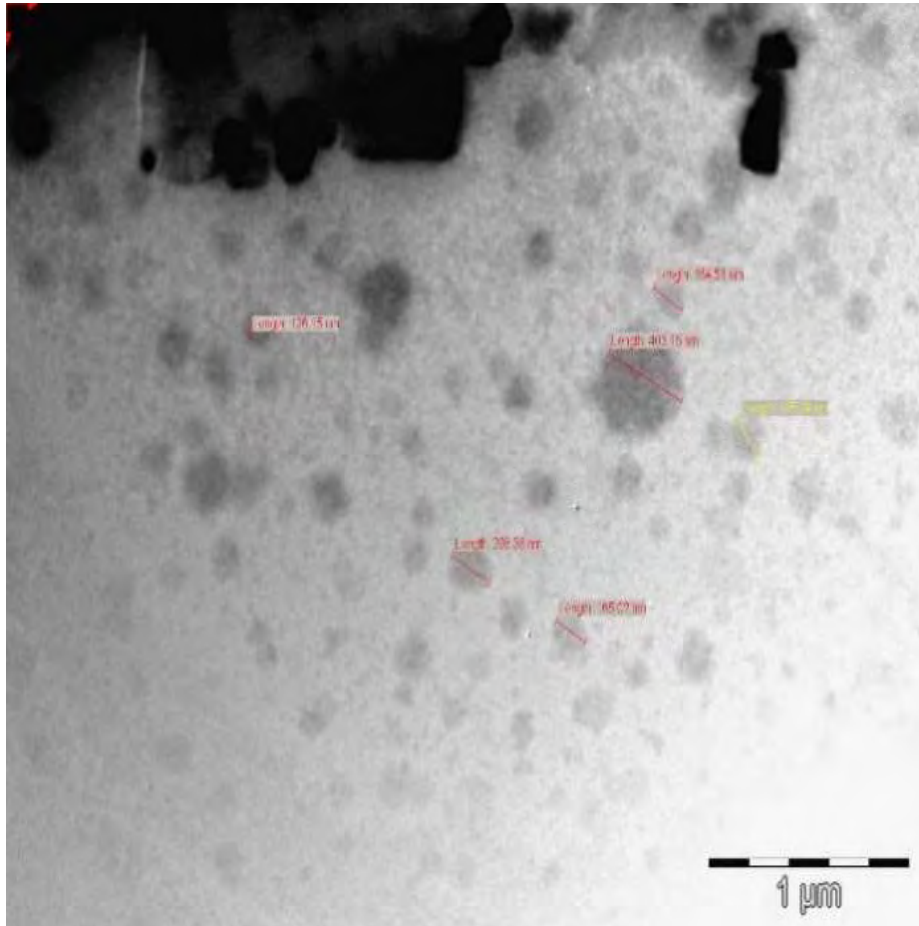


Figure 7.15. Transmission electron image of formulation emulsion F4.

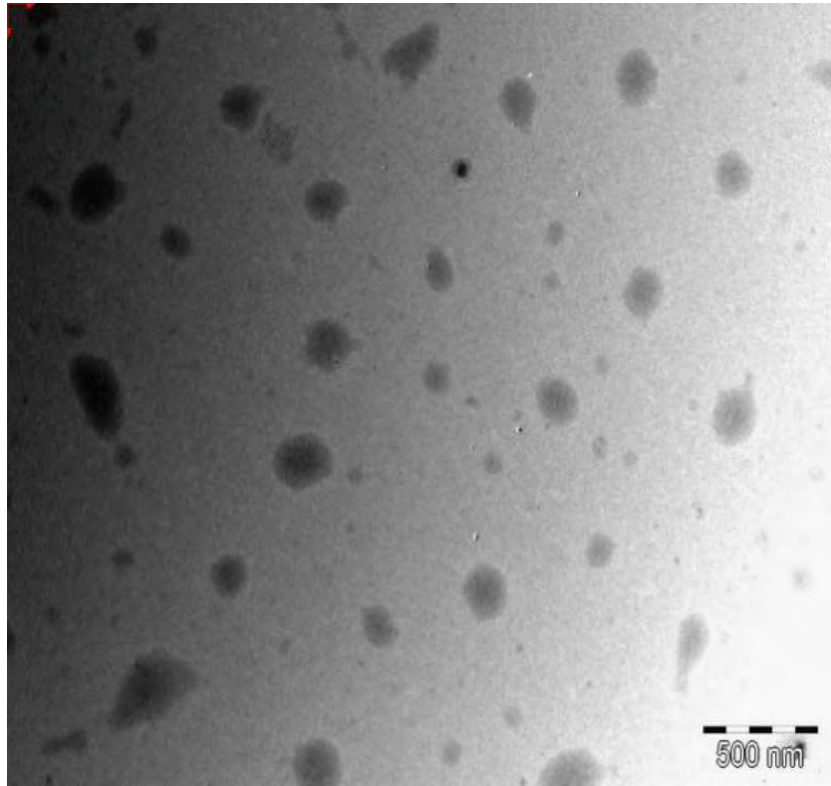


Figure 7.16. Transmission electron image of formulation nano-emulsion F2.

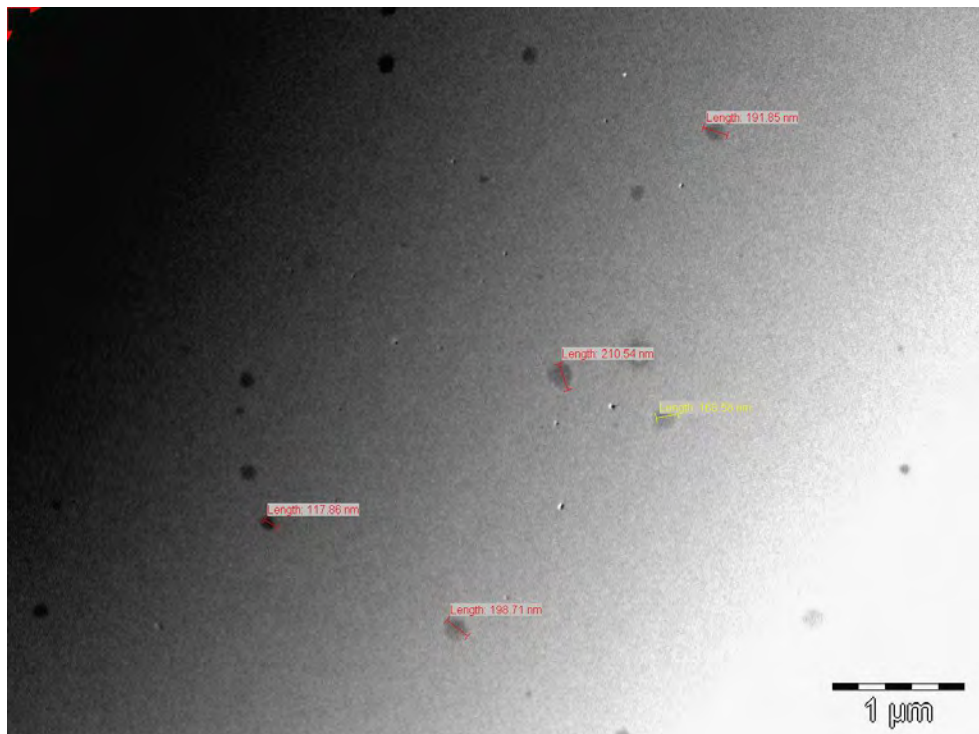


Figure 7.17. Transmission electron image of formulation nano-emulsion F3.